Doctoral Thesis in Environmental Engineering, Mining and Energy

Economic and environmental analysis of applying ammonia as carbon free fuel in internal combustion engine driven agricultural vehicle performed in whole life cycle approach

Mateusz Proniewicz

Silesian University of Technology
Gliwice, Poland, 2025

Author:
mgr inż. Mateusz Proniewicz
Department of Thermal Technology, Faculty of Energy and Environmental Engineering, Silesian University of Technology
e-mail: mateusz.proniewicz@polsl.pl

Supervisor:
prof. dr hab. inż. Andrzej Szlęk
Department of Thermal Technology, Faculty of Energy and Environmental Engineering, Silesian University of Technology
e-mail: andrzej.szlek@polsl.pl

Co-supervisor:
dr inż. Karolina Petela
Department of Thermal Technology, Faculty of Energy and Environmental Engineering, Silesian University of Technology
e-mail: karolina.petela@polsl.pl

Natura non nisi parendo vincitur
(Nature is only subdued by submission)
Sir Francis Bacon (1561–1626)

I dedicate this work to my wife and family

Preface

This thesis is submitted in fulfilment of the requirements for the degree of Doctor of Philosophy at Silesian University of Technology in Gliwice, Poland. The work was conducted at the Faculty of Energy and Environmental Engineering in the Department of Thermal Technology under the supervision of Professor Andrzej Szlęk and Dr. Karolina Petela.

This research has been a part of the “Ammonia as carbon free fuel for internal combustion engine driven agricultural vehicle” (ACTIVATE) project and has received funding from the Norway Grants 2014–2021 under the POLNOR2019 competition, operated by the National Centre for Research and Development, and from the Polish State Budget (Grant No. NOR/POLNOR/ACTIVATE/0046/2019-00).

Acknowledgements

Carrying out this work would not have been possible without certain individuals whom I wish to warmly acknowledge.

I would like to express my sincere gratitude to my supervisor, Professor Andrzej Szlęk, and my co-supervisor, Dr. Karolina Petela, for their guidance and support throughout this journey. Thank you for your time and patience.

I would also like to recognize the ACTIVATE project team for involving me in this work. Thank you for the collaboration and the many valuable experiences we have shared. I would also like to thank the project operator for providing financial support.

Finally, I would like to thank my wife, mother, and sister for their unconditional support. I also wish to acknowledge my late father, whose encouragement inspired me most to pursue this path. I am also grateful to my friends for their companionship throughout this journey.

Abstract

Ammonia may be considered a practical hydrogen carrier and diesel substitute for decarbonization in a CI engine used in a mini tractor intended for orchard operations. Environmental and economic assessments of such a solution are evaluated through life cycle assessment and life cycle costing methods. Life cycle assessment, performed using LCA for Experts software (formerly GaBi), accounts for multiple ammonia production pathways: ammonia based on hydrogen from steam methane reforming (grey), ammonia based on steam methane reforming with carbon capture and storage (blue), and ammonia based on hydrogen from electrolysis with electrical energy supplied by PV (green PV), wind (green wind), and a nuclear plant (pink). The analysis is based on experimentally gathered emissions data of the engine, where ammonia is utilized via a port injection setup, with rapeseed-based biodiesel serving as a pilot fuel. A mini tractor-specific working cycle of vehicle operation is considered, and the results are reported per hectare-year of the vehicle's operation (functional unit). For impact assessment, three midpoint ReCiPe categories are used – climate change, fossil depletion, and freshwater consumption – and two endpoint categories: human health and ecosystem quality.

First, an LCA of ammonia production methods compared to diesel is presented. The study shows that nuclear- and wind-based NH_3 minimize greenhouse gas emissions; however, pink ammonia increases fossil depletion and freshwater use due to uranium and cooling water burdens. Second, engine tests of a dual-fuel CI engine indicate slightly lower average efficiency than diesel, with the gap narrowing at high loads. However, partial load operation reveals elevated NO_x, N_2O, and NH_3 slip.

Complete LCA of the ammonia-fueled mini tractor shows that at the operational stage greenhouse gas emissions are reduced from approximately 88 kg CO_2 eq. for the diesel-fueled engine to approximately 72 CO_2 eq. for the ammonia-fueled one (–18 %), which can be assessed as a moderate reduction. This is due to the presence of N_2O emissions, a potent greenhouse gas, and the CO_2 from the pilot fuel for the ammonia-fueled engine. When the full life cycle is considered, climate reductions of 42–44 % are achieved when NH_3 is produced by wind or nuclear and the biodiesel carbon footprint is included. On a full life cycle basis, the results on fossil depletion show that green solar/wind ammonia allows for a 43–45 % reduction, whereas pink ammonia results in an impact increase of 78 % compared to the diesel-fueled engine. Full life cycle freshwater consumption rises 40–50 % for all NH_3 cases (apart from the nuclear route that rises to approximately twice that of diesel). Compared with the diesel scenario, full life cycle endpoint results show that the ammonia-fueled tractor causes about 47 % higher impact on human health and roughly double the impact on ecosystem quality, regardless of the ammonia source. When an SCR system using residual ammonia in the exhaust is considered to reduce NO_x and NH_3 emissions

from the operational phase, these impacts are reduced, but the human health impact still remains around 19 % higher and the ecosystem quality impact about 1.6–2 times higher than for diesel.

Life cycle costing employs a bottom-up approach, sourcing acquisition, operational, and end of life costs from laboratory and literature inputs, considering the same ammonia production pathways as in the environmental assessment. First, a price comparison of fuels on an energy basis is presented; ammonia is found to be economically competitive with diesel at a low natural gas price (below 6 $/MMBtu for the natural gas with carbon capture and storage pathway) or an electricity price below 38 $/MWh for electrolysis-based ammonia under a 1 $/l diesel price. Complete life cycle costing case study results indicate that the required upfront investment for an ammonia-fueled vehicle – which is about three times higher than a diesel vehicle – is the main challenge preventing overall economic competitiveness.

Considering uncertainty in the estimation of capital expenditure and volatile fuel markets, the estimated range of results shows that an ammonia-fueled tractor is 2–4 times more costly in total than that of a diesel mini tractor. To shift profitability in favor of ammonia from the orchard owner’s perspective, policymakers could implement a direct purchase incentive for a carbon-free vehicle, offsetting the high acquisition cost for orchard owners (a suggested range is 3000–8000 $, with 6000 $ being the default estimate), and include the cost of carbon emissions compliance for diesel to promote low carbon technologies.

Abstract in Polish language (Streszczenie)

Amoniak może być rozpatrywany jako praktyczny nośnik wodoru oraz substytut oleju napędowego służący do dekarbonizacji silnika o zapłonie samoczynnym stosowanym w mini ciągniku przeznaczonym do prac sadowniczych. Analiza środowiskowa oraz ekonomiczna takiego rozwiązania zostały przedstawione przy użyciu metod oceny cyklu życia i kalkulacji kosztów cyklu życia. Ocena cyklu życia, przeprowadzona przy użyciu oprogramowania LCA for Experts (dawniej GaBi), uwzględnia kilka ścieżek produkcji amoniaku: amoniak oparty na wodorze z reformingu parowego metanu (szary), amoniak z reformingu parowego metanu z wychwytywaniem i składowaniem CO_2 (niebieski) oraz amoniak z wodoru z elektrolizy zasilanej energią elektryczną przez fotowoltaikę (amoniak zielony, PV), wiatr (amoniak zielony, wiatr) i elektrownię jądrową (różowy). Analiza opiera się na eksperymentalnie zebranych danych dotyczących emisji silnika, w którym amoniak jest wykorzystywany w konfiguracji wtrysku pośredniego (port), a biodiesel na bazie rzepaku służy jako paliwo pilotażowe. Uwzględniono cykl pracy pojazdu dostosowany do mini ciągnika, a wyniki są podawane w przeliczeniu na hektar-rok eksploatacji pojazdu (jednostka funkcjonalna). Do oceny wpływu na środowisko wykorzystano trzy kategorie pośrednie ReCiPe – zmiana klimatu, wyczerpywanie zasobów kopalnych i zużycie wody słodkiej – oraz dwie kategorie końcowe: zdrowie ludzkie i jakość ekosystemu.

W pierwszym kroku przedstawiono analizę cyklu życia metod produkcji amoniaku w porównaniu z olejem napędowym. Wyniki pokazują, iż NH_3 wytwarzany z energii jądrowej i wiatrowej minimalizuje emisje gazów cieplarnianych, jednak różowy amoniak zwiększa wyczerpywanie zasobów kopalnych i zużycie wody słodkiej ze względu na eksploatację złóż uranu oraz zapotrzebowanie elektrowni na wodę chłodzącą. Następnie, wyniki eksperymentów silnika dwupaliwowego wskazują na nieco niższą średnią sprawność energetyczną niż w przypadku silnika zasilanego dieslem, przy czym różnica zmniejsza się przy dużych obciążeniach. Jednak praca silnika przy częściowym obciążeniu ujawnia podwyższony poziom emisji NO_x, N_2O oraz NH_3.

Kompletna analiza LCA mini traktora napędzanego amoniakiem pokazuje, że na etapie eksploatacji emisje gazów cieplarnianych zostały zmniejszone z około 88 kg ekw. CO2 dla silnika zasilanego olejem napędowym do około 72 kg ekw. CO2 dla silnika zasilanego amoniakiem (–18 %), co można ocenić jako umiarkowaną redukcję. Wynika to z obecności emisji N_2O, silnego gazu cieplarnianego, oraz emisji CO_2 pochodzących z paliwa pilotażowego w przypadku silnika zasilanego amoniakiem. Niemniej, z perspektywy pełnego cyklu życia wyniki wskazują, że redukcję emisji gazów cieplarnianych na poziomie 42–44 % osiąga się, gdy NH_3 jest wytwarzany z energii wiatrowej lub jądrowej oraz uwzględniony jest ślad węglowy biodiesla. W ujęciu pełnego cyklu życia wyniki w kategorii wyczerpywania zasobów kopalnych pokazują, że zielony amoniak, wytwarzany z energii słonecznej/wiatrowej, pozwala na redukcję o 43–45 %,

natomiast amoniak różowy powoduje wzrost wpływu o 78 % w porównaniu z silnikiem zasilanym olejem napędowym. Zużycie wody słodkiej wzrasta o 40–50 % dla wszystkich rozpatrywanych wariantów NH_3 (z wyjątkiem ścieżki jądrowej, dla której zużycie to wzrasta do około dwukrotności poziomu dla oleju napędowego). W porównaniu do diesla wyniki w kategoriach końcowych, w ujęciu pełnego cyklu życia, wskazują, że traktor zasilany amoniakiem powoduje około 47 % wyższy wpływ na zdrowie ludzkie oraz w przybliżeniu dwukrotnie wyższy wpływ na jakość ekosystemu, niezależnie od zastosowanego źródła amoniaku. Uwzględnienie układu SCR wykorzystującego amoniak obecny w spalinach w celu redukcji emisji NO_x i NH_3 powstających na etapie eksploatacji pojazdu prowadzi do obniżenia tych oddziaływań, jednak wpływ na zdrowie ludzkie pozostaje o około 19 % wyższy, a wpływ na jakość ekosystemu pozostaje o około 1,6–2 razy większy niż w przypadku oleju napędowego.

Rachunek kosztów cyklu życia opiera się na podejściu oddolnym, uwzględniającym koszty pozyskania, eksploatacji i utylizacji na podstawie danych laboratoryjnych i literaturowych, przy czym uwzględniono te same metody produkcji amoniaku, co w ocenie środowiskowej. Najpierw przedstawiono porównanie cen paliw w przeliczeniu na jednostkę energii; wykazano, że amoniak jest konkurencyjny ekonomicznie w stosunku do oleju napędowego przy niskiej cenie gazu ziemnego (poniżej 6 USD/MMBtu dla gazu ziemnego z wychwytywaniem i składowaniem dwutlenku węgla) lub cenie energii elektrycznej poniżej 38 USD/MWh dla amoniaku wytwarzanego w procesie elektrolizy przy cenie oleju napędowego wynoszącej 1 USD/l. Wyniki studium przypadku dotyczące całkowitych kosztów cyklu życia wskazują, że głównym wyzwaniem uniemożliwiającym konkurencyjność ekonomiczną jest wysoka wartość inwestycji początkowej dla pojazdu napędzanego amoniakiem, która jest około trzykrotnie wyższa niż w przypadku pojazdu z silnikiem diesla.

Uwzględniając niepewność w szacowaniu nakładów kapitałowych i niestabilność rynków paliwowych, szacowany zakres wyników pokazuje, że ciągnik napędzany amoniakiem wymaga 2–4 razy wyższych kosztów całkowitych niż mini ciągnik zasilany dieslem. Opłacalność stosowania amoniaku w pojeździe z punktu widzenia właścicieli sadów może zostać zwiększona przez decydentów politycznych poprzez wprowadzenie bezpośredniej dopłaty do zakupu pojazdów bezemisyjnych, w celu skompensowania wysokich kosztów nabycia pojazdu (w przedziale 3000–8000 USD, przy czym domyślnym szacunkiem jest 6000 USD), oraz uwzględnienie kosztu emisji dwutlenku węgla w cenie oleju napędowego, co może zwiększyć opłacalność technologii o niskim śladzie węglowym.

List of publications

This thesis consists of a series of four publications listed below. The papers are presented in full in the Appendix.

I. **Proniewicz, M.**, Petela, K., Szlęk, A., & Adamczyk, W. (2024). Life cycle assessment of selected ammonia production technologies from the perspective of ammonia as a fuel for heavy-duty vehicle. *Journal of Energy Resources Technology-Transactions of the Asme*, *146*, Article 3, 030905. https://doi.org/10.1115/1.4064371 (IF = 2.4)

II. **Proniewicz, M.**, Petela, K., Szlęk, A., Przybyła, G., Nadimi Karamjavan, E., Ziółkowski, Ł., Løvås, T., & Adamczyk, W. (2023). Energy and exergy assessments of a diesel-, biodiesel-, and ammonia-fueled compression ignition engine. *International Journal of Energy Research*, *2023*, 9920670. https://doi.org/10.1155/2023/9920670 (IF = 4.2)

III. **Proniewicz, M.**, Petela, K., & Szlęk, A. (2025). Life cycle assessment of ammonia as carbon-free fuel in internal combustion engine-driven orchard vehicle. *Fuel*, *400*, 135809. https://doi.org/10.1016/j.fuel.2025.135809 (IF = 7.5)

IV. **Proniewicz, M.**, Petela, K., & Szlęk, A. (2025). Life cycle costing of an ammonia-fueled internal combustion engine-driven orchard vehicle. *Energy*, *334*, 137814. https://doi.org/10.1016/j.energy.2025.137814 (IF = 9.4)

Apart from these articles, the author also authored/co-authored the following works related to the topic investigated in this thesis:

I. **Proniewicz, M.**, Petela, K., & Szlęk, A. (2022). LCA and LCC framework for special purpose vehicles based on a case study of mini-tractor for orchard operations. In B. Elmegaard, E. Sciubba, A. M. Blanco-Marigorta, J. K. Jensen, W. Brix Markussen, W. Meesenburg, N. Arjomand Kermani, T. Zhu, & R. Kofler (Editors), *Proceedings of ECOS 2022, 35th International Conference on Efficiency, Cost, Optimization, Simulation and Environmental Impact of Energy Systems*.

II. Adamczyk, W., Przybyła, G., Nadimi Karamjavan, E., Peczkis, G., Lovas, T., Petela, K., **Proniewicz, M.**, Pasternak, M., Lewandowski, M., Emberson, D., Bjorgen, K., Rutczyk, B., & Sachajdak, A. (2023). Zastosowanie amoniaku jako paliwa do napędu silników

tłokowych. In J. T. Cieśliński, D. Mikielewicz, & J. Wajs (editors), *XXV Jubileuszowy Zjazd Termodynamików 11-14 września 2023 r., Gdańsk. Książka abstraktów*.

Author contribution statement

The first author's contributions to each paper comprising this thesis are provided below, in accordance with the CRediT (Contributor Roles Taxonomy). For Papers III and IV, full authorship statements appear at the end of the articles (after the Summary sections) in line with the journal guidelines. Contributions are identical across all four papers because the articles were prepared by the first author (calculations, tables, figures, text), and the co-authors contributed primarily through review and suggestions for improvement:

I. Mateusz Proniewicz: Writing – original draft, Methodology, Investigation, Formal analysis, Conceptualization, Data curation.

II. Mateusz Proniewicz: Writing – original draft, Methodology, Investigation, Formal analysis, Conceptualization, Data curation.

III. Mateusz Proniewicz: Writing – original draft, Methodology, Investigation, Formal analysis, Conceptualization, Data curation.

IV. Mateusz Proniewicz: Writing – original draft, Methodology, Investigation, Formal analysis, Conceptualization, Data curation.

Table of contents

List of figures

List of tables

Nomenclature

ASU – Air Separation Unit
CI – Compression Ignition
EoL – End of Life
GHG – Greenhouse Gases
GWP – Global Warming Potential
IEA – International Energy Agency
ICE – Internal Combustion Engine
LCA – Life Cycle Assessment
LCC – Life Cycle Costing
LCOE – Levelized Cost of Electricity
LHV – Lower Heating Value
NG – Natural Gas
SCR – Selective Catalytic Reduction

Chapter 1 – Introduction

1.1. Background

One of the pillars of civilization's development is its use of energy. Global direct primary energy consumption has been continuously growing over the years, increasing from 27 972 TWh in 1950 to 167 584 TWh in 2024. This energy is primarily based on fossil fuels as gas, oil, and coal consumption accounted for 72 % of global direct primary energy in 1950 and increased to 85 % in 2024 [1]. However, intensive exploitation of fossil fuels is linked to the emissions of greenhouse gases (GHG), which in turn impact the climate. According to climate models, greenhouse gas emissions caused by human activity increase the global average temperature, affecting the ice quantity in the polar caps, sea levels, and the frequency of extreme events [2]. This culminated in the adoption of the Paris Agreement, an international treaty on climate change, recognized by 195 parties during the UN Climate Change Conference (COP21) in Paris, France, on 12 December 2015. The primary outcome was an agreement towards decarbonization in order to limit the increase in the global average temperature to below 2 °C relative to pre-industrial levels, and to undertake further initiatives to fall below 1.5 °C. A scientific comparison of the impacts of global warming of 1.5 °C and 2 °C and GHG emission pathways has been elaborated in the report prepared by the Intergovernmental Panel on Climate Change (IPCC) in 2018 [3].

Decarbonization is a broad term for a process in which entities or individuals adopt dedicated strategies for reducing their carbon impact [4]. Technically, this can be achieved, for instance, through enhancing energy efficiency, electrification, adoption of alternative energy sources such as bio-based feedstocks or hydrogen, and carbon capture and storage (CCS) technologies [3], depending on the analyzed system.

For sectors that are strongly dependent on fossil fuels, such as agriculture, construction, or transportation, where diesel-fueled heavy-duty machinery like tractors, trucks, excavators, mobile cranes, and others are commonly used, decarbonization is not a trivial task. Electrification, which may be feasible for passenger vehicles, is challenging for heavy-duty vehicles due to their high power requirements and the need to maintain acceptable driving range. Because batteries have lower energy density and slower charging rates compared to liquid fuels [5], alternatives may be considered. Based on the EU–27's statistics, between 2015 and 2023, final consumption of gas oil and diesel oil grew by 2487 thousand tonnes of oil equivalent (ktoe) in agriculture and forestry, and by 1755 ktoe in the construction sector [6].

One option is to replace fossil diesel with bio-based diesel. Biofuels are commonly grouped into generations based on feedstock and conversion pathway [7], [8]:

i. 1st generation: conversion of vegetable oils/animal fats to biodiesel (transesterification) and fermentation of sugars/starches (e.g., sugarcane, corn) to alcohol fuels. The key limitation is competition with food and arable land.

ii. 2nd generation: conversion of lignocellulosic residues and wastes (e.g., cereal straw, sugar cane bagasse, forest residues) via biochemical or thermochemical routes. Limitations are costly pretreatment and overall process complexity.

iii. 3rd generation: algae/aquatic biomass and other microbes; lipid extraction or conversion of algal bio-oils. Limitations are low lipid yields, energy-intensive harvesting/dewatering (mixing, filtration, centrifugation) and contamination risk in open ponds.

iv. 4th generation: genetically optimized feedstocks (algae and other microbes) designed to increase the yield of lipids and ease their extraction, with integrated CO_2 capture and sequestration. While it aims to address the challenges of the 3rd generation, it remains an early-stage technology with high initial investment.

Because the carbon is biogenic, switching to biofuels can reduce life cycle GHG emissions [8]; however, existing limitations motivate further options.

Hydrogen has gained interest as a versatile energy carrier that can replace or work alongside existing fuels in multiple applications. It is characterized by a high lower heating value (LHV) on a mass basis (2.4 times higher compared to methane [9]), a lack of carbon emissions upon its combustion, and renewability when produced by water electrolysis using renewable electrical energy [10]. It is seen as particularly promising for industry (steel production), transportation, heating, and electricity production [11]. Additionally, it can also be converted into other hydrogen-based fuels like synthetic methane, ammonia, or methanol. Interest in hydrogen and its derivatives is reflected in initiatives such as the U.S. Regional Clean Hydrogen Hubs (H2Hubs) and the EU's Hydrogen Valleys under the Clean Hydrogen Partnership. However, for mobile applications hydrogen poses a challenge for efficient storage; it can be stored either as a liquid at low temperatures (saturation temperature around –253 °C at 1 bar [12]) or as a gas under high pressure (700 bar) [13].

From this point of view, ammonia emerges as a promising alternative for heavy-duty applications. Similar to hydrogen, its molecule does not contain carbon atoms and therefore its combustion does not involve any carbon emissions. It is mainly produced in a Haber–Bosch process [14] in the reaction of hydrogen with nitrogen; given that nitrogen is obtained from air, ammonia can be classified as renewable if renewable hydrogen is used. Ammonia's saturation temperature is around −34 °C at 1 bar [15], and as such its storage is much more feasible compared to hydrogen;

if pressurized to 20 bar it remains liquid up to 50 °C [16]. A comparison between ammonia and hydrogen on an energy basis is presented in Table 1; even though the LHV of hydrogen on a mass basis is around 6.45 times higher, on a volume basis in the liquid state it is actually 0.67 times lower. Ammonia as a hydrogen-derived fuel is explicitly mentioned in the *Renewable fuels of non-biological origin in the European Union* report published by the European Commission in 2022.

Table 1. Comparison of lower heating values (LHV) of liquefied ammonia and hydrogen [17].

	LHV, MJ/kg	LHV, MJ/l	Density, kg/m3
Liquefied ammonia (1 bar, -33.6 °C)	18.6	12.7	682
Liquefied hydrogen (1 bar, -253 °C)	120	8.5	70.9

From an ICE perspective, although ammonia's lower heating value per kilogram of fuel is about 44 % of that of diesel [18], its lower stoichiometric air–fuel ratio results in a similar energy content per kilogram of stoichiometric fuel-air mixture (2.64 vs 2.77 MJ/kg-mixture) [18]. Consequently, for the same amount of inducted air, a comparable amount of energy can be delivered using ammonia, which supports the feasibility of this fuel in ICE applications. However, ammonia's high auto-ignition temperature, low laminar burning velocity, and long quenching distance contribute to incomplete combustion, leading to ammonia slip and nitrogen oxide emissions (NO_x) [19]. These can be addressed through engine optimization, dual-fuel operation, or aftertreatment systems such as selective catalytic reduction (SCR) [20]. This shows that while ammonia might be successfully used in an ICE, the engine must be adjusted accordingly. Its combustion characteristics make it particularly suitable for engines operating at low rotational speeds, such as those used in marine, railway, or agricultural applications.

1.2. Objectives and research gap

From the discussion provided in Section 1.1, it may be concluded that technically ammonia can be utilized in an ICE operating in a vehicle. However, a question arises about the environmental and economic implications of this fuel switch in a life cycle approach.

If the engine were fueled by pure ammonia, no carbon emissions would be present during its operation. However, since ammonia has a lower energy content per kilogram of fuel than diesel, a greater amount of ammonia must be consumed by the engine to deliver the same output. If ammonia production had a high impact on the environment through intensive energy or resource use, resulting in considerable GHG emissions, the benefits of reducing GHG during the operation phase of the vehicle may be offset or even exceeded by the carbon emissions occurring during the production of ammonia. This is particularly important given that currently hydrogen is primarily produced from natural gas via steam methane reforming (SMR), but is anticipated to be produced in larger quantities from renewable-based pathways in the upcoming years [21].

Next, due to the difficulties with pure ammonia combustion, dual-fuel operation has been considered to achieve the engine's stable operation, in line with literature suggestions [22], with biodiesel serving as the pilot fuel. Detailed analysis of the engine's emissions under varying conditions and dual-fuel operation is another factor toward complete understanding of the fuel switch. Since ammonia combustion results, among others, in nitrous oxide (N_2O) emissions [20], [23], which is a strong GHG with Global Warming Potential (GWP) of 273 [24], this factor must be accounted for.

Another aspect of the fuel switch is the economic comparison between the two options, specifically, cost comparison between them. This can be divided into two primary parts:

i. Expenditure required to purchase a diesel- or ammonia-fueled vehicle, given that technologically an ammonia-fueled vehicle involves certain modifications (dual-fuel adaptation, SCR).

ii. Expenditure required to run the diesel- or ammonia-fueled vehicle, given the different amounts of fuel consumed under the same operating conditions and their respective costs, noting that the cost of ammonia depends on the source of hydrogen.

To address these research questions, the specific objectives of this work can be formulated as follows:

1. Defining the differences between the impact on the environment of ammonia- and diesel-fueled mini tractor based on life cycle assessment (LCA).

2. Assessing the economic performance of ammonia- and diesel-fueled mini tractor based on life cycle costing (LCC).

To fully characterize the use of ammonia as a fuel for a mini tractor, a comparison to a diesel baseline using the same functional unit and performance assumptions is necessary. Without this reference case, the LCA and LCC would report only absolute impacts and costs, which do not provide enough information for an informed fuel switch decision.

Literature quoted in Section 1.1, supported by other works [23], [25], [26], [27], clearly shows that ammonia's potential and advantages as a fuel have been noticed, along with its disadvantages. There are published LCA studies on applying ammonia in an ICE context [28], [29], but they are set in passenger vehicles for transportation and power generation contexts. Conversely, LCC studies on alternative fuel options focus primarily on hydrogen [30], [31], [32]; for heavy-duty applications, several bus assessments have been published [33], [34], [35]. The lack of dedicated

research on the environmental analysis of ammonia's application as a fuel in a compression ignition (CI) engine used in agriculture for orchard operation is the first major research gap this study fulfills. The second major gap is the lack of research on the economic assessment of such a solution, specifically, lack of information on purchasing and operating an ammonia-fueled mini tractor used in an orchard.

The agricultural context of this study is justified by the fact that ammonia is already commonly used in the agricultural sector and, as such, its logistics can leverage an existing base of ports, storage, and carriers built for the fertilizer industry. According to the International Energy Agency (IEA), production of ammonia – used both directly and as the base for nitrogen fertilizers – accounts for 2 % of global energy use and 1.3 % of CO_2 emissions [36]. The experience of the agricultural sector with ammonia could facilitate ammonia deployment in other uses, like using it for the machinery. Additionally, using ammonia as a fuel in such an application can also support sustainable food production, which is another ongoing challenge.

1.3. LCA and LCC approach

LCA and LCC are both methods that quantify environmental impacts and total costs, respectively, of a given product or asset throughout its lifespan, i.e., from its production/acquisition, operation with maintenance, and utilization [37], [38]. The LCA structure follows the ILCD handbook [37] which is in line with the ISO 14040 and 14044 standards on LCA, and consists of the following parts:

i. Goal and scope – specifies the decision context, functional unit, and system boundaries.

ii. Life cycle inventory (LCI) – quantifies all relevant inputs (materials, energy) and outputs (emissions, wastes, products) of the system across the life cycle.

iii. Life cycle impact assessment (LCIA) – translates inventory flows into environmental impact categories.

iv. Interpretation – analyzes LCIA results towards conclusions and recommendations.

The goal of the LCA presented in this work is in line with the first objective of the study presented in Section 1.2, i.e. comparing the environmental impacts of diesel- vs. ammonia-fueled mini tractor (SCOUT 15-T), which is achieved by performing two independent LCAs under consistent comparison assumptions: one for an ammonia-fueled mini tractor with biodiesel serving as the pilot fuel in port injection mode, and one for the reference diesel mini tractor. The LCA is a cradle to grave type, i.e., from resource extraction to product utilization; system boundaries with major phases are schematically presented in Figure 1. Hectare-year of tractor operation has been selected

as the functional unit. The LCA has been performed using the LCA for Experts software (prev. GaBi).

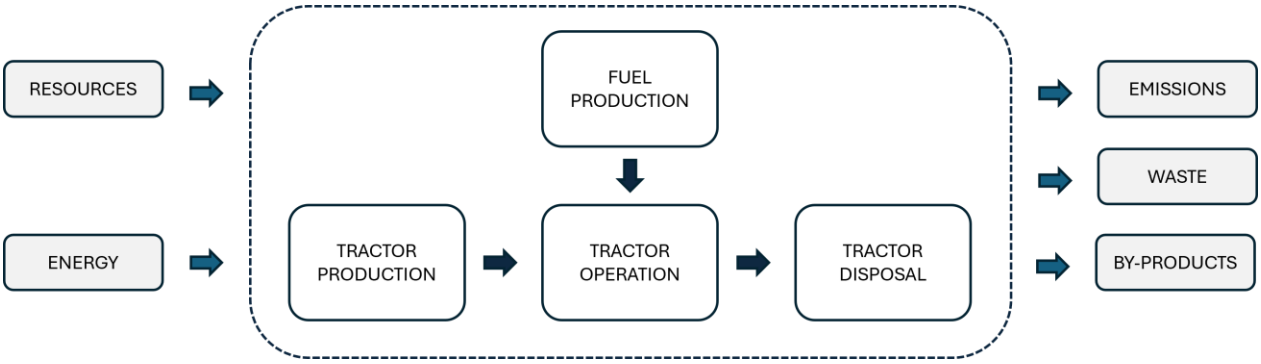

Figure 1. Schematic overview of the system boundaries for the LCA study.

For the ammonia-fueled case, fuel production represents the complete pathway of ammonia production for several scenarios from fossil- to renewable-based routes, whereas the tractor operation represents emissions gathered from experimental measurements of the ammonia-fueled engine. Conversely, for the diesel-fueled LCA, fuel production pertains to diesel, and emissions are based on experiments of the diesel-fueled engine. The same approach has been applied to estimate the environmental impact of the tractor production and disposal phases (end of life, EoL) in the two cases.

Life cycle inventory is based on primary experimental data for the operation phase and secondary data for other phases. Secondary data include Sphera's Managed LCA Content database (software database) [39] and literature; the database is based on industry data and its reliability is ensured by a third party review. Life cycle impact assessment is based on selected environmental categories using the ReCiPe method, and is followed by the interpretation. While LCA is standardized at the framework level, its application in this study required several case-specific developments, including defining tractor- and orchard-specific system boundaries and operating scenario, constructing consistent life cycle inventories by collecting and processing primary experimental data for the ammonia- and diesel-fueled engine, and aggregating secondary data for fuel production pathways and other life cycle phases.

The structure of the life cycle costing is in line with the LCA approach; a schematic overview of the system boundaries of the LCC is shown in Figure 2.

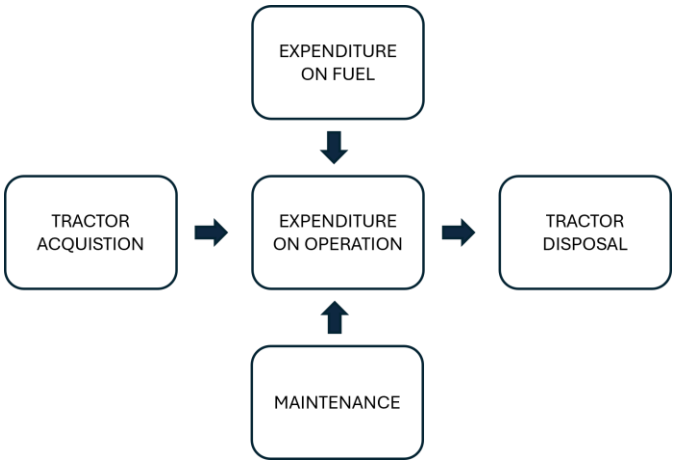

Figure 2. Schematic overview of the system boundaries for the LCC study.

For an ammonia-fueled mini tractor, tractor acquisition refers to the price of a standard mini tractor (CI engine) equipped with apparatus allowing for the utilization of ammonia via a port injection system; the pilot fuel uses a direct injection setup with biodiesel substituting diesel. For the reference diesel-fueled case, this value is represented by its market price. The operation phase constitutes expenditure on fuel, considering that ammonia can be based on either fossil or renewable pathways, as well as the vehicle's maintenance. Tractor disposal represents the price of disposing of the vehicle's body.

1.4. Thesis outline

In this work, ammonia is analyzed as a fuel for a mini tractor suitable for an agriculture setting, specifically for orchard operations, from environmental and economic perspectives. As stated in Section 1.2, crucial aspects of the LCA are ammonia production pathways and the engine's emissions. Since these topics require thorough discussion, a dedicated paper on each of these topics has been prepared, and the final findings from the LCA and LCC are published in the two following studies. This document should be interpreted as a guide through these papers with the following structure.

Chapter 1 provides an introduction to the topic including the background, objectives and research gaps, the LCA and LCC approaches, and the thesis's structure.

Chapter 2 is devoted to the estimation of environmental impacts of several ammonia production pathways. This is achieved through a dedicated LCA on ammonia production routes and represents a summary of the first paper comprising the thesis, particularly regarding the applied methods and key results.

Chapter 3 focuses on the comparison of the engine's performance and its emissions when fueled by ammonia or diesel, across the entire map of the engine's operation considering varying shaft speeds and loads. It gives an overview of the methods and major results from the second published paper.

Chapter 4 presents a comprehensive LCA of an ammonia-fueled mini tractor in comparison to a reference vehicle, drawing from the investigated ammonia production pathways from Paper I and the engine's emissions from Paper II. It directly addresses the first specific objective of the thesis and outlines the third paper's methodology and results.

Chapter 5 elaborates on LCC of an ammonia-fueled mini tractor in reference to the diesel-fueled vehicle. It responds to the thesis's second objective and summarizes the fourth paper's approaches employed and key findings.

Chapter 6 concludes the findings of this research.

Most figures and tables shown in this document are either directly taken from the published papers or have been slightly refined.

Chapter 2 – Ammonia production pathways

Paper I addresses the LCA of selected ammonia production pathways from the perspective of using ammonia as a fuel in a heavy-duty vehicle. Based on this paper, an overview of the considered technologies, modeling approach, impact categories, and environmental results is provided in this chapter.

2.1. Technology overview

The primary industrial method for ammonia production is the Haber–Bosch process, valued for its technological maturity and scalability [40], [41], and is therefore used here as the representative baseline for ammonia's production. Alternative methods – including electro- or photocatalytic nitrogen reduction and chemical looping – are still under development and lie outside the scope of this study [42], [43].

The Haber–Bosch process is based on the exothermic reaction of nitrogen and hydrogen in accordance with equation 1. For iron-based catalysts, the process conditions are set between 150–300 bar and 350–525 °C to achieve a high conversion rate [44].

$$N_2 + 3H_2 \leftrightarrow 2NH_3 \quad (1)$$

Nitrogen needed for the process is derived from atmospheric air; the following sources of hydrogen are considered in this study, which determine the type of ammonia:

i. Grey ammonia – hydrogen from steam methane reforming

ii. Blue ammonia – hydrogen from steam methane reforming with carbon capture and storage

iii. Green ammonia – hydrogen from water electrolysis driven by solar or wind energy

iv. Pink ammonia – hydrogen from water electrolysis driven by nuclear energy

Grey and blue ammonia can be referred to as fossil-based ammonia. The SMR is performed in two steps: first, an endothermic reaction of methane with steam, in accordance with equation 2, is performed under 3–25 bar and 700–850 °C [45]. To increase the hydrogen yield, the water-gas shift reaction follows, in line with equation 3 [46].

$$CH_4 + H_2O \rightarrow CO + 3H_2 \quad (2)$$

$$CO + H_2O \rightarrow CO_2 + H_2 \quad (3)$$

Around 30–40 % of the gas is used to deliver heat, causing the emissions of "diluted" CO_2 upon its combustion; the rest participates in the reaction and results in the "process" CO_2 emissions [11]. The difference between grey and blue ammonia is that absorption- or adsorption-based CO_2 capture coupled with CO_2 storage is applied for blue ammonia, resulting in considerably lower CO_2 emissions.

Green and pink ammonia come from water electrolysis, where water is decomposed into hydrogen and oxygen under the applied voltage. There are three most common types of electrolyzers: alkaline, proton exchange membrane (PEM) and solid oxide electrolysis cells (SOEC). Electrical efficiency is the highest for the SOEC type (74–81 %), followed by alkaline and PEM (63–70 %, 56–60 %, respectively); however, it is the least developed technology and is characterized by the highest CAPEX (2800–5600 $/kWe). On a CAPEX basis, alkaline is the most beneficial (500–1400 $/kWe), followed by PEM (1100–1800 $/kWe) and SOEC. Alkaline and PEM are both low-temperature electrolyzer types operated under moderate pressures: 60–80 °C at 1–30 bar and 50–80 °C at 30–80 bar, respectively, SOEC operates at 1 bar under 650–1000 °C (high-temperature electrolysis) [11].

2.2. Modeling approach

To evaluate the environmental impact of ammonia production technologies from the perspective of using it as fuel in ICE CI, a cradle to gate type analysis (from raw material extraction through processing to ammonia production) with a functional unit of 1 MJ on an LHV basis has been performed.

The environmental impacts of grey (SMR) and blue ammonia (SMR coupled with CCS) are taken directly from aggregated datasets in the software (black-box models) [39]:

i. Ammonia (NH3) production mix, without CO2 recovery

ii. Ammonia (NH3) synthesis with CO2 recovery, where CO2 is a by-product

Stages included in both datasets cover: gas extraction, methane reforming, and ammonia synthesis in the Haber–Bosch process, using data representative of Europe. In the grey route, CO_2 from SMR is released into the air. In the blue route, carbon capture is applied to the "process CO_2" stream. The recovered CO_2 is modeled as a by-product; no allocation is performed between NH_3 and CO_2 outputs.

Green ammonia is modeled based on an alkaline electrolyzer as the most representative technology (60 % of worldwide installed capacity in 2023 [20]) with a literature-based electrolysis model using upstream processes sourced from the software database. The cradle to gate approach includes: electrolyzer manufacturing, water preparation, nitrogen production, and electrical energy production. Quantitatively electrolysis per one kg of H_2 is modeled as follows [47]:

- Electricity: 53 kWh
- Water: 9 kg
- Steam: 0.11 kg
- Nitrogen: 0.00029 kg

Three electricity cases are assessed – PV and wind (green ammonia), and nuclear (pink ammonia) – with identical process parameters. The electrolyzer manufacturing inventory follows literature data [47]. Finally, H_2 from electrolysis and N_2 from an air separation unit (ASU) react at a 3:1 ratio in a recycle loop; overall conversion is 98 % with 2 % of H_2 treated as an emission. A complete list of processes sourced from the software database to model green ammonia is presented in Table 2. Datasets relate primarily to the European market.

Table 2. Upstream processes for modeling green ammonia [39].

Input	Description
Ammonia synthesis	
Electricity from photovoltaic	PV power supply including panel manufacture, installation, operation over 30 years, and end of life.
Electricity from wind power	Onshore/offshore wind generation with turbine manufacturing, transport, installation, operation and maintenance (O&M), and dismantling.
Electricity from nuclear	Mix of pressurized water and boiling water reactors for nuclear generation; includes reactor and fuel life cycle, including decommissioning.
Water (desalinated; deionized)	Tap water treated by ion-exchange/desalination to produce water for the process.
Process steam from natural gas 90 %	Industrial steam produced in natural gas plants, with flue gas cleanup (dust, SO_x, NO_x); 90 % quality.
Nitrogen (gaseous)	Nitrogen from cryogenic air separation (ASU/Linde).
Electrolyzer manufacturing	
Copper	Refined copper from mining to smelting/refining and delivery.

Stainless steel sheet	Sheet/plate production based on melting via electric arc furnace.
Nickel	Class-1 nickel production covering mining, beneficiation, refining, and transport.
Aluminum sheet	Rolled aluminum sheet including alumina production, extrusion/rolling, and scrap remelting.
Polyvinyl chloride (PVC) sheet	PVC sheet manufacture covering polymerization, extrusion/calendering, cooling, and cutting.
Acrylonitrile butadiene styrene	Acrylonitrile butadiene styrene production via common polymerization routes.
Aniline	Aniline produced by catalytic hydrogenation of nitrobenzene.
Purified terephthalic acid	Oxidation of p-xylene in air using metal catalysts.
Nitric acid	Manufactured by catalytic oxidation of ammonia (Ostwald process).
Hydrochloric acid	Based on mixed industrial routes, but primarily as a by-product of chlorination/halogen-exchange processes.
Lubricant oil	Refinery by-product stream; includes crude extraction through refining and blending.
Carbon monoxide	CO obtained from syngas processing/cryogenic separation.
Gypsum plaster	Production from raw gypsum through calcination to hemihydrate (β-hemihydrate).
Electricity grid mix	Average EU-28 grid electricity mix.
Thermal energy from natural gas	Heat supplied from natural gas-fired heat plants.

Since the destination of ammonia is its utilization as fuel in ICE CI, a comparison to diesel production has been included. Diesel is modeled using Sphera's Managed LCA Content dataset: Diesel mix at the refinery [39]. The system boundary reflects a multi-output refinery and includes primary processes such as atmospheric/vacuum distillation, desulfurization, cracking (hydro- and catalytic), alkylation/polymerization, and blending. Since the refinery yields multiple products, the model applies allocation by mass and net calorific value across outputs (e.g., diesel, lubricant oil). The dataset is valid for the European market.

2.3. Impact categories

Reported impact categories for the LCIA of ammonia production pathways follow the ReCiPe 2016 v1.1 method [48]:

i. Climate change (kg CO2 eq.; midpoint): measure of GHG contributions to radiative forcing affecting global average temperature.

ii. Fossil depletion (kg oil eq.; midpoint): measure of depletion of fossil fuels.

iii. Freshwater consumption (m^3; midpoint): measure of freshwater exploitation.

iv. Human health (disability-adjusted life years, DALYs; endpoint): holistic measure of damage to health aggregated from midpoint categories (including: climate change, ozone depletion, ionizing radiation, fine particulate matter formation, photochemical ozone formation, cancer and non-cancer toxicity, water use).

v. Ecosystem quality (species years; endpoint): holistic measure of time-integrated species loss across terrestrial, freshwater, and marine systems, accumulated from midpoint categories (including climate change, photochemical ozone formation, acidification/eutrophication, terrestrial toxicity, water/land use).

The ReCiPe method is selected as it often yields higher endpoint scores than Eco-indicator 99 or IMPACT 2002+ [49], and as such can be considered a pragmatic choice. Categories are selected to enable a reliable comparison with diesel: the three midpoints capture the most material technology differences (GHG, fossil depletion, freshwater consumption), while the two endpoints provide a holistic impact from multiple mechanisms. Impacts are considered within a 100-year timeframe (hierarchist perspective within the ReCiPe method).

2.4. Environmental results

Figure 3 compares five ammonia routes with diesel across three midpoint indicators on a normalized scale. For climate change, the order among ammonia options is: grey, blue, green PV, green wind, pink (nuclear). Versus diesel production alone, the green wind and pink cases are lower (with pink at around half of diesel). Because the functional unit is 1 MJ (LHV), diesel's production footprint is relatively small, as a smaller amount of diesel is required to provide 1 MJ compared to ammonia. However, the dominant effect when using diesel in ICE comes from its combustion. Therefore, a scenario including a stoichiometric estimate of diesel CO_2 emissions is added. Grey ammonia is the only option that exceeds diesel's total (including combustion), confirming that SMR-based ammonia is not climate benign; blue is lower but still high since capture targets only "process CO_2." Green and pink routes are preferred overall, with PV the least favorable of the three electricity cases. For fossil depletion, both green routes are lowest; diesel, grey, and blue are mid-range, while pink is the highest. Freshwater consumption is dominated by the nuclear case, while diesel is the lowest.

Figure 4 shows upstream contributions for the green and pink routes (grey, blue, and diesel are aggregated database processes and cannot be disaggregated). Across all three midpoints, results are driven primarily by the electricity supply. Nuclear has the lowest climate change burden among the three electricity options, whereas PV and wind are higher due to panel/turbine manufacturing. In contrast, fossil depletion and freshwater consumption are the highest for the nuclear case. This is primarily due to the uranium fuel cycle – uranium resource use on an energy basis is included in the fossil depletion category in the ReCiPe 2016 v1.1 method – and to the cooling water requirements of nuclear plants, which drive freshwater consumption. The lowest scores in these categories are achieved for wind, with PV lying between wind and nuclear. Other upstream steps (electrolyzer manufacturing, water preparation, ASU) are secondary contributors.

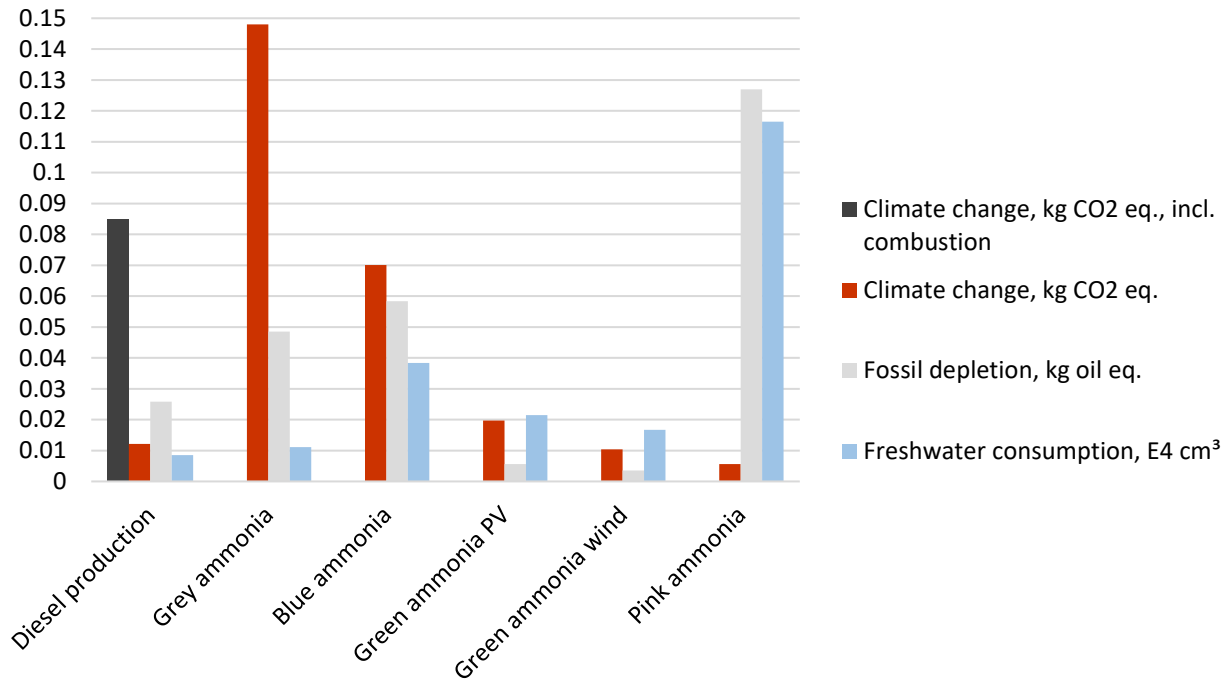

Figure 3. Midpoint category results for ammonia production pathways.

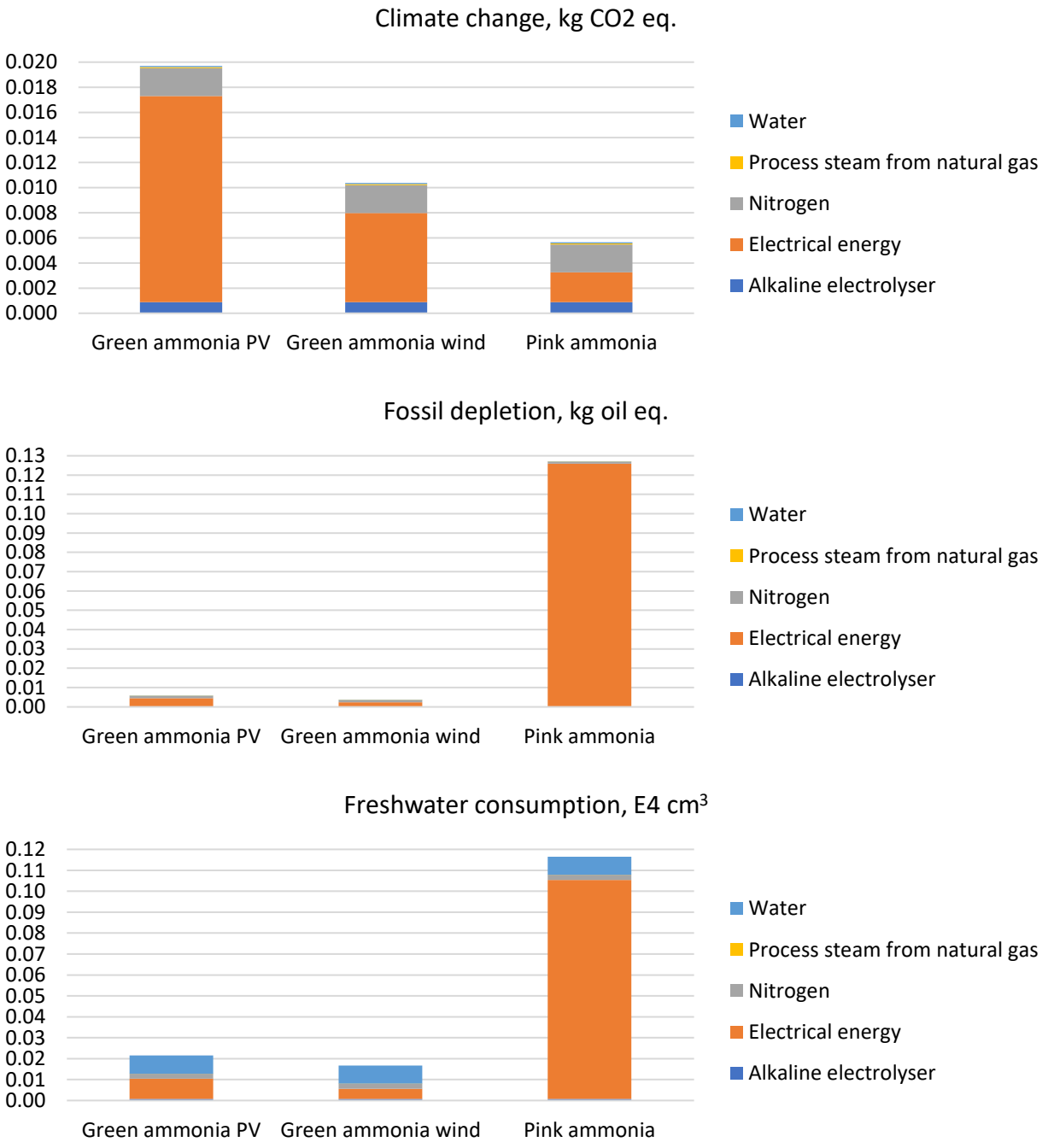

Figure 4. Contributions of upstream processes to midpoint categories for green and pink ammonia production pathways.

Figure 5 reports endpoint results with ecosystem quality with respect to terrestrial, freshwater, and marine impacts on a normalized scale (scientific notation). Human health broadly mirrors the climate change trend (as climate change is the primary midpoint category affecting human health): pink is lowest, then green wind, green PV, with diesel production also low on its own but

higher when including combustion; grey is the highest, and blue in between. Ecosystem quality is primarily driven by its terrestrial impact among the three components; green PV shows the largest terrestrial impact (due to material-intensive PV manufacturing and EoL handling), whereas wind, pink, blue, and grey follow at similar, lower levels, with diesel at the lowest; however, the differences are modest except for PV. For ecosystem quality in terms of freshwater, the spread is small: diesel incl. combustion is highest, and green wind is the lowest. For marine ecosystems, grey ammonia is highest; diesel incl. combustion follows at around five times lower value; green wind is the lowest.

Human health endpoint category is mostly affected by climate change across all pathways; the secondary driver varies by route: fine particulate matter formation and cancer toxicity for green ammonia, and fine particulate matter formation and water use for grey, blue, and pink cases. Ecosystem quality is primarily driven by the terrestrial toxicity midpoint category. A complete discussion on this topic is provided in Paper I (Section 3).

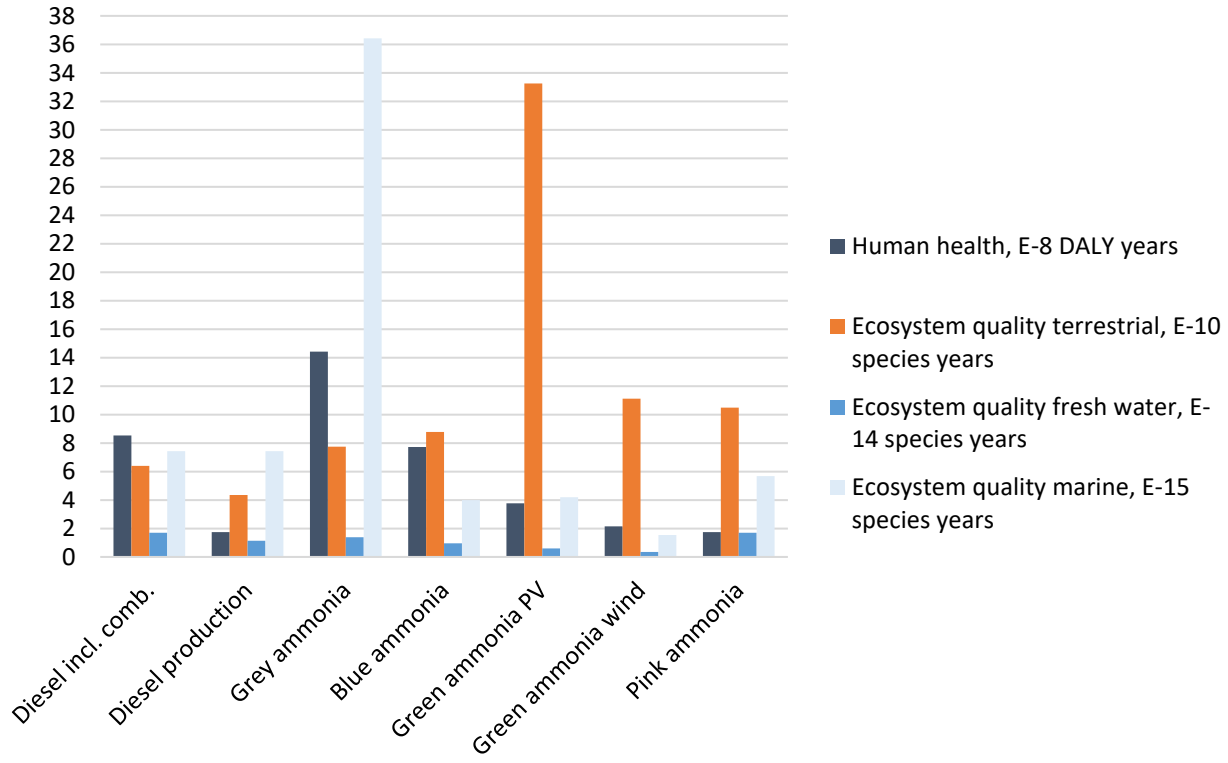

Figure 5. Endpoint category results for ammonia production pathways.

Chapter 3 – Ammonia- and diesel-fueled engine performance

The engine's performance in Paper II is discussed by means of energy and exergy assessments. From the LCA perspective, a complete energy balance of the engine is not required; only fuel consumption and emissions are essential for the LCA, which is one of the two primary goals of this research. However, efficiency can serve as an indirect indicator: if the ammonia-fueled engine achieved noticeably lower thermal or exergy efficiency, it would imply higher fuel consumption to deliver the same power output. Therefore, primary emissions and thermal efficiency comparisons are included in this guide; the detailed energy and exergy balances reported in Paper II should be treated as complementary information but are not elaborated in detail in this document.

Three supply modes were tested in Paper II: pure diesel (reference), pure biodiesel, and ammonia (with biodiesel). While the pure biodiesel test is not required for the LCA of an ammonia-fueled vehicle, it was included to provide a more comprehensive view of the fuel switch implications in an ICE CI engine. Regardless, this guide focuses primarily on the ammonia- and diesel-fueled engine; the comparison to biodiesel presented in Paper II should be treated as contextual, complementary results as well.

3.1. Experimental setup and fuel details

Experiments were run on a Lifan C186F (mini tractor class). Ammonia utilization was realized through port injection: gaseous NH_3 was injected into the intake manifold to premix with air before the cylinder, while pilot fuel biodiesel was injected directly. A schematic of the test rig is shown in Figure 6. While no SCR is used for the data reported here, it can be connected to the exhaust line (as shown in Paper II, Section 2). NH_3 mass flow rate was measured using a Coriolis meter, while air volumetric flow rate was measured using a turbine flowmeter. Air, fuel, and exhaust temperatures were recorded with thermocouples. Shaft torque and speed were controlled using an electric machine operated as a brake. All signals were integrated and controlled in LabVIEW. Exhaust composition was measured on a wet basis by FTIR (Gasmet DX4000), with a CAPELEC CAP 3201 providing O_2 measurement and gas analyzer SMG200 M PM10 verification. Recorded variables included: fuel consumption; CO_2, CO, CH_4, NO_x, NH_3, SO_2, PM10; and other exhaust components. Measurement points were taken at steady state under ambient conditions (open hall). Major engine characteristics, along with fuel elemental analyses and LHV, are provided in Table 3.

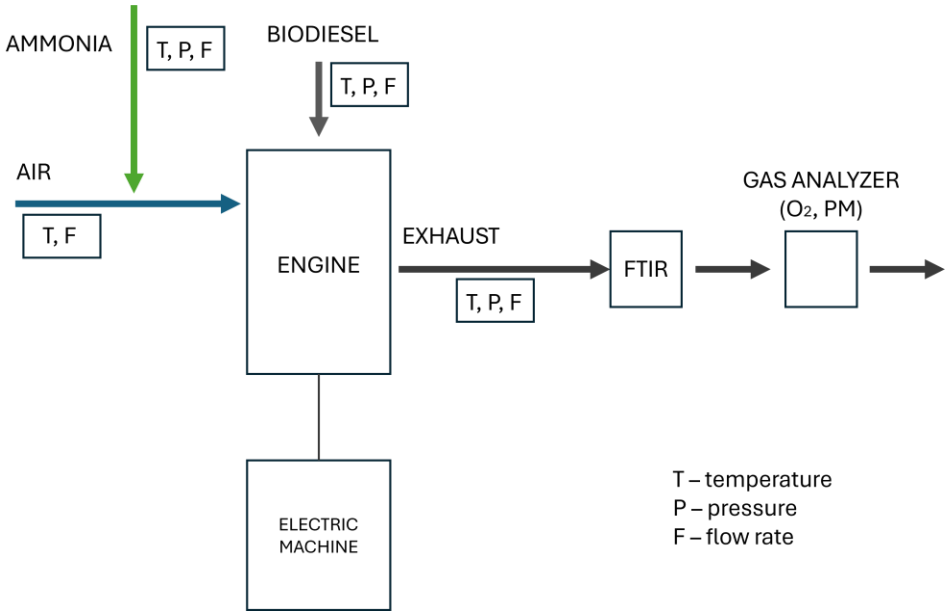

Figure 6. Schematic of the test rig used in the experiments.

Table 3. Engine and fuel characteristics.

Engine	Model: LIFAN C186F, 4-stroke, 1-cylinder, forced air cooling Displacement: 418 cm^3 Compression ratio: 16.5:1 Max theoretical power: 6.4 kW
Diesel	C = 0.8078, H = 0.1556, O = 0.0363, N = 0.0003 LHV = 42.4 MJ/kg
Biodiesel	C = 0.7533, H = 0.1397, O = 0.1070, N = 0.0000 LHV = 37.4 MJ/kg
Ammonia	C = 0.0000, H = 0.1760, O = 0.0000, N = 0.8240 LHV = 18.6 MJ/kg

3.2. Engine performance comparison

Tests covered shaft speeds 2700, 2400, 2100, 1800, 1500, 1200 rpm. At 2700 rpm, torques of 12, 8, 4 Nm were applied (loads 100, 67, 33 %). At the other speeds, torques of 17, 12, 8, 4 Nm were used (loads 100, 71, 47, 24 %). For ammonia-fueled operation, the biodiesel mass flow rate was fixed at the minimum value that allowed stable combustion (corresponding to 4 Nm); introducing NH_3 flow resulted in an increased torque. The point 2700 rpm / 12 Nm was the upper bound for the ammonia-fueled engine. Pure diesel and biodiesel could reach higher shaft speeds and torque but with high smoke emissions; therefore, an operational range between 1200 rpm / 4 Nm and 2700 rpm / 12 Nm was adopted for comparison.

The following emissions with regard to both ammonia- and diesel-fueled engines are outlined in Figure 7: CO_2, N_2O, NH_3, and NO_x (sum of NO and NO_2). CH_4, another potent greenhouse gas, is not presented since it was at a similar level for both fueling options and therefore does not affect the comparative assessment. N_2O and NH_3 emissions for diesel are zero and are omitted as well. Fuel consumption comparison is presented in Table 4. It should be noted that in Paper II some other variables have been reported (Section 2, Tables 5–8), such as exhaust temperature, water content, and others, but not all of them; a complete list of all emissions has not been published as they serve as source data that can be shared upon request, as stated in the Data Availability statement. Selected emissions from these experiments have been additionally tabulated in Paper III, Supplementary Material (Table S5). In this guide, fuel consumptions and primary emissions from the fuel switch perspective are provided as mass flow rates (as measured, wet basis). While both in Paper II and III the torque is understood as load and is shown in percentages, in Figure 7 it is reported in source units (Nm). Data were logged continuously and grouped at steady state operating points; outliers were also removed, leading to tightly clustered points, so the calculated uncertainties presented in Paper II are very small and therefore have not been repeated in this guide.

Based on the Figure 7, it is apparent that CO_2 emissions are higher for the diesel-fueled case; higher rpm and load indicate higher fuel consumption and thus explain the increasing CO_2. The peak occurs at 2400 rpm and 17 Nm (100 % load). For the ammonia-fueled case, CO_2 originates solely from the biodiesel pilot and is therefore lower (biogenic CO_2). The trend resembles the diesel-fueled scenario. However, analysis of NO_x emissions across the engine map shows that the ammonia-fueled engine emits considerably more NO_x than diesel. This is expected, since oxidizable nitrogen is present both in the intake air (N_2) and in the ammonia fuel (NH_3). The peak occurs at 1800 rpm / 17 Nm. Conversely, the ammonia-fueled engine also forms N_2O, with the highest levels at high rpm and moderate load (around 8 Nm), which is particularly notable because N_2O is a potent GHG. The NO_x/N_2O patterns reflect combustion kinetics and mixing (burning velocity, quenching, pilot-fuel/NH_3/air ratios) and local in-cylinder temperature, oxygen availability, and residence time. At high rpm and high torque, NH_3 slip appears, consistent with increased NH_3 mass flow. Because ammonia has a lower LHV, the combined fuel mass flow (biodiesel and ammonia) is higher than for diesel.

Comparison of GHG emissions as CO_2 equivalent – including CO2 (GWP = 1), CH_4 (GWP = 27), and N_2O (GWP = 273) – to CO_2 from the diesel-fueled case is also presented in Table 4. Since the ammonia-fueled engine exhibits relatively high N_2O, there are operating points where total GHG emissions are higher than diesel (e.g., 2700 rpm at all loads; 2400 rpm at 12 and 8 Nm). This shows that whether the fuel switch achieves its primary decarbonization purpose depends strongly on engine operating conditions.

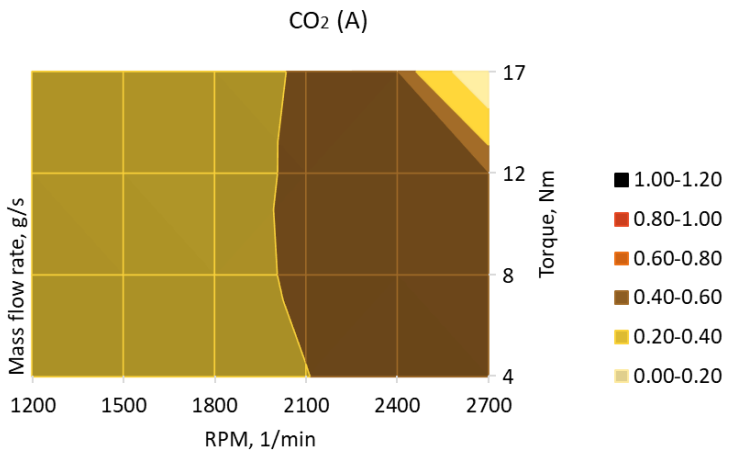
CO2 (A)
Mass flow rate, g/s
Torque, Nm
RPM, 1/min
1200
1500
1800
2100
2400
2700
4
8
12
17
1.00-1.20
0.80-1.00
0.60-0.80
0.40-0.60
0.20-0.40
0.00-0.20

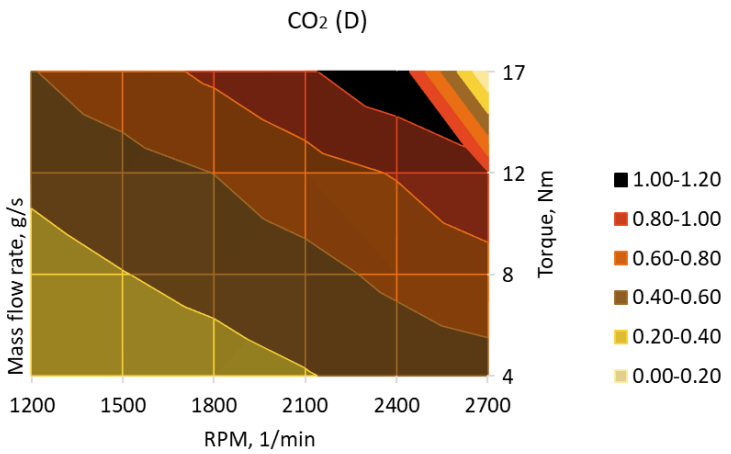
CO2 (D)
Mass flow rate, g/s
Torque, Nm
RPM, 1/min
1200
1500
1800
2100
2400
2700
4
8
12
17
1.00-1.20
0.80-1.00
0.60-0.80
0.40-0.60
0.20-0.40
0.00-0.20

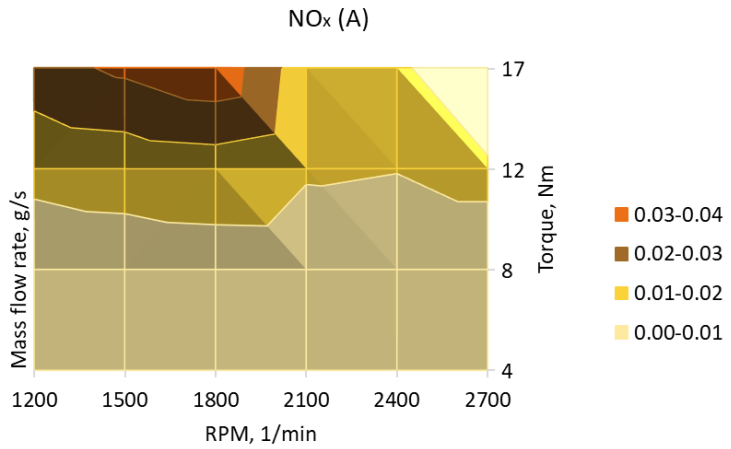
NOx (A)
Mass flow rate, g/s
Torque, Nm
RPM, 1/min
1200
1500
1800
2100
2400
2700
4
8
12
17
0.03-0.04
0.02-0.03
0.01-0.02
0.00-0.01

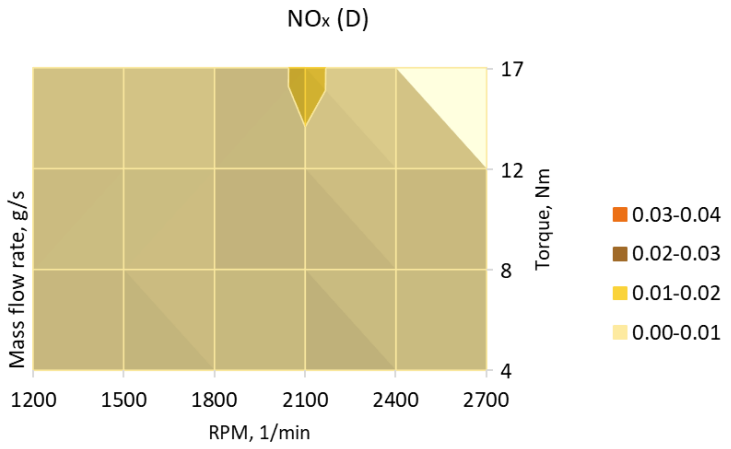
NOx (D)
Mass flow rate, g/s
Torque, Nm
RPM, 1/min
1200
1500
1800
2100
2400
2700
4
8
12
17
0.03-0.04
0.02-0.03
0.01-0.02
0.00-0.01

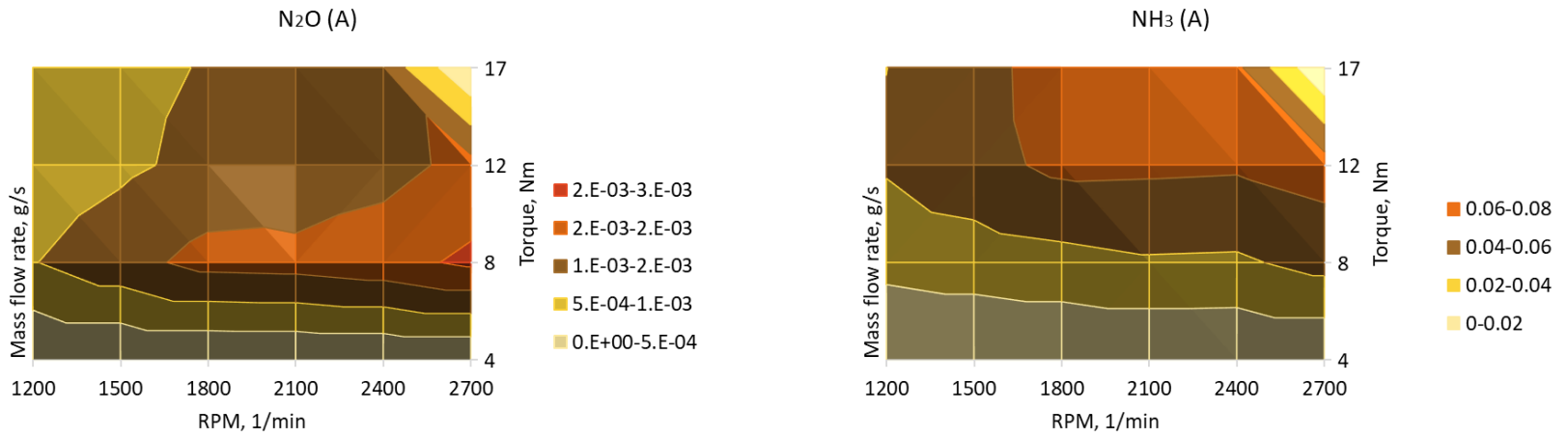

Figure 7. Comparison of emissions for ammonia- and diesel-fueled operation (D = diesel; A = ammonia).

Table 4. Comparison of fuel consumption and GHG emissions for ammonia- and diesel-fueled operation (D = diesel; A = ammonia).

RPM, 1/min	Load, Nm	Diesel (D), g/s	Biodiesel, g/s (A)	Ammonia, g/s (A)	GHG, CO2 eq./s (D)	GHG, CO2 eq./s (A)
2700	12.00	0.323	0.202	0.412	0.951	1.012
2700	8.00	0.249	0.203	0.232	0.733	1.126
2700	4.00	0.180	0.195	0.000	0.523	0.529
2400	17.00	0.400	0.184	0.492	1.152	0.871
2400	12.00	0.277	0.182	0.346	0.815	0.856
2400	8.00	0.220	0.181	0.175	0.648	0.996
2400	4.00	0.164	0.170	0.000	0.475	0.464
2100	17.00	0.334	0.154	0.480	0.979	0.728
2100	12.00	0.243	0.156	0.317	0.719	0.715
2100	8.00	0.182	0.155	0.169	0.537	0.893
2100	4.00	0.134	0.147	0.000	0.391	0.401
1800	17.00	0.291	0.129	0.428	0.842	0.653
1800	12.00	0.205	0.128	0.281	0.604	0.680
1800	8.00	0.156	0.132	0.142	0.461	0.823
1800	4.00	0.111	0.126	0.000	0.325	0.345
1500	17.00	0.252	0.111	0.356	0.723	0.548
1500	12.00	0.178	0.110	0.237	0.525	0.561
1500	8.00	0.134	0.111	0.124	0.397	0.672
1500	4.00	0.094	0.107	0.000	0.276	0.293
1200	17.00	0.214	0.093	0.284	0.604	0.442
1200	12.00	0.153	0.093	0.193	0.448	0.441
1200	8.00	0.110	0.091	0.105	0.324	0.520
1200	4.00	0.079	0.088	0.000	0.232	0.241

Aggregating power output of the engine versus the energy delivered in the fuel leads to the definition of thermal efficiency, according to equation 4 [50, p. 221]:

$$\eta = \frac{\dot{W}}{\dot{m}_{fuel} LHV_{fuel}} \tag{4}$$

where: η – thermal efficiency (–), $\dot{W}$ – power of the engine (kW), $\dot{m}_{fuel}$ – mass flow rate of fuel (g/s). For the ammonia-fueled engine, the denominator in equation 4 includes both ammonia and biodiesel.

The comparison of thermal efficiency between the two fueling options is outlined in Figure 8. The diesel case follows the typical pattern: peak efficiency at mid/high loads, with low efficiency at minimum load. The ammonia with biodiesel pilot case behaves more linearly with an increase

in load and peaks at the maximum load for all speeds; at 100 % load its efficiency is generally close to diesel (apart from 2700 rpm), while at mid-loads it is typically around 2–3 percentage points lower; this highlights the need for optimization of the combustion process (pilot/ammonia ratio, injection timing, etc.). From an LCA perspective, the implication is straightforward: if ammonia is used via port injection with default pilot settings, the engine should be operated at high loads to minimize the efficiency difference; mid-load operation is where the efficiency gap versus diesel is most visible.

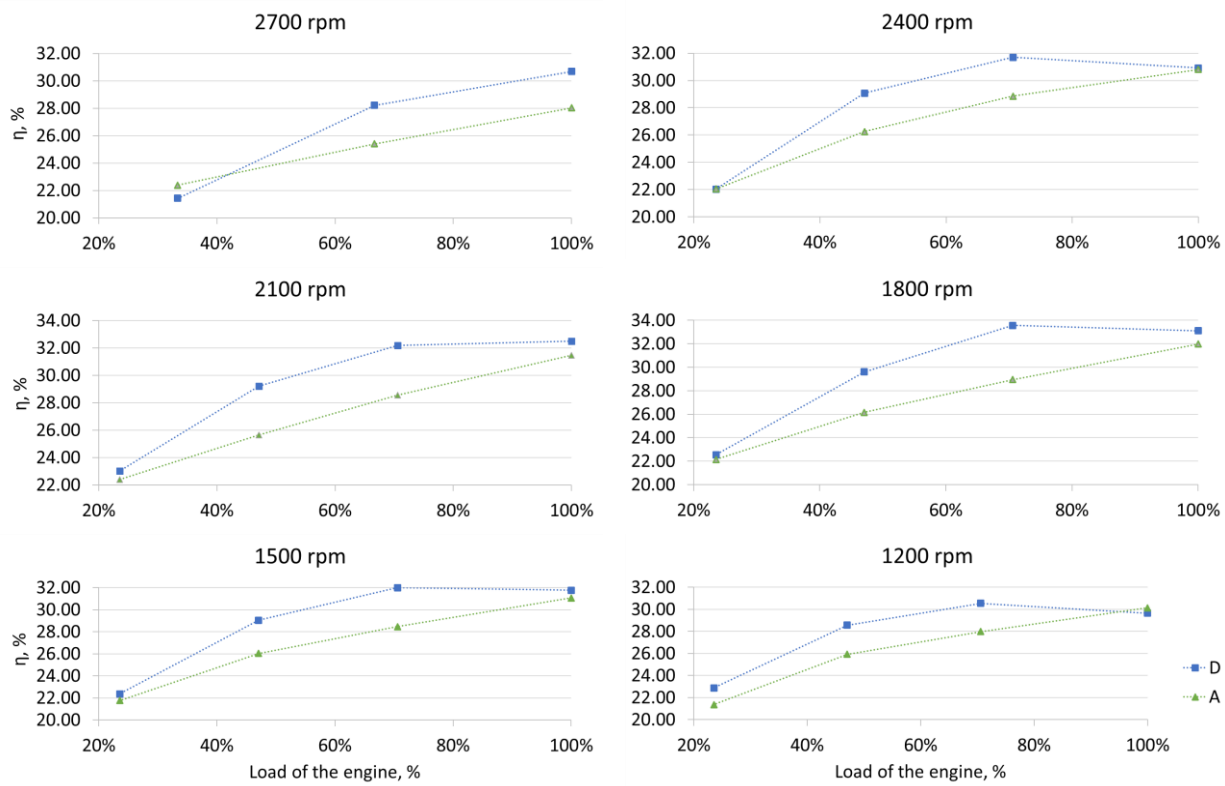

Figure 8. Thermal efficiency as a function of engine load and speed for the two fueling options (D = diesel; A = ammonia).

Chapter 4 – LCA of an ammonia-fueled mini tractor

Collating fuel production pathways elaborated in Chapter 2 – Ammonia production pathways with engine's emissions shown in Chapter 3 – Ammonia- and diesel-fueled engine performance, a comprehensive LCA of an ammonia- and diesel-fueled vehicle can be presented, as seen in Paper III. System boundaries for the ammonia-fueled mini tractor analysis, as a central focus of this research, are outlined in Figure 9. The LCA is a cradle to grave type of assessment and includes all the vehicle's phases: production, operation, and utilization.

To complete the discussion on the assumptions of the LCA, the subsequent aspects are discussed in this chapter: mini tractor manufacturing, biodiesel production, mini tractor operation and utilization, followed by the environmental results. The impact categories are the same as in the case of Paper I, elaborated in Section 2.3.

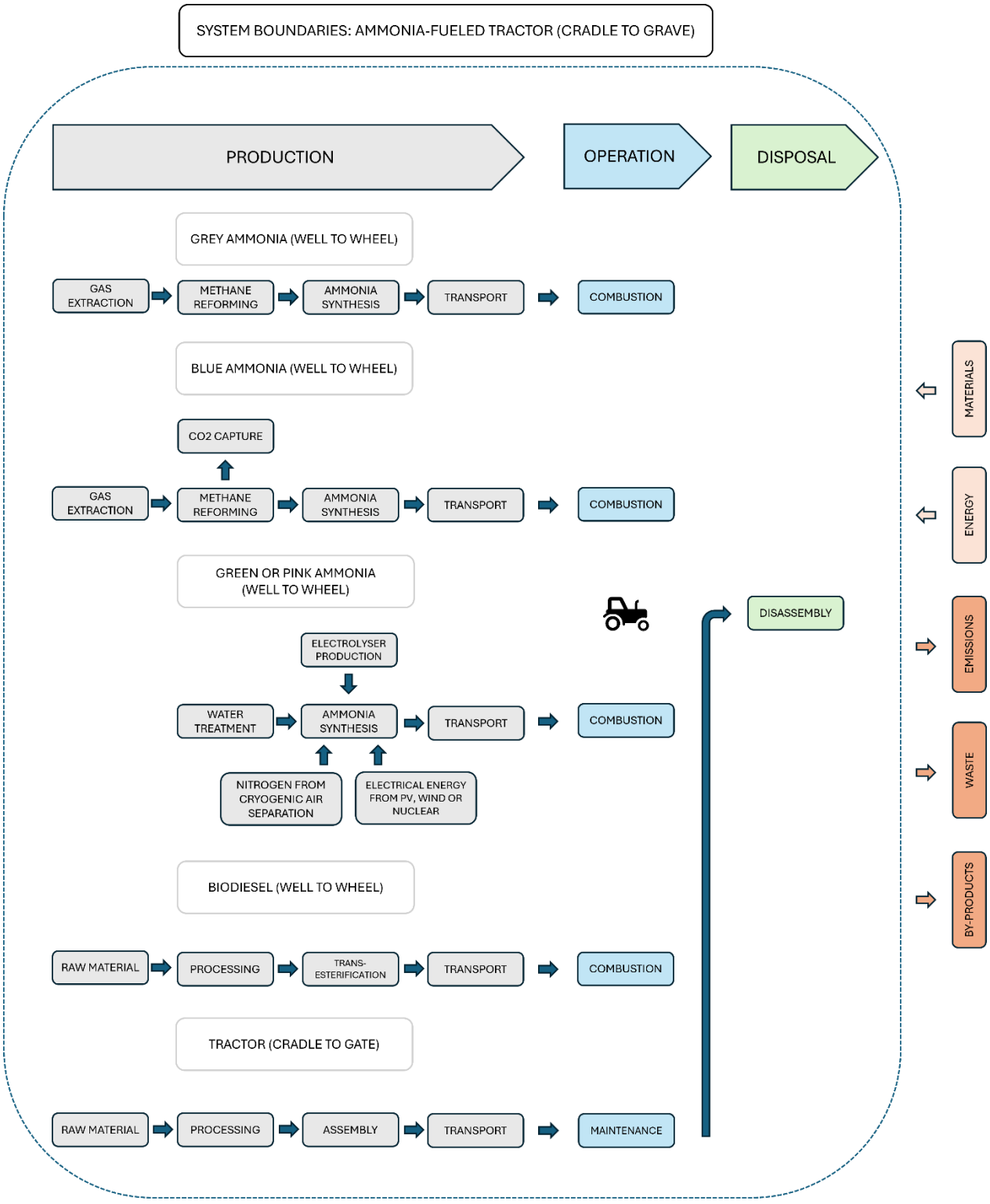

Figure 9. System boundaries for the LCA of an ammonia-fueled mini-tractor.

4.1. Modeling approach

4.1.1. LCA phases

Mini tractor production phase is modeled through Sphera's Managed LCA Content dataset [39]: Farm tractor production (vehicle manufacturing including its maintenance, without the EoL phase). It represents industry-based material composition in a cradle to gate scope and includes maintenance parts replaced over 5 years. The inventory is based on a typical farm tractor weighing around 13.3 t; the inventory is linearly scaled to the 540 kg mini tractor, which is the weight of the SCOUT 15-T vehicle. The dataset is globally applicable.

Since the engine runs in dual-fuel mode, biodiesel production is included for a complete vehicle LCA. Biodiesel is modeled as produced via transesterification of oils/fats with methanol using a literature-based data inventory [51]. Following the conclusions from this work, the supercritical methanol route with propane co-solvent is adopted as the lowest impact option versus the alkali- and acid-catalyzed pathways. Allocation by energy content (LHV) splits burdens between biodiesel and glycerol (the by-product of the transesterification process). The characterization of inputs used for biodiesel modeling is provided in Table 5. Additionally, biodiesel and ammonia transport is modeled as 150 km by road in a Euro V freight truck (hence the well to wheel caption in Figure 9).

End of life phase is modeled using the Car shredder process from the software database [39]. It covers vehicle shredding with partial disassembly of used parts beforehand. The dataset reflects the German market. A recapitulation of the modeling approach to each LCA phase is provided in Table 6.

Table 5. Modeling approach and characterization of biodiesel production.

Input	Modeling approach	Input	Description
Oil	Aggregated process from the software database	Rapeseed (canola) oil, refined	Oil preparation including cultivation, harvesting, processing/milling, and refining; dataset based on the German market.
Propane	Aggregated process from the software database	Propane at refinery	Propane as a refinery co-product with allocation by mass and energy content; dataset set in a European perspective.
Steam	Aggregated process from the software database	Process steam from natural gas 95 %	Industrial steam produced in natural gas plants, with flue gas cleanup (dust, SO_x, NO_x); 95 % quality.
Electricity	Aggregated process from the software database	Electricity grid mix	Average EU-28 grid electricity mix.

Methanol	User defined model based on literature data (upstream from the database)	User defined model of methanol production	Methanol production is modeled separately via natural gas steam reforming, using the inventory from [52]. Inputs include EU electricity and natural gas mixes, oxygen from air separation, and sodium hydroxide from a mix of mercury-, diaphragm-, and membrane-cell electrolysis. Desalinated (ion-exchange) water and freshwater of moderate scarcity are considered. All processes use European data.

Table 6. Modeling approach for the LCA phases.

Phase	Modeling approach
Mini tractor construction	Aggregated process from the software database
Ammonia production	Grey and blue ammonia: aggregated process from the software database Green and pink ammonia: user defined model based on literature data (upstream from the database)
Biodiesel production	User defined model based on literature data (upstream from the database)
Diesel production	Aggregated process from the software database
Mini tractor operation	User defined model based on experimental data
Mini tractor utilization	Aggregated process from the software database

4.1.2. Working cycle

Given that the investigated engine is appropriate for a mini tractor used in agriculture for orchard operations and that the emissions depend on the engine's conditions, it is important to characterize the engine's operation in detail. To achieve this, the working cycle of a mini tractor has been determined based on the following assumptions. First, typical orchard activities and their annual frequencies for a representative apple orchard were determined from the literature [53], as shown in Table 7.

Table 7. Orchard management activities and their frequencies [53].

Activity	Annual frequency
Branch and leaves sweeping and raking	2
Mechanical weed removal (hoeing)	1
Grass mowing	8
Pruning	2
Fruit harvest	1
Tree fertilizing	4
Insecticide and fungicide application	20

In the second step, a scaled CAD model of the orchard was prepared to simulate tractor movement by task using the routes, as outlined in Figure 10:

i. Sweeping / hoeing / mowing: depart storage, drive to orchard, traverse each alley twice with the device engaged, return.

ii. Spraying: depart storage, drive to orchard, traverse each alley once with a trailed sprayer, return.

iii. Harvesting / pruning: depart storage, drive to orchard, traverse each alley once to collect fruit or prunings with a towed trailer, return to storage when the trailer is full (it is assumed that the tractor returns to storage after each alley).

Next, a theoretical gearbox model was defined: orchard activities were split into sub-activities (drive to orchard through a gravel road, make a turn, drive through a vertical alley, make another turn, etc.), and gear–speed combinations were assigned to each sub-activity. For instance, for the sweeping activity the sub-activity of driving through a vertical alley was assumed to be realized at gear 3 and speed 4 km/h (over the distance of the vertical alley), then a turn to the horizontal alley at gear 2 and speed 2 km/h, and then movement through a horizontal alley at gear 3 and speed 4 km/h. The goal of this was to determine all operating points of the engine and the distance covered at each point.

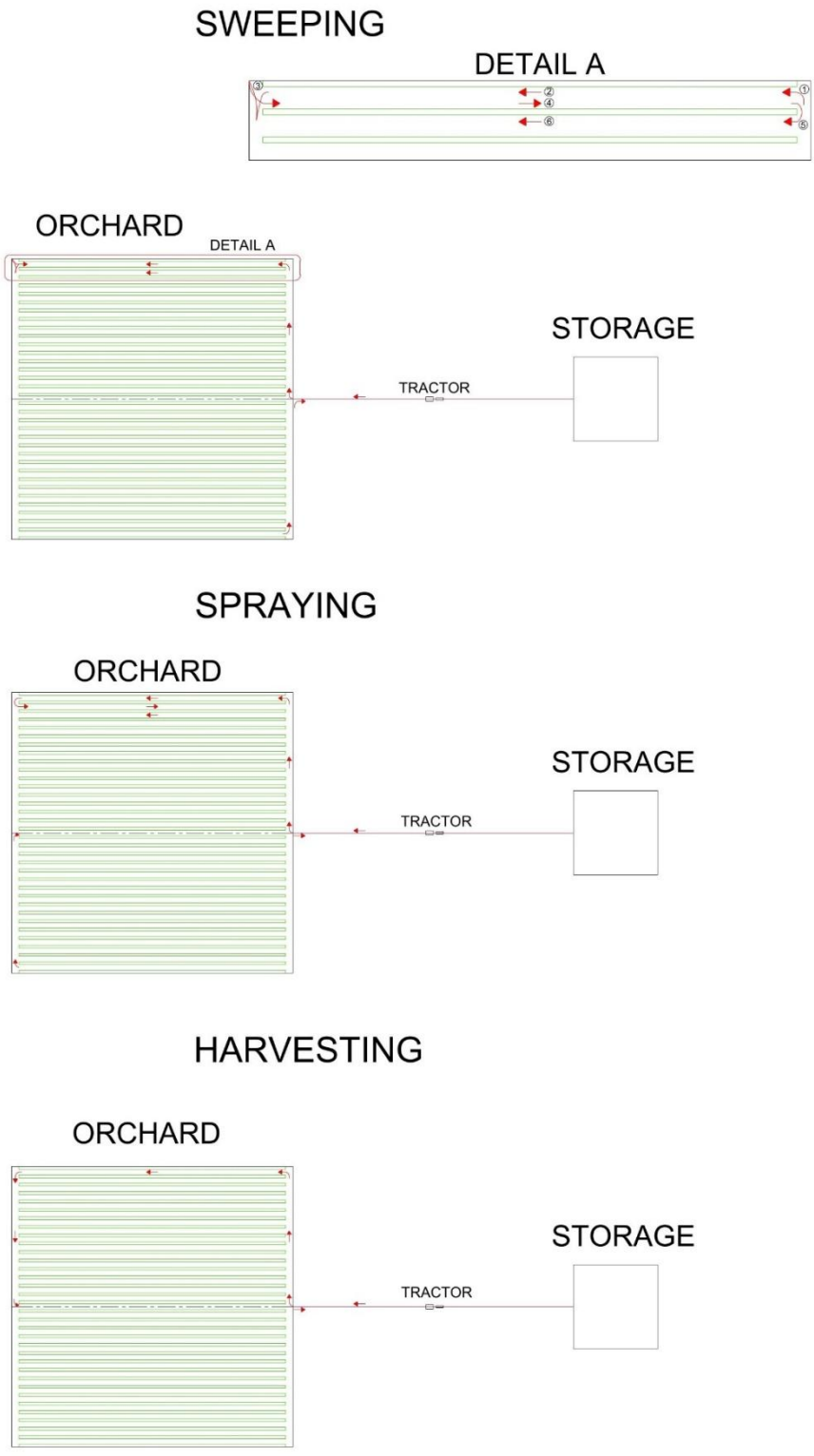

Figure 10. Schematic of orchard activities.

Factoring the mini tractor's characteristics (externally determined transmission losses depending on the gear and speed of this mini tractor), rolling resistance, air drag, and considering the type of the activity, engine conditions (rpm and torque) were determined. Differences in weights of the attached equipment were considered (for instance, a sweeper used for sweeping causes different rolling resistance than a mower used for mowing). Moreover, for sweeping, mowing, and hoeing the respective devices increase the load of the engine since the engine must supply power for both vehicle movement as well as device operation (the trailed sprayer used for spraying has been assumed to have a separate engine). To address this, maximum torque (17 Nm defined from the measurements) at the rpm determined for the working speed of each device (e.g., 4 km/h for sweeping) has been considered. Weights and working speeds of the devices compatible with the mini tractor follow the SCOUT catalogue, presented in Table 8. Based on the set of operating points determined from the working cycle and the engine map from the experiments, fuel consumptions and emissions were calculated by interpolating from the measured data.

Table 8. Orchard implements used with the tractor, with assumed weights and operating speeds.

Equipment	Mass, kg	Operating speed, km/h	Comment
Hooked sweeper	80	4	–
Side hoe	100	4	–
Rotary mower	50	6	–
Sprayer (trailed)	180 (+ tank up to 400)	4	Tank mass decreases during spraying.
Trailer (towed)	80 (+ full load 500)	1	Average speed while traversing an horizontal alley.

To illustrate this approach, Figure 11 highlights the engine's power over time for a sweeping example. The tractor accelerates from storage, slows on entering the orchard, and reaches a peak of approximately 4.2 kW when the sweeper is engaged. This cycle repeats across all 33 alleys (highlighted in red in Figure 11), followed by the return to storage. For hoeing and mowing activities, the chart's shape is the same, with the only difference being a different peak power. For spraying, harvesting, and pruning, the change in the engine's power over time is straightforward, as those activities involve only movement of the vehicle with attached trailer/sprayer. Finally, measured emissions and fuel consumption were integrated over distances

using the working cycle, yielding an input–output operation phase model for the diesel- and ammonia-fueled scenarios. The functional unit is management of a 1-ha apple orchard over one year.

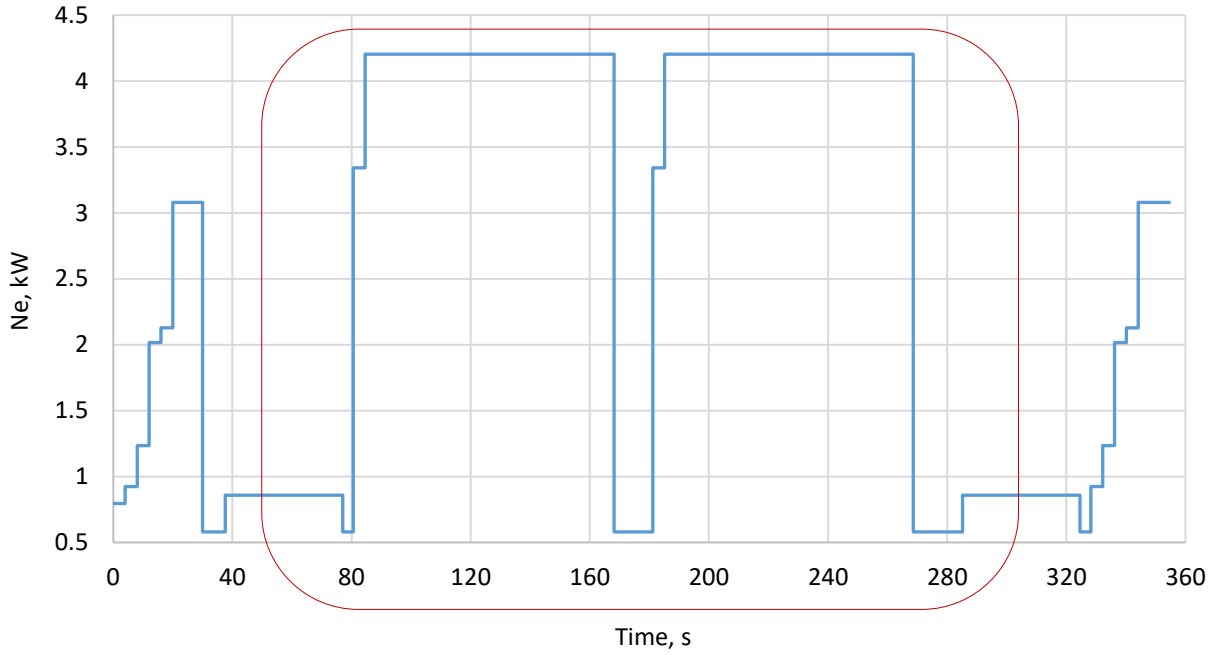

Figure 11. Engine power over time during the sweeping activity.

4.1.3. Selective catalytic reduction

High NO_x and ammonia slip from the engine's operation can be mitigated with SCR, as noted in Section 1.1. To address this, a simplified SCR model using two reactions shown in equations 5 and 6 has been considered as an additional scenario for the LCA of the ammonia-fueled engine [54]:

$$NO + NO_2 + 2NH_3 \rightarrow 2N_2 + 3H_2O \quad (5)$$

$$4NO + 4NH_3 + O_2 \rightarrow 4N_2 + 6H_2O \quad (6)$$

Given that the quantity of NO is higher than NO_2 at all points:

i. Reaction I: NH_3 reacts first with the available N_2 and an equal molar amount of NO (1:1:2 molar ratio of NO:NO_2:NH_3). Then:

   a. If NH_3 is insufficient, it is fully consumed and the unreacted NO/NO_2 leave the exhaust.

b. If NH_3 is sufficient, reaction II applies with the remaining NO.

ii. Reaction II:

a. If NH_3 is sufficient, all remaining NO is reduced; any excess NH_3 appears as ammonia slip.
b. If NH_3 is insufficient, it is fully consumed and the residual NO exits.

This reaction-based approach uses only the NH_3 present in the exhaust (no external dosing). Results are reported before and after SCR, and no N_2O reduction is considered, as this requires dedicated research, particularly with regard to the catalyst used, as some catalysts might actually promote additional unfavorable N_2O formation [55].

4.2. Environmental results

Climate change results are presented in Figure 12 (a). Reference fuel production pertains to diesel for the diesel-fueled vehicle and biodiesel for the ammonia-fueled vehicle. For the diesel-fueled mini tractor, operation dominates climate change impact (approximately 70 %), followed by tractor production and diesel production; end of life is negligible. The operation burden is driven mainly by CO_2 (with contributions from CH_4 and N_2O). For the SMR-based (grey) ammonia case, ammonia production is responsible for approximately 47 % of total climate change impact. In the blue case (SMR with CCS), emissions from ammonia production are reduced by about half compared to the grey case. Electrolysis-based routes lower this further, with the pink (nuclear) scenario being the lowest. The operation phase is the largest contributor to climate change impact for all ammonia-fueled scenarios as well. Ammonia engines emit less CO_2 (non-zero due to the biodiesel pilot) but more N_2O than diesel, which impacts the GHG balance. In operation, the ammonia tractor totals approximately 72 kg CO_2 eq. versus around 88 kg CO_2 eq. for diesel – an 18 % reduction, which can be seen as moderate. The third contributor is the pilot fuel production (biodiesel). Biodiesel uses rapeseed oil from plants that absorb CO_2; this biogenic uptake is accounted for, which results in negative climate change impact, thus enhancing the decarbonization effect of the fuel switch. Mini tractor production impact is identical across scenarios, so its impact is the same in all categories. The retrofit (NH_3 tank and fuel line) adds less than 5 % to vehicle mass, with a negligible effect on production impacts. The aggregated climate change results, shown in Figure 12 (b), show the largest GHG reductions for electrolysis-based ammonia from wind and nuclear, at about 42 % and 44 % respectively.

Fossil depletion results are shown in Figure 13 (a). Impacts are driven by fuel pathways and vehicle manufacturing. Grey NH_3 (SMR) is similar to diesel; blue (SMR+CCS) is slightly higher (CCS burden). Renewable NH_3 is the lowest – reductions of approximately 43 % (PV) and 45 % (wind) vs. diesel. The nuclear case is 78 % higher than diesel, driven by uranium resource use. Biodiesel

adds to fossil depletion (rapeseed supply chain), but remains below vehicle production impact. Freshwater consumption results are presented in Figure 13 (b). Vehicle production dominates across all cases, with fuel production next. All ammonia-fueled scenarios are around 40–50 % higher than diesel, mainly due to water use in the reference biodiesel (rapeseed) supply chain. Among ammonia sources, the nuclear pathway is highest, which is due to the nuclear plant's water demand.

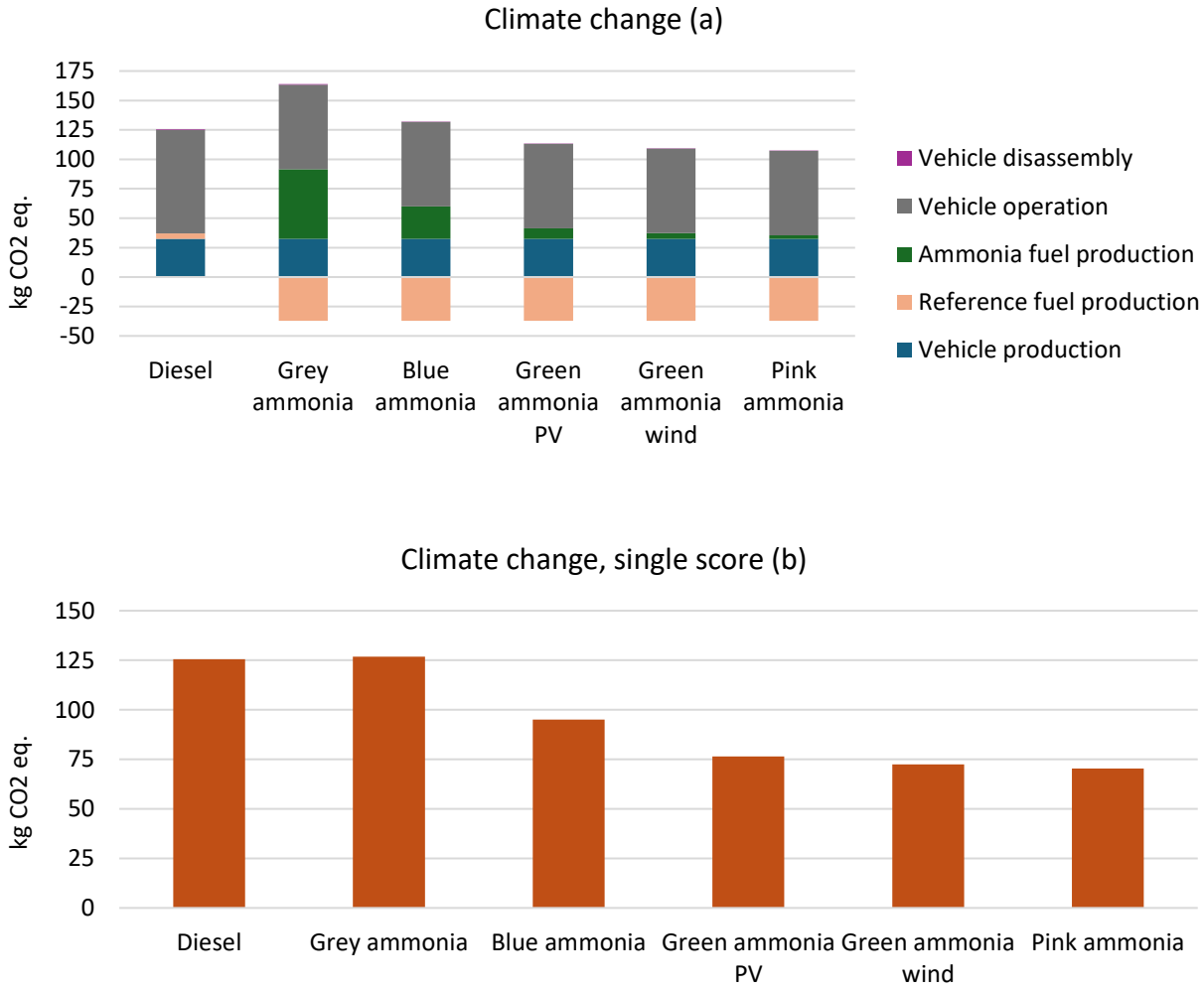

Figure 12. Climate change results.

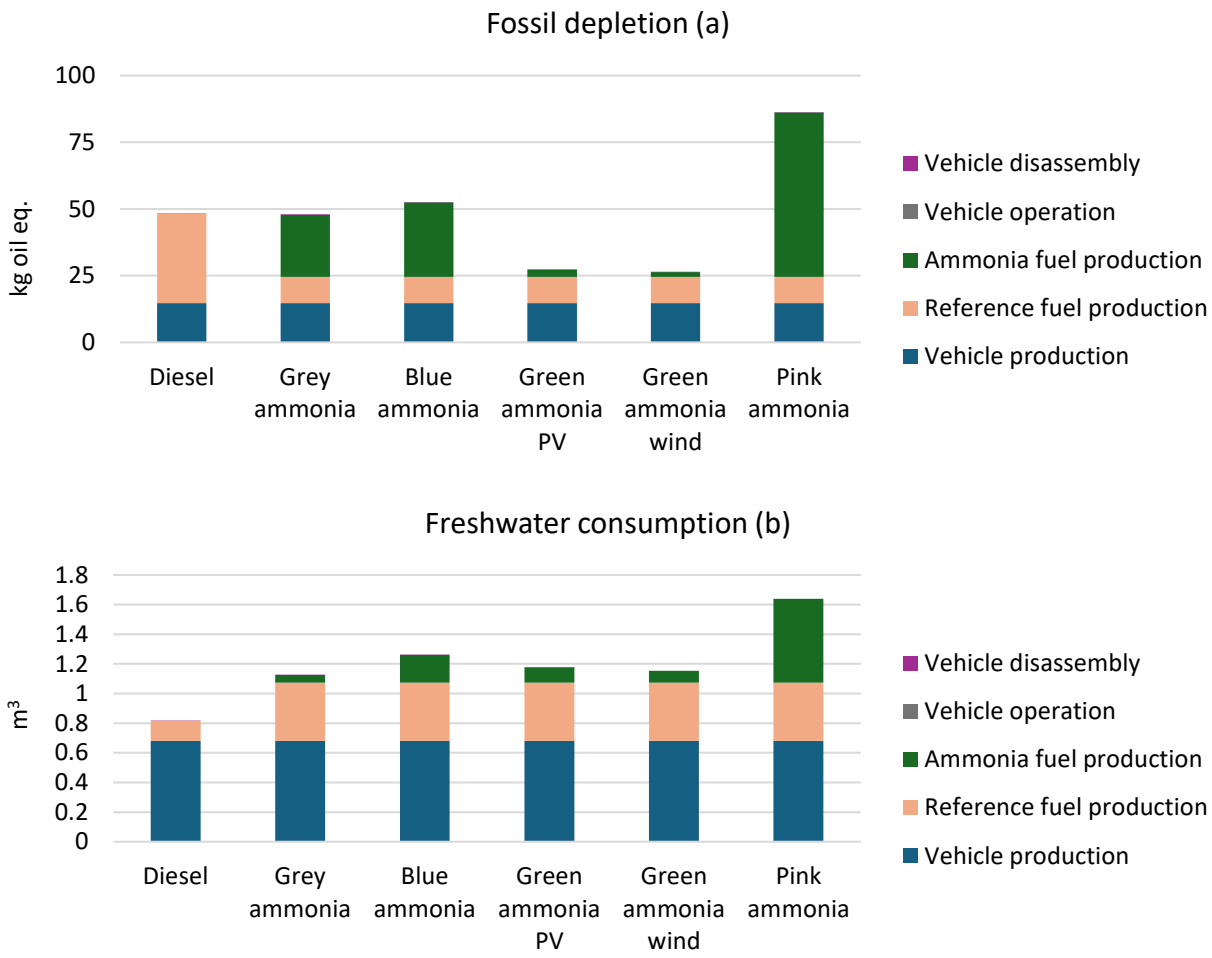

Figure 13. Fossil depletion and freshwater consumption results.

Figure 14 (a) shows the results for the human health endpoint category and that, for the diesel case, diesel production and vehicle production contribute most; their impact is driven by the human toxicity midpoint category (which is a measure of emitted carcinogens expressed in 1.4-dichlorobenzene equivalents). For the ammonia cases, operation dominates, followed by vehicle production, primarily caused by elevated NH_3 and NO_2 emissions (treated as secondary PM within ReCiPe). Overall, the human health endpoint is around 47 % higher for ammonia scenarios than for diesel. Figure 14 (b) shows that, for the diesel case, vehicle production dominates ecosystem quality impacts, followed by diesel production and operation. In the ammonia cases, biodiesel production adds to this category as it is around 2.5 times higher than diesel production (due to land use from rapeseed cultivation). Ammonia production also contributes; among routes, electrolysis is the strongest, with PV-based electricity highest (due to the terrestrial toxicity impact caused by manufacturing and EoL of PV, as noted in Section 2.4). The operation phase is also larger for the ammonia cases: about 5 times more than diesel; again driven by the elevated NO_x and NH_3.

Overall, the ammonia-fueled mini tractor achieves around 2 times higher impact than diesel for this category.

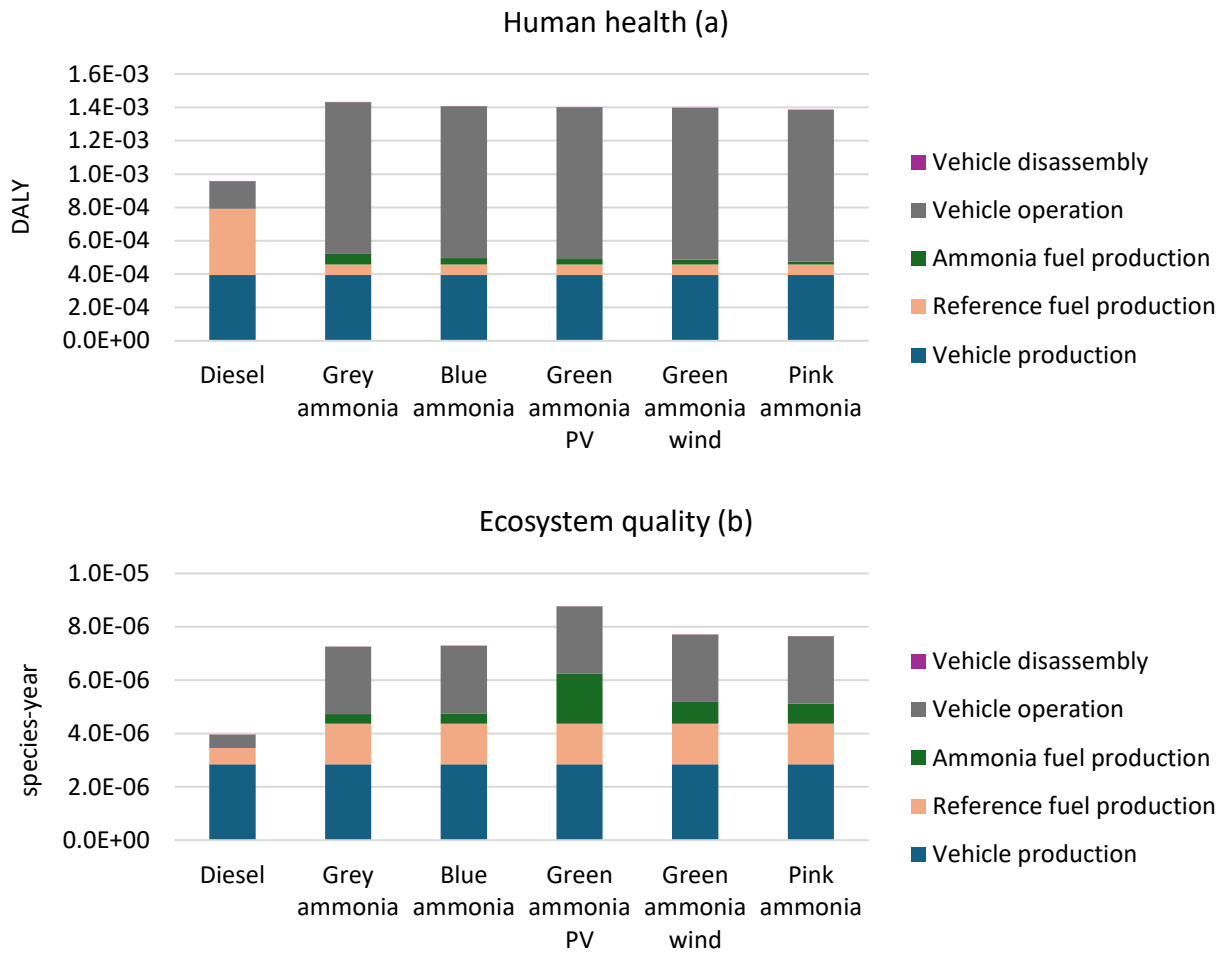

Figure 14. Human health and ecosystem quality results.

If SCR is applied to the ammonia engine's exhaust, the changes in endpoint categories take values shown in Figure 15. With SCR, impacts drop by around 20 % for human health and 10 % for ecosystem quality. Even after SCR, the ammonia-fueled vehicle remains around 19 % higher than diesel in human health, and between 1.6–2 times higher in ecosystem quality. These reductions, although limited by a simplified model where only residual NH_3 is used, confirm the need for SCR but do not change the primary burden driver: the operation phase remains the key phase to consider.

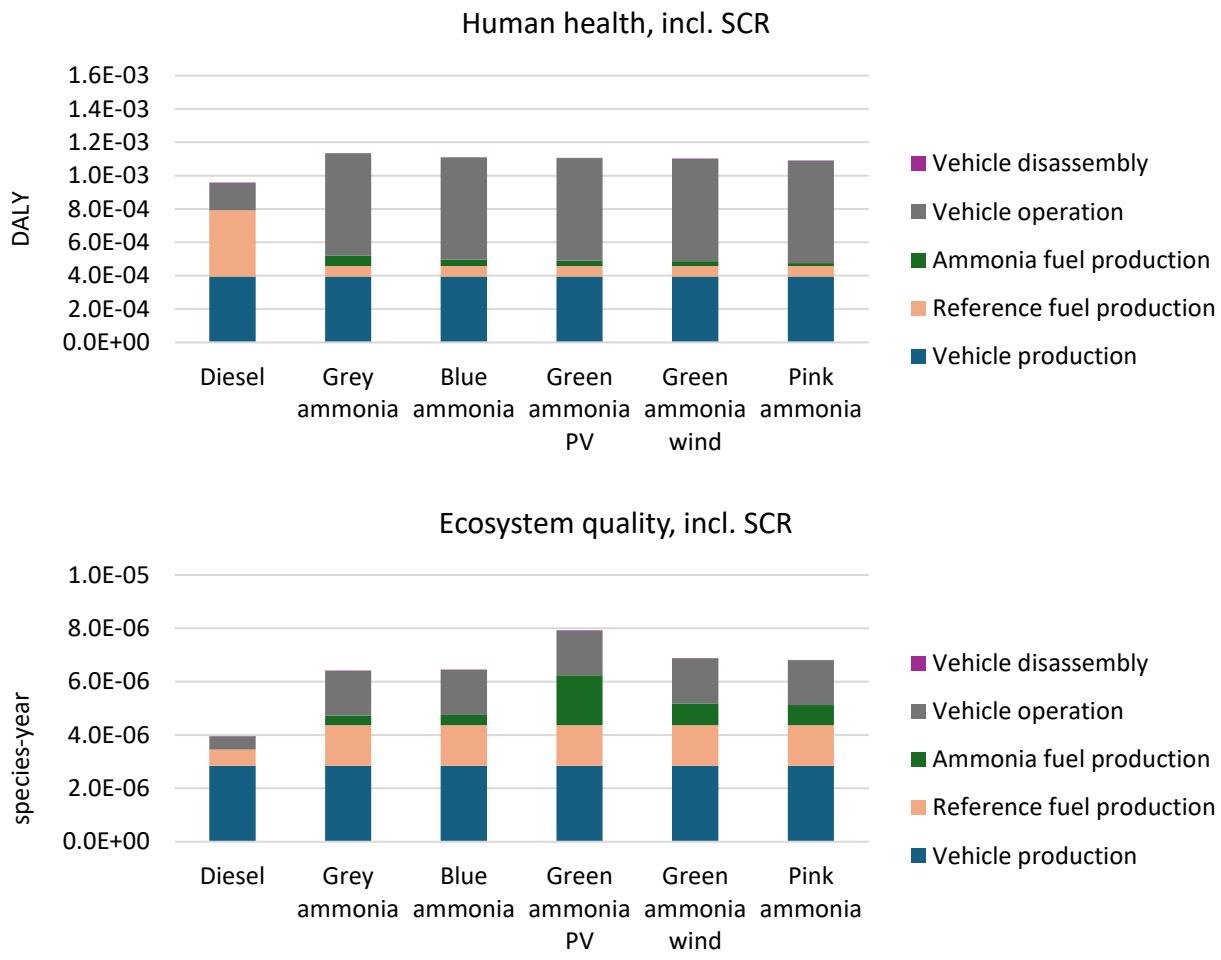

Figure 15. Human health and ecosystem quality results including SCR.

Chapter 5 – LCC of an ammonia-fueled mini tractor

While Papers I–III address the environmental impacts of ammonia- and diesel-fueled mini tractors across multiple ammonia pathways, Paper IV addresses the cost comparison, aligned with the second objective of this research. The LCC targets parity thresholds for capital and operating costs; these thresholds can inform policymaking when designing incentives for wider ammonia adoption.

Subsequent subchapters outline the modeling approach and assumptions (capital/operational costs for multiple ammonia sources), the fuel cost break-even analysis (ammonia vs. diesel/biodiesel), and the LCC case study results with sensitivity analysis.

5.1. Modeling approach

5.1.1. System boundaries

The analysis is set from a small orchard owner's perspective choosing a new mini-tractor: i) diesel-fueled or ii) ammonia-fueled (same chassis as for diesel, engine adapted for port injected NH_3). Options are mutually exclusive; the assessment compares each as a standalone purchase. The LCC includes capital cost, operating cost (fuel and maintenance), and EoL cost. The analysis uses primarily U.S. market data and context (treated as international) and reports all values in 2024 $. System boundaries are shown in Figure 16.

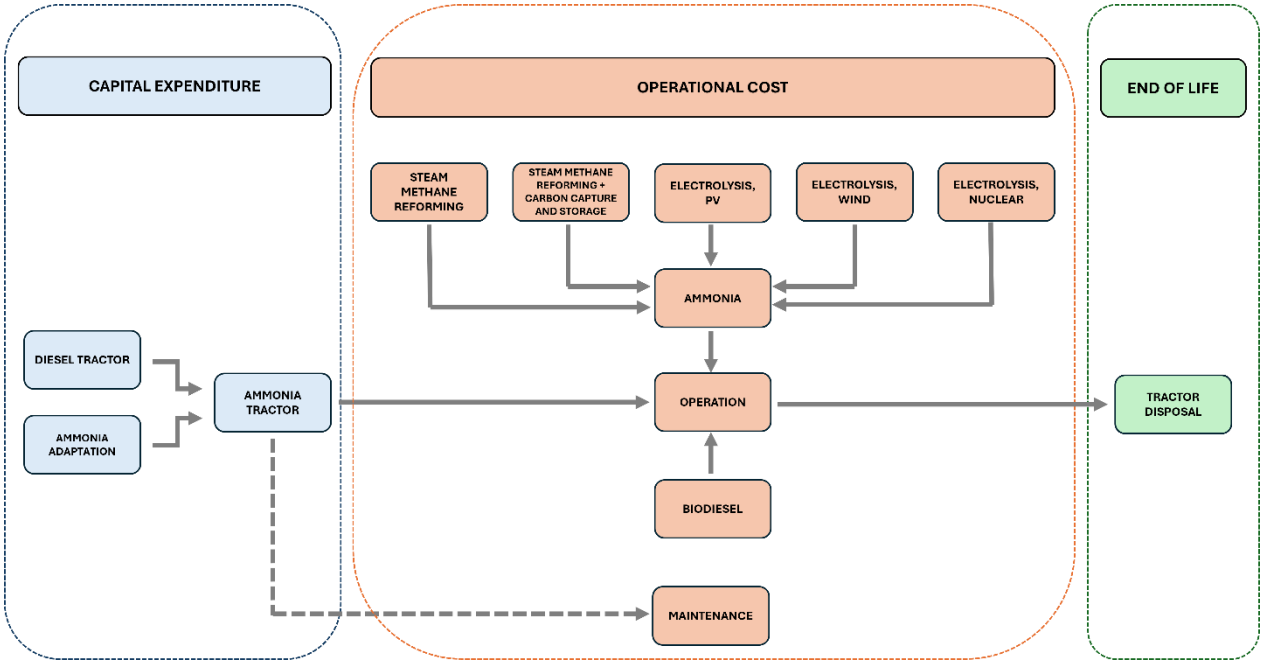

Figure 16. System boundaries for the LCC of an ammonia-fueled mini-tractor.

The capital expenditure of an ammonia-fueled mini tractor is calculated by equation 7. The difference between the two vehicles is the cost of the ammonia setup; dealer distribution and margin are treated as the same value for the two cases.

$$\mathrm{PRICE_{T,NH3}} = \mathrm{PRICE_{T,DIESEL}} + \mathrm{COST_{NH3\_SETUP}} = \mathrm{COST_{T,DIESEL}} + \mathrm{M_{SALES}} + \mathrm{COST_{NH3\_SETUP}} \quad (7)$$

where: $\mathrm{PRICE_{T,NH3}}$ – price for the ammonia-fueled mini tractor, $\mathrm{PRICE_{T,DIESEL}}$ – price for the diesel-fueled mini tractor, $\mathrm{COST_{NH3\_SETUP}}$ – cost of additional equipment for ammonia utilization, $\mathrm{COST_{T,DIESEL}}$ – cost of producing the diesel-fueled tractor, $\mathrm{M_{SALES}}$ – dealer distribution and margin.

Fuel cost includes NH_3 (multiple supply pathways in accordance with the LCA) and the biodiesel pilot. Maintenance and EoL are treated in a simplified manner as a proportional part of the purchase cost.

5.1.2. Capital expenditure

As noted in the Section 1.3, the capital expenditure of an ammonia-fueled mini tractor considers the price of a diesel tractor and its adaptation for port injected ammonia. The cost for the adaptation setup, numerically presented in Table 9, is based on inputs from the laboratory work performed within the project ACTIVATE and is based on the following assumptions:

i. Mini tractor purchase price is taken from the Polish market (treated as internationally representative).

ii. Ammonia tank comprises a 10-liter steel cylinder, shipping and insurance from Asia (China), and a customs duty. Inclusion of shipping and customs duty should be seen as a conservative approach representing an upper bound of the ammonia tank cost.

iii. The NH_3 adaptation package cost is estimated using the price of a commercial diesel LPG/CNG adaptation kit. This relies on an engineering analogy: both systems require similar types of components (fuel line, reducer, injectors, electronic control unit, switch, sensors) with comparable function and complexity, so the LPG/CNG kit price is used as an approximation of the NH_3 fuel line and associated components.

iv. SCR cost is based on a vanadium catalyst sourced from literature [56].

v. Factory service (assembly labor) based on consultations with an industrial company: front-end (controllers, sensors, etc.) 32 h; rear-end (tank, fuel line, etc.) 8 h; refueling valve 4 h. A factory rate of 90 $/h is assumed.

Additionally, annual maintenance cost is assumed as 2 % of capital expenditure, and EoL as 20 %, for both mini tractors, following the literature approach [33].

Table 9. Capital expenditure items for an ammonia-fueled tractor.

Item	Cost, $
SCOUT T-15 (baseline; diesel)	**2500**
Ammonia tank	580
Ammonia implementation equipment	900
Selective catalytic reduction	330
Factory service	3960
Total	**8270**

5.1.3. Operational costs

Operational costs for the LCC depend on the ammonia/biodiesel prices for the ammonia-fueled vehicle and the diesel price for the diesel-fueled vehicle, as well as the quantity of fuel consumed by the engine. Annual fuel consumptions have been calculated for the LCA (Chapter 4 – LCA of an ammonia-fueled mini tractor); for the LCC the same annual quantities are used. Diesel and biodiesel prices used in this study come directly from the statistical data [57]. Ammonia costs are defined through cost functions that depend on the ammonia production pathway; the same pathways as for the LCA are considered.

Ammonia cost function for the natural gas route has been determined based on the IEA report [11] and follows equation 8. The cost comprises a fixed term (CAPEX and fixed operation and maintenance costs) and a gas-dependent variable term, and – for blue ammonia – a CCS surcharge. The values reported in IEA [11] represent averaged data; no specific reformer/CCS method is considered.

$$TC_{ng} = FC_{ng} + VC_{ng} + CCS = FC_{ng} + X_{ng} \cdot NG + Y_{ng} + CCS \quad (8)$$

where: TC_{ng} – total cost of ammonia production ($/t$NH_3$) for the natural gas-based route; FC_{ng} – fixed cost for the natural gas-based route ($/t$NH_3$), VC_{ng} – variable cost for the natural gas-based route ($/t$NH_3$), CCS – fixed term for carbon capture and storage ($/t$NH_3$), X_{ng} and Y_{ng} – empirical coefficients of a linear function linking the natural gas price ($/MMBtu) and ammonia variable cost, NG – natural gas price ($/MMBtu).

Following [58], the fixed cost term has been set to 110 $/t NH_3 (in 2019 $). Based on the total ammonia cost from the report [11] and the fixed cost term, the coefficients of the cost function have been determined. Aggregated fossil-route costs are summarized in Table 10. All values have been reported in 2024 $.

Table 10. Cost aggregation for fossil-based ammonia.

Cost, $/tNH$_3$	Natural gas price at 3.5 $/MMBtu	Natural gas price at 12 $/MMBtu
FC_{ng}	131	131
VC_{ng}	131	405.5
CCS*	95.5	95.5
TC_{ng} grey ammonia	262	536.5
TC_{ng} blue ammonia	357.5	632

*CCS – refers to the blue ammonia production pathway

Values in Table 10 represent pre-shipment costs. Assuming that the plant were located in Asia, adding marine freight increases the cost by 70–130 $/tNH$_3$ [59] (South Korea to the U.S. transport). Additionally, if a carbon pricing scheme were applied, e.g., California's Cap-and-Trade at 35 $/tCO$_2$ (average for 2024), compliance adds about 80.5 $/tNH$_3$ for grey ammonia (at 2.3 tCO$_2$/tNH$_3$ intensity) and 45.5 $/tNH$_3$ for blue ammonia (at 1.3 tCO$_2$/tNH$_3$ intensity) [11].

Electrolysis-based ammonia cost function also follows the IEA report [11]. In the study, the ammonia production cost was defined for alkaline electrolyzer CAPEX of 455–894 $/kWe and 64–74 % efficiency (LHV). By grouping CAPEX of 455 $/kWe with 74 % efficiency, and 894 $/kWe with 64 %, "low" and "high" cost functions were determined according to equation 9.

$$TC_{el} = FC_{el} + VC_{el} = FC_{el} + X_{el} \cdot EL + Y_{el} \quad (9)$$

where variables are defined analogously as in the case of equation 8, with the difference being X_{el} and Y_{el}, which represent empirical coefficients of a linear function linking the electrical energy price ($/MWh) and ammonia variable cost, and EL being the price of electricity.

In line with recent literature [60], this study adopts 400 $/kWe CAPEX and 67 % efficiency for alkaline electrolysis. The fixed term is scaled from the 455 $/kWe case, and the variable-cost function for 67 % is interpolated between the IEA low (74 %) and high (64 %) cases. Electrolysis-route cost aggregation is reported in Table 11.

Table 11. Cost aggregation for electrolysis-based ammonia (CAPEX 400 $/kWe, 67 % efficiency).

Electricity price, $/MWh	21.5	62
TC_{el}, $/tNH$_3$	273.5	681
FC_{el}, $/tNH$_3$	57.5	57.5
VC_{el}, $/tNH$_3$	216	623.5

To capture the expenditure related to using ammonia in an ICE, a retail markup is included because the orchard owner purchases the fuel from a distributor. The markup comprises: distribution (fuel transport), storage (facility maintenance), tax rate, and retail margin. Pipeline transport from the plant to storage is assumed; pipeline and storage costs follow [61]. The tax rate refers to the Superfund Chemical Excise Tax. Local distribution to stations, retail margins, and other taxes are embedded within an extra 10 $/tNH$_3$ markup. The price structure for fossil- and electrolysis-based ammonia at low and high natural-gas/electricity prices is presented in Figure 17. While the variable term is the largest contributor in most cases, all components must be considered; none are negligible.

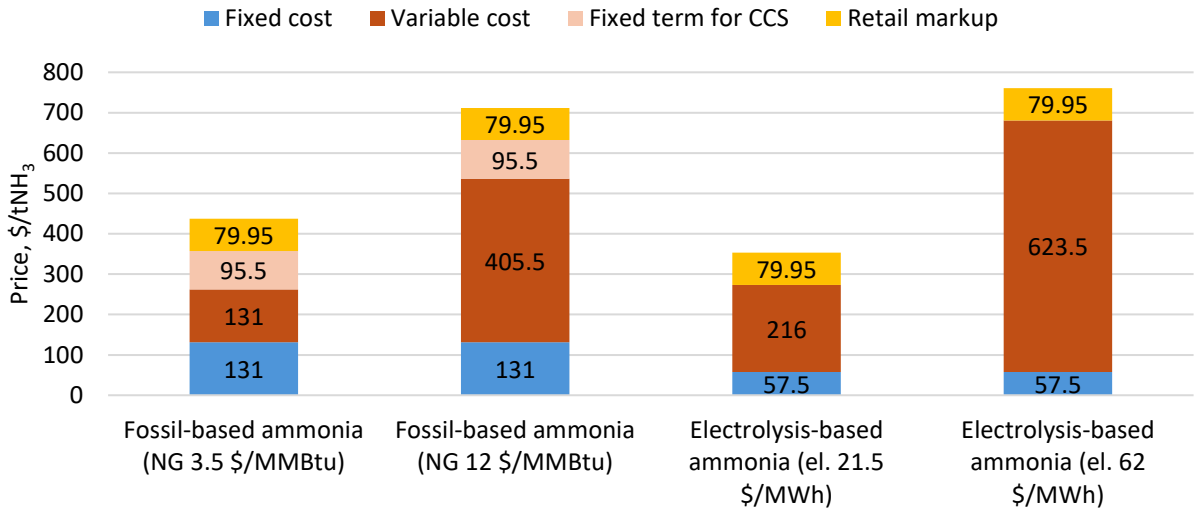

Figure 17. Ammonia price structure for fossil- and electrolysis-based pathways.

5.1.4. LCC case study assumptions

Life cycle costing assumptions for the case study of a mini tractor include:

i. Time horizon: 10 years

ii. Diesel/biodiesel: first-year prices are sourced from the U.S. Department of Energy (2024 average retail) [57]. Changes in prices over time follows the U.S. Energy Information Administration (EIA) forecasts [62].

iii. Ammonia: for grey and blue ammonia, the initial natural gas price and its trajectory over the years come from the EIA predictions [63]. For electrolysis-based ammonia, the electricity prices are taken from the IEA's Levelised Cost of Electricity (LCOE) Calculator [64], no variation over time is included:

a. green PV – utility-scale solar PV (median case, 100 MW)
b. green wind – onshore wind (≥1 MW, median case, 100 MW)
c. pink – long-term operation (10 years, 1000 MW)

A real discount rate of 5 % is applied to all operating cash flows (including maintenance) as a midpoint between the stable market (3 %) and high-risk benchmarks (7 %) [65]. First-year prices are aggregated in Table 12. The 10-year change trajectory for diesel/biodiesel and natural gas is shown in Figure 18 (year 1 = 100 %).

Table 12. Initial prices used in the LCC (year 1).

Fuel/electrical energy	Value	Unit
Diesel	1.06	$/l
Biodiesel	1.20	$/l
Natural gas	4.58	$/MMBtu
Electrical energy, PV	52.7	$/MWh
Electrical energy, wind	46.5	$/MWh
Electrical energy, nuclear	43.0	$/MWh

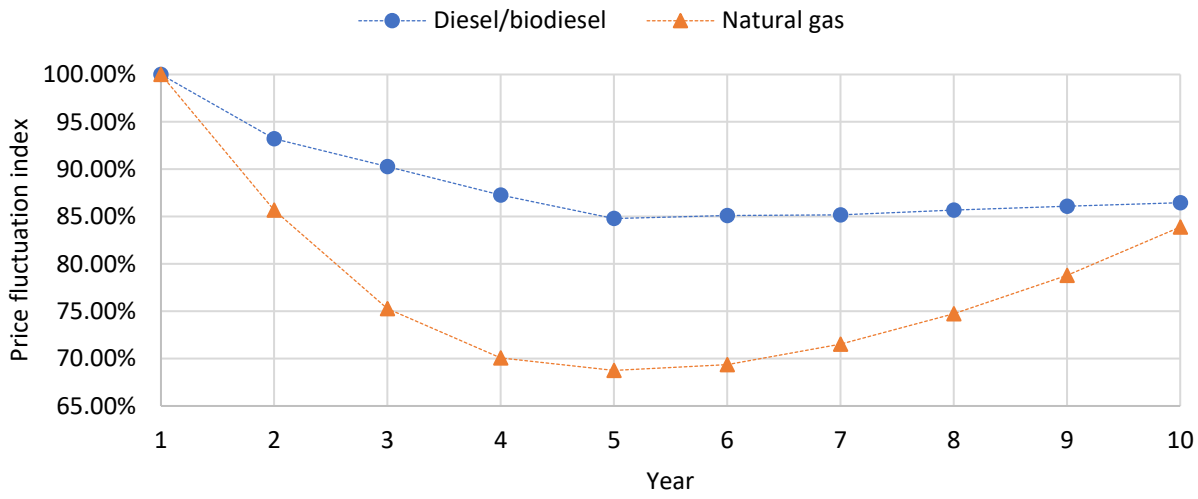

Figure 18. Ten-year price trajectories for diesel/biodiesel and natural gas [62], [63].

5.2. Economic results

5.2.1. Fuel cost break-even analysis

First part of the results regards the ammonia comparison to diesel and biodiesel on an LHV basis. Figure 19 compares LHV-based prices per 1 GJ for:

i. Green: electrolysis-based ammonia

ii. Grey low: NG-based ammonia at 3.5 $/MMBtu

iii. Grey high: NG-based ammonia at 12 $/MMBtu

iv. Blue low: NG-based ammonia coupled with CCS at 3.5 $/MMBtu

v. Blue high: NG-based ammonia coupled with CCS at 12 $/MMBtu

vi. Diesel low: minimum retail between 2013 and 2023 based on [57], at 0.74 $/l (reported in 2024 $)

vii. Diesel high: maximum retail between 2013 and 2023 based on [57], at 1.70 $/l

viii. Biodiesel low: analogously to diesel, at 0.98 $/l

ix. Biodiesel high: analogously to diesel, at 1.71 $/l

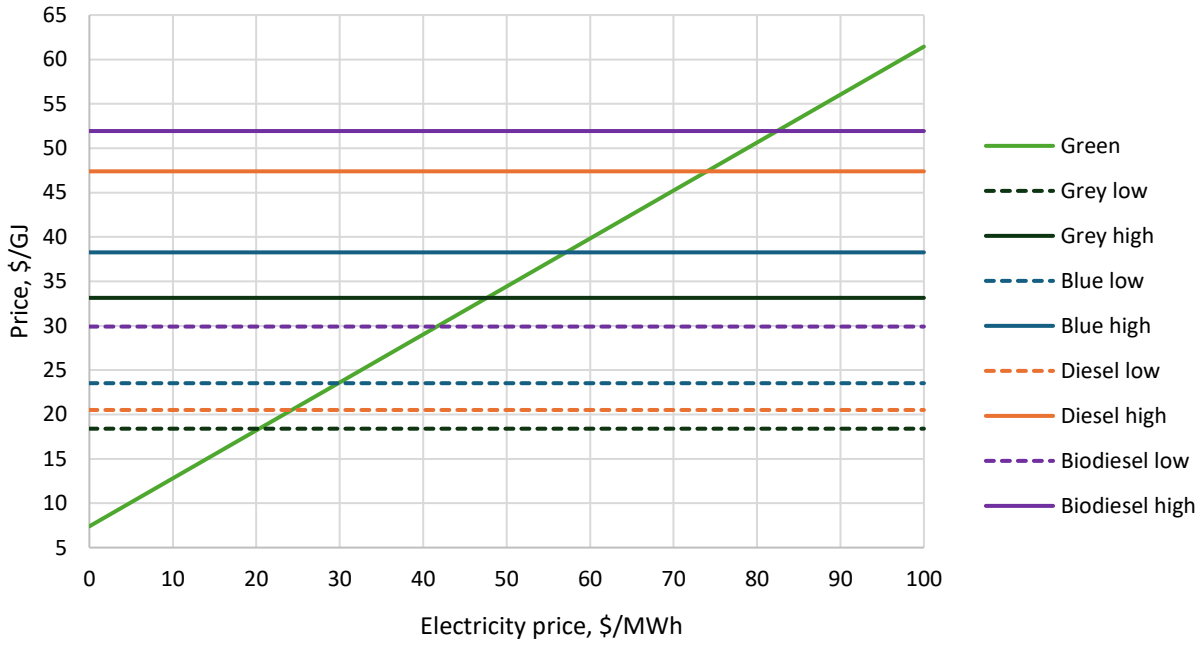

Figure 19. Price comparison of ammonia and other fuels per GJ.

At low gas prices, the break-point electricity price is 20.5 $/MWh vs. grey low ammonia and 30 $/MWh vs. blue low. IEA's LCOE yields around 40 $/MWh for nuclear (LTO, 1000 MW), onshore wind (≥1 MW), and utility-scale PV under best conditions; in such cases green and pink ammonia

cannot compete with NG-based routes. At high gas prices, break-points rise to 47 $/MWh (grey high) and 57 $/MWh (blue high). Under such conditions, green and pink ammonia can undercut NG-based ammonia, but outcomes are case-specific. For diesel, the low price is between grey low and blue low, giving a green ammonia break-point of 24 $/MWh; at high diesel, the break-point is 74 $/MWh. For biodiesel, break-points are 42 $/MWh (low) and 82.5 $/MWh (high). Biodiesel is generally the costliest option.

Values presented in Figure 19 regard pre-shipment conditions. Adding shipping at 70 $/t$NH_3$ increases the price of all ammonia routes, and so ammonia becomes relatively more expensive versus conventional fuels; green ammonia must then rely on lower electricity prices to compete (the required break-even electricity price drops, e.g., from 24 to 17.5 $/MWh under low diesel conditions). However, applying a carbon charge at 35 $/tCO2 to grey and blue ammonia increases their costs and makes electrolysis-based ammonia comparatively more attractive – the break-even electricity price rises (e.g., grey low from 20.5 to 28 $/MWh; blue low from 30 to 34 $/MWh). Nonetheless, whether green ammonia is the best option is case-specific and requires a dedicated analysis considering local electricity prices, natural gas prices, logistics, and the applicable carbon policy. A complete discussion on this subject is provided in Paper IV (Section 3.1).

5.2.2. LCC case study

Second part of the results regards the LCC case study under the assumptions elaborated in the Section 5.1.4. Figure 20 aggregates all cost components for the ammonia-fueled tractor (by ammonia source) versus the diesel reference. Baseline refers to the capital expenditure of the diesel-fueled mini tractor, adaptation is the cost of converting it to ammonia; pilot fuel pertains to diesel in the diesel case and biodiesel in the ammonia case.

The LCC of the ammonia tractor is around three times that of the diesel tractor, primarily because the capital expenditure of the ammonia-fueled vehicle is about 3.3 times the price of the diesel vehicle; this is driven by equipment and factory services aggregated in a bottom-up estimate. As shown in Table 9, factory service is the largest single cost item (around half of the total capital expenditure of the ammonia-fueled mini tractor), based on the assumption of 44 h of assembly at 90 $/h for a one-time retrofit. Since this assumption is derived from consultations with industry, it is treated as a conservative yet valid approach. The obtained value also serves as a starting point for the sensitivity analysis. Pilot fuel cost is higher for the diesel case than for the ammonia case, reflecting higher diesel use versus the smaller biodiesel pilot quantity with ammonia. Ammonia contributes only 2–3 % of the total LCC. For grey/blue routes, this stems from low NG prices in the assessment (range of 3.15–4.58 $/MMBtu). Electrolysis-based ammonia at 43–53 $/MWh (Table 12) is costlier than NG-based at low gas prices, consistent with the fuel comparison shown in Figure 19. Diesel prices near 1 $/l (28 $/GJ) indicate that grey and blue ammonia at low NG can be cheaper than diesel on an energy basis. Green ammonia would require electricity below 38

$/MWh to be more competitive than diesel, below the range used here. Because biodiesel is around 1.1 $/l and the ammonia setup still consumes pilot biodiesel, total fuel spend for the ammonia tractor is around 10–30 % higher than for the diesel tractor, depending on the ammonia production pathway. Ammonia prices are pre-shipment and exclude carbon compliance.

Maintenance and EoL are modeled as fractions of acquisition cost; consequently, they are around 3.3 times higher for the ammonia tractor.

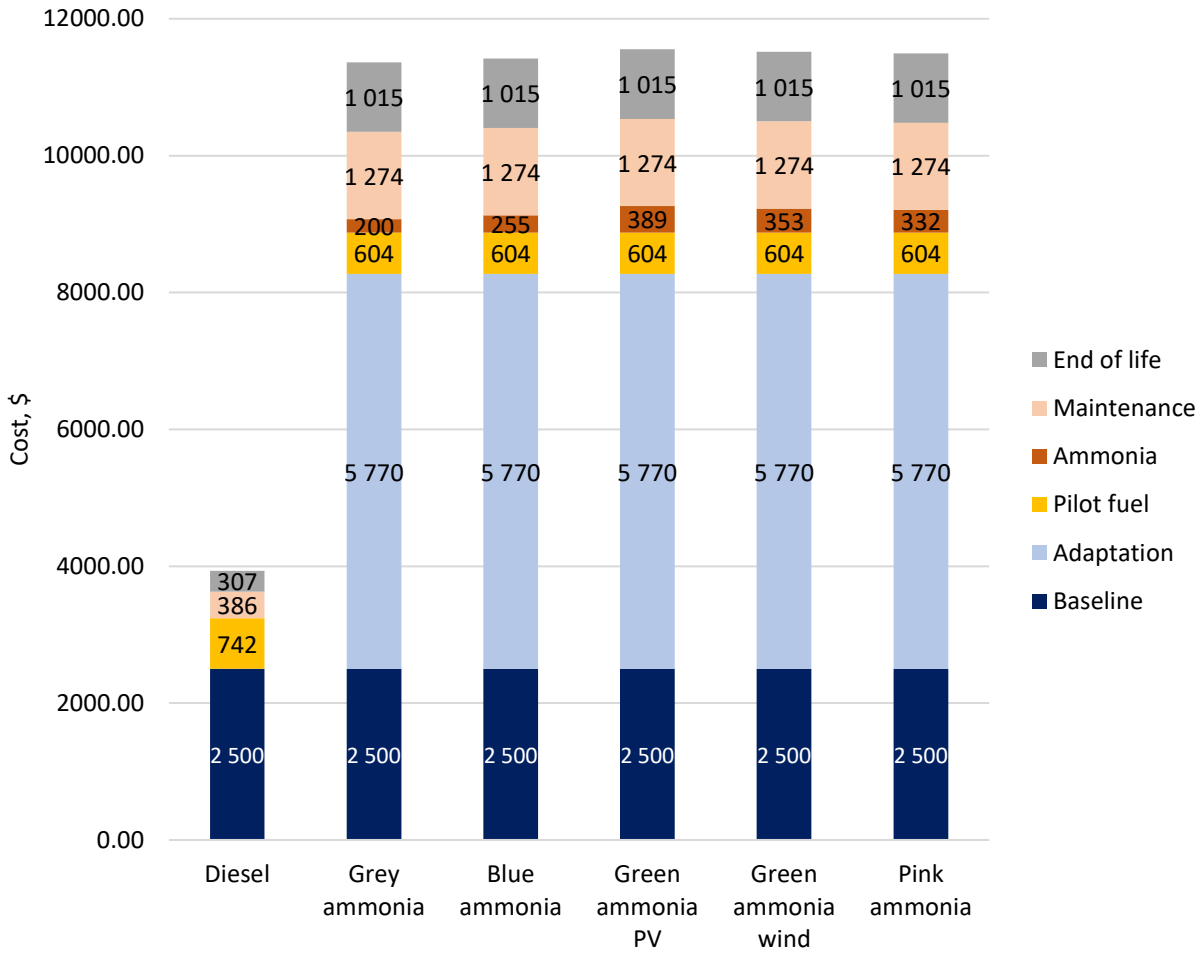

Figure 20. LCC results for an ammonia-fueled mini-tractor.

5.2.3. Sensitivity analysis

Figure 20 shows that the ammonia-fueled tractor is much costlier than the diesel reference, mainly due to acquisition cost. However, the bottom-up capital expenditure may deviate from real-world values: high-volume production could lower equipment and factory-service rates, but increased safety and control measures or a different SCR type could raise costs. The diesel baseline price may also vary by manufacturer/distributor. Fuel prices are based on certain assumptions and follow

informed trends which might not reflect the future precisely as well. Therefore, there is a need to define the LCC results within a range rather than as exact values.

First, a ± 30 % sensitivity range, as an early-stage estimate range [66], is applied to capital expenditure items: (i) baseline tractor, (ii) ammonia hardware (tank with adaptation unit), (iii) SCR, and (iv) factory service, as shown in Figure 21 (a). Factory service has the largest impact on the capital expenditure of the ammonia-fueled vehicle (48 % in the default): a 30 % cut produces around 1200 $ savings; baseline, hardware, and SCR follow in that order. From the sensitivity analysis of the capital expenditure from a policy perspective, an incentive equal to hardware, SCR, and factory service (all components needed to transform a diesel-fueled mini tractor to an ammonia-fueled vehicle) would fall around 4500–7000 $ (if only one item deviates from default, as in the case of this calculation).

Maintenance and EoL scale with capital expenditure; across scenarios they range from 142–189 $/year (maintenance) and 1416–1892 $ (EoL), as shown in Figure 21 (b).

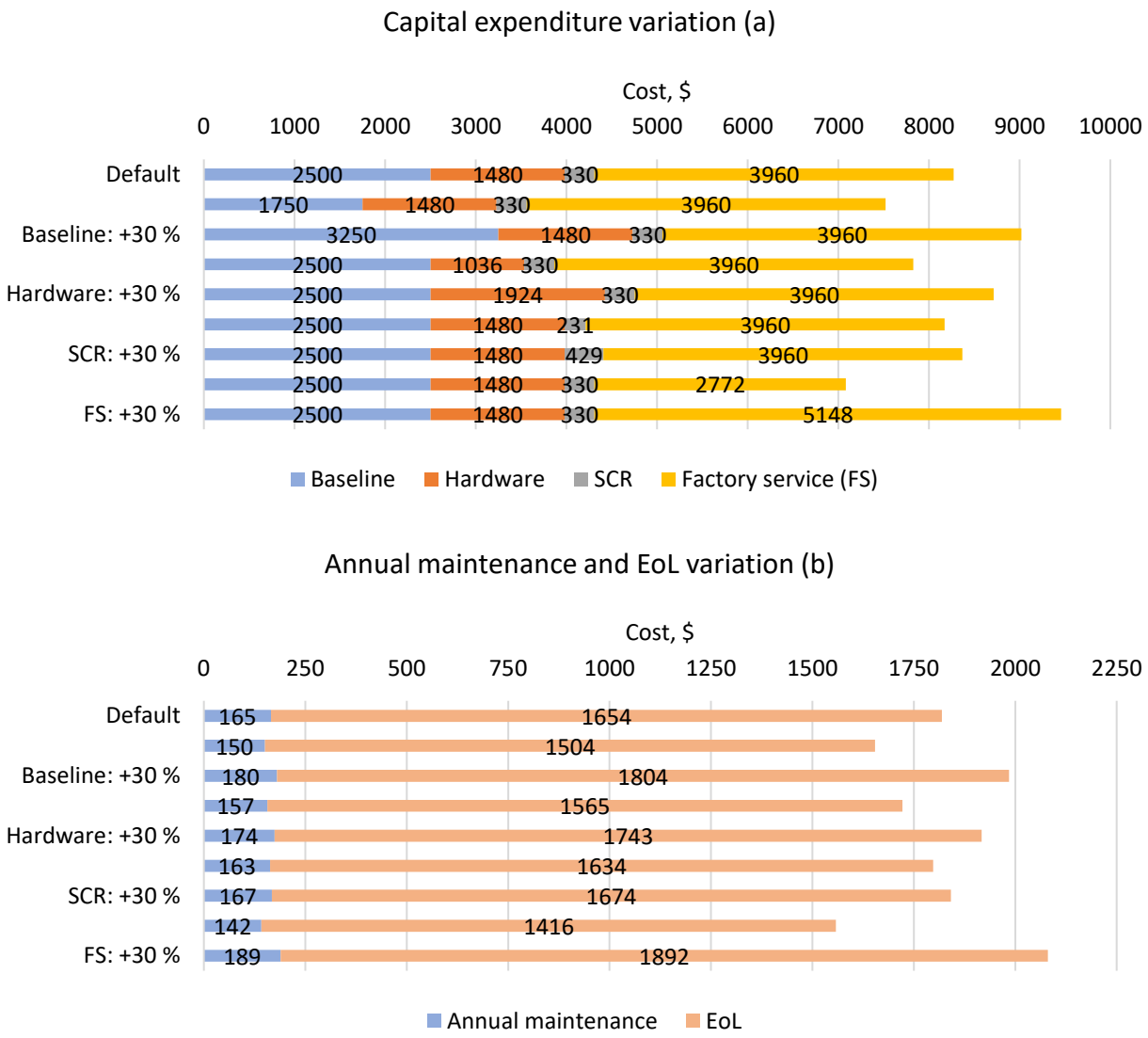

Figure 21. Sensitivity analysis: (a) capital expenditure; (b) maintenance and EoL.

Second, because the LCC is an arithmetic sum and ammonia costs follow the linear functions, shown in Section 5.1.3, changes in natural gas or electricity prices shift ammonia costs – and thus total LCC – linearly. The effect of electricity price on total discounted ammonia cost – 389 $ for green PV at 52.7 $/MWh, 353 $ for green wind at 46.5 $/MWh, and 332 $ for pink at 43 $/MWh – is seen in Figure 20. However, these values do not include shipping and carbon-compliance costs noted in Section 5.1.3. If 70 $/t$NH_3$ is added for shipping for all ammonia and 35 $/t$CO_2$ for carbon-emission compliance for grey and blue pathways, ammonia's share of LCC rises by about one percentage point (from 2–3 % to 3–4 %, depending on scenario). This is illustrated in Figure 22. Given ammonia's small share, these adders do not change the LCC's primary conclusions.

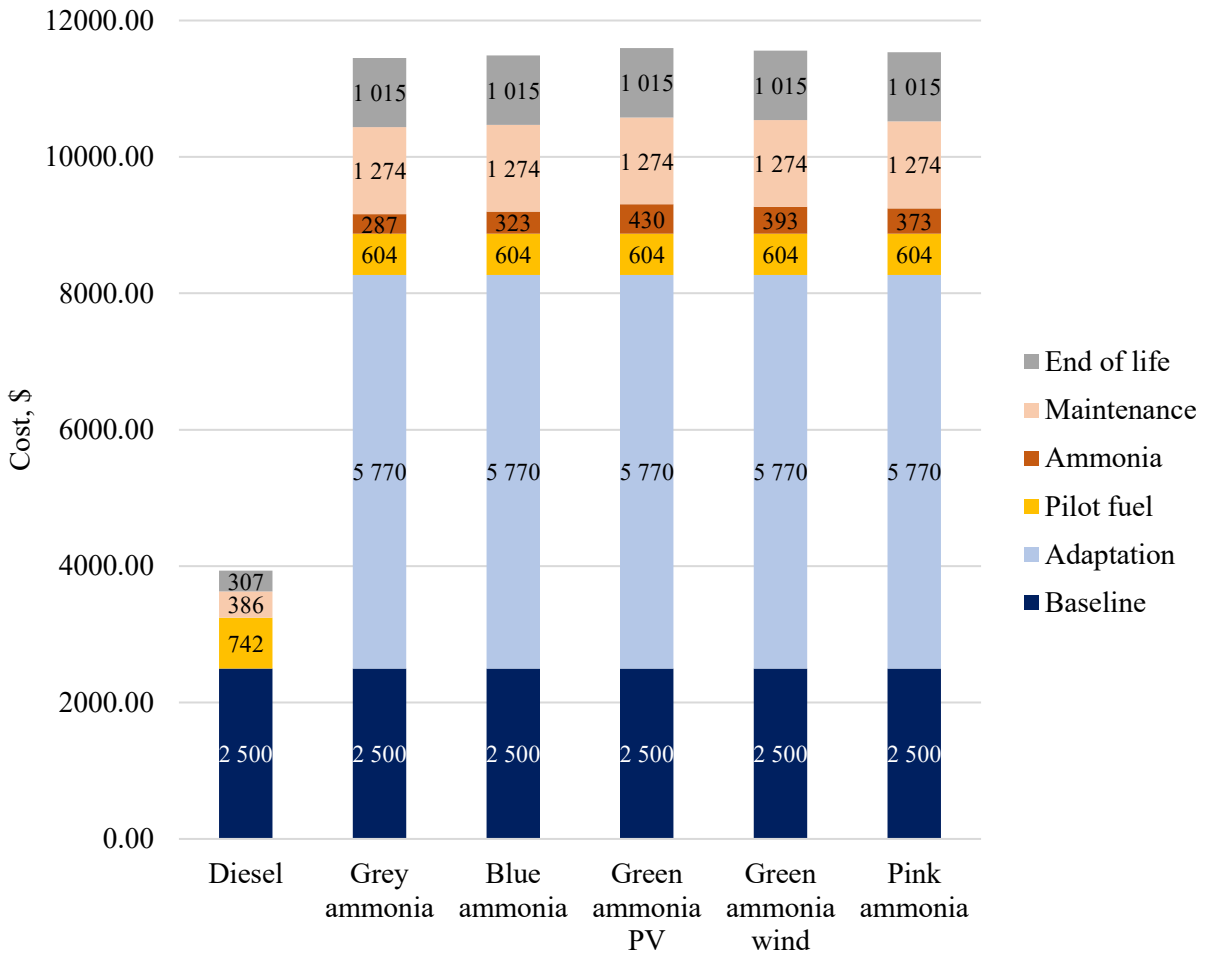

Figure 22. LCC results for an ammonia-fueled mini-tractor, including shipping and carbon-emission compliance for ammonia.

Additional comment must be made regarding the cost of pilot fuel. Over the 10-year horizon, fuel trajectories can be condensed to the following discounted-average prices: diesel 0.94 $/l, biodiesel 1.07 $/l, natural gas 3.59 $/MMBtu, and electricity 52.7 $/MWh (PV, used as a conservative upper bound for electrolysis). In the ammonia-fueled tractor, ammonia quantity exceeds pilot fuel volume, yet the high biodiesel price makes the pilot share dominate total fuel cost across the analyzed cases. Setting a minimum biodiesel price (Section 5.2.1) reduces the gap versus the diesel tractor (total pilot fuel cost would be reduced from 604 $, shown in Figure 20, to 553 $) but generally does not achieve parity, especially for blue or electrolysis-based ammonia at the electricity level assumed. In short, with current price levels, pilot biodiesel cost is an important factor; parity of fuel contributions for the ammonia- and diesel-fueled mini tractor would require either meaningfully cheaper biodiesel, lower electricity/natural gas prices, or both. A complete discussion on this topic is shown in Paper IV (Section 3.3.2).

Based on the capital expenditure and fuel price variations described earlier, a range of LCC results can be defined, shown by the best-case (BS) and worst-case (WS) scenarios.

Best case (BS) – favorable market assumptions:

i. Capital expenditure: –30 % for all items

ii. Biodiesel: 0.98 $/l

iii. Natural gas: 3.5 $/MMBtu

iv. Electricity: 43.0 $/MWh

Worst case (WS) – adverse market assumptions:

i. Capital expenditure: +30 % for all items

ii. Biodiesel: 1.71 $/l

iii. Natural gas: 12 $/MMBtu

iv. Electricity: 52.7 $/MWh

v. Ammonia price includes carbon-compliance and transport

Figure 23 compares BS and WS scenarios. Because ammonia's share of total LCC is small (about 2–3 % in the default case), the three ammonia sourcing options cluster to similar values within each scenario. Depending on market conditions, the following conclusions may be drawn:

i. Capital expenditure for the ammonia-fueled tractor is 2.3–4.3 times that of the diesel tractor.

ii. Fuel cost (ammonia plus pilot fuel) is 1.1–2.0 times that of the diesel-fueled tractor, except for grey ammonia, which approaches diesel fuel cost under low biodiesel and low NG prices.

iii. Maintenance and EoL, modeled as fractions of acquisition cost, are 2.3–4.3 times higher for the ammonia tractor than for the diesel tractor.

This comparison should be seen as a more realistic LCC range given the possible alterations from the default scenario seen in Figure 20.

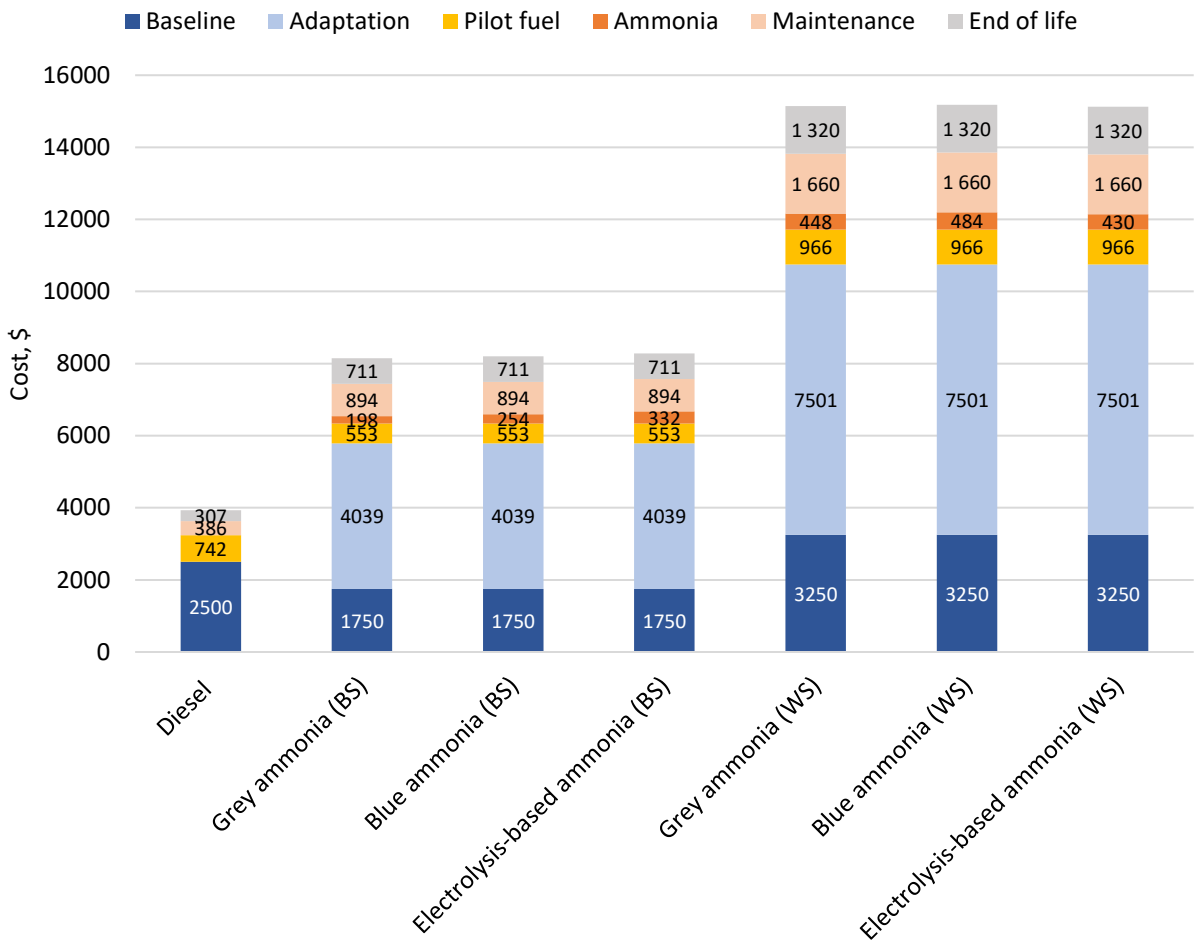

Figure 23. Range of estimated LCC results.

Chapter 6 – Summary

Ammonia's decarbonization potential and practical advantages over hydrogen make it a promising option within a hydrogen-based economy. It can be stored and refueled similarly to LPG or CNG, and agriculture's existing ammonia infrastructure facilitates its deployment for mini tractor fueling. Two primary objectives of this work, i.e. i) evaluating the differences between the impacts on the environment of an ammonia-fueled and a diesel-fueled mini tractor based on life cycle assessment, and ii) comparing the economic performance of an ammonia-fueled and a diesel-fueled mini tractor based on life cycle costing analysis, have been achieved in this study. The following conclusions have been obtained.

An environmental impact assessment of ammonia production pathways indicates that, among the pathways analyzed, the preferred option under the climate change criterion is electrolysis-based ammonia produced using nuclear electricity. However, its high freshwater consumption and fossil depletion (driven by uranium use) can be constraining, particularly where water is scarce or resource availability is limited. In such contexts, wind-powered electrolysis may be the better choice: it markedly lowers impacts in those two categories while still delivering a low climate change burden, which is the primary motivation for alternative fuels. Relative to diesel, all ammonia pathways except grey (SMR without CCS) meet the decarbonization objective, with blue ammonia offering only modest improvement. At the endpoint level, vehicle fueled with ammonia produced using nuclear or wind electricity shows the lowest human health impact. However, regardless of the ammonia production pathway, it worsens ecosystem quality relative to diesel, with PV-based ammonia performing particularly poorly in this category. Nonetheless, ammonia's tangible potential to mitigate global warming is shown.

Analysis of the performance of the ammonia-fueled engine versus the diesel case shows that, on average, the ammonia-fueled engine is less efficient than diesel, but the difference diminishes under high load (torque) across most speeds of the shaft. Notably, while less CO_2 is emitted by the ammonia-fueled engine, there is apparent formation of NO_x and N_2O, particularly under partial-load operating conditions of the engine.

Premise stated in Chapter 1 – Introduction, i.e. that ammonia allows for decarbonization of heavy-duty machinery as it can be produced renewably and combusts without direct carbon, has been confirmed on the basis of the life cycle assessment for the mini tractor used in the orchard. However, the level of the decarbonization effect depends on the engine operation; for instance, if it were operated only near the strongest N_2O formation (high rpm and moderate torque, e.g. 2700/2400 rpm at 8 Nm torque), a different outcome might be achieved. This emphasizes the need for accounting for real engine operation for a reliable environmental assessment;

for an ammonia-fueled engine used in a different instance (e.g. heavy machinery used in the construction sector) its working cycle should reflect real conditions.

Relative to diesel, the ammonia-fueled tractor investigated in this research shows lower operational GHGs (approximately 72 kg CO2 eq. vs. around 88 kg, an 18 % reduction), which is limited by the CO_2 from the pilot fuel and N_2O formation. Over the full life cycle, switching to ammonia with a biodiesel pilot fuel reduces the climate change impact to a greater extent – between 42–44 % – when ammonia is produced via wind or nuclear power and the biodiesel footprint is included. For fossil depletion, solar/wind-derived ammonia scenarios yield between 43–45 % reductions, whereas the nuclear-derived ammonia mini tractor increases depletion by around 78 %. Freshwater consumption is higher across all ammonia routes (40–50 % above diesel), with the nuclear pathway approaching a twofold increase.

Ammonia-vehicle scenarios increase the human health endpoint category by approximately 47 % compared to diesel, mostly due to secondary particulate formation from NH_3/NO_x, and roughly double the ecosystem quality impact owing to both operational emissions and fuel production burdens. Adding SCR, based on a theoretical approach utilizing residual ammonia present in the exhaust, lowers the human health impact by approximately 20 % and ecosystem quality by about 10 %, yet still, post-SCR, the human health result remains 19 % above diesel and ecosystem quality is still 1.6–2 times higher.

In sum, ammonia in a dual-fuel CI engine is a viable substitute that can aid decarbonization of hard to electrify, heavy-duty machinery, such as the mini tractor used for orchard operations. On a climate change basis, nuclear-based ammonia is the preferred option; however, its high impact on fossil depletion and water consumption should be considered for long-term resource planning and in water-constrained regions; green wind ammonia achieves a marginally higher score on climate change, yet has much lower impacts on both fossil depletion and freshwater consumption. It may be cautiously concluded that electrolysis-based ammonia with electrical energy supplied by a wind turbine is the best scenario. Still, endpoint analysis reveals that elevated NO_x and NH_3 emissions from the engine combustion must be addressed, as, for all scenarios, the ammonia-fueled mini tractor performs worse in terms of human health and ecosystem quality.

To improve the technical and environmental performance of the engine, combustion optimization would bring the most benefits (which is additionally confirmed by means of the exergy balance presented in Paper II). Ammonia/biodiesel ratio, injection timing, cylinder design improvements, or exhaust gas recirculation could be investigated towards optimizing the port injection setup; alternatively, a direct injection setup might be considered. The obtained results should be interpreted considering the fact that the ammonia-fueled engine represents a prototype configuration which can be improved, whereas the diesel engine is a mature commercial design.

The primary goal would be to improve the thermal efficiency of the engine and minimize the formation of NO_x/N_2O and ammonia slip. Further research should also address the SCR configuration, particularly with regard to the type of catalysts and ammonia dosing, to facilitate the goal of emission reduction. Ultimately, higher generations of biodiesel used as pilot fuel (not competing with food and causing indirect land use change) should be considered.

Life cycle costing assessment has identified the conditions necessary for the ammonia-fueled mini tractor to become competitive with a diesel-fueled vehicle and yields the following conclusions.

First, the cost ranking between natural gas-based and electrolysis-based ammonia depends on gas and electricity prices. At low gas prices (3.5 $/MMBtu), electrolysis would need electricity below roughly 20–30 $/MWh which is unlikely in most cases. At higher gas prices (12 $/MMBtu), electrolysis-based ammonia can become cheaper if electricity is about 47–57 $/MWh, which is achievable in optimal renewable or nuclear cases (around 40–46 $/MWh). Second, versus diesel: at a low diesel price (0.74 $/l), only grey ammonia at low gas prices is competitive; electrolysis would require electricity under 24 $/MWh, which is unlikely. At a high diesel price (1.70 $/l), parity is reachable if electricity is below 74 $/MWh – feasible in many cases.

For the case study of the full LCC, the capital expenditure of the ammonia-fueled mini tractor is about 3.3 times higher than that of the standard diesel vehicle under the stated assumptions. Combined fuel costs for the ammonia tractor are 10–30 % higher than for diesel; this gap can decrease by lowering ammonia or biodiesel prices, but because biodiesel contributes the larger share of the combined fuel spend, reducing the biodiesel price would be particularly effective. Parity requires biodiesel around 0.62–0.96 $/l, depending on the ammonia pathway. Adding shipping and carbon-compliance costs to ammonia increases total LCC only marginally. Considering capital expenditure uncertainty and market volatility in fuel prices, the ammonia-fueled tractor LCC is estimated at roughly 2–4 times that of the diesel mini tractor.

To improve cost-effectiveness, several strategies are available. Policymakers could offer a direct purchase incentive for carbon-free vehicles to offset the orchard owner’s acquisition costs – on the order of 3000–8000 $, about 6000 $ in the default case. Alternatively, targeted incentives for ammonia and biodiesel could bring their prices to diesel parity, or parity could be achieved if diesel prices reflected carbon-emission compliance costs from combustion. Accounting for these measures could shift profitability in favor of the ammonia-fueled mini tractor, providing a viable path to reduce agricultural emissions while enhancing energy security through diversified fuels.

To summarize, this work has presented complete LCA and LCC assessments of an ammonia-fueled mini tractor used in an orchard setting, based on primary experimental engine data, quantifying both environmental trade-offs and economic conditions for competitiveness. These results and the

underlying modelling framework might support future research on ammonia-fueled solutions and related policy measures.

References

[1] Global Change Data Lab, “Global direct primary energy consumption,” Our World in Data. Accessed: Oct. 10, 2025. [Online]. Available: https://ourworldindata.org/grapher/global-primary-energy

[2] M. J. Rogoff, “Introduction,” in *Solid Waste Recycling and Processing*, Elsevier, 2014, pp. 1–9. doi: 10.1016/B978-1-4557-3192-3.00001-4.

[3] Intergovernmental Panel on Climate Change (IPCC), “Summary for Policymakers,” in *Global Warming of 1.5°C: IPCC Special Report on Impacts of Global Warming of 1.5°C above Pre-industrial Levels in Context of Strengthening Response to Climate Change, Sustainable Development, and Efforts to Eradicate Poverty*, Masson-Delmotte, V., Zhai, P., Pörtner, H.-O., Roberts, D., Skea, J., Shukla, P. R., Pirani, A., Moufouma-Okia, W., Péan, C., Pidcock, R., Connors, S., Matthews, J. B. R., Chen, Y., Zhou, X., Gomis, M. I., Lonnoy, E., Maycock, T., Tignor, M., and Waterfield, T., Eds., Cambridge, UK; New York, NY, USA: Cambridge University Press, 2018, pp. 3–24. Accessed: Oct. 10, 2025. [Online]. Available: https://doi.org/10.1017/9781009157940.001

[4] A. D. Valdivia and M. P. Balcell, “Connecting the grids: A review of blockchain governance in distributed energy transitions,” *Energy Research & Social Science*, vol. 84, p. 102383, Feb. 2022, doi: 10.1016/j.erss.2021.102383.

[5] P. K. Senecal and F. Leach, “Diversity in transportation: Why a mix of propulsion technologies is the way forward for the future fleet,” *Results in Engineering*, vol. 4, p. 100060, Dec. 2019, doi: 10.1016/j.rineng.2019.100060.

[6] Eurostat, “Complete energy balances,” Eurostat Data Browser. Accessed: Oct. 18, 2024. [Online]. Available: https://ec.europa.eu/eurostat/databrowser/view/NRG_BAL_C__custom_17917152/default/table

[7] A. M. N. Renzaho, J. K. Kamara, and M. Toole, “Biofuel production and its impact on food security in low and middle income countries: Implications for the post-2015 sustainable development goals,” *Renewable and Sustainable Energy Reviews*, vol. 78, pp. 503–516, Oct. 2017, doi: 10.1016/j.rser.2017.04.072.

[8] H. Naveed, A. H. Al-Muhtaseb, F. Jamil, S. Al-Maawali, and R. Al-Hajri, “Prospects of R&D in the biofuel sector/industry,” in *Environmental Sustainability of Biofuels*, Elsevier, 2023, pp. 163–181. doi: 10.1016/B978-0-323-91159-7.00021-7.

[9] “Higher Calorific Values of Common Fuels: Reference & Data,” The Engineering ToolBox. Accessed: Jul. 16, 2025. [Online]. Available: https://www.engineeringtoolbox.com/fuels-higher-calorific-values-d_169.html

[10] T. Abbasi and S. A. Abbasi, “‘Renewable’ hydrogen: Prospects and challenges,” *Renewable and Sustainable Energy Reviews*, vol. 15, no. 6, pp. 3034–3040, Aug. 2011, doi: 10.1016/j.rser.2011.02.026.

[11] IEA, “The Future of Hydrogen,” Jun. 2019. [Online]. Available: https://www.iea.org/reports/the-future-of-hydrogen

[12] “Hydrogen - Density and Specific Weight vs. Temperature and Pressure,” The Engineering ToolBox. Accessed: Jul. 16, 2025. [Online]. Available: https://www.engineeringtoolbox.com/hydrogen-H2-density-specific-weight-temperature-pressure-d_2044.html
[13] H. T. Hwang and A. Varma, “Hydrogen storage for fuel cell vehicles,” *Current Opinion in Chemical Engineering*, vol. 5, pp. 42–48, Aug. 2014, doi: 10.1016/j.coche.2014.04.004.
[14] M. Shi and X. Meng, “Photothermal catalysis: From principles to applications,” *International Journal of Hydrogen Energy*, vol. 48, no. 89, pp. 34659–34676, Nov. 2023, doi: 10.1016/j.ijhydene.2023.05.253.
[15] “Ammonia - NH3 - Thermodynamic Properties,” The Engineering ToolBox. Accessed: Jul. 16, 2025. [Online]. Available: https://www.engineeringtoolbox.com/ammonia-d_971.html
[16] “Ammonia - Properties at Gas-Liquid Equilibrium Conditions,” The Engineering ToolBox. Accessed: Jul. 16, 2025. [Online]. Available: https://www.engineeringtoolbox.com/ammonia-gas-liquid-equilibrium-condition-properties-temperature-pressure-boiling-curve-d_2013.html
[17] J. N. Klüssmann, L. R. Ekknud, A. Ivarsson, and J. Schramm, “Ammonia Application in IC Engines”.
[18] A. J. Reiter and S.-C. Kong, “Demonstration of Compression-Ignition Engine Combustion Using Ammonia in Reducing Greenhouse Gas Emissions,” *Energy Fuels*, vol. 22, no. 5, pp. 2963–2971, Sep. 2008, doi: 10.1021/ef800140f.
[19] C. Kurien and M. Mittal, “Review on the production and utilization of green ammonia as an alternate fuel in dual-fuel compression ignition engines,” *Energy Conversion and Management*, vol. 251, p. 114990, Jan. 2022, doi: 10.1016/j.enconman.2021.114990.
[20] P. Dimitriou and R. Javaid, “A review of ammonia as a compression ignition engine fuel,” *International Journal of Hydrogen Energy*, vol. 45, no. 11, pp. 7098–7118, Feb. 2020, doi: 10.1016/j.ijhydene.2019.12.209.
[21] International Energy Agency (IEA), “Global Hydrogen Review 2024,” IEA, Paris, 2024. Accessed: Oct. 13, 2025. [Online]. Available: https://www.iea.org/reports/global-hydrogen-review-2024
[22] C. Tornatore, L. Marchitto, P. Sabia, and M. De Joannon, “Ammonia as Green Fuel in Internal Combustion Engines: State-of-the-Art and Future Perspectives,” *Front. Mech. Eng.*, vol. 8, p. 944201, Jul. 2022, doi: 10.3389/fmech.2022.944201.
[23] M.-C. Chiong *et al.*, “Advancements of combustion technologies in the ammonia-fuelled engines,” *Energy Conversion and Management*, vol. 244, p. 114460, Sep. 2021, doi: 10.1016/j.enconman.2021.114460.
[24] United States Environmental Protection Agency (EPA), “Understanding Global Warming Potentials,” United States Environmental Protection Agency. Accessed: Oct. 13, 2025. [Online]. Available: https://www.epa.gov/ghgemissions/understanding-global-warming-potentials
[25] D. R. MacFarlane *et al.*, “A Roadmap to the Ammonia Economy,” *Joule*, vol. 4, no. 6, pp. 1186–1205, Jun. 2020, doi: 10.1016/j.joule.2020.04.004.

[26] A. Valera-Medina, H. Xiao, M. Owen-Jones, W. I. F. David, and P. J. Bowen, “Ammonia for power,” *Progress in Energy and Combustion Science*, vol. 69, pp. 63–102, Nov. 2018, doi: 10.1016/j.pecs.2018.07.001.
[27] L. Kumar and A. K. Sleiti, “Systematic review on ammonia as a sustainable fuel for combustion,” *Renewable and Sustainable Energy Reviews*, vol. 202, p. 114699, Sep. 2024, doi: 10.1016/j.rser.2024.114699.
[28] Dincer, I., & Bicer, Y., “Comprehensive Evaluation of NH3 Production and Utilization Options for Clean Energy Applications,” University of Ontario Institute of Technology, Ontario, Canada.
[29] Y. Bicer and I. Dincer, “Life cycle assessment of ammonia utilization in city transportation and power generation,” *Journal of Cleaner Production*, vol. 170, pp. 1594–1601, Jan. 2018, doi: 10.1016/j.jclepro.2017.09.243.
[30] S. T. Thompson *et al.*, “Direct hydrogen fuel cell electric vehicle cost analysis: System and high-volume manufacturing description, validation, and outlook,” *Journal of Power Sources*, vol. 399, pp. 304–313, 2018, doi: 10.1016/j.jpowsour.2018.07.100.
[31] P. Halder *et al.*, “Performance, emissions and economic analyses of hydrogen fuel cell vehicles,” *Renewable and Sustainable Energy Reviews*, vol. 199, p. 114543, Jul. 2024, doi: 10.1016/j.rser.2024.114543.
[32] B. Wang, Z. Li, J. Zhou, Y. Cong, and Z. Li, “Technological-economic assessment and optimization of hydrogen-based transportation systems in China: A life cycle perspective,” *International Journal of Hydrogen Energy*, vol. 48, no. 33, pp. 12155–12167, Apr. 2023, doi: 10.1016/j.ijhydene.2022.12.189.
[33] J. Ally and T. Pryor, “Life cycle costing of diesel, natural gas, hybrid and hydrogen fuel cell bus systems: An Australian case study,” *Energy Policy*, vol. 94, pp. 285–294, Jul. 2016, doi: 10.1016/j.enpol.2016.03.039.
[34] E. Szumska, M. Pawełczyk, and V. Pistek, “Evaluation of the Life Cycle Costs for urban buses equipped with conventional and hybrid drive trains,” *The Archives of Automotive Engineering – Archiwum Motoryzacji*, vol. 83, no. 1, pp. 73–86, Mar. 2019, doi: 10.14669/AM.VOL83.ART5.
[35] A. M. Kuyumcu, B. Bingül, F. Akar, and A. Yıldız, “Well-to-wheel carbon footprint and cost analysis of gasoline, diesel, hydrogen ICE, hybrid and fully electric city buses,” *Energy*, vol. 301, p. 131685, Aug. 2024, doi: 10.1016/j.energy.2024.131685.
[36] International Energy Agency (IEA), “Ammonia Technology Roadmap,” IEA, Paris, 2021. [Online]. Available: https://www.iea.org/reports/ammonia-technology-roadmap
[37] European Commission, Joint Research Centre (JRC), Institute for Environment and Sustainability, “International Reference Life Cycle Data System (ILCD) Handbook – General guide for Life Cycle Assessment – Detailed guidance,” European Commission, Joint Research Centre (JRC), Luxembourg, ILCD Handbook, 2010.

[38] P. Iradukunda, E. M. Mwanaumo, and J. Kabika, “A review of integrated multicriteria decision support analysis in the climate resilient infrastructure development,” *Environmental and Sustainability Indicators*, vol. 20, p. 100312, Dec. 2023, doi: 10.1016/j.indic.2023.100312.
[39] Sphera Solutions, Inc., “Search Life Cycle Assessment Datasets,” Sphera. Accessed: Oct. 13, 2025. [Online]. Available: https://lcadatabase.sphera.com/
[40] Y. Bicer, I. Dincer, C. Zamfirescu, G. Vezina, and F. Raso, “Comparative life cycle assessment of various ammonia production methods,” *Journal of Cleaner Production*, vol. 135, pp. 1379–1395, Nov. 2016, doi: 10.1016/j.jclepro.2016.07.023.
[41] S. Ghavam, M. Vahdati, I. A. G. Wilson, and P. Styring, “Sustainable Ammonia Production Processes,” *Front. Energy Res.*, vol. 9, p. 580808, Mar. 2021, doi: 10.3389/fenrg.2021.580808.
[42] E. Fu, F. Gong, S. Wang, and R. Xiao, “Chemical Looping Technology in Mild-Condition Ammonia Production: A Comprehensive Review and Analysis,” *Small*, vol. 20, no. 1, p. 2305095, Jan. 2024, doi: 10.1002/smll.202305095.
[43] “Green ammonia synthesis,” *Nat. Synth*, vol. 2, no. 7, pp. 581–582, Jun. 2023, doi: 10.1038/s44160-023-00362-y.
[44] C. W. Ong, N. Chang, M.-L. Tsai, and C.-L. Chen, “Decarbonizing the energy supply chain: Ammonia as an energy carrier for renewable power systems,” *Fuel*, vol. 360, p. 130627, Mar. 2024, doi: 10.1016/j.fuel.2023.130627.
[45] Riis, T., Hagen, E. F., Vie, Preben, and Ulleberg, Øystein, “Hydrogen production R&D: Priorities and gaps,” International Energy Agency (IEA), Paris, 2006.
[46] J. Xu and G. F. Froment, “Methane steam reforming, methanation and water-gas shift: I. Intrinsic kinetics,” *AIChE Journal*, vol. 35, no. 1, pp. 88–96, Jan. 1989, doi: 10.1002/aic.690350109.
[47] Sundin, C., “Environmental Assessment of Electrolyzers for Hydrogen Gas Production,” Master’s thesis, KTH Royal Institute of Technology, Stockholm, Sweden, 2019. Accessed: Oct. 13, 2025. [Online]. Available: https://api.semanticscholar.org/CorpusID:210721338
[48] Huijbregts, M. A. J. *et al.*, “ReCiPe 2016 v1.1: A harmonized life cycle impact assessment method at midpoint and endpoint level. Report I: Characterization,” National Institute for Public Health and the Environment (RIVM), Bilthoven, The Netherlands, 2016–0104a, 2016.
[49] P. Stavropoulos, C. Giannoulis, A. Papacharalampopoulos, P. Foteinopoulos, and G. Chryssolouris, “Life Cycle Analysis: Comparison between Different Methods and Optimization Challenges,” *Procedia CIRP*, vol. 41, pp. 626–631, 2016, doi: 10.1016/j.procir.2015.12.048.
[50] J. Szargut, *Termodynamika*, 7th ed. Warsaw, Poland: Polish Scientific Publishers PWN, 2013.
[51] S. Morais, T. M. Mata, A. A. Martins, G. A. Pinto, and C. A. V. Costa, “Simulation and life cycle assessment of process design alternatives for biodiesel production from waste vegetable oils,” *Journal of Cleaner Production*, vol. 18, no. 13, pp. 1251–1259, Sep. 2010, doi: 10.1016/j.jclepro.2010.04.014.

[52] Z. Chen, Q. Shen, N. Sun, and W. Wei, “Life cycle assessment of typical methanol production routes: The environmental impacts analysis and power optimization,” *Journal of Cleaner Production*, vol. 220, pp. 408–416, May 2019, doi: 10.1016/j.jclepro.2019.02.101.
[53] University of Maine, “Calendar of Apple Orchard Management Activities,” Cooperative Extension: Garden and Yard. Accessed: Oct. 18, 2024. [Online]. Available: https://extension.umaine.edu/gardening/manual/calendar-apple-orchard-management-activities/
[54] Y.-K. Park and B.-S. Kim, “Catalytic removal of nitrogen oxides (NO, NO2, N2O) from ammonia-fueled combustion exhaust: A review of applicable technologies,” *Chemical Engineering Journal*, vol. 461, p. 141958, Apr. 2023, doi: 10.1016/j.cej.2023.141958.
[55] Y. Jung *et al.*, “Nitrous oxide in diesel aftertreatment systems including DOC, DPF and urea-SCR,” *Fuel*, vol. 310, p. 122453, Feb. 2022, doi: 10.1016/j.fuel.2021.122453.
[56] F. Posada, S. Chambliss, and K. Blumberg, “Costs of emission reduction technologies for heavy-duty diesel vehicles,” The International Council on Clean Transportation, 2016.
[57] “Alternative Fuels Data Center,” U.S. Department of Energy, Energy Efficiency & Renewable Energy. Accessed: Jan. 23, 2025. [Online]. Available: https://afdc.energy.gov/fuels/prices.html
[58] B. Shiozawa, “The Cost of CO2-free Ammonia,” Ammonia Energy Association. Accessed: Jan. 23, 2025. [Online]. Available: https://ammoniaenergy.org/articles/the-cost-of-co2-free-ammonia/
[59] Y. Seo *et al.*, “Technical–Economic Analysis for Ammonia Ocean Transportation Using an Ammonia-Fueled Carrier,” *Sustainability*, vol. 16, no. 2, p. 827, Jan. 2024, doi: 10.3390/su16020827.
[60] E. Vartiainen *et al.*, “True Cost of Solar Hydrogen,” *Solar RRL*, vol. 6, no. 5, p. 2100487, May 2022, doi: 10.1002/solr.202100487.
[61] J. R. Bartels, “A feasibility study of implementing an Ammonia Economy,” Master of Science, Iowa State University, Digital Repository, Ames, 2008. doi: 10.31274/etd-180810-1374.
[62] “Annual Energy Outlook 2023 Table: Table 12. Petroleum and Other Liquids Prices,” U.S. Energy Information Administration. Accessed: Jan. 24, 2025. [Online]. Available: https://www.eia.gov/outlooks/aeo/data/browser/#/?id=12-AEO2023&region=0-0&cases=ref2023&start=2021&end=2050&f=A&linechart=ref2023-d020623a.3-12-AEO2023~&map=&ctype=linechart&sourcekey=0
[63] “Annual Energy Outlook 2023 Table: Table 13. Natural Gas Supply, Disposition, and Prices,” U.S. Energy Information Administration. Accessed: Jan. 24, 2025. [Online]. Available: https://www.eia.gov/outlooks/aeo/data/browser/#/?id=13-AEO2023&cases=ref2023&sourcekey=0
[64] IEA, “Levelised Cost of Electricity Calculator.” Accessed: Jan. 24, 2025. [Online]. Available: https://www.iea.org/data-and-statistics/data-tools/levelised-cost-of-electricity-calculator

[65] IEA, “Projected Costs of Generating Electricity 2020,” Paris, 2020. [Online]. Available: https://www.iea.org/reports/projected-costs-of-generating-electricity-2020
[66] AACE International, “Cost Estimate Classification System – As Applied in Engineering, Procurement, and Construction for the Process Industries,” AACE International, Recommended Practice 18R-97, rev 2016.

Appendix

Paper I

ASME Journal of Energy Resources Technology
Online journal at:
https://asmedigitalcollection.asme.org/energyresources

Life Cycle Assessment of Selected Ammonia Production Technologies From the Perspective of Ammonia as a Fuel for Heavy-Duty Vehicle

Mateusz Proniewicz[1]
Department of Thermal Technology,
Silesian University of Technology,
Konarskiego 22,
Gliwice 44-100, Poland
e-mails: Mateusz.Proniewicz@polsl.pl;
mproniewicz@polsl.pl

Karolina Petela
Department of Thermal Technology,
Silesian University of Technology,
Konarskiego 22,
Gliwice 44-100, Poland
e-mail: karolina.petela@polsl.pl

Andrzej Szlęk
Department of Thermal Technology,
Silesian University of Technology,
Konarskiego 22,
Gliwice 44-100, Poland
e-mail: Andrzej.Szlek@polsl.pl

Wojciech Adamczyk
Department of Thermal Technology,
Silesian University of Technology,
Konarskiego 22,
Gliwice 44-100, Poland
e-mails: Wojciech.Adamczyk@polsl.pl;
wadamczyk@polsl.pl

One of the promising options for the decarbonization of industry dependent on heavy-duty vehicles is to use alternative fuels such as ammonia. The study investigates the environmental impact of five selected ammonia production technologies and compares them to diesel fuel: ammonia based on hydrogen from steam methane reforming (gray), ammonia based on steam methane reforming with carbon capture and storage (blue), ammonia based on hydrogen from electrolysis with electrical energy supplied by: PV (green PV), wind (green wind), and nuclear plant (pink). Environmental impact is assessed using the ReCiPE method based on three midpoint and two endpoint categories: climate change, fossil depletion, freshwater consumption, human health, and ecosystem quality. The climate change results per 1 MJ (LHV) are as follows: gray ammonia at 0.148 kg CO_2 eq., blue ammonia at 0.0701 kg CO_2 eq., green ammonia PV at 0.0197 kg CO_2 eq., green ammonia wind at 0.01039 kg CO_2 eq., pink ammonia at 0.00565 kg CO_2 eq., and diesel (including its stoichiometric combustion) at 0.0851 kg CO_2 eq. The life cycle assessment (LCA) was performed using the LCA FOR EXPERTS (GaBi) software, with Sphera's comprehensive Managed LCA Content as the primary data source for the life cycle inventory. The study indicates nuclear and renewable-based routes to be the best options in terms of the climate change and human health categories; however, their high impact on freshwater consumption and ecosystem quality is revealed. Still, ammonia is proven to be an effective solution toward decarbonization, as compared to diesel, given its blue, green, or pink source. [DOI: 10.1115/1.4064371]

Keywords: life cycle assessment, diesel, ammonia, renewable energy, sustainability, alternative energy sources

1 Introduction

The climate crisis is the primary driver behind the current environmental policies aiming at decarbonization. According to the Intergovernmental Panel on Climate Change (IPCC), global warming is likely to reach 1.5 °C compared to 1850–1900 under intermediate, high, and very high GHG emissions scenarios [1]. One of the solutions to manage global warming is to substitute fossil fuels with alternatives such as ammonia. Ammonia is widely used as fertilizer, refrigerant, and chemical feedstock, contributing to 1.2% of total primary energy consumption and 1% of global greenhouse gas (GHG) emissions as of 2018 [2]. It is regarded as a promising fuel due to its high hydrogen content, the possibility to store and transport at low pressure (unlike hydrogen, which requires pressurizing to ca. 700 bar or cooling to a temperature of ca. −253 °C), and the possibility to transfer it through existing pipeline infrastructure with minor modifications and suitability for various applications such as combustion engines. Although the energy content of hydrogen on a mass basis is around six times higher than that of ammonia, its energy content on a volume basis (MJ/l) is ca. 1.5 times lower. A comparison of these properties is presented in Table 1.

Transportation, agriculture, and construction are the sectors that strongly depend on machinery fueled by diesel fuel—whereas the passenger vehicles are being electrified, this solution does not apply well for heavier vehicles like trucks, tractors, etc., due to the characteristics of the operation of heavy-duty vehicles: they require high power output and must be able to cover an acceptable range of distance. As such, ammonia seems to be a promising solution toward decarbonization for such cases; however, if the energy intensity of the production phase of the ammonia is too high, the switch of fuel in the engine from diesel to ammonia will not

[1]Corresponding author.

Contributed by the Advanced Energy Systems Division of ASME for publication in the JOURNAL OF ENERGY RESOURCES TECHNOLOGY. Manuscript received July 13, 2023; final manuscript received October 3, 2023; published online January 22, 2024. Assoc. Editor: Pawel Gladysz.

Table 1 Selected properties of ammonia and hydrogen as fuels, based on Ref. [3]

Fuel	Mass energy content (LHV), MJ/kg	Volume energy content (LHV), MJ/l	Density, kg/m^3
Cooled ammonia (liquefied, 1 atm, −33 °C)	18.6	12.69	682
Cooled hydrogen (liquefied, 1 atm, −253 °C)	120	8.5	70.85

achieve its goal—the surplus of emissions required for producing the ammonia might equal or exceed the avoided emissions in the operation phase of the tractor. Therefore, the investigation of the ammonia production cycle, from the perspective of ammonia as a fuel for the internal combustion engine, is required.

In recent years, several researchers reported the environmental impact of producing ammonia or hydrogen (which is essential for the production of ammonia through a Haber-Bosch process). Bhandari et al. [4] presented a review paper regarding hydrogen production through electrolysis identifying crucial process chains, indicating the global warming potential along with acidification potential to be the most often analyzed environmental categories. Koroneos et al. [5] conducted a comparative analysis of hydrogen production processes, namely steam reforming and electrolysis, using a functional unit of 1 MJ. The authors concluded that wind, hydropower, and solar thermal energy were the most favorable options due to the high CO_2 emissions associated with steam reforming and the unfavorable manufacturing process of PV solar panels. Lubis et al. [6] presented a life cycle assessment (LCA) of hydrogen production based on thermochemical water splitting (Cu–Cl) with heat supplied from the nuclear plant for 1 h of operation of the plant using the literature data for inventory analysis. The study revealed the construction phase of both nuclear plants and hydrogen plants to be major contributors to the environment, assessed through CML-2001 impact categories. Cetinkaya et al. [7] performed an LCA of five hydrogen production technologies, namely steam reforming of natural gas, coal gasification, water electrolysis from wind and solar, and thermochemical water splitting with a Cu–Cl cycle, for the case study of Toronto, Canada. The paper showed the lowest CO_2 eq. emissions for thermochemical water splitting, followed by wind and solar. In terms of the hydrogen production capacity, thermochemical splitting achieved values similar to methane reforming or coal gasification, contrary to wind and solar, which were suited for smaller capacities. Hacatoglu et al. [8] also focused on the LCA of nuclear-based copper–chlorine hydrogen production cycle. The assessment compared thermochemical hydrogen production obtained from nuclear with natural gas and renewable-based sources as well as gasoline in terms of 1 MJ of fuel with respect to energy return on investment (EROI) and mechanical efficiency of the internal combustion engine (in the case of gasoline) and fuel cells (for hydrogen). The authors concluded that nuclear-driven thermochemical hydrogen production seemed to be a promising technology as it utilized less fossil energy consumption than gasoline- or natural gas–based production pathway with GHG emissions similar to renewable-based sources (EROI of nuclear-based hydrogen also yielded similar value to the wind-based hydrogen). Hajjaji et al. [9] analyzed the environmental impact of hydrogen production methods considering the fossil methane, biological methane, and bioethanol-to-hydrogen systems assuming steam reforming, partial oxidation, and autothermal reforming. The LCA was conducted using SIMAPRO software; the environmental assessment was based on the CML 2000 and Eco-indicator 99 methods. The results proved that biomethane generates the lowest environmental burden. Tetteh and Salehi [10] highlighted the advantages of blue hydrogen, suggesting this technology is the most promising for the near-term energy transition perspective. They compared it to other common fuel production pathways through LCA, utilizing the GREET model (greenhouse gases, regulated emissions, and energy use in technologies). The study indicated a need for improvements in terms of nitrous and sulfur oxides, as well as in carbon capture and storage (CCS) efficiency development. Chen et al. [11] presented the LCA of a fuel cell vehicle (based on the example of Toyota Mirai), considering both the vehicle and fuel cycle with hydrogen as the analyzed fuel. The authors showed that global warming potential is fairly high in all life cycle stages. As for the fuel cycle, electrolysis was obtained to be the preferred option for hydrogen production, given hydropower or wind power as the source of electrical energy.

Ghavam's review paper [12] provided a comprehensive overview of ammonia production methods, ranging from the traditional Haber-Bosch process, which utilizes hydrogen from methane reforming to more innovative approaches, such as the use of hydrogen obtained from water electrolysis. The paper highlighted the potential benefits of using electrolysis to reduce greenhouse gas emissions but also noted that this process requires a significant quantity of pretreated water. Bicer et al. [13] performed the life cycle assessment for the case of four different ammonia production methods with the ammonia produced by the Haber-Bosch process with hydrogen being obtained through electrolysis considering hydropower, nuclear, biomass, and municipal waste resources. The analysis referred to 1 kg of ammonia with an LCA model built in SIMAPRO 7 software. The study revealed that the production of ammonia using municipal waste and hydropower sources yielded better environmental performance compared to nuclear and biomass cases. Hydropower was found to be the most efficient option in terms of energy and exergy efficiencies, while the use of municipal waste was identified as having the least environmental impact. In a summary report, Dincer and Bicer [14] discussed ammonia as a fuel in general, going through its most important applications. Chapter 7: Ammonia in Road Transportation presents the life cycle assessment of vehicles, distinguishing fuel and vehicle cycles. The authors compared hydrogen, electric, ammonia, compressed natural gas (CNG), diesel, liquefied petroleum gas, hybrid electric, gasoline, and methanol-fueled vehicles through the global warming environmental category. SIMAPRO 7.2 was utilized to carry out the LCA with the CML 2001 environmental assessment method. The lowest values were demonstrated for hydrogen, electric, and ammonia scenarios. Lasocki [2] presented a comparison of the environmental assessment of ammonia produced through the Haber-Bosch process with hydrogen coming from steam methane reforming (SMR) or partial oxidation of heavy oil and compared them to conventional engine fuels, gasoline, and diesel oil. The most common fuel production processes were assumed: gasoline was produced from light fractions and diesel oil from medium–heavy distillates. The author used the SIMAPRO 7 software for the LCA model with Ecoinvent databases and showed that conventional ammonia production processes achieved worse environmental performance than diesel and gasoline processes and indicated nuclear electrolysis or underground coal gasification with carbon capture storage as a promising option for further development. Angeles et al. [15] conducted a study on the potential use of ammonia as an automotive fuel, with a focus on the energy-intensive production processes and the implementation of ammonia in hybrid systems. The authors presented a well-to-wheel LCA of four ammonia production processes, two of which were fossil fuel–based (steam reforming and partial oxidation) and two were biomass-based (cyanobacterial and willow-based processes), along with three secondary fuels (gasoline, diesel, and dimethyl ether). The analysis was conducted on a light-duty internal combustion engine vehicle (ICEV), with a functional unit of 1 km distance driven by the vehicle. Carbon and nitrogen footprints were proposed as environmental indicators for evaluating the fuel cycles. The study's key conclusion was that the shift to biomass-based ammonia production was favorable, while fossil fuel–based production achieved little benefit. Chisalita

et al. [16] analyzed the synthesis of ammonia using the Haber-Bosch process, comparing conventional and green hydrogen sources. The study evaluated hydrogen production from SMR with two CO_2 capture technologies, hydrogen from electrolysis, and iron-based chemical looping (CLH), using the ReCiPe method and GaBi software. The functional unit was one metric ton of ammonia produced. The authors concluded that the use of CLH instead of SMR could be a promising solution due to the reduction in GHG emissions, with a 15% decrease in natural gas consumption and a 60% reduction in energy consumption in the air separation unit (ASU) stream; however, it is associated with high emissions to water and soil. The authors suggested the use of electrolysis with renewable sources of electricity as a potential alternative. Singh et al. [17] presented the LCA of selected ammonia production methods using SIMAPRO software and 1 kg of ammonia as a functional unit and comparing the following sources of hydrogen: underground coal gasification, steam methane reforming, biomass gasification, solar PV, and wind energy–based electrolysis, through CML 2001 method. The study found that biomass-based and wind-based methods are the most environmentally benign, emphasizing the relatively high impact of PV-based ammonia on acidification, eutrophication, and human toxicity due to the hazardous substances required for the manufacturing of the cells. Karaca et al. [18] analyzed nuclear ammonia synthesis through several hydrogen production methods in an LCA perspective, namely, electrolysis, high-temperature electrolysis, and three-, four-, and five-step thermochemical Cu–Cl cycles, utilizing SIMAPRO software and investigating five environmental categories. High-temperature electrolysis proved to be the most environmentally benign, with the lowest impact on all categories. Tallaksen et al. [19] investigated the ammonia production cycle using wind power through a cradle-to-gate approach. SIMAPRO v7.3 with Ecoinvent v2 was used for the assessment, with 1 kg of nitrogen (anhydrous ammonia in a tank) as a functional unit. The paper examined several cases considering the relationship between the background system (regional energy system) and foreground system (demand and supply for ammonia production), showing the complexity of relations between the wind farm size and its cost, grid power costs, and the emissions from the grid, which would strongly impact the production of hydrogen for ammonia generation. Ren et al. [20] presented the LCA of ammonia production from pulverized coal entrained flow (PEF) gasification technology and compared it to anthracite fixed bed (AFB) gasification technology. Studies revealed that fossil depletion and global warming were the main contributors to the overall environmental burden, with coal mining, coal washing, and electricity as dominant factors, while the PEF technology showed superiority in reducing the environmental burden compared with AFB technology. Further comparison of ammonia synthesis routes to ammonia produced from green and blue hydrogen exposed the potential of carbon emission reduction ratios of 90.9% and 42.9%, respectively. Zhang et al. [21] compared three pathways for ammonia production: coal-based, coke oven gas–based, and natural gas–based routes, using a case study from China and industry data for inventory analysis, with a functional unit of 1 kg of liquid ammonia and GaBi software used for the analysis. Authors showed that the natural gas–based route achieves lower environmental impact considering the greenhouse effect, acidification, and fossil energy depletion, while the development of water slurry gasification could be an alternative for the coal-based intermittent gasification technology, which is currently the most common solution.

The general conclusion from this review confirms that renewable-based ammonia would be the preferred variant of ammonia production, and utilizing it as a fuel represents a significant advancement in the decarbonization of transportation, as well as other sectors, although the ultimate choice of the technology requires a thorough analysis and depends on multiple variables. This study focuses on the well-to-wheel environmental assessments of the selected ammonia production methods using LCA FOR EXPERTS (GaBi) software and its database, which collates specific industry data, thus reflecting real-life conditions. In cases where data were unavailable in the database, specific literature was employed. The LCA follows the ISO 14044 and International Reference Life Cycle Data System (ILCD) handbook approach [22]. The goal, scope, and life cycle inventory are detailed in Sec. 2.2, and life cycle impact assessment (LCIA) and interpretation are discussed in Secs. 3 and 4. The assessment follows the attributional modeling, which focuses on determining the environmental impacts of a specific product as it exists in the current market. The analysis indicates the most environmentally benign method based on factual up-to-date data.

2 Materials and Methods

2.1 Overview of Ammonia Production Technology. This paper focuses on the Haber-Bosch process as the method of synthesizing ammonia, considering several sources of hydrogen. The considered cases in this work are as follows (color classifications are based on Ref. [23]):

(1) Gray hydrogen—based on steam methane reforming.
(2) Blue hydrogen—based on steam methane reforming with carbon capture and storage.
(3) Green hydrogen—based on water electrolysis supplied by electrical energy from photovoltaic or wind sources.
(4) Pink hydrogen—based on water electrolysis supplied by electrical energy from nuclear sources.

Subsequent subchapters provide an overall description of these technologies.

2.1.1 Haber-Bosch Process. The Haber-Bosch process is a recognized method of synthesizing ammonia due to its efficiency and ability to produce ammonia in large quantities. The process requires nitrogen (obtained from the air separation process) and hydrogen, which can be sourced from various methods. The reaction is exothermic, where hydrogen and nitrogen are combined at a 3:1 volume ratio in the presence of a catalyst. The reaction requires a temperature of 400 °C and a pressure of 150 bar [24]. It follows Eq. (1):

$$N_2 + 3H_2 \rightleftharpoons 2NH_3 \quad \Delta Hr^\circ = -92.4\,\text{kJ/mol} \tag{1}$$

where the heat of reaction, ΔHr°, is defined for standard conditions of 298 K and 1 atm. Since the nitrogen is available from the atmospheric air, the source of hydrogen determines the environmental impact of the ammonia production technology.

2.1.2 Steam Methane Reforming. SMR utilizes natural gas and water as feedstocks. About 30–40% of the gas is used for combustion, producing "diluted CO_2," while the remainder is converted to hydrogen and "process CO_2" [25]. The primary reaction for producing hydrogen is the endothermic conversion of methane and steam into carbon monoxide and hydrogen, as presented in Eq. (2):

$$CH_4 + H_2O \rightarrow CO + 3H_2 \quad \Delta Hr^\circ = +206.2\,\text{kJ/mol} \tag{2}$$

The process is conducted at a temperature range of around 700–850 °C and a pressure range of around 3–25 bar [26] under the presence of nickel catalysts. Then, water–gas shift reaction is used in order to obtain a higher H_2 share in the synthesis gas under iron or copper catalysts, according to Eq. (3):

$$CO + H_2O \rightarrow CO_2 + H_2 \quad \Delta Hr^\circ = -41.1\,\text{kJ/mol} \tag{3}$$

The complete technological chain with respect to synthesis gas includes also purification and/or CO_2 removal, methanation, and compression. Overall process efficiency is high, reaching up to 90%. Hydrogen processes through this method have a high purity of about 95–98% [27].

2.1.3 Steam Methane Reforming With Carbon Capture and Storage. Steam methane reforming technology is characterized

by high CO_2 emissions, present in both the synthesis gas and the furnace exhaust. A variety of technologies can be used for carbon capture; they can be generally classified as technologies that utilize:

- absorption (chemical or physical),
- adsorption (adsorbed beds or regeneration methods), and
- membrane (gas separation).

The selection of the technology is linked to the approach to CO_2 removal as there are three main options [26]:

(1) Post-combustion—the CO_2 is removed from the exhaust gas, which is a challenging option due to other impurities in the gas, dilute concentration of CO_2, and low pressure of exhaust (a common solution for this option is to use chemical solvents).
(2) Pre-combustion—the CO_2 is removed from the synthesis gas (which is the case of SMR + CCS technology) characterized by higher partial pressure of CO_2, which results in a better performance of separation and capture technologies.
(3) Oxyfuel-combustion—the combustion is performed with pure oxygen, resulting in the exhaust composition of CO_2 and H_2O (condensing water in the exhaust stream creates a pure CO_2 stream).

Capturing CO_2 from high-pressure synthesis gas can reduce emissions by up to 60%. If applied to the exhaust CO_2 emissions as well, approximately 90% emission reduction can be achieved [25]. The location of a plant using CCS technology also depends on storage options (e.g., storing in geological formations like gas fields) and transportation systems, such as pipelines and shipping.

2.1.4 Electrolysis. Electrolysis is a process of splitting the water into hydrogen and oxygen due to electrical voltage, according to Eq. (4):

$$H_2O + \text{voltage} \rightarrow H_2 + 0.5O_2 \quad \Delta Hr^\circ = +285.8\,\text{kJ/mol} \qquad (4)$$

There are a few methods of performing electrolysis, with alkaline electrolysis being the most popular, where the electrolyzer is constructed of two electrodes immersed in an aqueous KOH solution, and an ion-permeable separator is used to collect the gases in separate reservoirs. Alkaline electrolysis is characterized by an operating pressure of 1–30 bar and a temperature range of 60–80 °C. The average efficiency of the electrolysis process ranges between 60% and 81%, and the purity of obtained hydrogen is higher than 99.9% [28]. Electrolysis has the potential to be utilized effectively if waste heat from other processes is harnessed to elevate the water temperature. This can reduce the electrical energy demand, a concept known as high-temperature electrolysis. However, an important factor to be mindful of regarding the limitations of this technology is water consumption. To illustrate, if electrolysis were to completely replace current hydrogen production methods, it would require approximately double the water amount used in the SMR process for hydrogen production [25].

2.2 Life Cycle Assessment. The aim of the LCA is to evaluate and compare the environmental impacts of ammonia production methods considering several hydrogen sources in a cradle-to-gate approach. The functional unit is set as 1 MJ of lower heating value. The energy content was chosen as the functional unit because ammonia is analyzed as a fuel for internal combustion engines, allowing for a consistent comparison with other fuels. Ammonia is then compared to diesel, the fuel typically used in heavy-duty vehicles. LCA FOR EXPERTS (GaBi) software was used for the assessment due to its extensive database and the variety of options available for the analysis. A vast discussion regarding its advantages has been performed by Spatari et al. [29]. Subsequent subchapters describe the specific assumptions and sources of inventory for the analyses.

2.2.1 Gray and Blue Ammonia Production Models. Environmental impacts generated by the production of ammonia through steam methane reforming, both with and without carbon capture and storage, are modeled based on the LCA FOR EXPERTS (GaBi) database, specifically, Sphera's comprehensive Managed LCA Content (GaBi Professional Database). The impacts are modeled using the following processes:

(1) RER: Ammonia (NH_3) production mix, without CO_2 recovery
(2) RER: Ammonia (NH_3) synthesis with CO_2 recovery

Both processes are complete models of producing ammonia in a cradle-to-gate approach, using hydrogen obtained through steam methane reforming, covering the phases from the extraction of raw materials to the ready product, which is anhydrous ammonia. The models utilize data representative for Europe (RER). The schematic layout of a boundary system with major inputs/outputs is presented in Fig. 1. The inventory is primarily based on industry data from specific facilities, with supplementary data from the literature, environmental reports, or governmental statistics being used if needed. The quality of data is ensured by the technical and methodological assessment performed in regard to data quality indicators concerning technical, time-related, and geographical representativeness, completeness, methodological appropriateness with consistency, and uncertainty/precision. Each indicator is assessed on a five-level scale ranging from very poor to very good. The overall quality indicator for representing the environmental impact of gray and blue ammonia is defined as good, based on the process documentation described in the Managed LCA Content (GaBi Databases) available on the Sphera website [30].

Each process in the database is treated as a black box, meaning only the elementary flows (materials, energy requirements, and emissions) are available to the software user. However, it is not possible to analyze which component of ammonia production, throughout its technological chain, is the most crucial. The two models use identical assumptions. However, for gray ammonia production, the CO_2 emissions from the SMR are treated as emissions to air, not as a by-product.

2.2.2 Green Ammonia Production Model. Ammonia produced through electrolysis is modeled in the software, primarily drawing from literature. Figure 2 presents the scope, showcasing a case that utilizes a PV source of electrical energy. The other two considered cases of electrical energy for powering the electrolysis are wind energy and nuclear energy, which use an analogous approach, with the only difference being the source of electrical energy for electrolysis. Table 2 specifies the most important information about the processes used in the analysis. Generally, the electrolysis process and ammonia synthesis follow the energy/material requirements proposed in the literature, whereas the subprocesses are modeled based on the software database.

The exothermic reaction of ammonia synthesis in the Haber-Bosch process, as shown in Eq. (1), maintains the process; however, initial heating and pressurizing of reactants to the desired conditions is required. Moreover, the process is conducted in a recycle loop since single pass conversion of hydrogen and nitrogen into ammonia is characterized by a low efficiency. The overall conversion factor depends on the specific plant operation; in this work, 98% is assumed, meaning that 2% of hydrogen input to the plant is emitted into the atmosphere. The electricity requirement specific in Table 2 is considered to cover both the electrolysis itself and supplementary electrical energy consumption in the Haber-Bosch process. Sundin [31] proposed potassium hydroxide as the electrolyte; however, it is excluded from the analysis due to its unavailability in the software's database. Nevertheless, verifying its impact on the results, as presented in Ref. [31], its omission is acceptable since energy input for electrolysis, followed by raw materials for electrolyzer manufacturing and water for electrolysis dominate the impact of the technology on all environmental categories.

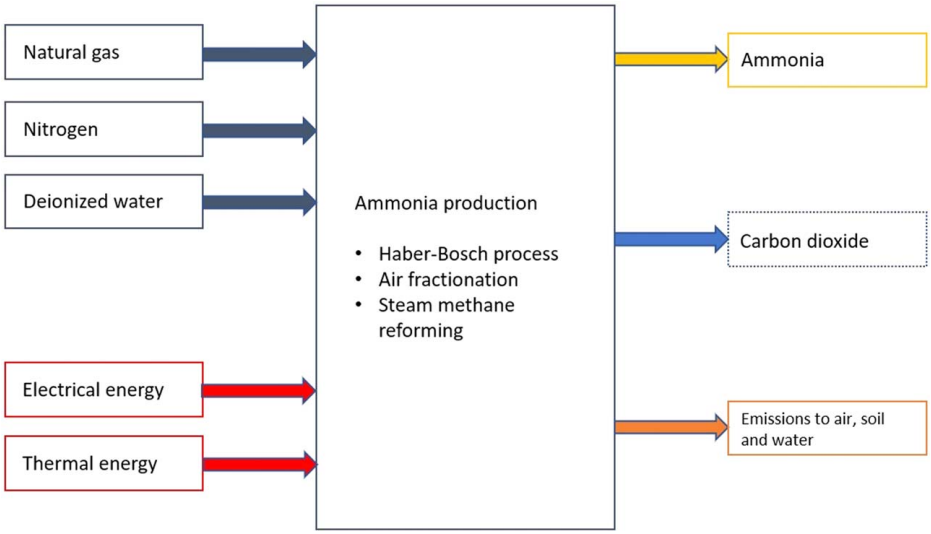

Fig. 1 Scheme of a boundary system for analyzed gray/blue ammonia production method based on Ref. [30]

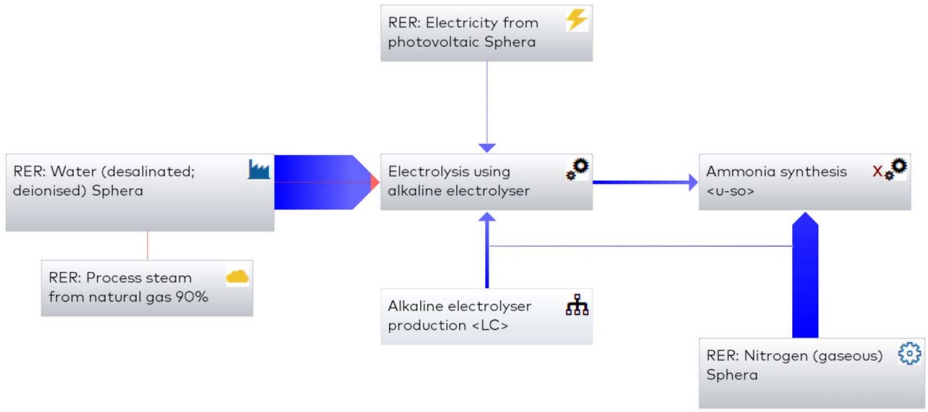

Fig. 2 Green ammonia model with alkaline electrolyzer utilizing PV source of electrical energy (screenshot from LCA FOR EXPERTS (GaBi) software)

Table 2 Green ammonia model—process characterization

Process	Source	Scope/comment	Data quality	Region
Electricity from photovoltaic	Software database	Production of electrical energy from PV. Manufacturing and operation phases are included with operational life time of the panels 30 years.	Good	Europe
Electricity from wind power	Software database	Production of electrical energy from wind turbines based on averaged onshore and offshore wind models including manufacturing, transportation, installation, operation, dismantling, and removal of the wind turbines.	Good	Europe
Electricity from nuclear	Software database	Production of nuclear energy based on mix of pressure water and boiling water reactors. Life cycle of infrastructure and fuel (uranium) including end-of-life phases.	Good	Europe
Water (desalinated; de-ionized)	Software database	De-ionization and desalination through ion exchange applied on tap water from groundwater.	Good	Europe
Process steam from natural gas 90%	Software database	Steam production in heat plants based on natural gas. Heat plant efficiency, fire technology, flue-gas desulfurization, NOx removal, and de-dusting norms at the national and regional levels are included.	Good	Europe
Nitrogen (gaseous)	Software database	Nitrogen production in a cryogenic separation of air (Linde process).	Good	Europe
Electrolysis	Literature	Water: 9 kg/kg H_2 [17] Electricity required: 53 kWh/kg H_2 [17] Nitrogen: 0.00029 kg/kg H_2 [31] KOH: 0.019 kg/kg H_2 [31] Steam: 0.11 kg/kg H_2 [31]	–	Global
Ammonia synthesis	Literature	Hydrogen to nitrogen 3:1 volume ratio [17], 98% conversion factor.	–	Global

Table 3 Inputs for alkaline electrolyzer—process characterization

Input	Scope/comment	Data quality	Region
Copper	Copper production through cradle-to-gate inventory based on pyrometallurgical, pyrometallurgical, and hydrometallurgical manufacturing routes.	Good	Global
Stainless steel sheet	Primary production steps in an electric steel making plant (with major process being the melting of stainless steel scrap in the electric arc furnace).	Good	Europe
Nickel	Production of class 1 nickel through cradle-to-gate inventory (including mining, beneficiation and ore preparation, extraction, refining, and transport phases.	Good	Global
Aluminum sheet	Aluminum sheets production by rolling process with data collection including production of alumina, primary aluminum, extrusion, and process scrap remelting.	Good	Europe
Polyvinyl chloride sheet	Polyvinyl chloride sheets manufacturing including cradle-to-gate inventory (with major technological processes being polymerization, blending and extrusion, calendering, cooling, and cutting).	Not evaluated	Europe
Acrylonitrile butadiene styrene	Acrylonitrile Butadiene Styrene (ABS) production based on averaged data including emulsion polymerization, bulk polymerization, or a combination of methods.	Not evaluated	Europe
Aniline	Aniline production through cradle-to-gate inventory via catalytic hydrogenation of nitrobenzene.	Good	Europe
Purified terephthalic acid	Terephthalic acid production, based on cradle-to-gate inventory, via oxidizing p-xylene in air with a catalyst of metal salts.	Good	Europe
Nitric acid	Nitric acid manufacturing in a cradle-to-gate approach, produced from the oxidation of ammonia with air.	Good	Europe
Hydrochloric acid	Hydrochloric acid production considering mix of technologies by-product of chlorination and halogen exchange reactions (e.g., production of methanol).	Very good	Germany
Lubricant oil	Lubricant oil production as a product of a refinery plant covering entirely supply chain from well drilling, crude oil production, and processing.	Good	Europe
Carbon monoxide	Carbon monoxide production via synthesis gas cryogenic separation (by-product hydrogen) through cradle-to-gate inventory.	Good	Germany
Gypsum plaster	Gypsum plaster production from raw material extraction to manufacturing, based on the beta-hemihydrate gypsum generation in a calcination of calcium sulfate dihydrate to hemihydrate.	Good	Europe
Water (desalinated; de-ionized)	Same as in Table 2.		
Electricity grid mix	Electrical energy production averaged from the mix of 28 European countries, covering main activity producers and autoproducers as well as electricity imports.	Good	Europe
Thermal energy from natural gas	Thermal energy production from natural gas specific heat plants averaged for 28 European countries accounting for specific technology standards such as efficiency, firing technology, flue-gas desulfurization, NOx removal, and de-dusting in respective countries.	Good	Europe
Process steam from natural gas 90%	Same as in Table 2.		

The life cycle inventory for the alkaline electrolyzer is presented in Table 3. The inventory for the alkaline electrolyzer production was primarily aggregated by Ref. [32] and then recalculated per 100 kg H2 by Ref. [31], considering the lifetime of the electrolyzer. Table 3 presents the key information about the upstream processes that constitute the manufacturing phase of the alkaline electrolysis, i.e., it aggregates the input flows. For instance, the first row shows the input "copper," which means that a complete process of copper production, considering its environmental impact, is embedded into the model. Table 3 does not specify the exact values used in the model since they follow the values presented by Ref. [31]. However, due to the complexity of the inventory, not all materials and processes were included in the model, as compared to the data presented in Refs. [31,32]. Specifically, some processes were not available in the software database. Nevertheless, since the share of those materials is relatively small (mass basis), it is assumed that the omission does not impact the results in any important way. The highest shares in the material inventory belong to steel and water, and the sum of all omitted materials constitutes less than 1%.

The production phase of equipment and machinery for the Haber-Bosch process was excluded from the system boundaries. Omission of infrastructure is, however, a common approach when analyzing the plants for which the emissions occur mostly during its operation (throughout the lifetime of technology, the relevance of infrastructure decreases as for each year the plant operates for a certain number of hours at given capacity, whereas the construction of infrastructure is performed a single time). Since the infrastructure for the Haber-Bosch process is not mentioned in the process documentation [30], it is considered to be outside of the boundary system, and therefore, the omissions of this infrastructure for the green ammonia model are consistent. Still, if the environmental impact generated due to the production and construction of the machinery were included in the models, the obtained values for each technology would be higher by the same difference as the Haber-Bosch process is a common process for all of the technologies. Therefore, the omission does not impact the conclusions based on the results at all, as the primary goal of the analysis is to compare the technologies and obtain the differences between these technologies rather than the absolute values.

2.2.3 Diesel Production Model. Since the objective of this work is to assess the ammonia production methods considering it as an alternative to diesel, diesel production technology is also examined. The environmental impact of diesel production is analyzed using the process detailed in Sphera's comprehensive Managed LCA Content: Diesel mix at the refinery. This process encompasses the entire supply chain of refinery products. The model incorporates averaged data from 28 European countries, which is characterized by good overall quality.

The schematic layout of the system boundary for the refinery plant is presented in Fig. 3. Since refinery plants are complex units, they include multiple processes of crude oil treatment, resulting in a set of products. Some major processes within a refinery plant, related to diesel production, include atmospheric and/or

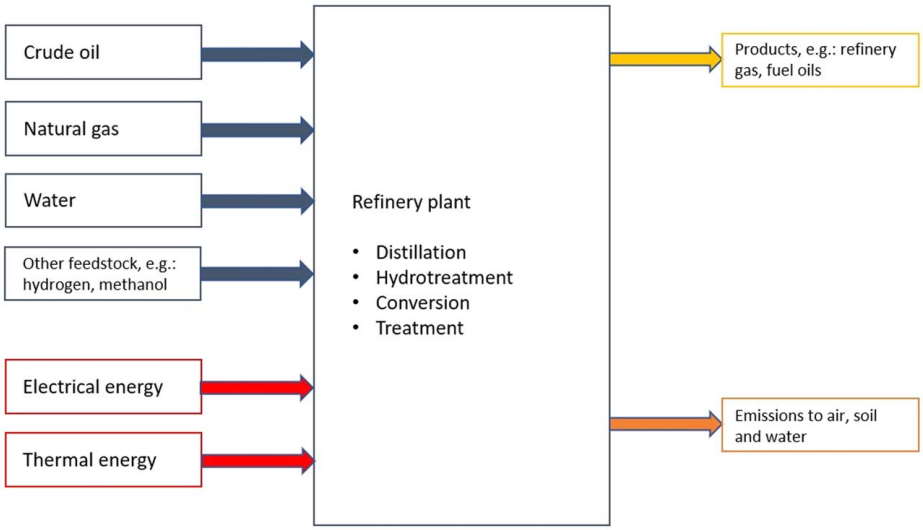

Fig. 3 Scheme of a boundary system for analyzed diesel production method based on Ref. [30]

vacuum distillation, desulfurization, cracking (hydrocracking and/or catalytic cracking), alkylation and polymerization, and blending. Detailed descriptions regarding the modeled processes within the refinery plant are available in the process documentation [30]. Depending on the type of crude oil being processed and the intended characteristics of the diesel being generated, different specific processing methods may be employed. The process employs allocation based on mass and net calorific value for its products; for example, lubricant oil is another product derived from the refinery plant.

2.3 Impact Categories. The environmental impact of the ammonia production methods is assessed through three midpoint and two endpoint categories from ReCiPe 2016 v1.1 method [33]:

(1) Midpoint: Climate Change—a measure of climate change caused by the emission of greenhouse gases that affect the radiative forcing capacity of Earth, causing an increase in global mean temperature, referred in kg CO_2 eq.
(2) Midpoint: Fossil Depletion—a measure of the reduction in future availability of fossil fuels caused by exploitation of these fuels in regard to the unit of product (production of 1 MJ of ammonia in this case), expressed in kg oil eq.
(3) Midpoint: Freshwater Consumption—a measure of water exploitation referred to as evaporation, incorporation into products and by-products or disposal to sea causing the loss in availability of freshwater for ecosystems, referred in m^3.
(4) Endpoint: Human Health—a value representing the number of years that are lost by a person due to the disease or accident, referred in DALYs (disability-adjusted life years).
(5) Endpoint: Ecosystem Quality—referred in species year as time-integrated species loss representing such loss at a local scale. It is divided between ecosystem quality considering terrestrial, freshwater, and marine ecosystems.

The choice of categories in the LCIA is arbitrary; however, it aims to enable a reliable comparison of the considered scenarios in alignment with the study's objectives. In this research, the ReCiPe method is adopted, since the endpoint categories account for many number of indicators. This can be perceived as a more rigorous approach, as it typically yields higher scores than methods like Eco-indicator 99 or IMPACT 2002+, as demonstrated by Ref. [34]. Three midpoint categories have been recognized to be the most important in terms of the comparison of ammonia to diesel, whereas the collective impact of various categories is aggregated within the endpoint categories, thus allowing for a more holistic assessment. The human health category encompasses the following midpoint categories: climate change, ozone depletion, ionizing radiation, fine particulate matter formation, photochemical ozone formation, cancer toxicity, non-cancer toxicity, and water use through characterization factors that reflect the impact of these categories on human health. Ecosystem quality: terrestrial category is constructed based on climate change, photochemical ozone formation, acidification, toxicity, water use and land use, ecosystem quality: fresh water based on climate change, eutrophication, toxicity and water use, ecosystem quality: marine uses eutrophication and toxicity midpoint categories [33]. The ReCiPe method defines also a third endpoint category, which is resource scarcity; however, it does not have a constant midpoint to endpoint factor, as it uses the absolute surplus ore potential, which is determined by the prices of minerals. Consequently, the endpoint category, as defined in Ref. [33], is expressed in dollars. Economic considerations are not discussed in this work, and therefore, the analysis is limited to the two endpoint categories.

The ReCiPe method distinguishes between three primary perspectives: individualistic, hierarchist, and egalitarian. The impact categories considered in this paper utilize the hierarchist perspective, which is rooted in the scientific consensus about the plausibility of impact mechanisms and operates under the assumption that the impact's timeframe spans 100 years. A thorough discussion regarding the ReCiPe method is presented in the RIVM Report 2016-0104a [33].

3 Results

The results of five ammonia production methods, compared to diesel regarding the three selected midpoint indicators, are presented in Fig. 4. Since each indicator is expressed in its own unit, a non-dimensional scale is used. Focusing primarily on the climate change category, among the ammonia production technologies, it is seen that the highest impact on climate change is achieved by gray ammonia, followed by blue, green PV, and green wind, with the lowest value obtained by the pink case. Collating these data with diesel production, it is seen that green wind and pink achieve actually a lower result, with the pink case achieving an impact nearly half that of diesel production. Diesel production has a relatively low climate change impact due to the difference in the lower heating values of diesel and ammonia (43.1 MJ/kg and 18.7 MJ/kg, respectively), implying a higher quantity of ammonia per 1 MJ. However, the major environmental impact of exploitation of the diesel comes from its combustion. As such, assuming diesel to be C12H24 and considering its stoichiometric combustion, a sum of

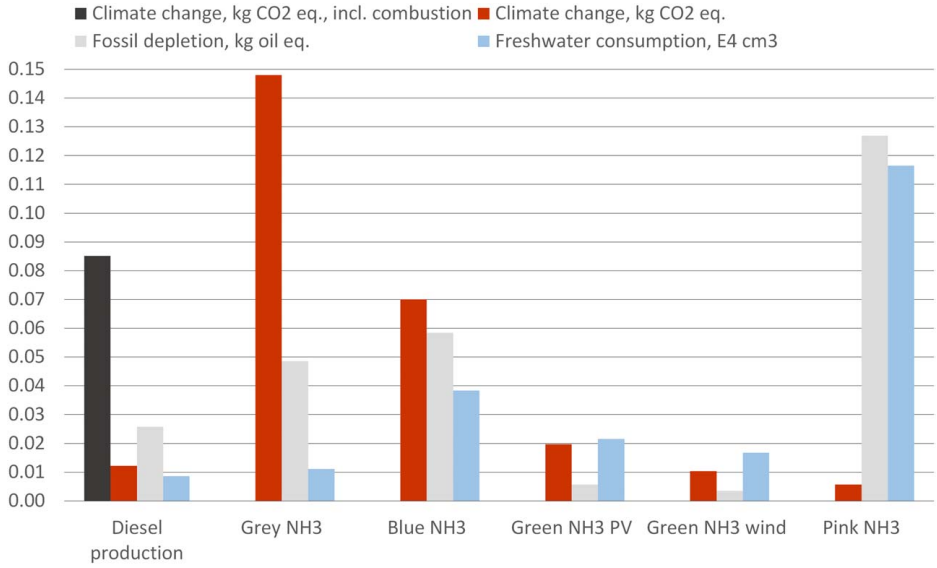

Fig. 4 Midpoint categories results per 1 MJ (LHV)

Table 4 Comparison of results for the climate change category in kg CO_2/kg NH_3

	Result	Singh et al. [17]	Zhang et al. [21]
Gray NH_3	2.768	3.032	1.900
Blue NH_3	1.311	–	–
Green NH_3 PV	0.368	1.277	–
Green NH_3 wind	0.194	0.496	–
Pink NH_3	0.106	–	–

its production and combustion is plotted on the chart using dark color. Naturally, the stoichiometry does not represent precisely the real emission of CO_2 since its specific emissions depend on a particular case, i.e., the engine, its power, and other characteristics. Still, it could be used as a useful estimate. Thus, gray ammonia is the only technology that affects climate change stronger than diesel, achieving nearly twice as much value as diesel including its combustion. It proves that utilizing ammonia produced from hydrogen generated via steam methane reforming is not environmentally benign. Blue ammonia generates considerably lower emissions but still achieves high impact since only "process CO_2" can be captured (explained in Sec. 2.1). Both green and pink methods are the preferred options, with green utilizing PV as the least favorable among these three. Fossil depletion is affected the least by both green methods, medium by diesel, gray, and blue cases, and in the strongest by pink ammonia that exploits fossil resources by ca. 2.5 times more than ammonia from steam methane reforming. Freshwater consumption is dominated by ammonia production using electrical energy from nuclear sources, which has a considerably higher impact than any other method. In contrast, the diesel case has the smallest impact on this category.

Table 4 presents specific results for climate change, recalculated per 1 kg of NH_3, compared to values from other researchers. The values calculated in this study generally correspond to the data reported by other researchers; however, specific values differ due to the assumptions regarding the boundary system for a given technology (e.g., whether plant construction and facility decommissioning are included), source of life cycle inventory, as well as methodology.

Since both green and pink ammonia production technologies have been built from the subprocesses, it is possible to track shares of each subprocess contributing to a respective environmental impact, as presented in Fig. 5. As expected, all three midpoint categories depend on the environmental impact of the electrical energy

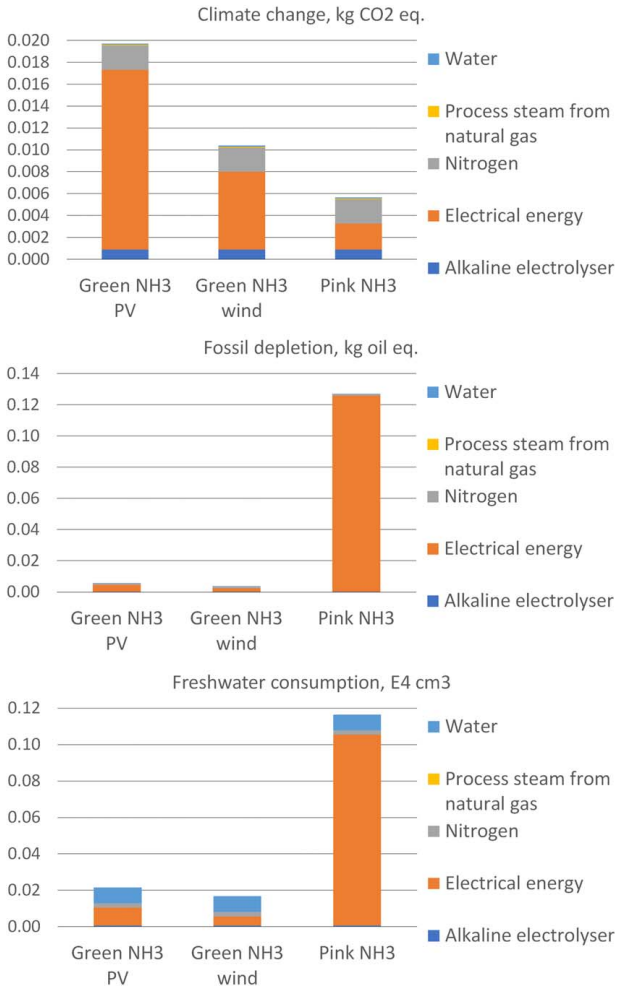

Fig. 5 Upstream processes' contributions on the selected midpoint categories for green PV, green wind, and pink ammonia

generation. Sphera's comprehensive Managed LCA Content indicates that nuclear electrical generation is the most environmentally benign in terms of climate change compared to PV or wind. This is mostly due to the environmental burden associated with the

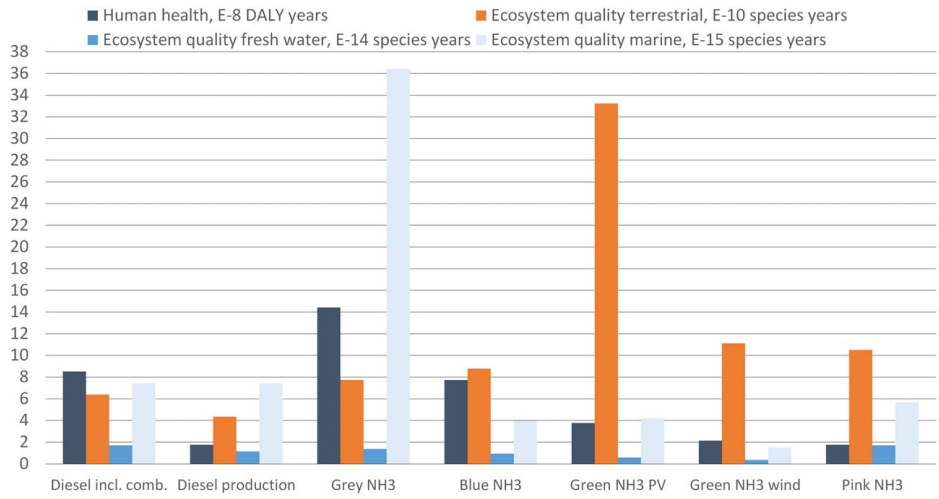

Fig. 6 Endpoint categories results per 1 MJ (LHV)

manufacturing of PV panels and wind turbines. However, in terms of the fossil depletion and freshwater consumption categories, it is clear that the exhaustion of uranium sources along with the water requirements for the plant generate a much higher impact than PV or wind. For both fossil depletion as well as freshwater consumption, the wind-based case achieves the lowest environmental impact.

The results of endpoint categories for the analyzed technologies are presented in the Fig. 6. The ecosystem quality indicator is divided between its impact on terrestrial, freshwater, and marine ecosystems for the purpose of a better visualization; however, the impact of the technologies on the ecosystem quality depends almost exclusively on the terrestrial ecosystem, as indicated by the units in the legend. When aggregating several midpoint categories related to human health, the general trend mirrors that of climate change. It is caused by the fact that climate change is the midpoint category that affects human health in the strongest way, which is seen in the Table 5. The lowest impact on human health is achieved by the pink ammonia followed by the green technologies: wind and PV. Diesel production also achieves a low value of climate change impact, but, as previously mentioned, it should be considered including its combustion. Gray ammonia presents the highest damage to human health caused primarily by high greenhouse gas emissions. Ecosystem quality terrestrial is affected in the strongest way by the green ammonia PV, which is caused by the exhaustion of the specific materials used for PV manufacturing. Green technology based on the wind, pink, blue, and gray ammonia follow, with the least impact caused by the diesel; however, the difference between the technologies is relatively small, apart from the green based on PV. As for the ecosystem quality regarding the fresh water, the differences between technologies are small, with the highest impact achieved by the diesel incl. its combustion and the lowest impact generated by green utilizing wind energy. In terms of marine ecosystem quality, gray ammonia has the strongest impact. Diesel incl. combustion follows with ca. 5 times lower value; the lowest impact is generated by green ammonia based on wind energy.

The value of an endpoint indicator depends on the specific midpoint indicator for a given technology and its characterization factor, as described in Ref. [33]. Tables 5 and 6 present the contribution of respective midpoint categories on the final value of human health and ecosystem quality for the terrestrial ecosystem. Beyond the climate change midpoint category, the endpoint analysis shows that fine particulate matter formation and cancer toxicity have the strongest impact on human health for both green and pink cases. Ecosystem quality is affected the strongest by the climate change and toxicity midpoint categories.

Phase contributions for green and pink models in regard to particulate matter formation, cancer toxicity, and ecosystem toxicity are presented in Fig. 7. The human toxicity category accounts for the toxicity (measure of human intake of a chemical and accumulation in a human food chain) in regard to cancerogenic non-cancerogenic substances. Terrestrial ecotoxicity accounts for the increase in the concentration of the chemicals leading to disappeared fraction of species. They are measured in kg 1.4-dichlorobenzene-equivalents (1.4-DB eq.). It is seen that fine particulate matter formation is dependent mostly on the source of electrical energy, alkaline electrolyzer phase follows. Cancer toxicity is determined primarily by the specific materials used for the alkaline electrolysis, with a considerable contribution from the wind energy caused by the specific emissions occurring during the life cycle of the wind turbines. Terrestrial ecotoxicity is defined similarly by

Table 5 Contribution of midpoint categories on the human health in DALY years

Midpoint category	Diesel incl. comb.	Diesel production	Gray NH_3	Blue NH_3	Green NH_3 PV	Green NH_3 wind	Pink NH_3
Climate change	7.91×10^{-08}	1.13×10^{-08}	1.38×10^{-07}	6.52×10^{-08}	1.83×10^{-08}	9.66×10^{-09}	5.26×10^{-09}
Ozone depletion	6.89×10^{-12}	6.89×10^{-12}	4.90×10^{-10}	1.23×10^{-10}	2.41×10^{-12}	1.38×10^{-12}	8.81×10^{-13}
Ionizing radiation	2.65×10^{-13}	2.65×10^{-13}	4.26×10^{-12}	9.86×10^{-12}	2.16×10^{-12}	2.28×10^{-12}	2.91×10^{-10}
Fine particulate matter formation	5.77×10^{-09}	5.77×10^{-09}	5.70×10^{-09}	1.10×10^{-08}	1.67×10^{-08}	7.99×10^{-09}	7.29×10^{-09}
Photochemical ozone formation	2.29×10^{-11}	2.29×10^{-11}	4.23×10^{-11}	7.66×10^{-11}	3.95×10^{-11}	1.53×10^{-11}	1.31×10^{-11}
Cancer toxicity	6.93×10^{-11}	6.93×10^{-11}	5.54×10^{-11}	6.96×10^{-11}	2.11×10^{-09}	3.41×10^{-09}	2.10×10^{-09}
Non-cancer toxicity	5.18×10^{-11}	5.18×10^{-11}	1.26×10^{-12}	2.11×10^{-12}	1.54×10^{-11}	4.07×10^{-12}	8.06×10^{-12}
Water use	1.88×10^{-10}	1.88×10^{-10}	2.44×10^{-10}	8.45×10^{-10}	4.73×10^{-10}	3.68×10^{-10}	2.56×10^{-09}

Table 6 Contribution of midpoint categories on the ecosystem quality terrestrial in species year

Midpoint category	Diesel incl. comb.	Diesel production	Gray NH_3	Blue NH_3	Green NH_3 PV	Green NH_3 wind	Pink NH_3
Climate change	2.38×10^{-10}	3.42×10^{-11}	4.14×10^{-10}	1.96×10^{-10}	5.52×10^{-11}	2.91×10^{-11}	1.58×10^{-11}
Photochemical ozone formation	3.47×10^{-12}	3.47×10^{-12}	6.12×10^{-12}	1.11×10^{-11}	5.71×10^{-12}	2.21×10^{-12}	1.90×10^{-12}
acidification	6.97×10^{-12}	6.97×10^{-12}	5.61×10^{-12}	1.11×10^{-11}	1.59×10^{-11}	8.53×10^{-12}	8.04×10^{-12}
Toxicity	3.49×10^{-10}	3.49×10^{-10}	3.40×10^{-10}	6.43×10^{-10}	3.24×10^{-09}	1.07×10^{-09}	1.01×10^{-09}
Water use	1.20×10^{-12}	1.20×10^{-12}	1.55×10^{-12}	5.38×10^{-12}	3.01×10^{-12}	2.34×10^{-12}	1.63×10^{-11}
Land use	3.93×10^{-11}	3.93×10^{-11}	5.97×10^{-12}	1.09×10^{-11}	7.04×10^{-12}	4.51×10^{-12}	2.17×10^{-12}

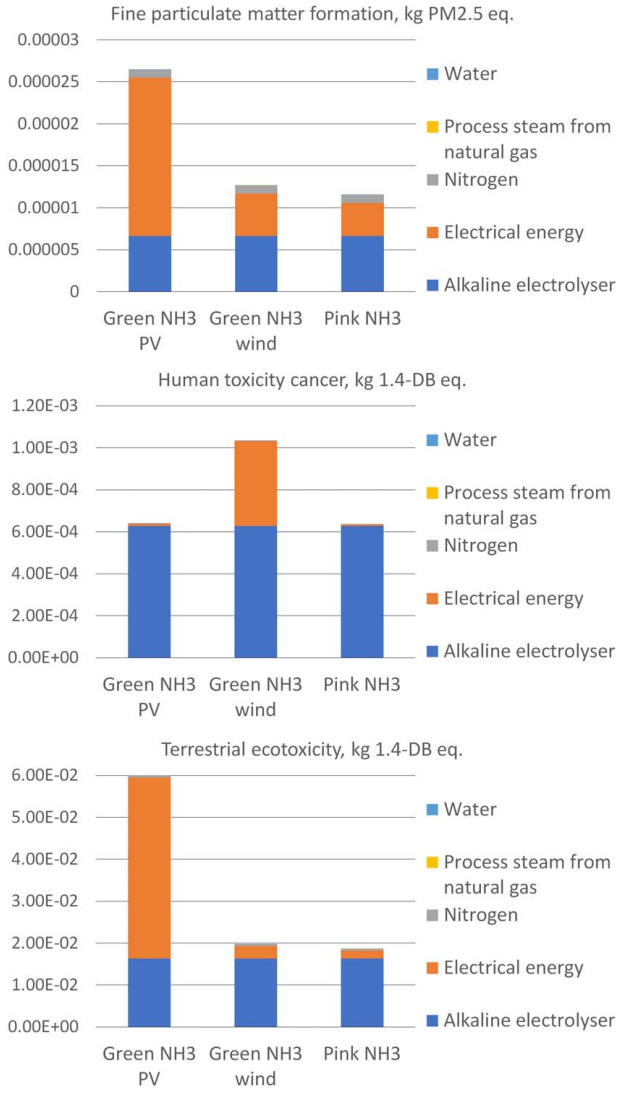

Fig. 7 Upstream processes' contributions on the additional midpoint categories for green PV, green wind, and pink ammonia

electrolyzer manufacturing and the source of electrical energy, with the life cycle of PV panels contributing to this category in the largest share.

The ISO 14044 and ILCD handbook approach [22] suggests normalization and weighting as additional steps. These can further refine the interpretation of results and provide a singular comparative score for the technologies. In this study, two selected endpoint ReCiPe categories are considered to represent the aggregated results, given multiple midpoint categories, in terms of their impact on human health as well as ecosystem quality. Normalization and weighting on these categories are not applied since the research aims at demonstrating both the strong and weak points of selected technologies rather than selecting a unique solution.

4 Conclusions

The unequivocal choice of the technology that could be considered to be the most environmentally benign is not a trivial task when conducting the LCA assessment. The ultimate decision as to which technology would be the most preferred depends on the specific criteria defined by the decision maker, typically involving a trade-off between environmental considerations and economic profitability. A promising approach toward linking these two criteria would be to consider the environmental costs occurring throughout the life cycle of the technology (such as damage to human health), with the main difficulty being the appropriate definition of such costs.

Based on the climate change criterion, which is addressed by essentially all researchers indicated in Sec. 1, the best option among the analyzed cases would be to select ammonia based on electrolysis using electrical energy from a nuclear source. However, its high impact on freshwater consumption, as well as fossil depletion (uranium), might be a limitation, e.g., when selecting the location of such plant under limited resource availability or freshwater scarcity. In such a case, green ammonia utilizing electrical energy from wind might be a better decision given its considerably lower impact on these two categories while still maintaining a relatively low climate change impact. Still, the freshwater consumption for electrolysis-based routes is roughly twice as much as for steam methane reforming. Comparing the ammonia technologies to diesel through a climate change perspective, as the major reason for developing alternative fuels is the negative effect of diesel production and its combustion, it is seen that all scenarios, apart from gray-based ammonia, achieve this aim, noting that blue ammonia generates little benefit. Analysis of the results of endpoint categories indicates that nuclear and wind-based ammonia achieve the lowest impact on human health; however, all of the ammonia technologies worsen the ecosystem quality compared to diesel, noting the especially high impact of PV energy on this category. As such, a need for improvement in terms of the PV life cycle and its manufacturing is revealed. Nevertheless, ammonia proves to be an interesting alternative compared to diesel fuel and could be used to mitigate the global warming issue.

The study's results, based primarily on the regularly updated data from Sphera's comprehensive Managed LCA Content, confirm that electrolysis-based ammonia is the most promising option. Future research could investigate high-temperature electrolysis and/or perform detailed investigation of ammonia production, given the intermittency of renewable sources (such as wind energy).

Acknowledgment

The research leading to these results has received funding from the Norway Grants 2014–2021 under POLNOR2019 competition operated by the National Centre for Research and Development and from Polish State Budget (Grant No. NOR/POLNOR/ACTIVATE/ 0046/2019-00).

Conflict of Interest

There are no conflicts of interest.

Data Availability Statement

The datasets generated and supporting the findings of this article are obtainable from the corresponding author upon reasonable request.

References

[1] Masson-Delmotte, V., Zhai, P., Pirani, A., Connors, S., Péan, C., Berger, S., Caud, N., et al., 2021, "IPCC, 2021: Summary for Policymakers," *Climate Change 2021: The Physical Science Basis. Contribution of Working Group I to the Sixth Assessment Report of the Intergovernmental Panel on Climate Change*, Cambridge University Press, Cambridge, United Kingdom and New York, NY, pp. 3–32.

[2] Lasocki, J., 2018, "Ammonia and Conventional Engine Fuels: Comparative Environmental Impact Assessment," E3S Web Conf., **44**, p. 00091.

[3] Klüssmann, J. N., Ekknud, L. R., Ivarsson, A., and Schramm, J., 2020, "Ammonia Application in IC Engines," IEA-AMF Technology Collaboration Programme on Advanced Motor Fuels.

[4] Bhandari, R., Trudewind, C. A., and Zapp, P., 2014, "Life Cycle Assessment of Hydrogen Production via Electrolysis—A Review," J. Cleaner Prod., **85**, pp. 151–163.

[5] Koroneos, C., Dompros, A., Roumbas, G., and Moussiopoulos, N., 2004, "Life Cycle Assessment of Hydrogen Fuel Production Processes," Int. J. Hydrogen Energy, **29**(14), pp. 1443–1450.

[6] Lubis, L. L., Dincer, I., and Rosen, M. A., 2010, "Life Cycle Assessment of Hydrogen Production Using Nuclear Energy: An Application Based on Thermo-Chemical Water Splitting," ASME J. Energy Resour. Technol., **132**(2), p. 021004.

[7] Cetinkaya, E., Dincer, I., and Naterer, G. F., 2012, "Life Cycle Assessment of Various Hydrogen Production Methods," Int. J. Hydrogen Energy, **37**(3), pp. 2071–2080.

[8] Hacatoglu, K., Rosen, M. A., and Dincer, I., 2012, "Comparative Life Cycle Assessment of Hydrogen and Other Selected Fuels," Int. J. Hydrogen Energy, **37**(13), pp. 9933–9940.

[9] Hajjaji, N., Pons, M. N., Renaudin, V., and Houas, A., 2013, "Comparative Life Cycle Assessment of Eight Alternatives for Hydrogen Production From Renewable and Fossil Feedstock," J. Cleaner Prod., **44**, pp. 177–189.

[10] Tetteh, D. A., and Salehi, S., 2023, "The Blue Hydrogen Economy: A Promising Option for the Near-to-Mid-Term Energy Transition," ASME J. Energy Resour. Technol., **145**(4), p. 042701.

[11] Chen, Yisong, Hu, Xu, and Liu, Jiahui, 2019, "Life Cycle Assessment of Fuel Cell Vehicles Considering the Detailed Vehicle Components: Comparison and Scenario Analysis in China Based on Different Hydrogen Production Schemes," Energies, **14**(15), p. 3031.

[12] Ghavam, S., Vahdati, M., Wilson, I. A. G., and Styring, P., 2021, "Sustainable Ammonia Production Processes," Front. Energy Res., **9**.

[13] Bicer, Y., Dincer, I., Zamfirescu, C., Vezina, G., and Raso, F., 2016, "Comparative Life Cycle Assessment of Various Ammonia Production Methods," J. Cleaner Prod., **135**, pp. 1379–1395.

[14] Dincer, I., and Bicer, Y., 2017, "Mitacs Accelerate Project Final Report Application Ref.: IT08015 Comprehensive Evaluation of NH_3 Production and Utilization Options for Clean Energy Applications," University of Ontario Institute of Technology.

[15] Angeles, D. A., Are, K. R. A. G., Razon, L. F., and Tan, R. R., 2017, "Carbon and Nitrogen Footprint Optimisation of Ammonia as an Automotive Fuel," Chem. Eng. Trans., **61**, pp. 271–276.

[16] Chisalita, D. A., Petrescu, L., and Cormos, C. C., 2020, "Environmental Evaluation of European Ammonia Production Considering Various Hydrogen Supply Chains," Renewable Sustainable Energy Rev., **130**, p. 109964.

[17] Singh, V., Dincer, I., and Rosen, M. A., 2018, "Chapter 4.2-Life Cycle Assessment of Ammonia Production Methods," *Exergetic, Energetic and Environmental Dimensions*, I. Dincer, C. O. Colpan, and O. Kizilkan, eds., Academic Press, Amsterdam, The Netherlands, pp. 935–959.

[18] Karaca, A. E., Dincer, I., and Gu, J., 2020, "A Comparative Life Cycle Assessment on Nuclear-Based Clean Ammonia Synthesis Methods," ASME J. Energy Resour. Technol., **142**(10), p. 102106.

[19] Tallaksen, J., Bauer, F., Hulteberg, C., Reese, M., and Ahlgren, S., 2015, "Nitrogen Fertilizers Manufactured Using Wind Power: Greenhouse Gas and Energy Balance of Community-Scale Ammonia Production," J. Cleaner Prod., **107**, pp. 626–635.

[20] Ren, K., Zhang, T., Tan, X., Zhai, Y., Bai, Y., Shen, X., Jia, Y., and Hong, J., 2021, "Life Cycle Assessment of Ammonia Synthesis Based on Pulverized Coal Entrained Flow Gasification Technology in China," J. Cleaner Prod., **328**, p. 129658.

[21] Zhang, Y., Liu, H., Li, J., Deng, Y., Miao, X., Xu, D., Liu, S., Xie, K., and Tian, Y., 2022, "Life Cycle Assessment of Ammonia Synthesis in China," Int. J. Life Cycle Assess., **27**(1), pp. 50–61.

[22] European Commission—Joint Research Centre—Institute for Environment and Sustainability, 2010, *International Reference Life Cycle Data System (ILCD) Handbook—Framework and Requirements for Life Cycle Impact Assessment Models and Indicators*, 1st ed., EUR 24586 EN, Publications Office of the European Union, Luxembourg.

[23] Lubbe, F., Rongé, J., Bosserez, T., and Martens, J. A., 2023, "Golden Hydrogen," Curr. Opin. Green Sustain. Chem., **39**, p. 100732.

[24] Darmawan, A., Aziz, M., Ajiwibowo, M. W., Biddinika, M. K., Tokimatsu, K., and Lokahita, B., 2022, "Chapter 5—Integrated Ammonia Production From the Empty Fruit Bunch," *Innovative Energy Conversion From Biomass Waste*, A. Darmawan, and M. Aziz, eds., Elsevier, New York, pp. 149–185.

[25] Future of hydrogen, 2019, "Seizing Today's Opportunities," Report Prepared by the IEA for the G20, Japan.

[26] Riis, T., Hagen, E. F., Vie, P. J. S., and Ulleberg, Ø, 2006, "Hydrogen Production and Storage: R&D Priorities and Gaps," IEA.

[27] Lejda, K., 2013, "Wodór w Aplikacjach do Środków Napędu w Transporcie Drogowym," Wydawnictwo KORAW.

[28] Brauns, J., and Turek, T., 2020, "Alkaline Water Electrolysis Powered by Renewable Energy: A Review," Processes, **8**(2), p. 248.

[29] Spatari, S., Betz, M., Florin, H., Baitz, M., and Faltenbacher, M., 2001, "Using Gabi 3 to Perform Life Cycle Assessment and Life Cycle Engineering," Int. J. Life Cycle Assess., **6**(2), pp. 81–84.

[30] Sphera., (n.d.), Managed LCA Content (GaBi Databases), https://sphera.com/life-cycle-assessment-lca-database/, Accessed April 1, 2023.

[31] Sundin, C., 2019, "Environmental Assessment of Electrolyzers for Hydrogen gas Production," Master's thesis, KTH Royal Institute of Technology School of Engineering Sciences in Chemistry, Biotechnology and Health.

[32] Koj, J., Wulf, C., Schreiber, A., and Zapp, P., 2017, "Site-Dependent Environmental Impacts of Industrial Hydrogen Production by Alkaline Water Electrolysis," Energies, **10**(7), p. 860.

[33] Huijbregts, M. A. J., Steinmann, Z. J. N., Elshout, P. M. F., Stam, G., Verones, F., Vieira, M. D. M., Hollander, A., Zijp, M., and van Zelm, R., 2016, "Recipe 2016 v1.1 a Harmonized Life Cycle Impact Assessment Method at Midpoint and Endpoint Level Report I: Characterization," National Institute for Public Health and the Environment.

[34] Stavropoulos, P., Giannoulis, C., Papacharalampopoulos, A., Foteinopoulos, P., and Chryssolouris, G., 2016, "Life Cycle Analysis: Comparison Between Different Methods and Optimization Challenges," Procedia CIRP, **41**, pp. 626–631.

Paper II

Hindawi
International Journal of Energy Research
Volume 2023, Article ID 9920670, 20 pages
https://doi.org/10.1155/2023/9920670

Research Article

Energy and Exergy Assessments of a Diesel-, Biodiesel-, and Ammonia-Fueled Compression Ignition Engine

Mateusz Proniewicz,[1] **Karolina Petela**,[1] **Andrzej Szlęk**,[1] **Grzegorz Przybyła**,[1] **Ebrahim Nadimi**,[1] **Łukasz Ziółkowski**,[1] **Terese Løvås**,[2] **and Wojciech Adamczyk**[1]

[1]*Department of Thermal Technology, Silesian University of Technology, Gliwice, Poland*
[2]*Department of Energy and Process Engineering, Norwegian University of Science and Technology (NTNU), Trondheim, Norway*

Correspondence should be addressed to Mateusz Proniewicz; mproniewicz@polsl.pl

Received 20 April 2023; Revised 27 June 2023; Accepted 7 July 2023; Published 14 August 2023

Academic Editor: Amin Paykani

The research is aimed at investigating ammonia in a compression ignition internal combustion engine as a promising alternative fuel towards decarbonization. This study presents energy and exergy assessments of a low-power engine for three cases of fuel supply, diesel oil, biodiesel oil, and ammonia with pilot biodiesel oil, across the entire engine's range. While diesel or biodiesel was administered directly into the engine cylinder, the ammonia was delivered through port injection. The results show that the maximum thermal efficiency of 33.56% and exergy efficiency of 31.88% were found at 1800 rpm and 71% load for the diesel fuel system. For the biodiesel fuel system, the efficiencies were 32.72% and 30.93%, respectively, at 1800 rpm and 100% load, and for the ammonia with pilot biodiesel system, they were at 31.98% and 30.04%, respectively, for the same rpm and load. The exergy assessment indicates that exergy destruction, which accounts for the irreversibility of processes such as combustion and friction, is responsible for the greatest loss of useful energy. Optimizing these processes could significantly improve the engine's performance for all three fuel cases. This research found that ammonia could successfully substitute diesel or biodiesel fuel, as the engine's efficiency was comparable in all three tested scenarios; however, further research and optimization in terms of the ammonia-fueled engine emissions are required.

1. Introduction

Reliability, durance, and high compressive resistance have made a diesel engine a preferred application in heavy-duty vehicles, commonly used in transportation, construction, agriculture, and other sectors. However, due to the negative effect of the use of fossil fuels on climate change, there is a need to develop alternative sources of energy to decrease the emissions of greenhouse gases. This conclusion has been summarized during the 2015 Paris Agreement, resulting in the aim of the European Union of at least 55% of greenhouse gas reduction by 2030 compared to 1990 (updated in December 2020). One option to substitute fossil diesel fuel is to use a biodiesel. Technically, biodiesel consists of a mono-alkyl ester of fatty acids, produced from animal fats or plant oils (feedstock) in a transesterification process [1]. There are two main advantages of this fuel from an environmental perspective. Firstly, it is a renewable source since it is produced from resources that are continuously replenished. Secondly, it is considered carbon-neutral because the plants used for a feedstock absorb carbon dioxide during growth, thereby offsetting the CO_2 emissions that occur due to the production and combustion of the fuel [1]. In the case of a lipid feedstock, defined as waste cooking oil or animal fats/tallow and grease, the life-cycle emissions are low since the feedstock has been produced in a nonrelated process [2]. Still, there are several drawbacks associated with biodiesel. Biofuel crops compete with plants that could be otherwise used for food production, in terms of land, material, and energy consumption. This competition could result in a negative impact of the biodiesel on the environment in terms of its life cycle, considering other environmental categories than CO_2 emissions, such as land use change. There have been clearance cases of natural vegetation and forests to

grow soybeans or palm oil trees [2]. Another disadvantage in terms of its wide commercialization is the high cost of the biodiesel compared to diesel, ranging from 70% to 130% higher, as noted by the European Federation for Transport and Environment in 2022 [3]. Another option to substitute the diesel is the use an alternative like hydrogen or ammonia. Ammonia is a promising fuel due to its high energy density (caused by high hydrogen content) and a possibility of being produced from renewable sources, since it is formed from hydrogen and nitrogen, where the hydrogen can be produced via electrolysis supplied by sustainable sources. Moreover, it does not emit carbon emissions during combustion, and it can be stored and transported at moderate pressures. While sustainability is an advantage characterizing both of these fuels, hydrogen requires pressurization to approximately 700 bar or cooling to a temperature of approximately -253°C, depending on whether it is stored in gaseous or liquid form. This makes it challenging to apply broadly in the transportation sector. Easier storage, lower flammability, and a possibility to detect the ammonia by smell are some of the other advantages of ammonia over hydrogen. Furthermore, it is widely used as a fertilizer (80% of ammonia production [4]), and therefore, it already has the established infrastructure for its handling. The use of ammonia in the internal combustion engine (ICE) is limited by the parameters that make it difficult to operate: high resistance to autoignition, low flame speed, and corrosivity. As such, currently, most research is focused on implementing ammonia in spark ignition engines [5]. Yet another option in terms of substituting diesel would be electrification; however, it does not apply well to heavy vehicles that require high power output along with an acceptable range of distance. One way to assess the feasibility of utilizing an alternative fuel in the internal combustion engine is to perform an energy assessment that is based on the first law of thermodynamics. It quantifies the energy flows within the system boundaries and, therefore, allows for the estimation of energy conversion and identification of losses occurring during the operation of the engine. However, it is the second law of thermodynamics that allows for a deeper understanding of system performance, performed by assessing the quality of respective flows by means of exergy. Exergy is defined as the useful work potential considering the reference state, otherwise called as availability [6]. Exergy assessment indicates the processes in which energy is degraded, thus revealing the lost opportunities to perform work. Energy and exergy analyses are both useful tools towards the assessment of engine performance as they provide the information regarding the engine's performance and sources of energy losses and indicate which processes could be improved.

In recent years, a lot of research has been dedicated to the analysis of internal combustion engines (ICE) utilizing various fuel mixtures like diesel oil, biodiesel, methanol, hydrogen, ammonia, or mixtures of these fuels, in terms of the performance of the engine, emissions, and combustion analysis. Damanik et al. [7] presented a review of diesel engine performance and exhaust emission characteristics for diesel with biodiesel blends. They discussed the promising option of utilizing biodiesel blends with nanoadditives that decrease the carbon monoxide, nitrogen oxide, and unburned hydrocarbon emissions, while increasing the engine thermal efficiency, emphasizing that specific results depend on the biodiesel properties. Abedin et al. [8] presented a review paper on the energy balance of internal combustion engines presenting two approaches to the energy balance and discussing the case studies of alternative fuels. In a further study, Abedin et al. [9] analyzed three methods of introducing biodiesel to the engine, i.e., blend, fumigation, and emulsion, in terms of the engine performance and emissions. Thermal efficiency decreased for blend and fumigation strategies but grew in the emulsion mode. Carbon monoxide and hydrocarbon emissions increased for fumigation and emulsion strategies, but they declined in the case of the blend mode. Abdelrazek et al. [10] presented a numerical investigation comparing a direct injection diesel engine powered by base diesel oil and soybean biodiesel fuel under various load conditions. Findings showed that using soybean biodiesel fuel resulted in a decrease in carbon monoxide and hydrocarbon emissions and an increase in nitrogen oxides and carbon dioxide emissions, compared to base diesel. Additionally, an increase in brake-specific fuel consumption and a decrease in brake thermal efficiency were reported. Karpanai Selvan et al. [11] analyzed the performance of a set of the biodiesel-blended fuels in a diesel engine. It was revealed that the algae oil (AO10D) achieved higher efficiency at roughly similar levels of emissions, across the engine's load range. Thiyagarajan et al. [12] discussed the effect of hydrogen addition to biodiesel oil for the CI engine. The study revealed improvements in engine performance and reduced emissions, except for an increase in nitrogen oxides. Through numerical investigations, Ghazal [13] studied the impact of blending hydrogen with diesel in a CI engine and found improved performance, reduced emissions, and shortened ignition lag. Similarly, Jafarmadar [14] numerically investigated the mix of hydrogen and diesel and discovered a decrease in exergy efficiency as the hydrogen proportion increased. Lastly, Taghavifar et al. [15] showed a numerical analysis of hydrogen, DME, and diesel fuel systems in the CI engine which revealed that the hydrogen system offered the highest power and lowest indicated specific fuel consumption. Nadimi et al. [16] examined ammonia/biodiesel dual fuel combustion using the same small-sized single-cylinder compression ignition engine setup as in this study. Running the engine at 1500 rpm with fixed biodiesel and varied ammonia flows, the study found that ammonia could supply 69.4% of the input energy under stable conditions; however, high nitrogen oxide emissions along with ammonia slip were identified. In the further research, Nadimi et al. [17] analyzed the possibility of replacing diesel oil with an ammonia/diesel-operated engine, based on the experiments for 1200 rpm at full load varying the diesel-to-ammonia contribution ratio. The work showed that 84.2% of the input energy could be replaced by ammonia, while achieving lower carbon emissions; however, there were still high nitrogen oxides and ammonia emissions. Kuta et al. [18] investigated the dual-fuel CI ammonia engine emissions and an after-treatment process with $V_2O_5/SiO_2–TiO_2$ SCR, again using the same experimental setup as [16, 17],

comparing the diesel to ammonia (constant diesel mass flow with varying ammonia contributions). Implementation of the SCR unit allowed for a considerable reduction of nitrogen oxide emissions; however, still, the high emissions of ammonia remained unsolved. Zhang et al. [19] investigated the performance and emission characteristics of a two-stroke low-speed engine using an ammonia/diesel dual direct injection system. The work revealed that timing of diesel injection, which ignites the ammonia spray, not only enhances the indicated thermal efficiency by speeding up ammonia combustion but also minimizes NOx emissions.

Numerous papers regard the energy and exergy assessments of diesel, biodiesel, or a mixture of these two; however, relatively few papers consider the exergy assessment of utilizing alternative fuels, such as hydrogen or ammonia in the case of ICE. Al-Najem and Diab [20] performed an energy-exergy analysis on an eight-cylinder diesel engine obtaining ca. 35% of thermal efficiency. The authors discussed that around 50% of the energy contained in the fuel had been lost due to cooling and exhaust gases, whereas, based on the exergy assessment, 47% and 16% of energy in the exhaust gases and cooling water, respectively, could be potentially utilized. Şanli and Uludamar [21] reported the energy and exergy analyses of a fueled CI engine, comparing diesel to biodiesel oils: hazelnut (HB) and canola (CB). The analysis considered different engine speeds using a four-stroke and four-cylinder engine. For all three cases, the highest thermal and exergy efficiencies were obtained for 1800 rpm. Among the three variants, diesel proved to be the most preferred option, followed by HB and CB. Çakmak and Bilgin [22] performed the energy and exergy assessments of a single-cylinder diesel engine considering biodiesel fuel blends. The engine was tested under different engine speeds at full load conditions. The work showed that the blends positively contributed to the performance of the engine. A similar conclusion was found by Karami et al. [23] who also investigated the impact of using binary and ternary blends on a compression ignition diesel engine in terms of its performance and energy and exergy balances. The results demonstrated that the blends increased the exergy efficiency with a peak for a tomato-papaya blend (TPD) and decreased the percentage of heat loss exergy. An opposite finding was presented by Kul and Kahraman [24]. The assessment explored the use of biodiesel blends in diesel fuel, with each case including 5% bioethanol, under different engine speeds. Pure diesel was the variant to have obtained the highest performance in terms of the thermal and exergy efficiencies. Similarly, Nazzal and Al-Doury [25] also investigated the effect of the additional biodiesel blends to diesel fuel in terms of its impact on the energy and exergy performance, considering different engine speeds for a single-cylinder diesel engine. They discussed that higher speeds of engine promote higher exergy destruction and that adding corn oil blends decrease the thermal and exergetic efficiencies. Another work on this matter was performed by Khoobbakht et al. [26] who presented an energy and exergy assessment of a four-cylinder diesel engine for blended biodiesel and ethanol in diesel fuel with regard to engine load and speed. The results presented the negative impact of the blends on the engine's efficiency. Hoseinpour et al. [27] analyzed the effect of gasoline fumigation on energy and exergy balances for CI engines, comparing diesel fuel and B20 (20% of waste cooking oil biodiesel by volume) as baseline variants, with the gasoline introduced at two different ratios. The study revealed that the gasoline fumigation for the B20 fuel achieved higher exergy efficiency compared to that for the purely diesel case at high load. Wang et al. [28] analyzed the energy and exergy performance of a turbocharged, spark ignition four-cylinder engine supplied by hydrogen. Exergy analysis indicated a high potential—theoretically more than 59% of exergy efficiency, utilizing waste heat recovery. Yu et al. [29] compared the gasoline port injection (GPI) with hydrogen direct injection (HDI) to GPI with gasoline direct injection (GDI) in a spark ignition four-cylinder engine in terms of the energy and exergy analyses under lean burn conditions at different HDI fractions and air ratios. For both injection strategies, the thermal efficiency increased with the rise of hydrogen/gasoline direct injection fraction, and the thermal efficiency improvement achieved by HDI was higher on average by 0.64% than in the case of the GDI. The same conclusion applies to the exergy efficiency, thus showing the potential of alternative fuels. Sun et al. [30] compared two injection strategies: gasoline port fuel injection with gasoline direct injection (PFI with GDI) and port fuel injection with hydrogen direct injection (PFI with HDI) in terms of heat and exergy performance. They obtained that most of the total exergy is attributed to the exergy destruction and that utilizing hydrogen decreases the proportion of destruction. Table 1 presents a summary of energy and exergy efficiencies drawn from selected papers. All cases included, except the last one, pertain to a diesel engine using a direct injection strategy. The specific differences between the results in Table 1 can be attributed to variations in the engines tested and the characterization of the experiments. Despite these differences, the results illustrate the range of expected values.

In this research, we perform a detailed analysis, based on the first and second laws of thermodynamics, on a small compression ignition engine with port injection. This analysis spans different rotation speeds and shaft torques. Our primary objective is to explore the engine's performance across its entire range, comparing its default diesel oil fuel to a more environmentally friendly biodiesel and, finally, to ammonia, a promising alternative given environmental constraints. The secondary aim is to apply energy and exergy balance assessments to the internal combustion engine. This approach allows us to understand energy and exergy distributions, evaluate which fuel is used most efficiently, and identify potential areas for improvement. Achieving higher efficiency can lead to reduced fuel consumption and emissions, thus directly benefiting the environment.

2. Materials and Methods

The tests were performed on a single-cylinder engine Lifan C186F suited for a minitractor. The engine's specification is presented in Table 2. The engine was adjusted such that the gaseous ammonia was sent to the intake manifold to

Table 1: Comparison of selected literature on diesel engine energy and exergy efficiency.

Type of fuel	Operation condition	Maximum energy efficiency	Maximum exergy efficiency	Reference
Diesel	Constant load and speed	35.49%	34.33%	Al-Najem and Diab [20]
Biodiesel	Different load	26% at 100% load	—	Abdelrazek et al. [10]
Biodiesel or diesel	Different speed	38.85% at 1800 rpm for diesel	36.45% at 1800 rpm for diesel	Şanli and Uludamar [21]
Biodiesel/diesel mixture	Different load	46% at 100% load at 1500 rpm for AO10D	—	Karpanai Selvan et al. [11]
Biodiesel/diesel mixture	Different speed	40.41% at 2000 rpm for 10% blend	37.83% at 2000 rpm for 10% blend	Çakmak and Bilgin [22]
Biodiesel/diesel mixture	Different speed	32.12% at 1600 rpm for TPD blend	29.63% at 1600 rpm for TPD blend	Karami et al. [23]
Biodiesel/diesel mixture	Different speed	31.42% at 1400 rpm for pure diesel	29.38% at 1400 rpm for pure diesel	Kul and Kahraman [24]
Biodiesel/diesel mixture	Different speed	30.02% at 2500 rpm for pure diesel	28.16% at 2500 rpm for pure diesel	Nazzal and Al-Doury [25]
Biodiesel/diesel mixture	Different load/speed	36.61% at average	33.81% at average	Khoobbakht et al. [26]
Biodiesel or diesel/gasoline	Different load/speed	41.74% at 1300 rpm for pure B20 at 6.2 bar (break mean effective pressure)	38.32% at 1300 rpm for pure B20 at 6.2 bar (break mean effective pressure)	Hoseinpour et al. [27]
Ammonia/diesel	Constant load and speed	38% of indicated thermal efficiency for ammonia/ diesel fuel	—	Zhang et al. [19]
Hydrogen; implemented in a spark ignition engine via port injection	Different load/speed	35.1% at 2500 rpm at 0.8 MPa (brake mean effective pressure)	—	Wang et al. [28]

Table 2: Engine's specification.

Parameter	Value
Model, -	LIFAN
Engine type, -	CI, 4-stroke, 1-cylinder, forced air
Bore × stroke, mm × mm	86 × 70
Displacement, cm^3	418
Compression ratio, -	16.5 : 1
Intake valve opening, BTDC	14
Intake valve closing, ABDC	45
Exhaust valve opening, BBDC	50
Exhaust valve closing, ATDC	16
Start of injection, BTDC	15.5
Injection pressure, bar	200

mix with air before being sent to the cylinder. A Coriolis meter was used to measure the mass flow rate of ammonia, a turbine-type flowmeter was used to measure the mass flow rate of air, a thermocouple was used to measure the temperature of the exhaust gases, and an electric dynamometer was fitted to manage the engine's load and rotational speed. LabVIEW software and National Instruments hardware incorporated each of these characteristics. With an accuracy of 2% of the measurement range of the individual species, the FTIR Gasmet DX4000 was used to determine the composition of the exhaust gases. Next to the FTIR, an additional gas analyzer CAPELEC CAP 3201 was installed to provide verification and oxygen level with an accuracy of 3% of the measured value. The scheme of the experimental setup is presented in Figure 1. Nadimi et al. [16, 17] and Kuta et al. [18] have already presented the results from a different set of tests carried out using this experimental setup.

Fuels used for the purpose of the experiments have been purchased on the Polish market. The elementary analyses of diesel oil, biodiesel oil, and ammonia with corresponding lower heating values (LHV) are presented in Table 3.

Three tests considering three fuel supply scenarios were performed: diesel oil (D), biodiesel oil (B), and biodiesel oil with ammonia (B + A). The following considerations are applied:

(1) The points were measured once the engine was considered to achieve the steady state

(2) The reference conditions are the ambient conditions valid for the day and location of the tests (the tests were carried out in an open hall, thus using ambient air), summarized in Table 4

A set of measurements for each scenario included the following:

(1) *Applied shaft speed in rpm (revolutions per minute)*: 2700, 2400, 2100, 1800, 1500, and 1200

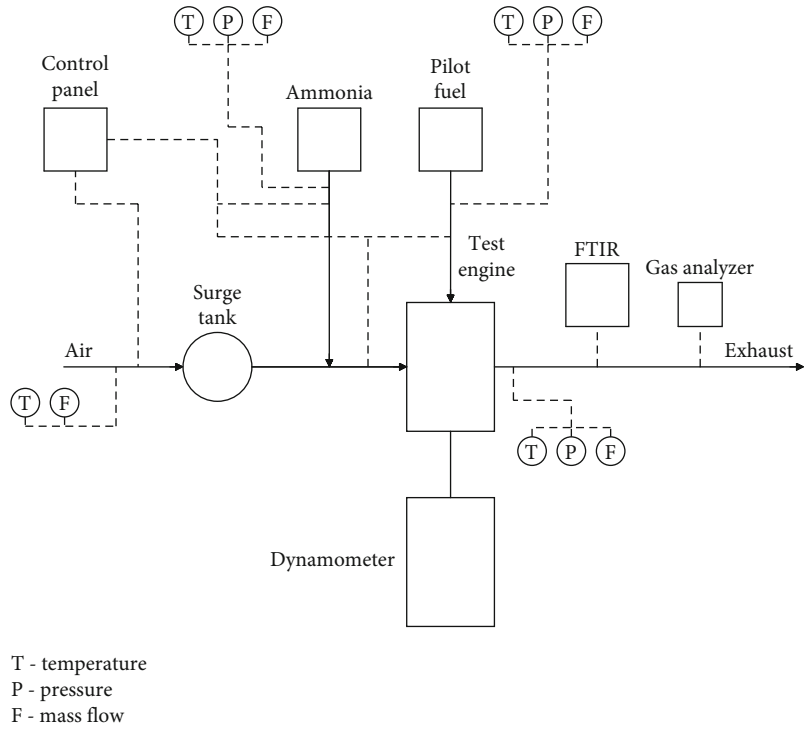

Figure 1: Diagram of experimental setup layout.

Table 3: Elementary analysis and LHV comparison of fuels.

Property	Diesel	Biodiesel	Ammonia
C, kg/kg	0.8078	0.7533	0.0000
H, kg/kg	0.1556	0.1397	0.1760
O, kg/kg	0.0363	0.1070	0.0000
N, kg/kg	0.0003	0.0000	0.8240
LHV, MJ/kg	42.4	37.4	18.6

Table 4: Ambient conditions (reference) of the three tests.

Parameter	D	B	B + A
Temperature, °C	1	3	3
Pressure, hPa	1034	1024.75	1018

(2) *Applied torque for 2700 rpm (Nm)*: 12, 8, and 4 referred to further as load in percentage (%): 100, 67, and 33

(3) *Applied torque for other speeds (Nm)*: 17, 12, 8, and 4 referred to further as load in percentage (%): 100, 71, 47, and 24

Shaft speed and torque were applied using an electric dynamometer. For a better presentation of the results, the torque range is presented in a dimensionless scale in a further part of this paper. In the case of the co-combustion of biodiesel with ammonia, the fixed mass flow rate of biodiesel was set, resulting in an applied torque of 4 Nm, and then, the increase of the torque was obtained by an increase of the ammonia mass flow rate. Such measurement design allowed for the capturing of the engine's performance throughout its operating range. The working point at 2700 rpm and 12 Nm represents the practical maximum—no higher torque was achievable when increasing the mass flow rate of ammonia. Pure diesel and biodiesel scenarios allowed for applying higher torque; however it resulted in excessive smoke emissions. Therefore, such an operating range has been considered to be practically operational.

The results of energy and exergy analyses depend on the engine's performance at respective points of operation. Therefore, a set of the most important results from the experiments is presented, as they will be supplementary for the discussion of the results. Tables 5–8 show fuel consumption; temperature of exhaust; temperature of the head of the engine; emissions of H_2O, CO_2, CO, NH_3, CH_4, and O_2; and excess air ratio. The values are presented with uncertainty defined according to equation [31]:

$$U = \sqrt{\frac{\sum \left(X_i - \bar{X}\right)^2}{n(n-1)}}, \tag{1}$$

where X_i and $\bar{X}$ stand for the measured and mean values, respectively, and n is the number of measurement results.

Excess air ratio is defined as

$$\lambda = \frac{n_a}{n_{\text{amin}}}, \tag{2}$$

where n_a is the kmol of air delivered for combustion referred

Table 5: Diesel-fueled engine-specific experiment results.

RPM, 1/min	Load	$\dot{m}_{fuel}$, g/s	T_{ex}, °C	T_{head}, °C	H_2O, %	CO_2, %	CO, %	CH_4, %	O_2, %	λ, -
2700	100%	0.322 ± 0.000	402.200 ± 0.230	71.660 ± 0.088	6.684 ± 0.008	6.548 ± 0.008	0.044 ± 0.000	0.001 ± 0.000	11.050 ± 0.331	2.36
2700	67%	0.249 ± 0.000	316.000 ± 0.111	62.910 ± 0.080	5.152 ± 0.005	5.048 ± 0.007	0.041 ± 0.000	0.001 ± 0.000	13.500 ± 0.405	3.13
2700	33%	0.180 ± 0.000	234.400 ± 0.127	53.190 ± 0.077	3.716 ± 0.005	3.485 ± 0.013	0.084 ± 0.001	0.002 ± 0.000	15.700 ± 0.471	4.42
2400	100%	0.400 ± 0.002	525.200 ± 0.050	81.300 ± 0.100	9.265 ± 0.003	9.089 ± 0.004	0.280 ± 0.002	0.002 ± 0.000	6.900 ± 0.207	1.62
2400	71%	0.276 ± 0.000	371.700 ± 0.025	68.800 ± 0.000	6.421 ± 0.008	6.336 ± 0.008	0.040 ± 0.000	0.001 ± 0.000	11.400 ± 0.342	2.41
2400	47%	0.220 ± 0.001	295.300 ± 0.075	59.150 ± 0.025	4.951 ± 0.011	4.858 ± 0.012	0.040 ± 0.000	0.001 ± 0.000	13.700 ± 0.411	3.13
2400	24%	0.163 ± 0.000	214.900 ± 0.124	46.190 ± 0.064	3.545 ± 0.006	3.327 ± 0.014	0.083 ± 0.001	0.002 ± 0.000	15.500 ± 0.465	4.16
2100	100%	0.333 ± 0.000	457.100 ± 0.193	75.380 ± 0.140	8.458 ± 0.012	8.394 ± 0.009	0.097 ± 0.001	0.002 ± 0.000	7.850 ± 0.235	1.71
2100	71%	0.243 ± 0.000	347.200 ± 0.177	72.590 ± 0.057	6.155 ± 0.012	6.066 ± 0.012	0.026 ± 0.000	0.001 ± 0.000	11.600 ± 0.348	2.38
2100	47%	0.182 ± 0.000	267.000 ± 0.172	64.800 ± 0.064	4.666 ± 0.013	4.491 ± 0.014	0.030 ± 0.000	0.001 ± 0.000	13.700 ± 0.411	3.28
2100	24%	0.133 ± 0.000	201.000 ± 0.104	56.800 ± 0.079	3.426 ± 0.004	3.123 ± 0.010	0.055 ± 0.000	0.002 ± 0.000	15.700 ± 0.471	4.58
1800	100%	0.291 ± 0.000	448.600 ± 0.140	81.150 ± 0.073	8.390 ± 0.007	8.269 ± 0.006	0.232 ± 0.001	0.004 ± 0.000	8.100 ± 0.243	1.70
1800	71%	0.204 ± 0.000	336.100 ± 0.126	76.960 ± 0.105	6.009 ± 0.005	5.894 ± 0.006	0.043 ± 0.000	0.002 ± 0.000	11.800 ± 0.354	2.44
1800	47%	0.156 ± 0.000	250.100 ± 0.157	63.990 ± 0.044	4.577 ± 0.011	4.398 ± 0.014	0.033 ± 0.000	0.002 ± 0.000	14.300 ± 0.429	3.26
1800	24%	0.111 ± 0.000	180.500 ± 0.123	55.200 ± 0.051	3.315 ± 0.008	2.919 ± 0.023	0.063 ± 0.000	0.002 ± 0.000	16.350 ± 0.490	4.65
1500	100%	0.251 ± 0.000	422.000 ± 0.188	75.240 ± 0.081	8.350 ± 0.020	8.205 ± 0.025	0.328 ± 0.004	0.008 ± 0.000	7.900 ± 0.237	1.66
1500	71%	0.178 ± 0.000	325.300 ± 0.061	76.460 ± 0.079	6.156 ± 0.003	6.053 ± 0.008	0.058 ± 0.000	0.003 ± 0.000	11.700 ± 0.351	2.36
1500	47%	0.134 ± 0.000	252.000 ± 0.238	69.430 ± 0.132	4.688 ± 0.004	4.511 ± 0.008	0.034 ± 0.000	0.003 ± 0.000	14.200 ± 0.426	3.17
1500	24%	0.094 ± 0.000	178.400 ± 0.156	59.420 ± 0.094	3.346 ± 0.010	2.992 ± 0.015	0.052 ± 0.000	0.003 ± 0.000	16.350 ± 0.490	4.62
1200	100%	0.214 ± 0.000	418.100 ± 0.398	80.960 ± 0.188	8.238 ± 0.032	8.342 ± 0.017	0.588 ± 0.010	0.018 ± 0.000	6.950 ± 0.208	1.48
1200	71%	0.152 ± 0.000	332.600 ± 0.085	79.560 ± 0.016	6.529 ± 0.006	6.471 ± 0.017	0.143 ± 0.001	0.008 ± 0.000	10.500 ± 0.315	2.08
1200	47%	0.109 ± 0.000	251.800 ± 0.165	74.510 ± 0.094	4.945 ± 0.007	4.754 ± 0.013	0.050 ± 0.000	0.005 ± 0.000	13.300 ± 0.399	2.93
1200	24%	0.078 ± 0.000	176.600 ± 0.257	61.510 ± 0.103	3.453 ± 0.011	3.207 ± 0.025	0.058 ± 0.000	0.005 ± 0.000	15.700 ± 0.471	4.35

Table 6: Biodiesel-fueled engine-specific experiment results.

RPM, 1/min	Load	$\dot{m}_{fuel}$, g/s	T_{ex}, °C	T_{head}, °C	H_2O, %	CO_2, %	CO, %	CH_4, %	O_2, %	λ, -
2700	100%	0.350 ± 0.002	415.700 ± 0.231	80.640 ± 0.129	6.658 ± 0.007	6.940 ± 0.006	0.072 ± 0.000	0.001 ± 0.000	10.600 ± 0.318	2.21
2700	67%	0.267 ± 0.000	313.600 ± 0.228	68.170 ± 0.067	4.993 ± 0.008	5.207 ± 0.015	0.042 ± 0.000	0.001 ± 0.000	13.300 ± 0.399	2.97
2700	33%	0.194 ± 0.000	234.600 ± 0.189	59.180 ± 0.071	3.522 ± 0.010	3.526 ± 0.014	0.073 ± 0.000	0.002 ± 0.000	15.600 ± 0.468	4.18
2400	100%	0.448 ± 0.000	517.900 ± 0.284	79.360 ± 0.161	9.049 ± 0.011	9.465 ± 0.016	0.349 ± 0.003	0.005 ± 0.000	9.200 ± 0.276	1.50
2400	71%	0.316 ± 0.000	384.800 ± 0.135	75.910 ± 0.079	6.390 ± 0.008	6.677 ± 0.012	0.065 ± 0.000	0.003 ± 0.000	12.900 ± 0.387	2.18
2400	47%	0.236 ± 0.000	291.600 ± 0.152	65.340 ± 0.065	4.802 ± 0.006	4.977 ± 0.018	0.043 ± 0.000	0.003 ± 0.000	13.900 ± 0.417	2.99
2400	24%	0.170 ± 0.000	214.500 ± 0.133	56.190 ± 0.039	3.431 ± 0.005	3.335 ± 0.010	0.071 ± 0.000	0.003 ± 0.000	15.800 ± 0.474	4.26
2100	100%	0.386 ± 0.000	449.400 ± 0.418	68.930 ± 0.227	8.278 ± 0.021	8.550 ± 0.017	0.176 ± 0.002	0.009 ± 0.000	9.500 ± 0.285	1.63
2100	71%	0.271 ± 0.000	341.100 ± 0.230	73.200 ± 0.079	5.899 ± 0.018	6.137 ± 0.018	0.050 ± 0.000	0.004 ± 0.000	13.700 ± 0.411	2.33
2100	47%	0.206 ± 0.000	264.500 ± 0.079	64.800 ± 0.055	4.546 ± 0.005	4.664 ± 0.005	0.039 ± 0.000	0.004 ± 0.000	15.700 ± 0.471	3.14
2100	24%	0.146 ± 0.000	193.300 ± 0.178	56.330 ± 0.052	3.286 ± 0.013	3.153 ± 0.017	0.060 ± 0.001	0.003 ± 0.000	17.900 ± 0.537	4.57
1800	100%	0.327 ± 0.000	419.800 ± 0.194	67.960 ± 0.200	7.829 ± 0.007	8.097 ± 0.027	0.293 ± 0.001	0.016 ± 0.000	9.400 ± 0.282	1.69
1800	71%	0.239 ± 0.000	326.300 ± 0.083	70.780 ± 0.047	5.795 ± 0.006	6.032 ± 0.004	0.087 ± 0.000	0.010 ± 0.000	13.100 ± 0.393	2.31
1800	47%	0.178 ± 0.000	250.200 ± 0.120	63.970 ± 0.053	4.470 ± 0.010	4.479 ± 0.027	0.054 ± 0.000	0.006 ± 0.000	15.800 ± 0.474	3.14
1800	24%	0.125 ± 0.000	178.600 ± 0.063	55.650 ± 0.048	3.188 ± 0.002	2.972 ± 0.009	0.075 ± 0.000	0.005 ± 0.000	17.800 ± 0.534	4.53
1500	100%	0.292 ± 0.000	423.200 ± 0.391	75.370 ± 0.240	8.344 ± 0.012	8.494 ± 0.018	0.476 ± 0.003	0.022 ± 0.000	8.300 ± 0.249	1.59
1500	71%	0.207 ± 0.000	327.800 ± 0.172	78.840 ± 0.088	6.004 ± 0.021	6.214 ± 0.022	0.097 ± 0.001	0.010 ± 0.000	12.500 ± 0.375	2.25
1500	47%	0.156 ± 0.000	250.200 ± 0.044	67.530 ± 0.039	4.645 ± 0.003	4.681 ± 0.012	0.058 ± 0.000	0.008 ± 0.000	14.300 ± 0.429	3.02
1500	24%	0.109 ± 0.000	179.600 ± 0.106	59.720 ± 0.064	3.331 ± 0.003	3.121 ± 0.010	0.062 ± 0.000	0.006 ± 0.000	16.200 ± 0.486	4.37
1200	100%	0.254 ± 0.002	440.800 ± 3.700	99.600 ± 0.400	8.491 ± 0.019	8.426 ± 0.045	1.368 ± 0.025	0.029 ± 0.000	7.800 ± 0.234	1.35
1200	71%	0.171 ± 0.000	324.200 ± 0.246	81.370 ± 0.052	5.910 ± 0.019	6.182 ± 0.021	0.162 ± 0.002	0.019 ± 0.000	11.600 ± 0.348	2.06
1200	47%	0.127 ± 0.000	243.600 ± 0.088	69.820 ± 0.044	4.668 ± 0.006	4.750 ± 0.014	0.084 ± 0.001	0.011 ± 0.000	14.000 ± 0.420	2.85
1200	24%	0.087 ± 0.000	165.800 ± 0.109	57.780 ± 0.035	3.301 ± 0.006	3.070 ± 0.012	0.078 ± 0.000	0.007 ± 0.000	16.300 ± 0.489	4.23

Table 7: Ammonia-fueled engine-specific experiment results.

RPM, 1/min	Load	$\dot{m}_{fuel}$, g/s	T_{ex}, °C	T_{head}, °C	H_2O, %	CO_2, %	CO, %	CH_4, %	O_2, %	λ, -
2700	100%	0.201 ± 0.000	387.100 ± 0.046	63.900 ± 0.033	11.700 ± 0.030	4.527 ± 0.033	0.067 ± 0.000	0.005 ± 0.000	10.200 ± 0.306	3.63
2700	67%	0.203 ± 0.000	310.400 ± 0.034	56.820 ± 0.019	7.527 ± 0.007	4.798 ± 0.021	0.093 ± 0.000	0.006 ± 0.000	12.900 ± 0.387	3.71
2700	33%	0.194 ± 0.000	234.600 ± 0.189	59.180 ± 0.071	3.522 ± 0.010	3.526 ± 0.014	0.073 ± 0.000	0.002 ± 0.000	15.600 ± 0.468	4.10
2400	100%	0.184 ± 0.000	446.200 ± 0.108	73.660 ± 0.049	15.860 ± 0.013	4.652 ± 0.027	0.085 ± 0.000	0.006 ± 0.000	9.000 ± 0.270	3.31
2400	71%	0.181 ± 0.000	360.900 ± 0.073	62.950 ± 0.071	10.620 ± 0.009	4.402 ± 0.060	0.057 ± 0.000	0.006 ± 0.000	10.500 ± 0.315	3.59
2400	47%	0.180 ± 0.000	284.900 ± 0.023	56.650 ± 0.021	7.139 ± 0.004	4.466 ± 0.022	0.075 ± 0.000	0.006 ± 0.000	13.300 ± 0.399	3.88
2400	24%	0.170 ± 0.000	214.500 ± 0.133	56.190 ± 0.039	3.431 ± 0.005	3.335 ± 0.010	0.071 ± 0.000	0.003 ± 0.000	15.800 ± 0.474	4.26
2100	100%	0.153 ± 0.001	422.900 ± 0.150	77.710 ± 0.069	16.280 ± 0.030	3.852 ± 0.026	0.078 ± 0.001	0.006 ± 0.000	6.900 ± 0.207	3.62
2100	71%	0.155 ± 0.000	326.900 ± 0.147	63.360 ± 0.084	10.080 ± 0.008	3.802 ± 0.054	0.040 ± 0.000	0.007 ± 0.000	11.100 ± 0.333	3.85
2100	47%	0.155 ± 0.000	260.300 ± 0.024	57.540 ± 0.029	6.849 ± 0.004	3.929 ± 0.013	0.056 ± 0.000	0.008 ± 0.000	13.700 ± 0.411	4.09
2100	24%	0.146 ± 0.000	193.300 ± 0.178	56.330 ± 0.052	3.286 ± 0.013	3.153 ± 0.017	0.060 ± 0.001	0.003 ± 0.000	17.900 ± 0.537	4.57
1800	100%	0.129 ± 0.000	391.000 ± 0.223	74.360 ± 0.083	15.950 ± 0.040	3.180 ± 0.049	0.090 ± 0.001	0.024 ± 0.000	7.000 ± 0.210	3.80
1800	71%	0.128 ± 0.000	303.100 ± 0.078	62.030 ± 0.065	10.050 ± 0.108	3.001 ± 0.028	0.052 ± 0.000	0.019 ± 0.000	11.500 ± 0.345	4.12
1800	47%	0.131 ± 0.000	244.400 ± 0.112	58.170 ± 0.009	6.638 ± 0.016	3.732 ± 0.014	0.066 ± 0.000	0.016 ± 0.000	14.000 ± 0.420	4.19
1800	24%	0.125 ± 0.000	178.600 ± 0.063	55.650 ± 0.048	3.188 ± 0.002	2.972 ± 0.009	0.075 ± 0.000	0.005 ± 0.000	17.800 ± 0.534	4.53
1500	100%	0.111 ± 0.000	372.000 ± 0.147	75.870 ± 0.095	16.200 ± 0.054	3.393 ± 0.041	0.133 ± 0.001	0.030 ± 0.000	7.250 ± 0.217	3.46
1500	71%	0.110 ± 0.000	291.500 ± 0.102	62.800 ± 0.078	10.440 ± 0.061	3.170 ± 0.031	0.070 ± 0.000	0.020 ± 0.000	11.950 ± 0.358	3.34
1500	47%	0.111 ± 0.000	234.900 ± 0.136	58.350 ± 0.018	6.790 ± 0.026	3.658 ± 0.015	0.071 ± 0.000	0.014 ± 0.000	14.600 ± 0.438	3.38
1500	24%	0.109 ± 0.000	179.600 ± 0.106	59.720 ± 0.064	3.331 ± 0.004	3.121 ± 0.011	0.062 ± 0.000	0.006 ± 0.000	16.200 ± 0.486	4.39
1200	100%	0.093 ± 0.000	353.000 ± 0.071	77.390 ± 0.108	16.450 ± 0.068	3.606 ± 0.033	0.175 ± 0.002	0.036 ± 0.000	7.500 ± 0.225	3.31
1200	71%	0.092 ± 0.000	279.800 ± 0.125	63.580 ± 0.090	10.840 ± 0.013	3.338 ± 0.034	0.088 ± 0.000	0.021 ± 0.000	12.400 ± 0.372	3.64
1200	47%	0.090 ± 0.000	225.400 ± 0.161	58.520 ± 0.027	6.941 ± 0.036	3.584 ± 0.015	0.076 ± 0.000	0.013 ± 0.000	15.200 ± 0.456	3.96
1200	24%	0.087 ± 0.000	165.800 ± 0.109	57.780 ± 0.035	3.301 ± 0.006	3.070 ± 0.012	0.078 ± 0.000	0.007 ± 0.000	16.300 ± 0.489	4.23

Table 8: Ammonia-fueled engine: ammonia consumption and emission in the exhaust experiment results.

RPM, 1/min	Load	Ammonia consumption, kg/h	NH_3, %
2700	100%	1.481 ± 0.000	1.468 ± 0.003
2700	67%	0.835 ± 0.000	1.047 ± 0.004
2700	33%	0.000 ± 0.000	0.000 ± 0.000
2400	100%	1.770 ± 0.000	1.540 ± 0.002
2400	71%	1.246 ± 0.000	1.439 ± 0.005
2400	47%	0.631 ± 0.000	0.879 ± 0.001
2400	24%	0.000 ± 0.000	0.000 ± 0.000
2100	100%	1.726 ± 0.000	1.627 ± 0.005
2100	71%	1.140 ± 0.000	1.476 ± 0.002
2100	47%	0.608 ± 0.000	0.916 ± 0.002
2100	24%	0.000 ± 0.000	0.000 ± 0.000
1800	100%	1.542 ± 0.000	1.625 ± 0.004
1800	71%	1.011 ± 0.000	1.452 ± 0.002
1800	47%	0.511 ± 0.000	0.911 ± 0.002
1800	24%	0.000 ± 0.000	0.000 ± 0.000
1500	100%	1.282 ± 0.000	1.576 ± 0.004
1500	71%	0.852 ± 0.000	1.463 ± 0.005
1500	47%	0.444 ± 0.000	0.947 ± 0.003
1500	24%	0.000 ± 0.000	0.000 ± 0.000
1200	100%	1.022 ± 0.000	1.528 ± 0.004
1200	71%	0.693 ± 0.000	1.473 ± 0.007
1200	47%	0.378 ± 0.000	0.984 ± 0.003
1200	24%	0.000 ± 0.000	0.000 ± 0.000

per kg of fuel and n_{amin} is the stoichiometric amount of air required to combust the fuel. In the case of the experimental results of the ammonia-fueled engine, seen in Table 7, the excess air ratio is referred per the amount of pilot fuel (biodiesel).

The values, along with their associated uncertainties, were calculated on a dataset that had been progressively fragmented over time and refined by the removal of outlier points. The objective was to conduct the measurement as soon as the engine reached a steady-state condition. Hence, all measured values were continuously logged, and once there was no significant variance between subsequent measurements, the data for a specific operating point was recorded. This was followed by a data-cleaning process, which resulted in a final set of measured values that were closely aligned. When equation (19) was applied to such closely clustered measurement values, the resulting uncertainty was very small. The exception is O_2 that was measured by an additional gas analyzer, and therefore, it uses a fixed value of uncertainty. The uncertainties for exhaust components like CO, CH_4, and NH_3 are essentially zero, since they were measured in ppm, whereas the presented values regard the percentage shares. The emissions are not referred per 5% of O_2 share, which is required for the comparison of the emissions from different engines and is a common literature approach, e.g., [16], but they are shown directly in a form they are used for energy and exergy balances.

From the experimental results reported in Tables 5 and 6, it is evident that high loads and speed of the shaft require high fuel consumption, thus promoting higher temperatures of both exhaust and engine's head which is true at all shaft speeds for all three cases. The excess air ratio decreases along with the increase in the load, and it achieves similar values to the corresponding loads, independently of the rpm. A low excess air ratio corresponds to high H_2O, CO_2, CO, and CH_4 at low O_2, and these proportions reverse with an increase of the excess air ratio. On average, the ammonia-fueled scenario, presented in Tables 7 and 8, achieves a lower temperature of exhaust and engine's head. Since the carbon emissions for this case originate from a pilot dosage equivalent to 4 Nm of applied torque, as explained in Section 2, such a solution allows for the reduction of CO_2 and CH_4 emissions. A high load promotes high H_2O and NH_3 shares due to high ammonia consumption and ammonia slip; CO_2, CO, and CH_4 take roughly similar values for 100%, 71%, and 47% loads at any given rpm.

3. Energy and Exergy Analysis Approach

The mass and energy balances of the control volume in a steady-state condition can be written consecutively as

$$\sum \dot{m}_{in} = \sum \dot{m}_{out}, \tag{3}$$

$$\sum \dot{m} h_{in} = \sum \dot{m} h_{out}, \tag{4}$$

where the subscripts "in" and "out" stand for the inlet and outlet, respectively; $\dot{m}$ refers to the mass flow rate; and h refers to the specific enthalpy.

The energy balance can be rewritten as

$$\dot{Q}_{air} + \dot{E}_{fuel} = \dot{W} + \dot{Q}_{lost} + \dot{Q}_{exh}, \tag{5}$$

where $\dot{Q}$ with subscript "air" stands for the energy rate delivered by air, $\dot{E}$ with subscript "fuel" stands for the fuel energy rate, $\dot{W}$ stands for the power of the engine, $\dot{Q}$ with subscript "lost" stands for net heat transfer rate lost to the environment (later also noted as cooling losses), and $\dot{Q}$ with subscript "exh" stands for the energy rate of the exhaust gases equal to the physical enthalpy of the exhaust gases.

Considering the intake air to be at the same temperature as the reference conditions, the physical enthalpy of air entering the control volume can be neglected; the same consideration applies to the physical enthalpy of fuel. Potential and kinetic energies of fluid streams are omitted.

Fuel energy rate can be expressed as

$$\dot{E}_{fuel} = \dot{m}_{fuel} LHV_{fuel}, \tag{6}$$

where $\dot{m}$ with subscript "fuel" stands for the mass flow rate of fuel and LHV with subscript "fuel" indicates the lower heating value of the fuel.

Enthalpy of exhaust gases is expressed as

$$\dot{Q}_{\text{exh}} = \sum \dot{m}_{\text{exh},i} \Delta h_{\text{exh},i}, \tag{7}$$

where $\dot{m}$ with subscript "exh,i" stands for the mass flow rate of the i component of exhaust gases and Δh with subscript "exh,i" represents the difference of specific enthalpy of the i component of exhaust gases at the measured and reference state temperatures, and it is defined as

$$\Delta h_i = h_i - h_{i,0}. \tag{8}$$

Heat transfer rate lost to the environment is calculated by closing the energy balance. Thermal efficiency of the engine is calculated as

$$\eta = \frac{\dot{W}}{\dot{E}_{\text{fuel}}}. \tag{9}$$

Based on the defined energy balance, the exergy balance of the control volume equals to the following:

$$\dot{\text{E}}\text{x}_{\text{fuel}} = \dot{\text{E}}\text{x}_{\text{w}} + \dot{\text{E}}\text{x}_{\text{lost}} + \dot{\text{E}}\text{x}_{\text{exh}} + \dot{\text{E}}\text{x}_{\text{dest}}, \tag{10}$$

where Ėx with subscript "fuel" indicates the exergy fuel rate, Ėx with subscript "w" stands for the exergy work rate, Ėx with subscript "lost" means the exergy rate lost to the environment, Ėx with subscript "exh" stands for the exergy of exhaust gases, and Ėx with subscript "dest" represents the exergy destruction rate.

Th exergy fuel rate is defined as

$$\dot{\text{E}}\text{x}_{\text{fuel}} = \dot{m}_{\text{fuel}} \varepsilon_{\text{ch,fuel}}, \tag{11}$$

where $\varepsilon_{\text{ch,fuel}}$ stands for the specific chemical exergy of fuel.

For liquid fuels, the standard chemical exergy of fuel can be calculated based on its elemental analysis. There are several approaches proposed in the literature, as summarized by Michalakakis et al. [32]. In this work, the equation proposed by Szargut is used [33] to determine the chemical exergy of diesel and biodiesel:

$$\varepsilon_{\text{ch,fuel}} = \text{LHV}_{\text{fuel}} \left[1.047 + 0.0154 \frac{\text{H}}{\text{C}} + 0.0562 \frac{\text{O}}{\text{C}} + 0.5904 \frac{\text{N}}{\text{C}} \left(1 - 0.175 \frac{H}{C} \right) \right], \tag{12}$$

where H, C, O, and N represent the mass fractions of hydrogen, carbon, oxygen, and nitrogen, respectively, from the ultimate analysis of the fuel sample.

The standard chemical exergy of ammonia is taken directly from the literature (Szargut [34]), and it is equal to 337.9 kJ/mol.

The exergy work rate is equal to the net work of the engine:

$$\dot{\text{E}}\text{x}_{\text{w}} = \dot{W}. \tag{13}$$

Table 9: Ambient environment (reference) definition.

Component	Mol fraction, %
yCO	7.00E-04
$y\text{CO}_2$	3.45E-02
$y\text{H}_2\text{O}$	3.03
$y\text{N}_2$	75.67
$y\text{O}_2$	20.35
$y\text{NH}_3$	6.00E-07
$y\text{CH}_4$	1.74E-04
Rest	9.15E-01

The exergy rate lost to the environment equals to

$$\dot{\text{E}}\text{x}_{\text{lost}} = \sum \left(1 - \frac{T_0}{T_m} \right) \dot{Q}_{\text{lost}}, \tag{14}$$

where T with subscript "0" is the temperature at the reference state and T with subscript "m" stands for the temperature of the system boundary where heat is transferred to the environment, as explained in [35]. Most analyses found in the literature used for the experiment the water-cooled engine, and therefore, the temperature of cooling water is used as this temperature, e.g., [24, 26]; however, since the engine used in the experiment is cooled by air, the temperature of the head of the engine is here considered.

The exergy of exhaust gases can be written as

$$\dot{\text{E}}\text{x}_{\text{exh}} = \sum \dot{m}_{\text{exh},i} \varepsilon_{\text{exh},i}, \tag{15}$$

where ε with subscript "exh,i" is the specific exergy of the i exhaust component defined as

$$\varepsilon_{\text{exh}} = \varepsilon_{\text{tm}} + \varepsilon_{\text{ch}}, \tag{16}$$

where ε with the subscript "tm" represents the specific thermomechanical exergy defined as

$$\varepsilon_{\text{tm}} = \Delta h - T_0 \Delta s, \tag{17}$$

where s stands for the specific entropy.

Specific chemical exergy of the exhaust gases is calculated according to the following formula:

$$\varepsilon_{\text{ch}} = \dot{R} T_0 \ln \frac{y_i}{y_{i,r}}, \tag{18}$$

where $\dot{R}$ is the universal gas constant equal to 8.314 J·mol^{-1}·K^{-1}, y_i is the molar fraction of the i component in the exhaust gases, and $y_{i,r}$ stands for the molar fraction of the i component in a reference environment.

The molar fractions of the components present in the environment are shown in Table 9. The assumption of ideal gases applies.

The components listed in Table 9 are taken from the following sources:

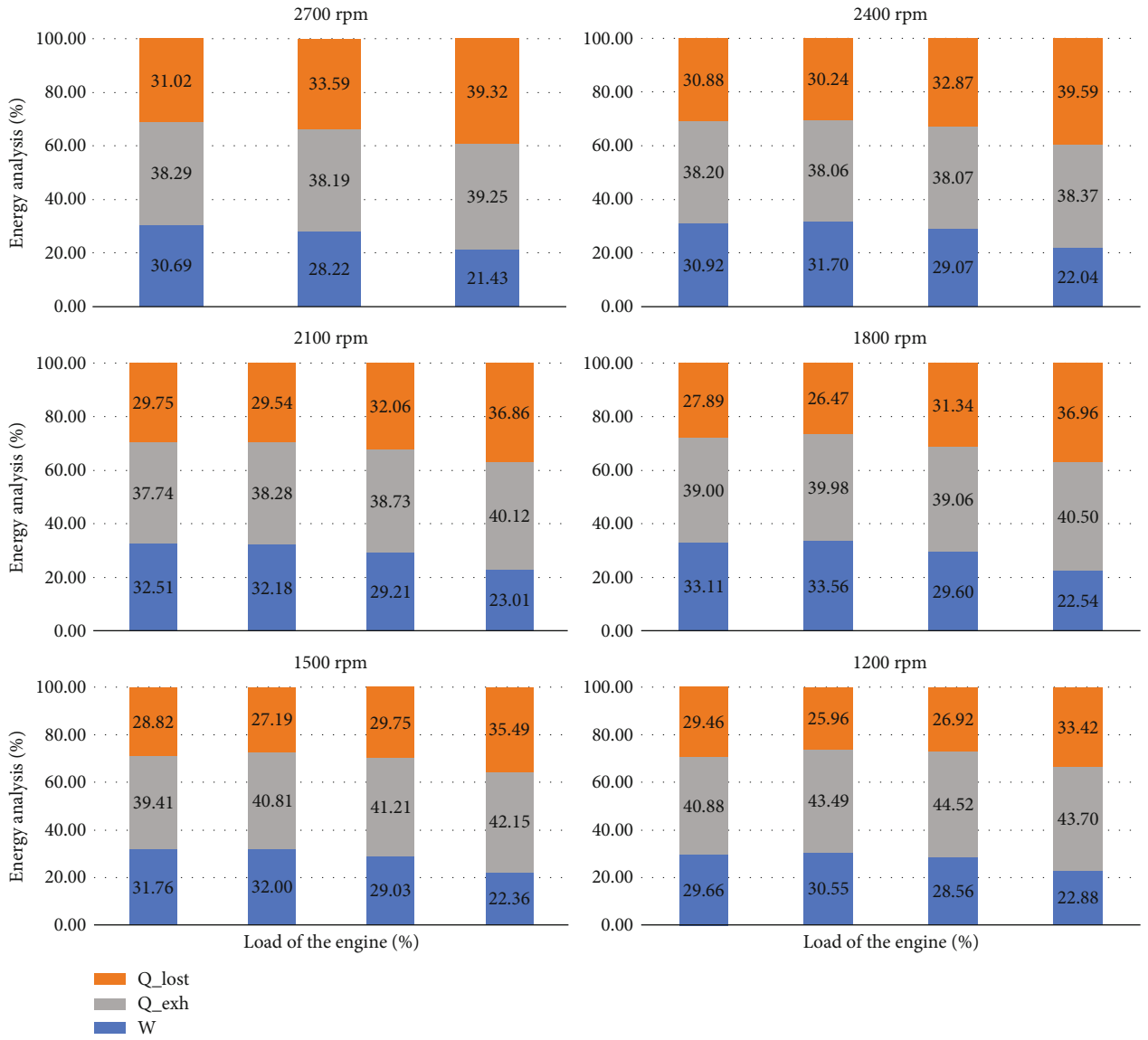

Figure 2: Results of energy analysis of diesel-fueled engine.

(1) Concentrations of CO, CO_2, H_2O, N_2, and O_2 follow the literature approach [21, 26]

(2) The concentration of NH_3 is considered to be 6 ppb (averaged global value of atmospheric NH_3 based on a satellite remote measurement), assumed from the review paper [36]

(3) The concentration of CH_4 is assumed from [37] (recalculated from the dry air composition)

It is common in the literature that the concentrations of NH_3 or CH_4 are not included in the energy and exergy balances (e.g., [21, 24, 26]); however, this paper is aimed at a detailed investigation of chemical exergy losses in the exhaust part, especially due to a high share of ammonia in the exhaust for the co-combustion of biodiesel with ammonia, as seen in Tables 7 and 8.

The exergy destruction rate is calculated from closing the exergy balance. It represents the rate of energy accounted in the irreversible processes such as combustion and friction.

Exergy efficiency is defined as

$$\psi = \frac{\dot{E}x_w}{\dot{E}x_{fuel}}. \tag{19}$$

4. Results

4.1. Diesel-Fueled Engine. Results of energy analysis applied on the measured data concerning the shaft's speeds and applied loads are presented in Figure 2. Thermal efficiency, a measure of how effectively an engine transforms the energy from the fuel into the useful work, is impacted by several factors that influence engine performance. These include exhaust losses, cooling efficiency, combustion effectiveness,

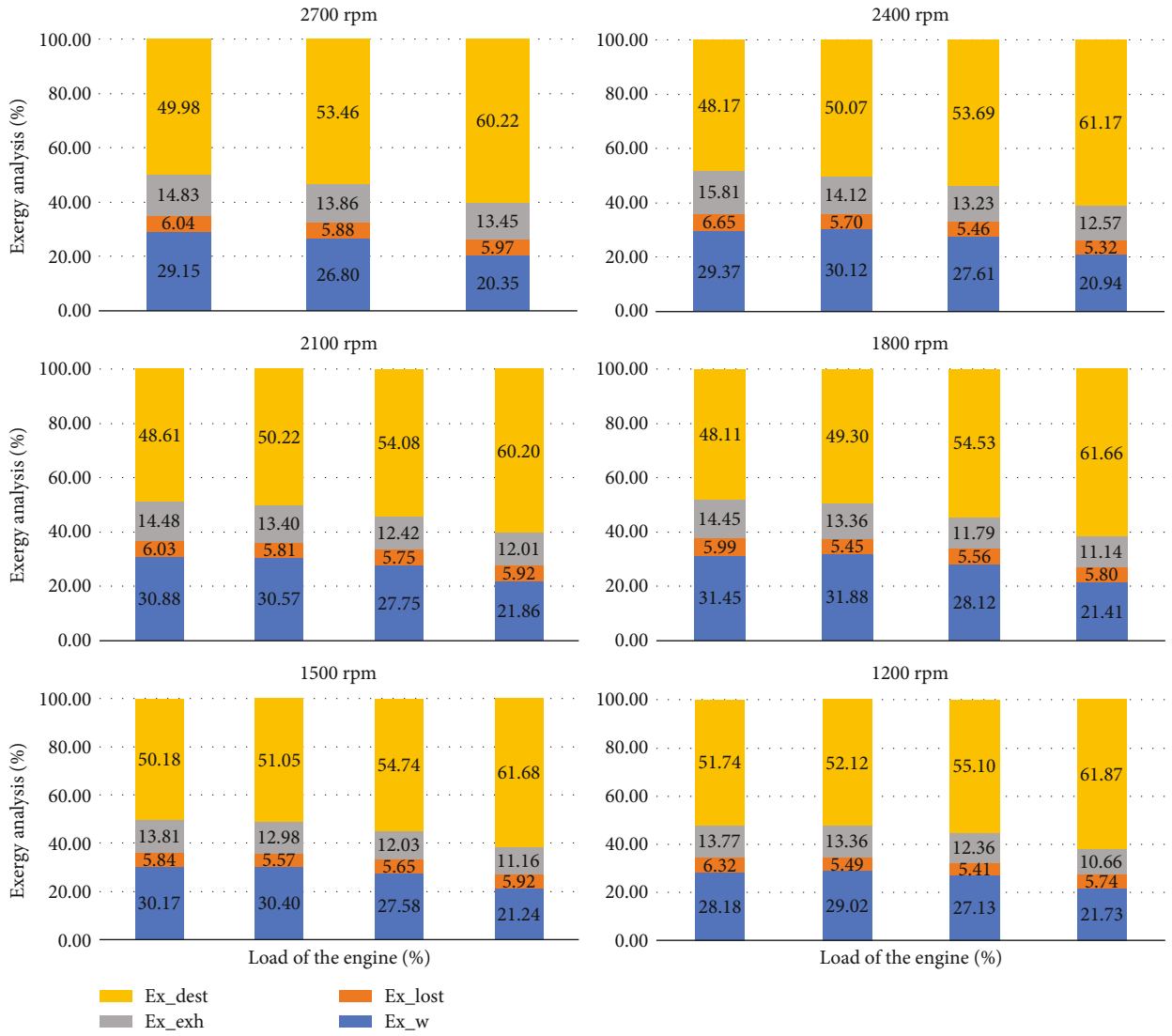

Figure 3: Results of exergy analysis of diesel-fueled engine.

and friction within the engine. Noting the case of 2400 rpm in Figure 2, these dependencies could be described in the following way. At 100% load and 2400 rpm, the engine achieves 30.92% of thermal efficiency which is due to the high temperature of exhaust gases at an excess air ratio of ca. 1.62. Peak efficiency of 31.70% for 2400 rpm is obtained at 71% load, at a lower temperature of the head of the engine resulting in a slight decrease in cooling losses and a lower exhaust temperature, even though the mass flow rate of the exhaust is higher (excess air ratio of 2.41, as presented in the Table 5). As a result, there is a slightly lower share of exhaust energy (analyzing the exergy efficiency for this point in Figure 3, it is seen that even though at 71% the exergy destruction associated with combustion is higher, lower shares of exhaust exergy and exergy lost to the environment result in an improvement in terms of the engine efficiency). Along with the decline in the load, the lower efficiencies are seen which are due to an increase in the ratio between friction losses and the engine-indicated work [17] (confirmed by the increased share of exergy destruction rate, seen in Figure 3) and high exhaust energy share caused by the higher exhaust mass flow rates (high excess air ratios of 3.13 and 4.16, as seen in Table 5, respectively, at 47% and 24% loads).

Collating it to the results at other rpm, the general trend is that the efficiencies take similar values at corresponding loads (e.g., for a load of 47%: efficiency is 29.21% at 2100 rpm and 29.03% and 1500 rpm), independently of the shaft's speed. In the case of 2700 rpm, the 100% load corresponds to 12 Nm of applied torque, and therefore, the behavior for 2700 rpm mirrors the trend of other rpm between the 71% load and 24% load, and so, the 100% load at 2700 rpm would be around the peak efficiency for this rpm. Noting the case of 2100 rpm, the highest efficiency is obtained at 100% load, not 71% as for other shaft speeds; however, the difference between the efficiencies for these two points is ca. 0.3 percentage point. At 71% load, there is a higher excess air ratio; however, a lower exhaust temperature compensates for the value of the exhaust energy, so that it is very similar at both of these points. The lower temperature of the

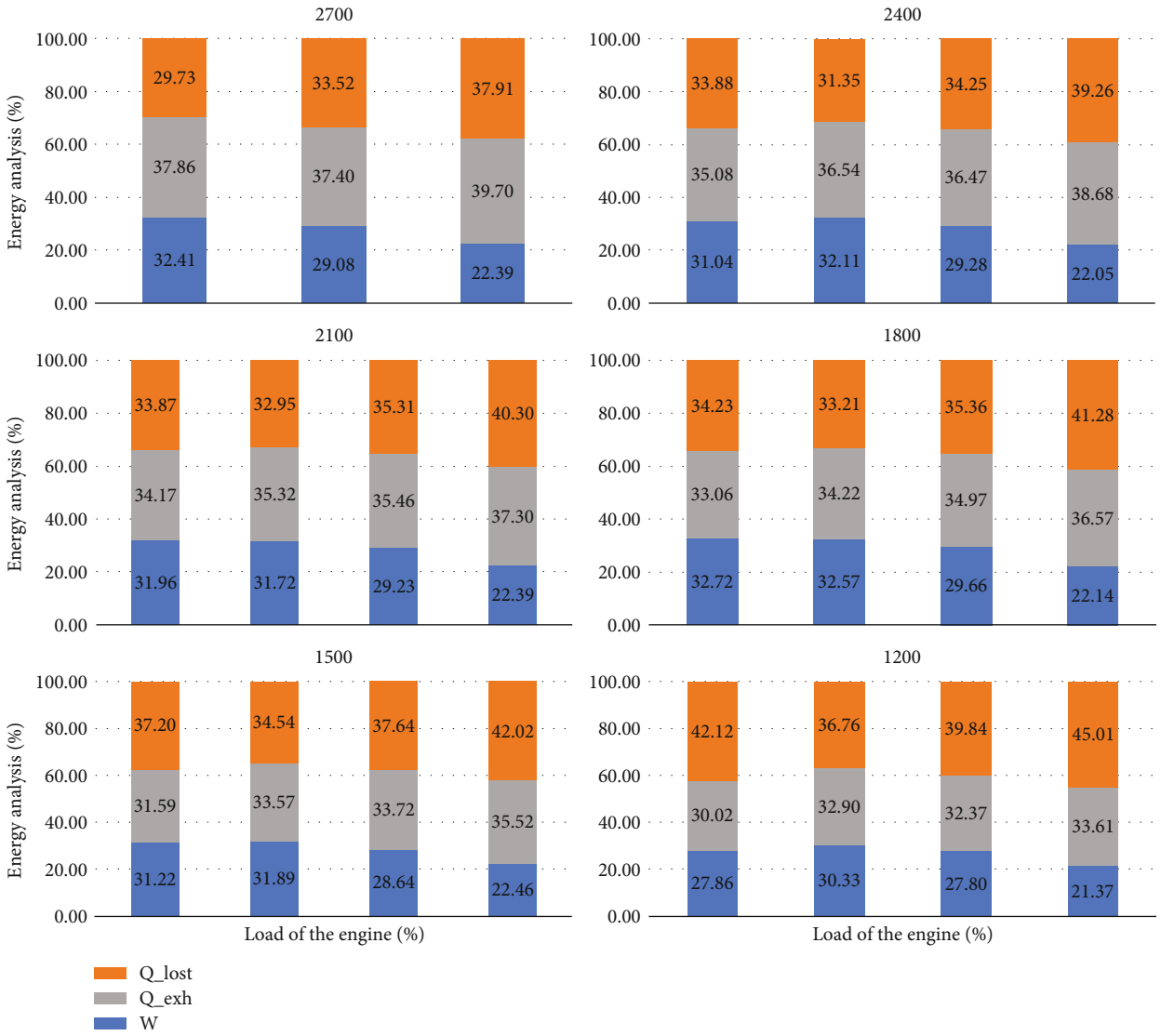

Figure 4: Results of energy analysis of biodiesel-fueled engine.

engine's head is registered at 71% load; however, since the 100% load is characterized by the lowest exergy destruction losses (accounting for combustion and friction; seen in Figure 3), a slightly higher efficiency is achieved at this point. Considering the thermal efficiency to be the main criterion of the engine's performance, the optimized operation of the diesel-fueled engine would be at medium-high loads, preferably between 1500 and 2400 rpm. Across the engine's working range, the peak efficiency of 33.56% is achieved at 1800 rpm with a load of 71%.

Applying exergy balance leads to the same conclusion. Based on Figure 3, it is seen that exergy efficiency follows the energy efficiency trend; however, it takes lower values, since it is defined based on the exergy fuel input. The peak exergy efficiency across the engine's operating range is achieved for the same point as in the case of energy efficiency (1800 rpm and 71% load) with the value of 31.88%. Noting the case of 2400 rpm, it is seen that it is the combustion process along with friction that is responsible for most of the energy degradation, seen by the highest share of exergy destruction at all loads. Exergy destruction increases along with the decrease in load; it is the highest at the 24% load at each rpm. The exergy of heat lost to the environment decreases with a decline in load which is caused by the lower temperature of the engine's head. In this work, the temperature of the engine head serves as a reference for determining the exergy rate lost to the environment; however, if the engine was cooled by the water and the temperature of cooling water would be used, which is the most common approach, e.g., [24, 26], it would decrease the share of exergy lost to the cooling by a few percentage points and increase the share of exergy destruction, thus not impacting the conclusions. The trend regarding the exergy of the exhaust is that a high temperature of exhaust gases, which occurs at high load, increases the share of exhaust exergy. It is seen that, independently from the rpm and load, for all cases, this value reaches above 10% in reference to the fuel exergy input.

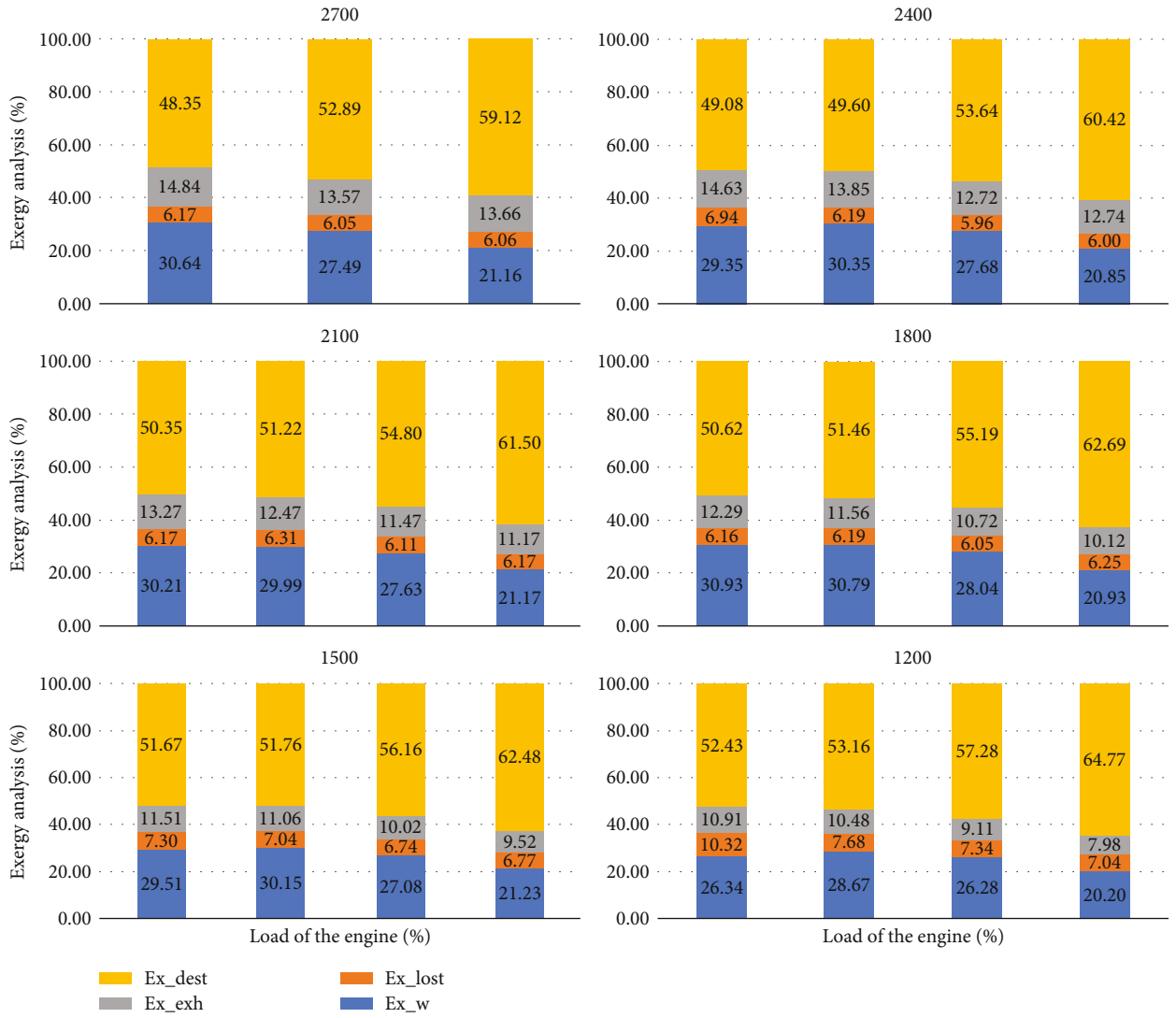

Figure 5: Results of exergy analysis of biodiesel-fueled engine.

Assuming a modification to the engine that would allow for a waste heat recovery system to transform all of the exhaust exergy into work, an efficiency of 45.90% could be found at 1800 rpm and a 100% load. However, from the second law of thermodynamics, it is known that such heat transfer cannot occur without any losses; therefore, such efficiency should be treated as a theoretical concept. The design of a waste heat recovery system aiming to recover as much exhaust exergy as possible depends on a variety of factors. These include the size and weight of the system, its cost, complexity, and the balance between efficiency gains and the operating conditions of the vehicle.

4.2. Biodiesel-Fueled Engine. The results of energy and exergy assessments for the biodiesel-fueled engine are presented in Figures 4 and 5. Noting the case of 2400 rpm, it is seen that the trends regarding the energy and exergy distributions remain similar to the case of the diesel-fueled scenario, and therefore, further description will aim at capturing the crucial differences. The peak efficiency occurs at 100% load at 2700, 2100, and 1800 rpm (for the diesel case, this is true only for 2700 and 2100 rpm); for other speeds, it occurs at 71% load. The reason for this trend is addressed in the previous Section 4.1; the explanation of this is best seen in Figure 5. For 2700, 2100, and 1800 rpm, the effect of lower exhaust exergy and exergy lost to the environment for the 71% load prevails at the lowest combustion losses at 100%; for the other speeds, it is the opposite. The overall highest thermal efficiency across the entire engine's range is 32.72%, for 1800 rpm and 100% load. This value is very close to the efficiency obtained at the same rpm but with a 71% load. Moreover, it is also near the efficiency achieved at a higher rpm of 2700, still at 100% load. The difference among these three efficiency values is less than one percentage point. The overall highest exergy efficiency is achieved at 1800 rpm and 100% load with the value of 30.93%, following the thermal efficiency trend.

Compared to the diesel case, for 2400 rpm and lower shaft speeds, the share of exhaust energy is a few percentage points lower (at all loads; at 2700 rpm, the differences are

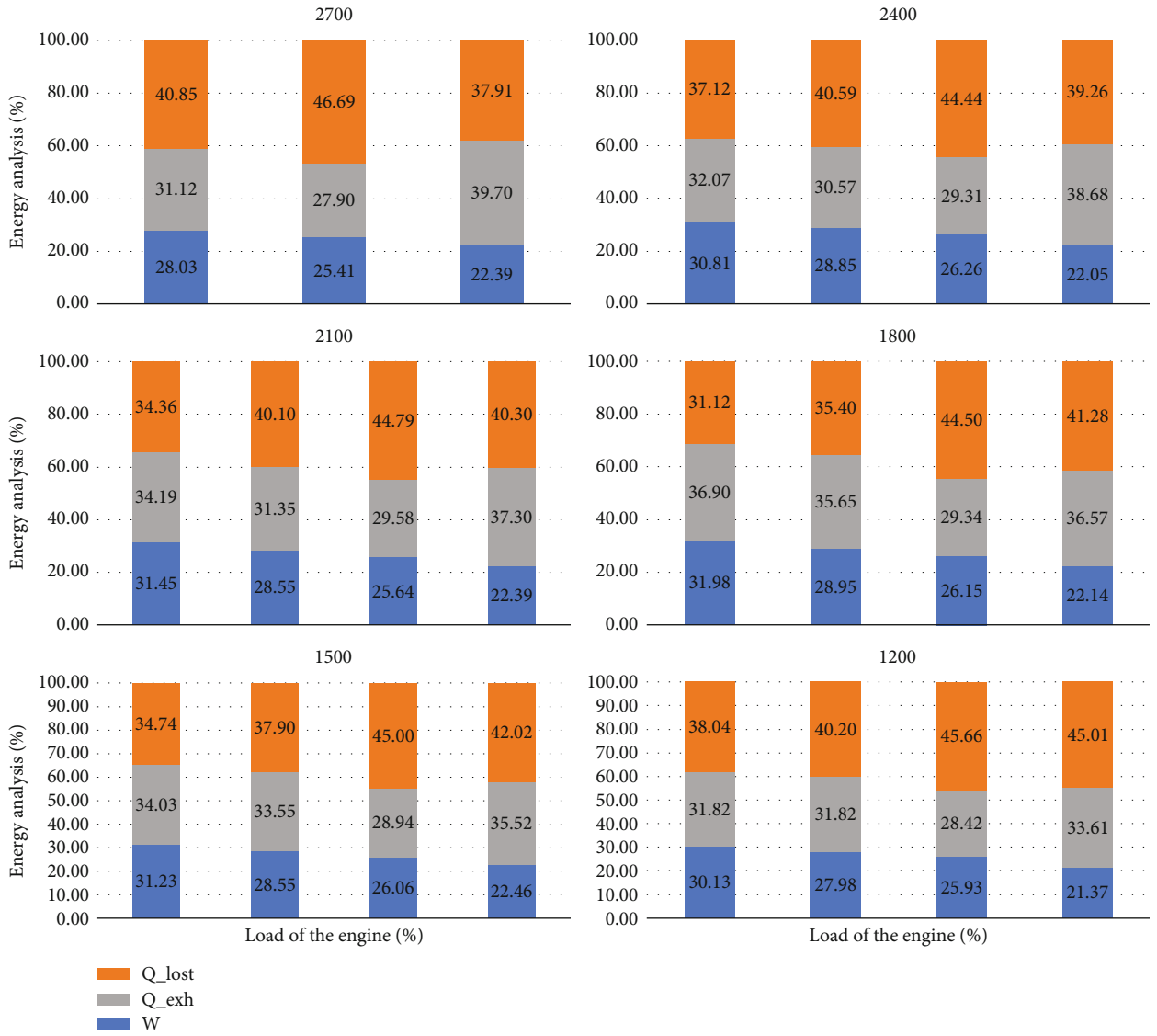

Figure 6: Results of energy analysis of ammonia-fueled engine.

even smaller). It is caused by the difference in the combustion process since a biodiesel-fueled engine is characterized by a higher fuel consumption due to its lower value of LHV, but lower excess air ratio, resulting in an overall lower mass flow rate of the exhaust. Shares of carbon monoxide and oxygen in the exhaust are higher indicating less complete combustion, as seen in Tables 5 and 6. This observation is confirmed by the exergy analysis which shows that the share of exergy destruction is higher for the biodiesel case (seen for 2400 rpm and lower rpm values, independently of loads). For 2700 rpm, it is actually the opposite, where the biodiesel case achieves slightly higher efficiency at all loads due to lower exergy destruction losses, noting the exhaust and cooling exergies to be similar. Theoretically, the maximum efficiency, given the waste heat recovery allowing for full utilization of the exhaust, would be the 45.48% at 2700 rpm and a 100% load.

4.3. Ammonia-Fueled Engine. Figures 6 and 7 present the results of energy and exergy analyses for the co-combustion of an ammonia-fueled engine. Noting that the biodiesel mass flow rate was set as a fixed value resulting in 4 Nm of applied torque, the results for the 24% load are the same as those in Figures 4 and 5. Focusing on Figures 6 and 7, independently of the shaft's speeds, the following trends can be observed. Low loads promote lower exhaust energy and an increase in the cooling, coupled with the decrease in thermal efficiency. A decreasing effect of the exhaust energy along with the decline in the torque is caused by a dominating effect of a declining temperature of the exhaust, even though there is an increase in the mass flow rate of the exhaust. In the case of the diesel and biodiesel variant, the differences between the exhaust energies at respective loads are smaller than in the case of the ammonia-fueled engine. Exergy destruction, accounting for the combustion and friction processes, increases with decline of the load which is the general trend. Exhaust exergy takes the highest value at the maximum load and gradually decreases (since it is related to the exhaust temperature). Decreasing the load also causes the decline in the

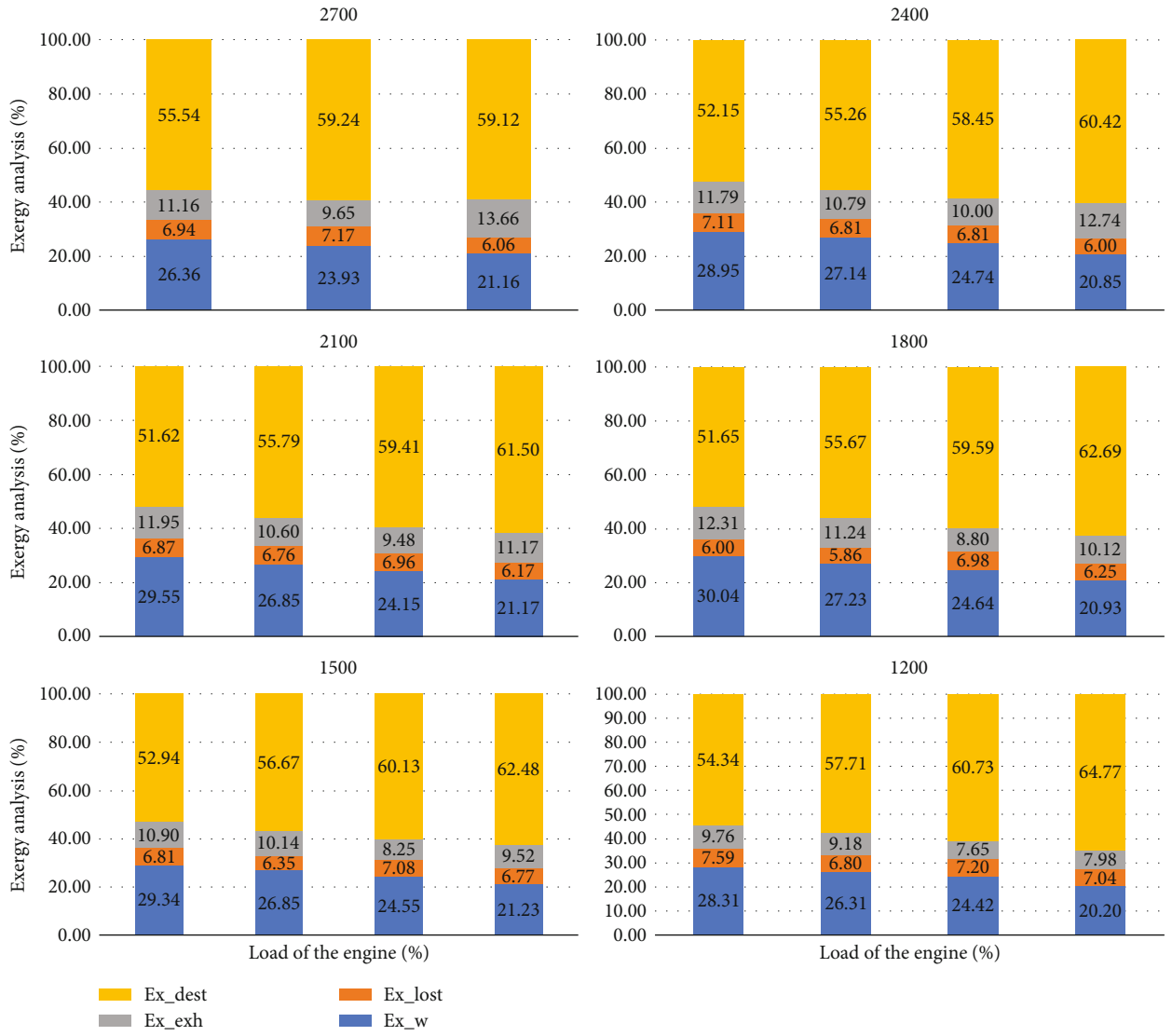

Figure 7: Results of exergy analysis of ammonia-fueled engine.

share of the cooling exergy (caused by a lower operating temperature). Described trends are generally true for the diesel and biodiesel variants as well; as such, the introduction of ammonia proves to be a feasible solution in terms of engine operation.

The comparison in terms of the ammonia-fueled variant to the diesel and biodiesel leads to the following observations. Firstly, introduction of ammonia to the engine changes the characteristic of efficiency; i.e., peak efficiency, throughout a set of the tested shaft's speeds, occurs at 100% load, not at 71% which is the case for diesel and biodiesel variants. This is true at all shaft speeds which is caused primarily by a better combustion of ammonia at the highest load. It can be observed by analyzing Table 8 which shows that for the case of the 71% load, the exhaust gases contain a similar share of ammonia in the exhaust, even though the mass flow rate of ammonia is lower. This is further confirmed by Figure 5 which proves that higher exergy destruction occurs at 71% compared to the 100% load. Still, in terms of the direct comparison of the efficiencies between these three type of fuels, it is seen that the ammonia-fueled variant achieves lower values in most cases, comparing the corresponding points. Secondly, further comparison of an ammonia-fueled variant to diesel reveals a lower exhaust energy than for the diesel case. This could be explained by a lower temperature of the exhaust gases for the ammonia-fueled variant and by values of the mass flow rates of the exhaust, compared to diesel at corresponding points. However, since the thermal efficiency is, for almost all cases, also lower, it implies the higher share of cooling losses, as seen when comparing Figures 2 and 6 (cooling losses are calculated by closing the energy balance, as explained in equation ((2))). The same relationship applies to the comparison of Figures 4–6 since the diesel and biodiesel cases represent very similar trends.

A comparison between the results of exergy assessments show that, for almost all cases independently of the shaft's speed or load, the exergy destruction has a higher share for ammonia than for diesel or biodiesel cases, roughly by 5 percentage points. It proves the need for engine optimization in

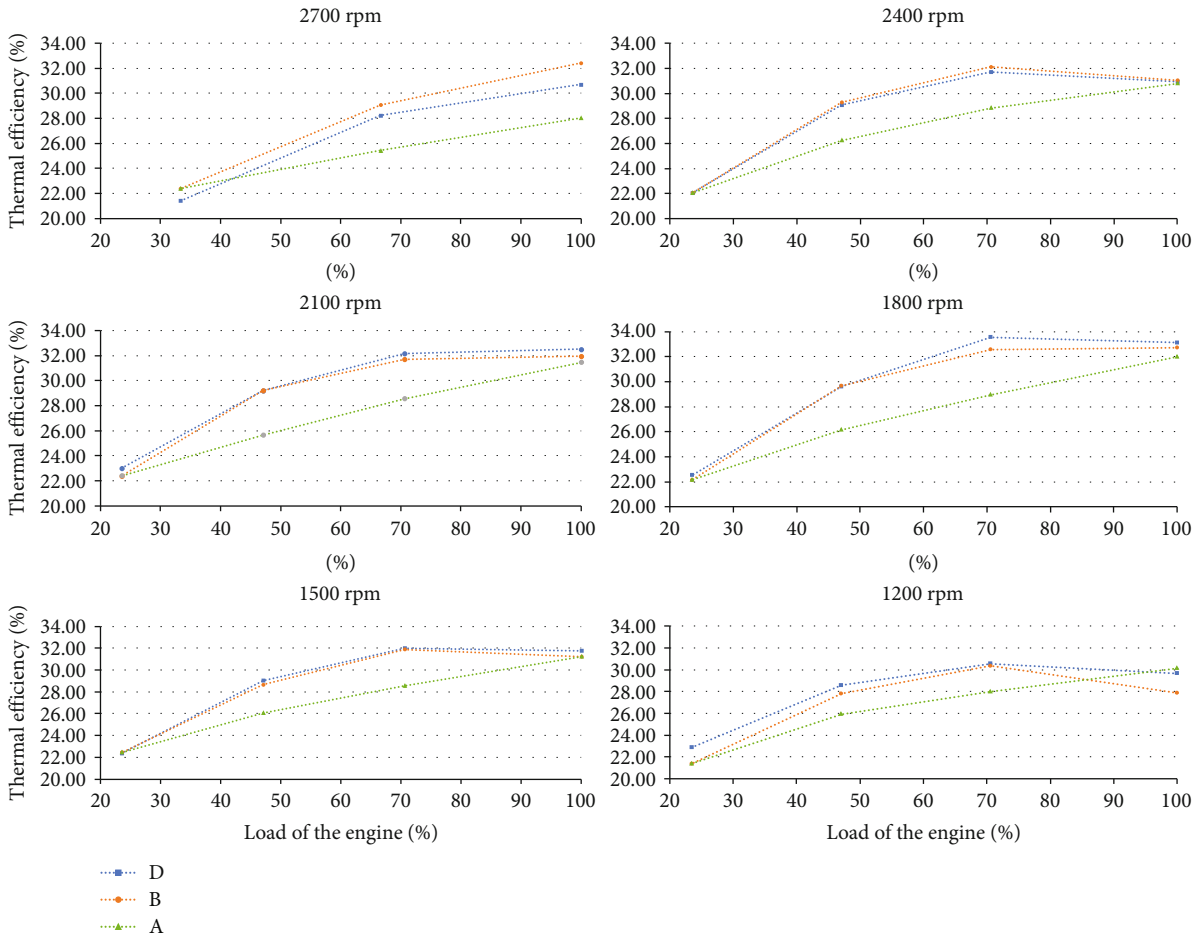

Figure 8: Thermal efficiency with respect to the engine's load and rpm.

terms of ammonia combustion. The share of exhaust exergy is higher for diesel and biodiesel cases compared to the ammonia-fueled engine which corresponds to the previously mentioned higher exhaust temperatures. A higher share of exergy lost to the environment (from the energy analysis) for the ammonia-fueled engine compared to diesel and biodiesel corresponds to the higher share of energy lost due to cooling.

The highest value of thermal efficiency across the engine's performance is achieved at 1800 rpm at 100% load with 31.98%; at the same point, the highest exergy efficiency is obtained to be 30.04%. An ideal waste heat recovery could theoretically increase this efficiency to 42.35%.

4.4. Fuel System Comparison. The results of particular analyses performed on the three types of fuel systems have been elaborated in the previous Sections 4.1, 4.2, and 4.3. Averaging the values over the engine's range (for a whole set of rpm as well as the load), the ammonia introduced to the engine, via port injection, impacts the energy balance of the engine in the following way (compared to diesel and biodiesel variants):

(1) Thermal efficiency is decreased

(2) Exhaust energy is decreased

(3) Heat lost due to cooling is increased

Exergy analysis leads to the following conclusions:

(1) Exergy efficiency and exergy of exhaust are decreased

(2) Exergy destruction and exergy of energy lost the environment are increased

Among these parameters, the thermal efficiency of the engine could be treated as the major criterion of the engine's performance. In order to understand the effect of introducing ammonia to this efficiency in a better way, Figure 8 has been plotted. It presents the thermal efficiency as a function of load with respect to a particular shaft's speed. A common trend for the efficiency of the diesel engine is that it achieves its peak value in between the engine operating range, as presented, e.g., by [23]. In the case of this study, it is generally seen that the engine is suited to perform more efficiently at high loads which correspond to the fact that the engine has been designed and tuned for the minitractor; such vehicles are designed to sustain high-load operation since they can be coupled with external devices and perform activities like mowing, spraying, sweeping, etc. Analyzing the diesel fuel trend, it is seen that a peak in between the engine's range

(71% load) is visible for 2400, 1800, 1500, and 1200 rpm; in the case of the 2700 and 2100 rpm, the highest value of thermal efficiency is at the 100% load. Low efficiency is noted at the lowest load of 24% for all shaft speeds. The results of thermal efficiency for the biodiesel-fueled engine indicate a similar trend. However, this behavior does not reflect the ammonia-fueled engine precisely, as, for this case, the peak occurs at the highest load for all speeds, and the relationship between the efficiency and the load is more linear. This could potentially indicate that even higher efficiencies might be achieved at higher loads, provided they fall within the engine's operating range (which could be verified on a larger-sized engine since the engine used in this study has been analyzed in terms of its whole range).

Independently of the load, at the highest rpm of 2700 and 2400, the peak efficiency is achieved by biodiesel. For 2100, 1800, 1500, and 1200 rpm, it is achieved by the diesel case, although, for this rpm, the ammonia-fueled variant achieves a very similar value (at 100% load; 0.2 percentage point difference). For most of the shaft's speeds, the differences between the three fuel systems at 24% and 100% are rather small. An apparent difference is seen for the 100% load at 2700 rpm, where the biodiesel-fueled engine achieved the higher efficiency by more than four percentage points compared to the ammonia-fueled variant. However, at medium loads, there is a difference of approximately two to three percentage points between the ammonia-fueled engine and the pure diesel and biodiesel cases. It shows the need for engine optimization in terms of adjusting the ammonia-pilot fuel ratio and optimizing the injection timing. If the engine was to be operated in a configuration that introduced ammonia, in order to minimize the thermodynamic losses, it should be operated at high loads. However, considering that the purpose of the engine is actually to perform activities designed for a minitractor, thus operating at high loads, ammonia introduction via port injection at default settings of the pilot fuel could be a feasible solution from the thermodynamic point of view.

The discussion presented so far is aimed at assessing the performance of the engine throughout its whole range, considering three types of fuel systems. However, as seen in Figure 8, for some points, the differences in the calculated results are very small. This is seen, for instance, at 2100 rpm and 100% load, where the thermal efficiency equals to 32.51%, 31.96%, and 31.45% for diesel, biodiesel, and ammonia scenarios, respectively. The underlying assumption behind the experimental research is the validity of the experiment data. The data provided are characterized by their uncertainty, as mentioned in Section 2; still, calculating the parameters such as the thermal efficiency based on these values are also characterized by an uncertainty which can be calculated using the uncertainty propagation method. Recalling equation (9) for the thermal efficiency, and equation (6) for the fuel energy rate, it is seen that the efficiency uncertainty depends on the measured value of the power of the engine, and the measured mass flow rate of fuel. The lower heating value of the respective fuel is also associated with an uncertainty; however, in order to simplify the calculations, it is going to be considered as a constant value. Under such an assumption, considering the partial derivatives of the thermal efficiency, the equation for the uncertainty of the thermal efficiency could be expressed as

Table 10: Efficiency and uncertainty comparison for three selected fueling systems for 2100 rpm and 100% load.

	Diesel	Biodiesel	Ammonia
η	32.509	31.962	31.454
$\delta\eta$	0.045	0.032	0.054

$$\delta\eta = \sqrt{\left(\frac{d\eta}{d\dot{W}}\delta\dot{W}\right)^2 + \left(\frac{d\eta}{d\dot{E}_{\text{fuel}}}\delta\dot{E}_{\text{fuel}}\right)^2}, \tag{20}$$

where $\delta\eta$ is the calculated uncertainty of the thermal efficiency, $\delta\dot{W}$ represents the uncertainty of the power of the engine, and $\delta\dot{E}_{\text{fuel}}$ stands for the uncertainty of fuel energy rate, calculated from the uncertainty propagation calculated for equation (6). The uncertainty of the fuel energy rate depends on the uncertainties of diesel, biodiesel, and ammonia mass flow rates.

Applying equation (20) on the example of 2100 rpm and 100% load, the results presented in Table 10 are obtained. It can be observed that the uncertainty associated with the calculated efficiency is small, which is a result of low uncertainties of the measured power and mass flow rates. This small uncertainty is primarily due to these values being derived from a set of measurements taken during the engine's steady-state operation, as explained in Section 2. While this process of uncertainty propagation could be repeated for other data points and calculated parameters, the resulting values are likely to be similarly small, given the observed trends. As such, the case study presented here is considered to provide sufficient understanding of these trends, and no further examination is carried out.

Results of the energy and exergy analyses for the diesel and biodiesel scenarios confirm the literature findings. Thermal and exergy efficiencies are similar to the values reported by the literature (close to 30-35%). Energy analysis indicates that about 65-70% of energy contained in the fuel is not effectively utilized, and the exergy balance proves the combustion and friction processes to account for most of the exergy destruction, e.g., [21, 24–26] (roughly around 50%).

From the thermodynamic point of view, ammonia seems to be a feasible solution; however, there are other crucial factors to consider prior to making ultimate conclusions regarding this technology. The first one would be to analyze the ammonia slip. For instance, as can be seen in Tables 7 and 8, at 2100 rpm and 71% load, the ammonia share in the exhaust is 1.627% at 6.9% oxygen level. This value is considered high given the toxic nature of ammonia. The second consideration should apply to NOx emissions. In this research, the NOx emissions have been excluded from the assessment since their impact on the energy and exergy balances is negligible. However, it is worth mentioning that even though NOx emissions are not critical for these specific assessments, they could have environmental implications,

especially in terms of the N_2O emission which is a greenhouse gas. Considering that the primary reason behind implementing an ammonia-fueled engine is to reduce the impact of the vehicle on climate change, high emissions of N_2O might offset the benefits of reducing carbon dioxide and methane. Even though a thorough investigation of the environmental impact of the ammonia-driven vehicle is outside the scope of this work, it could be a limiting factor towards widespread adoption of this technology.

5. Conclusions

In this work, a small-unit compression ignition (CI) engine is examined through energy and exergy assessments. These assessments are based on experimental data collected over the entire range of the engine, considering three fuel supply scenarios: diesel, biodiesel, and ammonia used in combination with biodiesel pilot oil. The ammonia was introduced to the engine using a port injection strategy. When considering the entire range of the engine, the maximum thermal efficiency of 33.56% and exergy efficiency of 31.88% were observed at 1800 rpm and 71% load for the diesel fuel system. For the biodiesel-fueled engine, thermal and exergy efficiencies of 32.72% and 30.93%, respectively, were achieved at 1800 rpm and full load. Lastly, the ammonia-fueled engine demonstrated thermal and exergy efficiencies of 31.98% and 30.04%, respectively, at 1800 rpm and full load. On average, the efficiency for the ammonia-fueled engine is slightly lower than in the case of diesel and biodiesel; however, this difference declines at maximum load (as in Figure 8), which is the trend observed for almost all of the shaft's speeds (apart from the highest 2700 rpm). For all three cases, the exergy destruction is responsible for the highest useful energy loss, and its optimization would bring the most improvement to the engine's performance.

A major advantage of utilizing ammonia in the internal combustion engine comes from the fact that it allows for the reduction of greenhouse gases such as CO_2 and CH_4. Still, further investigation towards the NH_3 slip and NOx emissions should be analyzed. One option would be to continue the development of the port injection system focusing on the optimization in terms of the ammonia-to-pilot fuel ratio, injection timing, or exhaust gas recirculation. Alternatively, a direct injection of ammonia could be a promising solution, especially towards solving the issue of NH_3 slip, as it would be aimed at improving the combustion. Direct injection could potentially improve the results of exergy assessment, since the ammonia-fueled scenario is characterized by a higher exergy destruction compared to the diesel and biodiesel cases.

To recapitulate, the work shows that from the thermodynamic point of view, ammonia can be a successful substitute of diesel and biodiesel oils for the compression ignition engine which is optimized to sustain heavy-load conditions, such as the analyzed engine, originally designed for a minitractor. However, the engine's optimization in terms its performance is required prior to the widespread popularisation of the technology.

Data Availability

Major data pertaining to this study are included. Supplementary data are available upon request.

Conflicts of Interest

The authors declare that they have no conflicts of interest.

Acknowledgments

The research leading to these results has received funding from the Norway Grants 2014-2021 under the POL-NOR2019 competition operated by the National Centre for Research and Development and from the Polish State Budget. The grant number is NOR/POLNOR/ACTIVATE/0046/2019-00.

References

[1] A. Aljaafari, I. M. R. Fattah, M. I. Jahirul et al., "Biodiesel emissions: a state-of-the-art review on health and environmental impacts," *Energies*, vol. 15, no. 18, p. 6854, 2022.

[2] US Energy Information Administration, "Biofuels explained - biofuels and the environment," 2022, https://www.eia.gov/energyexplained/biofuels/biofuels-and-the-environment.php.

[3] European Federation for Transport and Environment, "Biofuels twice as expensive as petrol and diesel in most cases," 2022, https://www.transportenvironment.org/discover/biofuels-are-twice-as-expensive-as-fossil-fuels/.

[4] L. Jakub, "Ammonia and conventional engine fuels: comparative environmental impact assessment," *E3S Web of Conferences*, vol. 44, article 00091, 2018.

[5] C. Mounaim-Rousselle and P. Brequigny, "Ammonia as fuel for low-carbon spark-ignition engines of tomorrow's passenger cars," *Frontiers in Mechanical Engineering*, vol. 6, p. 70, 2020.

[6] Y. A. Cengel and M. A. Boles, *Thermodynamics: An Engineering Approach*, McGraw-Hill College, Boston, MA, USA, 2006.

[7] N. Damanik, H. C. Ong, C. W. Tong, T. M. I. Mahlia, and A. S. Silitonga, "A review on the engine performance and exhaust emission characteristics of diesel engines fueled with biodiesel blends," *Environmental Science and Pollution Research*, vol. 25, no. 16, pp. 15307–15325, 2018.

[8] M. Abedin, H. Masjuki, M. Kalam, A. Sanjid, S. A. Rahman, and B. Masum, "Energy balance of internal combustion engines using alternative fuels," *Renewable and Sustainable Energy Reviews*, vol. 26, pp. 20–33, 2013.

[9] M. Abedin, A. Imran, H. Masjuki et al., "An overview on comparative engine performance and emission characteristics of different techniques involved in diesel engine as dual-fuel engine operation," *Renewable and Sustainable Energy Reviews*, vol. 60, pp. 306–316, 2016.

[10] M. Abdelrazek, M. Abdelaal, and A. El-Nahas, "Numerical simulation of a diesel engine performance powered by soybean biodiesel and diesel fuels," *Beni-Suef University Journal of Basic and Applied Sciences*, vol. 12, no. 1, 2023.

[11] B. Karpanai Selvan, S. Das, M. Chandrasekar et al., "Utilization of biodiesel blended fuel in a diesel engine - combustion engine performance and emission characteristics study," *Fuel*, vol. 311, article 122621, 2022.

[12] S. Thiyagarajan, E. Varuvel, V. Karthickeyan et al., "Effect of hydrogen on compression-ignition (CI) engine fueled with vegetable oil/biodiesel from various feedstocks: a review," *International Journal of Hydrogen Energy*, vol. 47, no. 88, pp. 37648–37667, 2022.

[13] O. H. Ghazal, "Performance and combustion characteristic of CI engine fueled with hydrogen enriched diesel," *International Journal of Hydrogen Energy*, vol. 38, no. 35, pp. 15469–15476, 2013.

[14] S. Jafarmadar, "Exergy analysis of hydrogen/diesel combustion in a dual fuel engine using three-dimensional model," *International Journal of Hydrogen Energy*, vol. 39, no. 17, pp. 9505–9514, 2014.

[15] H. Taghavifar, S. Khalilarya, S. Mirhasani, and S. Jafarmadar, "Numerical energetic and exergetic analysis of CI diesel engine performance for different fuels of hydrogen, dimethyl ether, and diesel under various engine speeds," *International Journal of Hydrogen Energy*, vol. 39, no. 17, pp. 9515–9526, 2014.

[16] E. Nadimi, G. Przybyla, D. Emberson, T. Lovas, L. Ziolkowski, and W. Adamczyk, "Effects of using ammonia as a primary fuel on engine performance and emissions in an ammonia/biodiesel dual-fuel CI engine," *International Journal of Energy Research*, vol. 46, no. 11, pp. 15347–15361, 2022.

[17] E. Nadimi, G. Przybyła, M. T. Lewandowski, and W. Adamczyk, "Effects of ammonia on combustion, emissions, and performance of the ammonia/diesel dual-fuel compression ignition engine," *Journal of the Energy Institute*, vol. 107, article 101158, 2023.

[18] K. Kuta, G. Przybyła, D. Kurzydym, and Z. Żmudka, "Experimental and numerical investigation of dual-fuel CI ammonia engine emissions and after-treatment with V_2O_5/SiO_2-TiO_2 SCR," *Fuel*, vol. 334, article 126523, 2023.

[19] Z. Zhang, W. Long, P. Dong et al., "Performance characteristics of a two-stroke low speed engine applying ammonia/diesel dual direct injection strategy," *Fuel*, vol. 332, article 126086, 2023.

[20] N. Al-Najem and J. Diab, "Energy-exergy analysis of a diesel engine," *Heat Recovery Systems and CHP*, vol. 12, no. 6, pp. 525–529, 1992.

[21] B. G. Şanli and E. Uludamar, "Energy and exergy analysis of a diesel engine fuelled with diesel and biodiesel fuels at various engine speeds," *Energy Sources, Part A: Recovery, Utilization, and Environmental Effects*, vol. 42, no. 11, pp. 1299–1313, 2020.

[22] A. Çakmak and A. Bilgin, "Exergy and energy analysis with economic aspects of a diesel engine running on biodiesel-diesel fuel blends," *International Journal of Exergy*, vol. 24, no. 1/2, p. 1, 2017.

[23] R. Karami, M. Hoseinpour, M. Rasul, N. Hassan, and M. Khan, "Exergy, energy, and emissions analyses of binary and ternary blends of seed waste biodiesel of tomato, papaya, and apricot in a diesel engine," *Energy Conversion andManagement: X*, vol. 16, article 100288, 2022.

[24] B. S. Kul and A. Kahraman, "Energy and exergy analyses of a diesel engine fuelled with biodiesel-diesel blends containing 5% bioethanol," *Entropy*, vol. 18, p. 387, 2016.

[25] I. Nazzal and R. Al-Doury, "Exergy and energy analysis of diesel engine fuelled with diesel and diesel-corn oil blends," *Journal of Advanced Research in Fluid Mechanics and Thermal Sciences*, vol. 63, pp. 92–106, 2019.

[26] G. Khoobbakht, A. Akram, M. Karimi, and G. Najafi, "Exergy and energy analysis of combustion of blended levels of biodiesel, ethanol and diesel fuel in a DI diesel engine," *Applied Thermal Engineering*, vol. 99, pp. 720–729, 2016.

[27] M. Hoseinpour, H. Sadrnia, M. Tabasizadeh, and B. Ghobadian, "Energy and exergy analyses of a diesel engine fueled with diesel, biodiesel-diesel blend and gasoline fumigation," *Energy*, vol. 141, pp. 2408–2420, 2017.

[28] X. Wang, B. G. Sun, and Q. H. Luo, "Energy and exergy analysis of a turbocharged hydrogen internal combustion engine," *International Journal of Hydrogen Energy*, vol. 44, no. 11, pp. 5551–5563, 2019.

[29] X. Yu, D. Li, P. Sun, G. Li, S. Yang, and C. Yao, "Energy and exergy analysis of a combined injection engine using gasoline port injection coupled with gasoline or hydrogen direct injection under lean-burn conditions," *International Journal of Hydrogen Energy*, vol. 46, no. 11, pp. 8253–8268, 2021.

[30] P. Sun, Z. Liu, X. Yu, C. Yao, Z. Guo, and S. Yang, "Experimental study on heat and exergy balance of a dual-fuel combined injection engine with hydrogen and gasoline," *International Journal of Hydrogen Energy*, vol. 44, no. 39, pp. 22301–22315, 2019.

[31] A. O. Hasan, A. I. Osman, A. H. Al-Muhtaseb et al., "An experimental study of engine characteristics and tailpipe emissions from modern DI diesel engine fuelled with methanol/diesel blends," *Fuel Processing Technology*, vol. 220, article 106901, 2021.

[32] C. Michalakakis, J. Fouillou, R. Lupton, A. Gonzalez Hernandez, and J. Cullen, "Calculating the chemical exergy of materials," *Journal of Industrial Ecology*, vol. 25, no. 2, pp. 274–287, 2021.

[33] J. Szargut, *Exergy Method: Technical and Ecological Applications*, WIT Press, 2006.

[34] J. Szargut, *Egzergia, Poradnik Obliczania i Stosowania*, Wydawnictwo Politechniki Slaskej, 2007.

[35] Y. J. Ramos da Costa, A. G. Barbosa de Lima, C. R. Bezerra Filho, and L. de Araujo Lima, "Energetic and exergetic analyses of a dual-fuel diesel engine," *Renewable and Sustainable Energy Reviews*, vol. 16, no. 7, pp. 4651–4660, 2012.

[36] A. Nair and F. Yu, "Quantification of atmospheric ammonia concentrations: a review of its measurement and modeling," *Atmosphere*, vol. 11, no. 10, p. 1092, 2020.

[37] Engineering Tool Box, "Air - molecular weight and composition," 2004, https://www.engineeringtoolbox.com/molecular-mass-air-d_679.html.

Paper III

Fuel 400 (2025) 135809

Contents lists available at ScienceDirect

Fuel

journal homepage: www.elsevier.com/locate/fuel

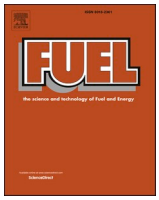

Full Length Article

Life cycle assessment of ammonia as carbon-free fuel in internal combustion engine-driven orchard vehicle

Mateusz Proniewicz *, Karolina Petela, Andrzej Szlęk

Silesian University of Technology, Faculty of Energy and Environmental Engineering, Department of Thermal Technology, Konarskiego 22, 44-100, Gliwice, Poland

ARTICLE INFO

Keywords:
LCA
Ammonia
Agriculture
Decarbonization
Energy transition
Sustainability

ABSTRACT

The study regards comparative LCA of ammonia- and diesel-fueled mini tractor destined for orchard activities. The LCA, compliant with ISO 14040 standards, encompasses production, operation, and utilization stages, considering both the vehicle and fuel life cycle. The analysis was conducted using the LCA for Experts software and utilizes hectare-year of tractor operation as a functional unit. Ammonia is synthesized via the Haber-Bosch process using the following sources of hydrogen: steam methane reforming (SMR), SMR with carbon capture and storage, and electrolysis using energy from PV, wind, and nuclear sources. The ammonia-fueled engine employs dual-fuel combustion with rapeseed oil-based biodiesel, utilizing a port injection strategy for ammonia. The operation phase is based on primary data sourced from experimental measurements, with fuel and vehicle production based on literature and Sphera's Managed LCA Content database. Environmental impacts are assessed using ReCiPe method, accounting for climate change (CC), fossil depletion, freshwater consumption, human health (HH), and ecosystem quality (EQ) environmental categories. Results show that electrolysis-based ammonia from wind and nuclear power achieves the highest climate change reductions, around 42 % and 44 %, respectively; however, nuclear scenario causes the highest impacts on fossil depletion and freshwater consumption. Nevertheless, high NO_x and NH_3 emissions from the operation phase, even including the residual ammonia-based SCR after-treatment method, render a stronger impact in terms of HH and EQ categories for the ammonia-fueled vehicle compared to the diesel scenario. Further improvements should target stronger reductions of NO_x, N_2O and NH_3 emissions, e.g. through combustion or after-treatment improvements.

1. Introduction

The climate crisis is a key driver behind the development of current decarbonization policies. One possible solution to address it is transitioning from fossil fuels, which release greenhouse gases (GHG), to alternatives like hydrogen or ammonia. Hydrogen is considered a promising energy carrier due to its high energy content per unit mass [1], clean emissions – producing only water vapor upon combustion – and its versatility in various applications (Chiesa et al., 2005; [2]. Renewable hydrogen is primarily generated via electrolysis[3]. However, its low density poses storage challenges, requiring either high pressurization (700 bar) or liquefaction at 20 K [4], both energy-intensive and costly, especially for vehicle applications [5]. As a result, ammonia is being explored as an alternative.

Ammonia molecule consists of one nitrogen and three hydrogen atoms, making it suitable for both direct applications, such as combustion engines [6] or fuel cells [7], and indirect uses as a hydrogen carrier [8,9]. Since ammonia contains no carbon, its complete combustion releases only nitrogen and water. Ammonia's physical properties resemble those of liquid propane, and it is commercially stored as a gas under moderate pressure (10 bar) or as a liquid at –33 °C [10]. Compared to hydrogen, ammonia offers a volumetric energy advantage, as presented in Table S1 (Supplementary materials). Ammonia is a widely used chemical, its production accounts for roughly 2 % of global energy consumption and 1.3 % of CO_2 emissions [11]. Due to its extensive use, ammonia's storage, management, and distribution infrastructure is already well-established, supporting its potential expansion for energy applications.

Decarbonizing sectors like agriculture, construction, and transportation is particularly challenging due to their dependence on diesel-

Abbreviations: CC, climate change; CCS, carbon capture and storage; EQ, ecosystem quality; EoL, end of life; GHG, greenhouse gases; HH, human health; LCA, life cycle assessment; LHV, lower heating value; SMR, steam methane reforming.

* Corresponding author.
E-mail addresses: mproniewicz@polsl.pl (M. Proniewicz), karolina.petela@polsl.pl (K. Petela), andrzej.szlek@polsl.pl (A. Szlęk).

https://doi.org/10.1016/j.fuel.2025.135809
Received 6 November 2024; Received in revised form 25 April 2025; Accepted 23 May 2025
Available online 26 May 2025

powered heavy machinery. In 2022, the EU-27's final energy consumption for petroleum and diesel, including industry and transport, totalled 226,092 toe. Road transportation accounted for 75.6 % of this, with agriculture and forestry contributing 6.5 %, and construction 2.2 % [12]. While passenger vehicles are being electrified, this solution is less viable for heavy-duty vehicles which require high power and adequate range, making ammonia a promising alternative for decarbonizing these sectors.

To realize the environmental benefits of switching from diesel to ammonia, several factors must be addressed. First, if ammonia production is too energy-intensive, the emissions saved during vehicle operation may be offset or even surpassed by those generated during production. Therefore, a detailed analysis of the environmental impact of ammonia production from different sources is essential. Second, technical feasibility of using ammonia in compression ignition (CI) engines must be evaluated. Due to ammonia's low flammability and high auto-ignition temperature compared to diesel, a dual-fuel mode is necessary for successful operation [13]. Additionally, emissions of NO_x and unburnt NH_3 must be considered [13]. In this context, a holistic life cycle assessment (LCA) comparing diesel- and ammonia-fueled vehicles is needed to understand the environmental impact of such transition.

The number of papers reviewing ammonia as a fuel has grown in recent years. MacFarlane et al. [14] explored the potential of an ammonia-based economy as a sustainable alternative for heavy transport, power generation, and energy storage, highlighting the technological advancements needed to scale production – from the current Haber-Bosch process to innovative electrochemical methods. Valera-Medina et al. [15] reviewed ammonia's use in power generation and CO_2 removal technologies, such as fuel cells, engines, gas turbines, and propulsion systems, with a focus on combustion behaviour in different blends. A systematic review on ammonia combustion by [16] indicated that extended ignition delay, low burning velocity, and NO_x emissions are primary challenges that can be addressed through blending or auxiliary technologies. Additionally, the study emphasized a knowledge gap regarding the technology readiness level for a wider implementation of ammonia-based technologies. Chiong et al. [17] reviewed combustion developments for ammonia-fueled engines, namely, spark ignition engines (SI), compression ignition (CI) engines, and gas turbines. For spark-ignition engines, a hydrogen blend from ammonia dissociation was found to be a practical approach to achieve acceptable thermal efficiency, while for CI engines, optimization of fuel injection was suggested as the most beneficial strategy for efficient ammonia utilization.

Exploring different fuelling options, Chai et al. [18] discussed ammonia, ammonia-hydrogen, and ammonia-methane possibilities, focusing on differences in reaction mechanisms depending on the applied blend, aiming towards better combustion characterization and progress in practical implementations. A review on ammonia/hydrogen-fueled engines by Xu et al. [19] emphasized the benefits of an ammonia-hydrogen blend setup and highlighted that storing hydrogen in the form of ammonia, integrated with ammonia decomposition for hydrogen derivation, was the preferred solution. Similarly, Qi et al. [20] also discussed an ammonia-hydrogen blend for an internal combustion engine, highlighting the engine's performance in such a setup and suggesting on-board ammonia decomposition.

Focusing on CI engines and green ammonia, Kurien & Mittal [21] elaborated on its production and utilization in a dual-fuel setup. They argued that ammonia's application is a feasible approach for the decarbonization of the automotive, marine, or power generation sectors. Their study stressed the need for advanced injection strategies in blending mode, coupled with an aftertreatment system, to be adopted towards addressing issues like high auto-ignition temperature, low burning velocity, and long quenching distance, which result in ammonia slip and NO_x emissions. Dimitriou & Javaid [22] also investigated the use of ammonia as a fuel for compression ignition engines, identifying challenges with unburned NH_3 and NO_x emissions. They emphasized the need for combustion improvements and advanced aftertreatment systems as well, suggesting that ammonia may be more suitable for applications without space constraints, such as marine or heavy-duty engines.

Several researchers have addressed the environmental impact of ammonia production. Bicer et al. [23] conducted LCA of ammonia production using the Haber-Bosch process with hydrogen from electrolysis powered by hydropower, nuclear, biomass, and municipal waste. The study evaluated environmental impacts like global warming potential, human toxicity, and abiotic depletion. It concluded that municipal waste had the lowest environmental impact, while hydropower offered the highest energy and exergy efficiency. Chisalita et al. [24] assessed the environmental impacts of various hydrogen production methods for ammonia synthesis, comparing traditional steam methane reforming with carbon capture technologies to alternatives like electrolysis and chemical looping with hydrogen (CLH). Both CLH and renewable-powered electrolysis showed strong potential for reducing greenhouse gas emissions, though they had notable impacts on water and soil. Singh et al. [25] conducted LCA of ammonia production using hydrogen from sources like underground coal gasification, SMR, biomass gasification, and solar- or wind-powered electrolysis, following the CML 2001 method. Biomass- and wind-based methods had the lowest environmental impacts, PV-based ammonia production had higher impacts on acidification, eutrophication, and human toxicity due to the hazardous materials in solar cell manufacturing. Proniewicz et al. [26] also presented LCA of ammonia production methods, comparing hydrogen from SMR, SMR with carbon capture and storage, and electrolysis powered by PV, wind, or nuclear energy. Electrolysis using nuclear or wind power showed the lowest greenhouse gas emissions.

Ammonia's application in compression ignition (CI) engine has been also discussed in literature. Cai et al.[27] investigated port injection configurations in a single-cylinder engine retrofitted from a heavy-duty diesel engine. The study, conducted under fixed conditions, focused on unregulated emissions like hydrogen cyanide (HCN). It revealed a complex interaction between injection timing and emissions, concluding that increasing the pilot fuel amount, raising the premixed gas inlet temperature, or adjusting combustion timing could help reduce HCN emissions. Nadimi et al. [28] explored the substitution of biodiesel with ammonia in a 6.4 kW dual-fuel compression ignition (CI) engine with port injection, operating at a fixed engine speed. The study found that approximately 70 % of biodiesel's energy could be replaced by ammonia, resulting in reduced CO_2, CO, and HC emissions but an increase in NO emissions.

A follow-up study by the same group evaluated higher ammonia-diesel ratios under similar conditions and revealed that 84.2 % of diesel energy could be replaced by ammonia, with the same emission trends observed [29,30]. In a study presented by Sonthalia et al. [31] sweet almond oil-based biodiesel was used as a substitute for diesel, which led to worsened engine performance and combustion characteristics. Improvement was achieved by introducing hydrogen gas; however, due to high NO_x emissions and safety concerns, ammonia was suggested as an alternative. In another study, Sonthalia et al. [32] investigated a CI engine fueled by sweet almond oil-based biodiesel and premixed ammonia with the aim of reducing CO_2 emissions through partial fuel substitution. Additionally, a calcite-based aftertreatment system was tested to further enhance CO_2 mitigation. Overall, they identified a viable setup that reduced greenhouse gas emissions while maintaining satisfactory performance. Proniewicz et al. [33] compared the energetic and exergetic performance of an ammonia-fueled engine, using port injection, to pure diesel and pure biodiesel scenarios for the same engine analyzed as [29,30]. The study demonstrated that, from a thermodynamic perspective, ammonia is a viable substitute for conventional fuels.

Aggregating the environmental impact of fuel production and vehicle emissions is a key focus of LCA studies for ammonia-fueled and heavy-duty vehicles. In a report chapter (Chapter 7), an LCA conducted by Dincer & Bicer, [34] compared several fueling options for a passenger

vehicle – including hydrogen, electricity, ammonia, compressed natural gas, diesel, gasoline, and methanol – evaluating their global warming potential, human toxicity, and abiotic depletion. Based on average fuel consumption and emissions per kilometer, they found ammonia and hydrogen to be the least environmentally harmful, and highlighted the significant environmental burden of battery production and disposal for electric vehicles. In another study, Bicer & Dincer, [35] assessed ammonia as a primary fuel for city transportation and power generation, assuming ammonia production via wind-powered electrolysis. The study concluded that switching to ammonia would bring environmental benefits in both the transport and power sectors.

Chang et al. [36] assessed the environmental impact of yard tractors powered by diesel, electric, LNG, and hydrogen fuel cells, focusing on their life cycle carbon footprints. Hydrogen fuel cells showed the lowest emissions, followed by electric and LNG. For diesel and LNG, the operation phase was the main emissions source, whereas for hydrogen and electric vehicles, the production stage (vehicle and fuel) was the largest contributor. Martelli et al. [37] evaluated the greenhouse gas emissions of an orchard tractor in Europe over 10 years using life cycle assessment based on field test data, finding that the operation phase accounted for around 90 % of total emissions.

Literature review confirms that ammonia has the potential to play a key role in the energy transition towards decarbonization and can serve as a viable substitute for fossil fuels in compression ignition engine used in heavy-duty vehicles. The primary objective of this study is to verify this premise. A comprehensive life cycle assessment of a mini tractor used in agriculture, powered by ammonia through port injection with pilot biodiesel fuel, is presented. The analysis of the operational phase of the vehicle is based on a detailed working cycle and emissions data gathered from experimental measurements, providing reliable insights regarding its actual operation. Several ammonia production pathways are also considered; in case the ammonia production is too energy-intensive, the emissions saved during vehicle operation could be offset. The study aims to inform about the cradle-to-grave environmental impacts for a heavy-duty vehicle, and to highlight the advantages and disadvantages of the fuel transition, as the results are benchmarked against the diesel baseline. While broader LCAs on ammonia utilization in engines exist, no literature has been found on dedicated life cycle assessments of an ammonia-fueled heavy-duty vehicle which is a gap that this study addresses.

2. Materials and methods

2.1. Goal and scope

The goal of this study is to evaluate the environmental impact of an

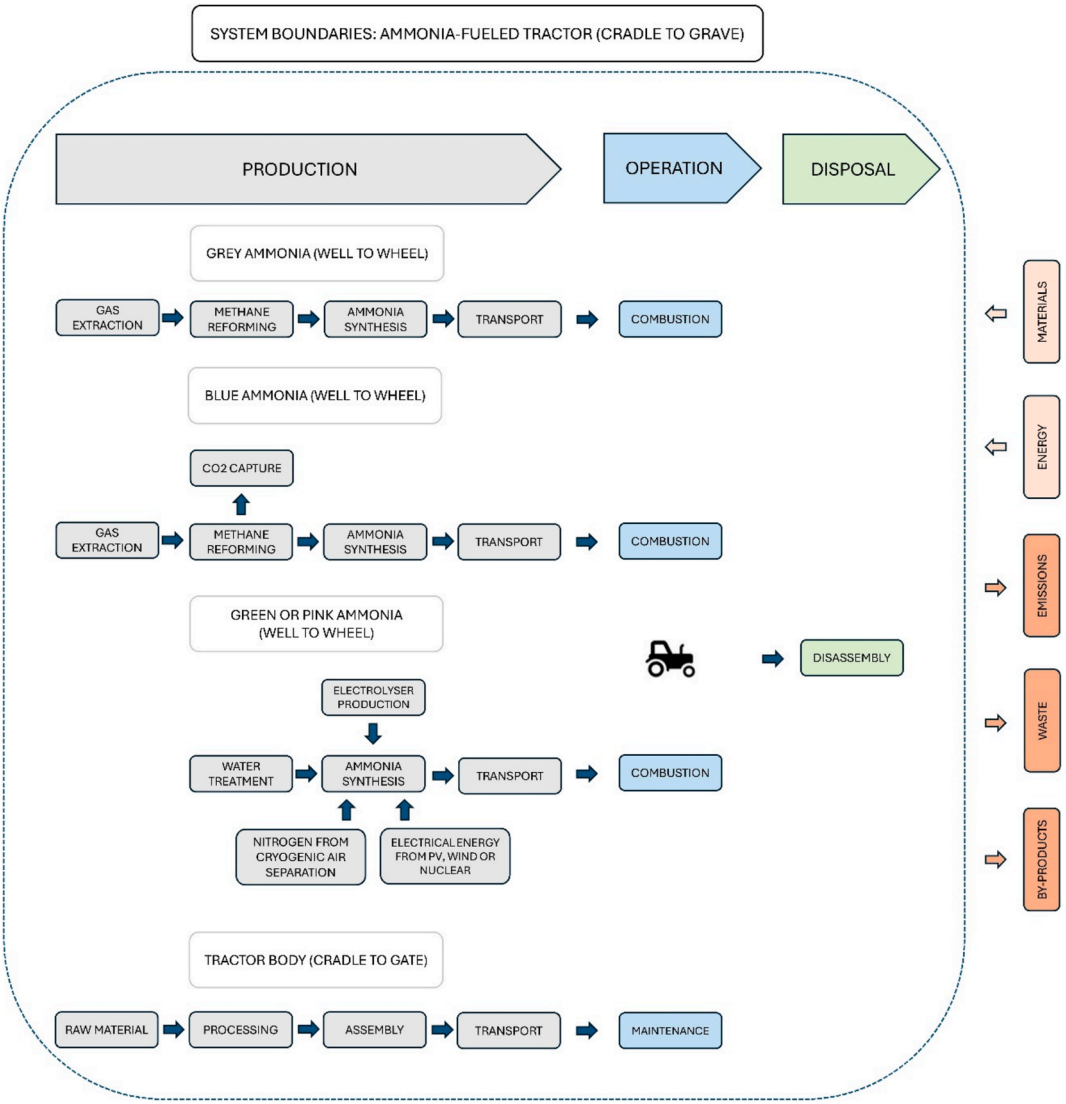

Fig. 1. LCA system boundaries of ammonia-fueled tractor.

ammonia-fueled mini tractor and compare it to its diesel-powered equivalent. In the proposed technological setup, ammonia is combusted in a compression ignition engine via port injection, with biodiesel as the pilot fuel. The life cycle assessment follows ISO 14040 standards and adopts a cradle-to-grave approach, covering all stages from raw material extraction to the end of life (EoL), as outlined in Fig. 1 and Fig. 2.

The production of ammonia in this study is modeled using the Haber-Bosch process, chosen for its technological maturity [23,25] and large-scale production capacity [38] making it the most representative method for ammonia production as a direct fuel. Biodiesel is selected as the secondary fuel due to its renewable nature [39] and high thermal efficiency in compression ignition engines reaching nearly 33 %[33]. Its production is based on the transesterification of rapeseed oil, consistent with the fuel used in the experiments. In the Haber-Bosch process, ammonia is synthesized from hydrogen – which can be produced through conventional or renewable methods – and nitrogen, typically derived from air separation.

The following ammonia production scenarios are considered in this work:

- **Grey ammonia**: Produced using hydrogen from steam methane reforming.
- **Blue ammonia**: Produced using hydrogen from steam methane reforming with carbon capture and storage.
- **Green ammonia**: Produced using hydrogen from water electrolysis powered by photovoltaic or wind energy.
- **Pink ammonia**: Produced using hydrogen from water electrolysis powered by nuclear energy.

The analyzed vehicle is SCOUT 15-T, mini tractor suitable for orchard operations. The functional unit is defined as a single hectare-year of tractor operation. LCA performed using LCA for Experts (GaBi) software adopts system boundaries for both ammonia- and diesel-fueled tractors shown in Fig. 1 and Fig. 2.

To evaluate the environmental impacts of diesel- and ammonia-fueled vehicles, five categories from the ReCiPe 2016 v1.1 method are assessed (hierarchist perspective, 100 year timeframe):

1. Climate change (midpoint), expressed in kg CO_2 equivalent.
2. Fossil depletion (midpoint), quantified in kg oil equivalent.
3. Freshwater consumption (midpoint), measured in cubic meters.
4. Human health (endpoint), expressed in DALYs (disability-adjusted life years).
5. Ecosystem quality (endpoint): quantified in species-years.

2.2. Life cycle inventory

The dataset for this analysis combines primary data on vehicle operation with secondary data for the production and disposal phases. Secondary data were obtained primarily from Sphera's Managed LCA Content database. This database ensures reliability through industry-sourced data and a thorough third-party review, covering aspects such as technical accuracy, relevance, completeness, precision, and methodological suitability. The approach to modeling each phase in the LCA, along with their respective process representations, is outlined in Table 1. Certain fuel production inventories utilize a hybrid approach, integrating a literature-based inventory with upstream data (e.g., electricity) sourced from the Sphera's Managed LCA Content.

2.2.1. Ammonia production pathways

The ammonia production pathways align with those shown in Fig. 1. The life cycle inventory for ammonia synthesis applied in this work is identical to that reported in our earlier, dedicated study of ammonia production pathways for ammonia's utilization as a fuel [26]. From an LCA perspective, ammonia production precedes vehicle operation and therefore it is treated as an upstream process. Accordingly, key modeling assumptions are described in this work; a thorough discussion of methodological details is provided in the cited publication.

The environmental impacts of grey and blue ammonia production (steam methane reforming with and without carbon capture and storage) are directly assessed from aggregated processes in the software database:

1. Ammonia (NH_3) production mix, without CO_2 recovery [43]
2. Ammonia (NH_3) synthesis with CO_2 recovery, where CO_2 is a by-product [44]

Both models represent the full life cycle from raw material extraction to anhydrous ammonia production via the Haber-Bosch process, using

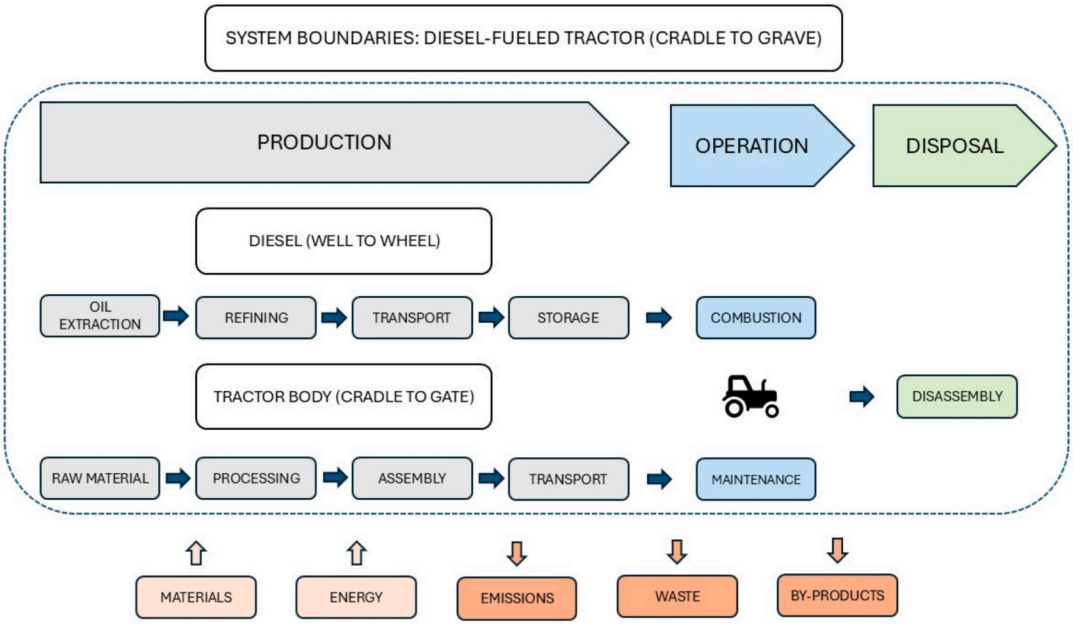

Fig. 2. LCA system boundaries of diesel-fueled tractor.

Table 1
Phases of LCA of the mini tractor.

Phase	Source	Process in software database	Description
Mini tractor construction	Sphera's Managed LCA Content	Farm tractor production (material composition, including Maintenance, without EoL)[40]	The process estimates farm tractor production using industry-sourced material composition, following a cradle-to-gate approach, and includes maintenance components replaced over a 5-year lifespan. The total materials used for both production and maintenance amount to approximately 13.3 tons in weight. Since the weight of the mini tractor used for the analysis is 540 kg, linear scaling is applied. The dataset is globally applicable.
Ammonia production	Literature data with upstream processes from the software database	User defined model	The process considers ammonia synthesized via Haber-Bosch process based on literature data requirements and distinguishes several ammonia sources. Detailed in section 2.2.1.
Biodiesel production	Literature data with upstream processes from the software database	User defined model	The process regards biodiesel production through transesterification based on supercritical methanol process using propane as co-solvent. Detailed in section 2.2.2.
Diesel production	Sphera's Managed LCA Content	Diesel mix at filling station[41]	The process treats the diesel as one of the co-products from a refinery plant that includes a set of specific processes: distillation, desulfurization, cracking alkylation and others. Diesel's contribution is based on mass allocation and net calorific value. The dataset is representative for Europe.
Tractor operation	Experiments	User defined model	The dataset comes from the experimental measurements of the engine used in the engine from a mini tractor destined for orchard operation. Detailed in sections 2.2.3 and 2.2.4.
Tractor utilization	Sphera's Managed LCA Content	Car shredder[42]	End of life phase is denoted by a shredding of the vehicle body considering partial disassembly of used parts prior to the shredding. The dataset is based on the German market.

data relevant to European conditions. For grey ammonia, CO_2 from SMR is emitted to the atmosphere, while in blue ammonia, CO_2 is recovered as a by-product. Steam methane reforming primarily uses natural gas and water, with 30–40 % of the gas consumed for combustion, producing "diluted CO_2," and the remainder for hydrogen generation and "process CO_2." Blue ammonia production cuts CO_2 emissions, but carbon capture applies only to "process CO_2." The recovered CO_2 is treated as a by-product, with no allocation between CO_2 and NH_3 outputs.

Ammonia production via electrolysis is modeled based on literature inputs. Quantities of respective flows are presented in Table 2. The upstream processes include electrical energy, pretreated water, steam (for heating) and nitrogen (for cleaning). The processes from the software database used to represent them are shown in Table S2.

Electrolyzer manufacturing is also considered and modeled separately. The alkaline electrolyser was selected due to its compatibility with renewable energy sources like solar and wind [45]. Key materials for electrolyser production include: copper, nickel, stainless steel, aluminum sheet, and PVC. Additional inputs such as aniline, purified terephthalic acid, nitric acid, hydrochloric acid, lubricant oil (a refinery by-product), carbon monoxide, gypsum plaster, and deionized water (from ion exchange) are also considered. Energy needs include thermal energy from natural gas heat plants and grid electricity (EU-28 average, 2020). All inputs are modeled using appropriate processes from the software database.

In the next step, the Haber-Bosch process synthesizes ammonia using hydrogen from the electrolyser and nitrogen from an air separation unit. Hydrogen reacts with nitrogen in a 3:1 ratio, achieving a 98 % conversion rate. Finally, ammonia transportation is also considered. It is assumed that ammonia is transported by road over a distance of 150 km in a Euro V standard freight truck.

2.2.2. Biodiesel production

Since the ammonia-fueled engine operates in dual-fuel mode, biodiesel production is also considered. Biodiesel is produced via transesterification, where oil or fat reacts with alcohol to form fatty acid alkyl esters, typically using a catalyst. Like ammonia, biodiesel production is modeled using literature inputs and upstream processes from the software database. Morais et al. [39] analyzed alkali-catalyzed, acid-catalyzed and supercritical methanol transesterification pathways; this study uses specific inventory data from this work which found supercritical methanol process with propane as a co-solvent to have the lowest environmental impact among the three methods. Therefore, this method is used to represent biodiesel production in this research. A list of inputs for transesterification is shown in Table 3. While the outputs from the transesterification process include biodiesel and glycerol (1000 kg and 106 kg, respectively), allocation by energy content (LHV) has been applied leading to reduction of quantities of inputs for the biodiesel production solely. The processes from the software databased used to represent them are summarized in Table S3. Biodiesel transportation for the end use is considered in the same way as for green ammonia, elaborated in section 2.2.1.

Additionally, methanol production is modeled separately using the natural gas steam reforming route, based on the inventory by [46]. Inputs include European mixes for electricity and natural gas, oxygen from air separation, and sodium hydroxide from a "mix" of mercury cell, diaphragm cell, and membrane cell electrolysis. Desalinated water via ion exchange and freshwater of moderate scarcity are also considered. All processes are based on European data. Quantities are detailed in the source paper [46].

2.2.3. Working cycle of a mini tractor

The operational phase models emissions from the tractor's use in a one-hectare apple orchard over a year. Annual orchard activities

Table 2
Electrolysis material and energy requirements per kg of hydrogen, based on [26].

Input	Quantity
Water	9 kg
Electrical energy	53 kWh
Nitrogen	0.00029 kg
Steam	0.11 kg

Table 3
Transesterification material and energy requirements per ton of biodiesel (energy allocation), based on [39].

Inputs	Quantity, kg/t
Oil	952.47
Methanol	105.33
Propane	0.02
High pressure steam	188.05
Medium pressure steam	229.17
Electricity (kWh)	3.84
Water cooling	487.95

Table 4
Orchard management activities and their frequency.

Activity	Frequency during a year
Branch and leaves sweeping and raking	2
Mechanical weed removal (hoeing)	1
Grass mowing	8
Pruning	2
Fruit harvest	1
Tree fertilizing	4
Insecticide and fungicide application	20

(Table 4) are based on an apple orchard management calendar from the University of Maine[47].

A scaled CAD model of the orchard was developed to simulate tractor performance for each task, based on the routes shown in Fig. S1:

- **Sweeping, hoeing, mowing**: the tractor leaves storage, travels to the orchard, passes through each alley twice with the equipment activated, and returns.
- **Spraying**: the tractor, with a sprayer attached, passes through each alley once, sprays, and returns to storage.
- **Harvesting, pruning**: the tractor, equipped with a trailer, travels through each alley once to collect fruit or prune, and returns to storage when the trailer is full.

Concurrently, a theoretical gearbox model was developed, breaking down orchard activities into sub-activities like road travel, turning, etc., applying gear and speed combinations to all sub-activities. This allowed for calculating the distances covered by vehicle at each operating point. To be able to reflect these operating points during experiments on a test rig, rolling resistances, transmission losses, and air drag were factored in, accounting for increased weight of tractor when orchard equipment like mower or sweeper is attached. This allowed the definition of a full set of engine operating points (shaft speed and torque) for all activities.

Additionally, for actions such as sweeping, mowing, and hoeing, activating the device adds load to the engine (while the sprayer operates with a separate engine). To account for this, the maximum load at assumed speed is used (maximum load determined from experiments). This is illustrated in Fig. 3 where engine power over time during sweeping is illustrated. The tractor accelerates from storage, slows down in the orchard, and reaches a peak of ~ 4.2 kW when the sweeper is activated. This pattern is repeated for all 33 alleys (highlighted in red color in Fig. 3). The final part shows the return to storage. Other tasks follow similar trends, with variations due to different equipment.

2.2.4. Experimental data

Implemented algorithm determined all engine operating points throughout its life cycle, which could be tested on a rig. A schematic of the experimental setup is shown in Fig. S2. Gaseous ammonia is introduced into the intake manifold, mixing with air before entering the combustion chamber, while the pilot fuel is delivered through the injector. Exhaust gases were analyzed using FTIR Gasmet DX400, with additional measurements for oxygen and PM via CAPELEC CAP 3201. Measured variables included fuel consumption, CO_2, CO, CH_4, NO_x, NH_3, SO_2, PM10, and other exhaust components. Key engine and fuel details are provided in Table S4.

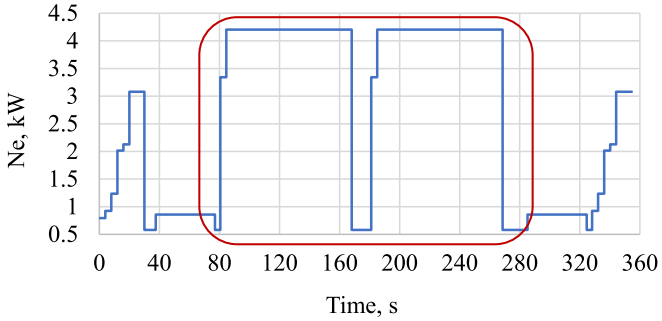

Fig. 3. Change in engine's power over time for sweeping activity.

A comparison of emissions at 2400 and 1200 RPM under various loads for the two fueling scenarios is shown in Table S5. For the ammonia-fueled engine, the pilot fuel provided 4 Nm of torque on the shaft, with torque increases achieved by adjusting ammonia flow. A 100 % load corresponds to 17 Nm, while the minimum load (24 %) represents 4 Nm, with the engine running solely on biodiesel. Due to ammonia's lower heating value, the total fuel mass flow (biodiesel and ammonia) exceeds that of diesel. As expected, the diesel scenario has higher CO_2 emissions and exhaust temperatures, leading to elevated NO_2 emissions, especially at low loads. However, total NO_x emissions ($NO + NO_2$) are higher for the ammonia-fueled engine at most points, due to nitrogen oxidation from both air and ammonia. The ammonia-fueled engine also emits unburnt ammonia (slip) and nitrous oxide (N_2O), a potent greenhouse gas with a Global Warming Potential of 273. Both scenarios showed traces of CH_4, but since emissions were comparable, it was not a focus of the study. Measured values are reported with their uncertainties (type A), which are very low due to the gradual refinement of the dataset by removing outliers. The last column in Table S5 provides a direct comparison of GHG emissions at respective engine points. Higher GHG emissions are confirmed for the ammonia-fueled vehicle at 71 % and 47 % load at 2400 rpm and at 47 % load at 1200 rpm.

Consequently, it can be concluded that using ammonia under such conditions does not serve its primary decarbonization purpose and that it would be more beneficial to operate on biodiesel alone under such loads, and switch to the ammonia-biodiesel mode at full load. However, the experiments were designed aiming to achieve:

a) Maximum fuel substitution: ammonia at its maximum share and using biodiesel only as a pilot fuel.
b) Practicality: utilizing ammonia in a simple manner, i.e., in a manner allowing for existing engine retrofitting rather than a complete engine and injection setup redesign, which might lead to increased costs.

LCA presented in this work serves to analyze the ammonia-fueled CI engine under these assumptions.

Experimental data used in this work is the same as that published by the authors of this study in [33], where energy and exergy balances of the ammonia-fueled engine were presented for various rpm and loads. This dataset is considered the most adequate since it encompasses a comprehensive map of engine operation, and vehicles like mini tractors often operate under partial load conditions (such as spraying), which it is necessary to consider for the validity of the LCA. The reliability of the dataset is additionally confirmed by the fact that several other experimental results performed on this test rig have been published [28–30,48].

Finally, measured emissions and fuel consumption were integrated over distances based on the working cycle and activity frequencies, forming an input–output model for diesel- and ammonia-fueled scenarios.

2.2.5. Selective catalytic reduction

High NO_x emissions revealed by experimental data may be reduced via an aftertreatment system, as suggested by literature [22,48]. In this study, a theoretical SCR reduction method is employed based on two reactions [49]:

$$NO + NO_2 + 2NH_3 \rightarrow 2N_2 + 3H_2O \quad (1)$$

$$4NO + 4NH_3 + O_2 \rightarrow 4N_2 + 6H_2O \quad (2)$$

Since at all measured points the concentration of NO is higher than that of NO_2, NH_3 first reacts with NO and NO_2 in a 1:1:2 M ratio, according to the reaction shown in eq. (1). In case the quantity of ammonia is less than required, all of it reacts with NO and NO_2, and the remaining NO and NO_2 are present at the exhaust outlet.

If sufficient quantity of ammonia is present to satisfy the reaction shown in eq. (1), remaining NO reacts with NH3 in a 1:1 ratio according to reaction presented in eq. (2). In case there is more ammonia than required for this reaction, all NO is reduced, and the surplus is released as ammonia slip in the exhaust gases. Conversely, if the quantity of ammonia is not sufficient, it reacts completely with NO, and the remaining NO is present at the exhaust outlet.

The applied method provides an idealized, reaction–based estimate of NO_x reduction and residual NH_3 within the SCR, i.e., no external ammonia injection for NO_x optimization is included. However, actual SCR performance depends on exhaust flow rate, temperature, the NO_x/NH_3 ratio, and catalyst formulation [50]. Consequently, full SCR optimization might require additional NH_3 dosing, which would increase overall NH_3 production – a factor to be considered from an LCA perspective. A comprehensive experimental campaign or CFD study, beyond the scope of this research, would be required to account for these factors and determine the final ammonia usage. Thus, the reaction–based estimation presented here represents an upper bound on emission reduction, assuming complete utilization of the ammonia already present in the exhaust.

The results section presents emissions before and after SCR, assuming no N2O reduction, as interactions between NO, NO_2, NH_3 and N_2O require dedicated analysis and are not considered among the primary reactions occurring during SCR operation[49].

3. Results

3.1. Life cycle impact assessment

Fig. 4 presents the climate change results across life cycle phases. Analysis of the diesel-fueled mini tractor shows that the operation phase contributes approximately 70 % of the total impact, followed by tractor production at about 26 %, and diesel fuel production at 3.7 %. Vehicle disassembly has negligible impact due to low energy requirements. High impact of the operation phase stems primarily from CO_2 emissions, but also from CH_4 and N_2O. Tractor production impacts result from manufacturing, processing, and assembling materials like steel, aluminum, thermoset and thermoplastic polymers, and glass, as noted in [37].

For SMR-based ammonia-fueled vehicle, ammonia fuel production emits approximately 59 kg CO_2 eq., corresponding to 47 % of the total impact on climate change. Steam methane reforming has high greenhouse gas emissions due to the methane reforming reaction and the need for high temperatures. In the blue ammonia-fueled vehicle, coupling SMR with CCS reduces emissions from ammonia production by approximately half. This impact can be further lowered by switching to electrolysis-based ammonia, with the lowest impact achieved in the pink scenario using nuclear energy for electricity generation. From the comprehensive comparison focused solely on the ammonia production methods [26]it is known that the electrical energy production phase dominates over the nitrogen and alkaline electrolyser manufacturing phases.

The operation phase is the largest contributor to the climate change impact across all ammonia-fueled scenarios for considered vehicle. While ammonia-fueled engines emit less CO_2 (still non-zero due to a biodiesel pilot fuel stream), they produce higher N_2O emissions

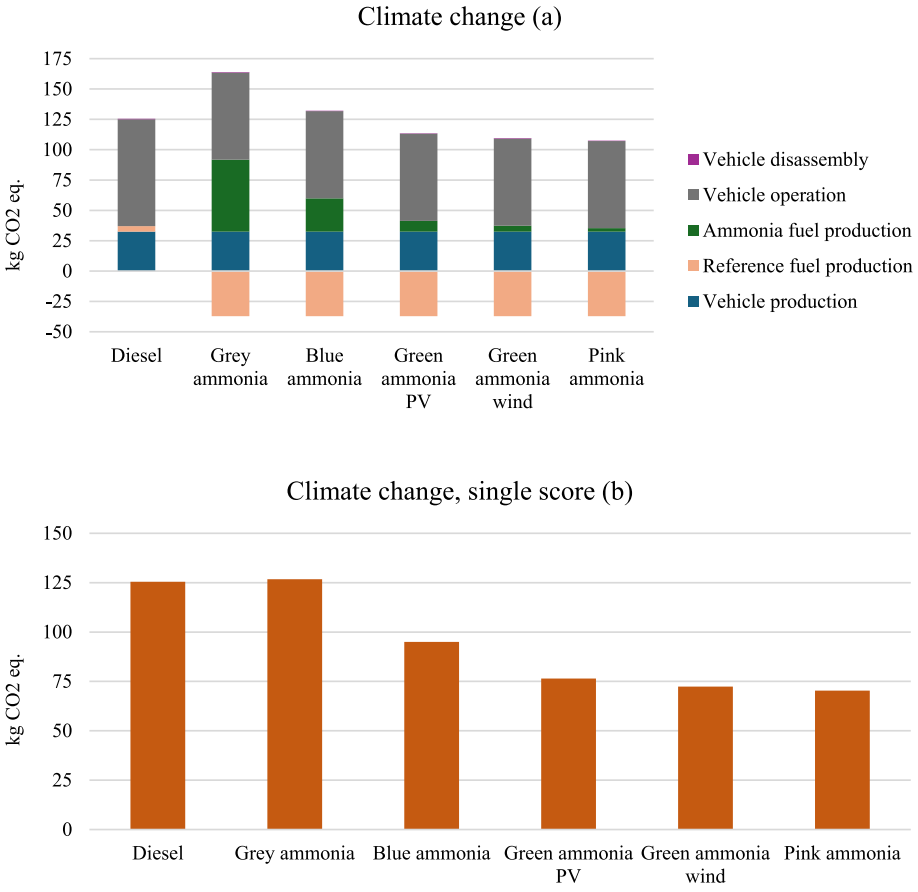

Fig. 4. Climate change results.

compared to diesel engines which results in significant GHG emissions over the life cycle. The ammonia-fueled tractor emits around 72 kg CO_2 eq. during operation, which is lower than the diesel case at approximately 88 kg CO_2 eq.; the reduction at 18 % can be considered as moderate.

The third phase affecting the climate change impact of the ammonia-fueled tractor is the reference fuel production, which represents biodiesel. Biodiesel production involves rapeseed oil derived from rapeseed plants that absorb CO_2. This absorption is accounted for in the calculations since the emission phase also includes CO_2, reflecting the biogenic carbon balance in the climate change results. The reference fuel production phase contributes −37 kg CO_2 eq., enhancing the decarbonization effect achieved by the fuel switch.

In all cases, mini tractor production has the same impact since the same vehicle must be manufactured – a trend consistent across all environmental categories analyzed. Retrofitting the tractor with an ammonia tank and transmission line increases its weight by less than 5 %, minimally affecting the environmental impact of production. Vehicle disassembly is practically negligible in the life cycle. Second part of Fig. 4 illustrates the aggregated climate change impact for the considered scenarios. The highest GHG emission reductions are achieved with electrolysis-based ammonia from wind power and nuclear sources, resulting in approximately 42 % and 44 % reductions, respectively.

Fig. 5(a) presents the results for the fossil depletion category. Fossil depletion depends primarily on fuel production pathways and vehicle manufacturing. Ammonia production from SMR, combined with biodiesel production via transesterification, yields a similar fossil depletion value to diesel production, resulting in comparable impacts for diesel and grey ammonia cases. Coupling SMR with CCS results in a slightly higher value, indicating increased resource exhaustion due to CCS requirements. Renewable-based ammonia achieves the lowest impacts in this category, resulting in 43 % and 45 % reductions compared to the diesel-fueled tractor for PV- and wind-based scenarios, respectively. Their contributions to fossil depletion stem from manufacturing and utilizing the PV panels and wind turbines. In the nuclear-based scenario, fossil depletion is approximately 78 % higher than diesel, primarily due to uranium resource exploitation in nuclear power plants. Biodiesel production, while generating lower impact than vehicle production, contributes to fossil depletion primarily due to resource extraction for rapeseed oil production.

Fig. 5(b) outlines the performance in freshwater consumption. Vehicle production dominates the impact in this category for all cases, followed by fuel production phases. All ammonia-fueled scenarios exhibit a higher impact compared to diesel, by around 40–50 %, primarily due to the high water usage in the production of the reference fuel, which involves rapeseed oil production. Regarding ammonia sources, the nuclear-based pathway requires considerably more water than the other options, resulting in nearly twice the impact on freshwater consumption compared to diesel.

Fig. 6(a) presents the results on human health. For the diesel-fueled tractor, the strongest contributors are diesel production and vehicle production phases, which have similar values, followed by vehicle operation. Since human health is an endpoint environmental category derived from ReCiPe midpoint categories, most impactful midpoint categories can be investigated. In the case of vehicle and diesel production, this is attributed to carcinogenic emissions associated with human toxicity, measured in 1,4-dichlorobenzene equivalents. For ammonia-fueled scenarios, fuel production phases have a weaker effect on outcomes. The strongest impact comes from the operation phase, followed by vehicle production. The most significant midpoint category here is fine particulate matter formation, primarily due to high emissions of ammonia from the ammonia-fueled engine, followed by

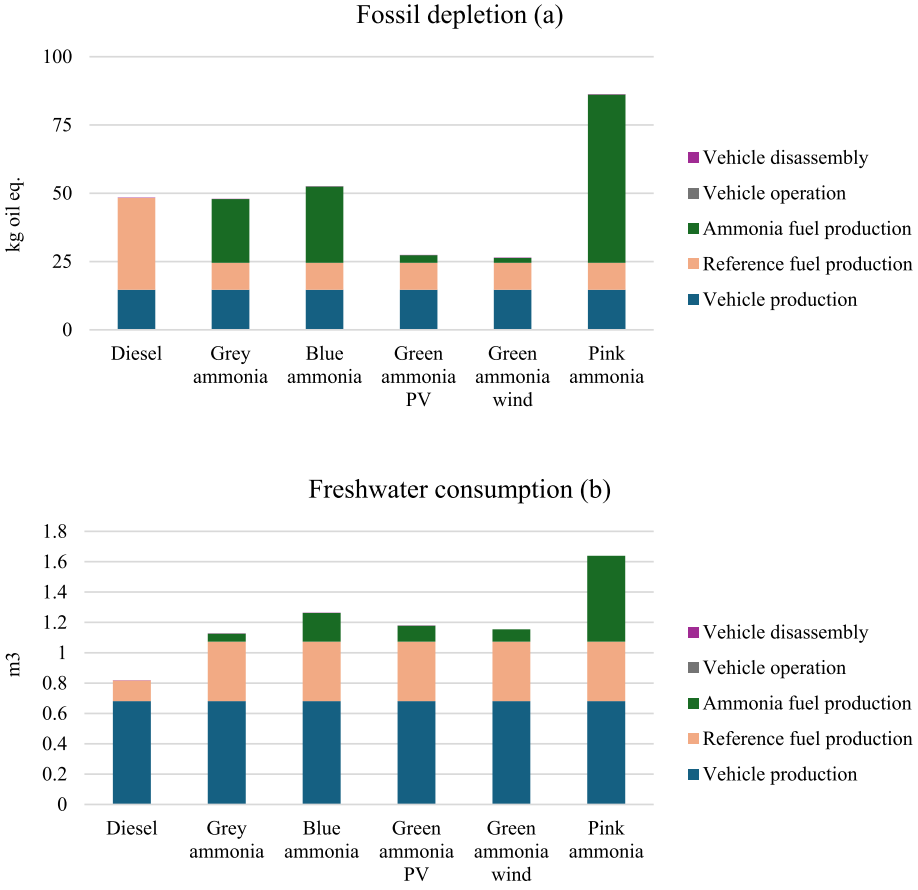

Fig. 5. Fossil depletion and freshwater consumption results.

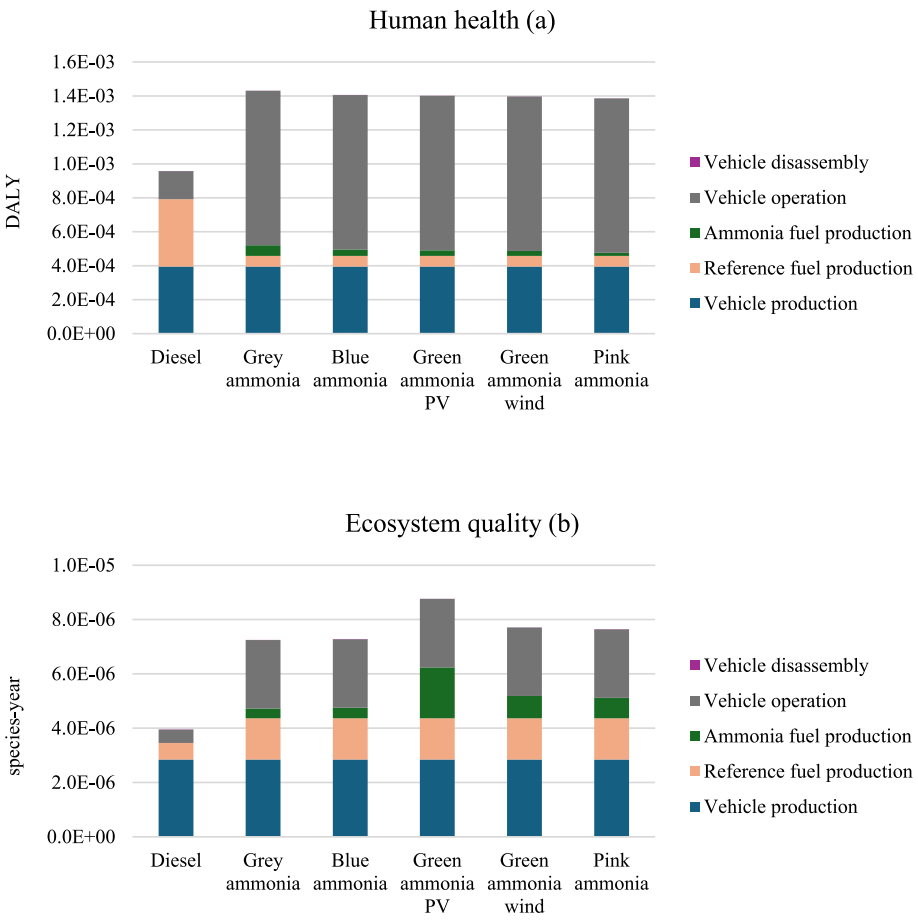

Fig. 6. Human health and ecosystem quality results.

nitrogen oxides – both known as secondary particulate matter. Consequently, all ammonia cases have approximately a 47 % higher impact on human health compared to diesel.

Fig. 6(b) presents the results on ecosystem quality. For the diesel-fueled vehicle, vehicle production dominates the environmental impact, followed by diesel production and fuel operation. This trend changes for ammonia-fueled cases. Biodiesel production has approximately 2.5 times higher impact compared to diesel production, primarily due to the land use midpoint category which is caused by rapeseed plant cultivation for rapeseed oil. In the dual-fuel scenario, ammonia production also contributes to this environmental category. The strongest contribution is observed for electrolysis-based ammonia, with the highest value associated with PV-based electrical energy, mainly due to its high impact on the terrestrial ecotoxicity midpoint category. This is attributed to manufacturing and end-of-life processes associated with handling heavy metals. Operation phase is also a considerable factor. For ammonia-fueled vehicles, this phase achieves approximately five times higher value, caused by significant impacts on terrestrial acidification and photochemical ozone formation, which result from high NO_x and NH_3 emissions. Overall, the green ammonia PV case results in a 2.2 times higher impact on ecosystem quality compared to diesel, while the remaining cases show approximately 1.9 times higher values.

To reduce operational impacts from high NO_x and NH_3 emissions, theoretical SCR is considered outlined in Fig. 7. This leads to the following reductions in endpoint categories:

1. Human health: from 9.1E to 04 DALY to 6.1E-04 DALY.
2. Ecosystem quality: from 2.5E to 06 species-year to 1.7E-04 species-year.

Exhaust treatment with SCR decreases environmental impacts by around 20 % for human health and around 10 % for ecosystem quality. In the human health category, this reduction results in the ammonia-fueled vehicle still having approximately 19 % higher impact than diesel across all cases. For ecosystem quality, PV-based ammonia is about 2 times higher than diesel, with other variants around 1.6 times higher. While both impacts are reduced compared to the non-SCR scenario – strengthening the need for SCR treatment – the reduction is moderate due to the use of residual ammonia in the simplified model. Applying SCR does not shift the primary environmental burden in the human health category; vehicle operation remains the main contributor for ammonia-based vehicles.

As mentioned in section 2.2.5, interactions between SCR and N_2O are not included; however, SCR might actually increase N_2O emissions depending on the catalysts used, as stated by [51]. This should be carefully considered in future research. Since LCA is inherently a linear model summing impacts from life cycle phases, the phases with the highest contributions proportionally affect the respective categories.

3.2. *Discrepancies from actual environmental impact*

LCA results should always be interpreted within the context of their aim and scope. This study relies on specific assumptions detailed earlier, but two issues require additional discussion.

First, farm tractor production impact is estimated using a parametrized process from Sphera's Managed LCA Content, where vehicle mass is an input. Analyzed tractor weighs 540 kg which is significantly less than the 13.3-tonne reference tractor used in the software. Since the software employs linear scaling based on mass, this likely leads to an underestimation of the production phase. This issue can be illustrated

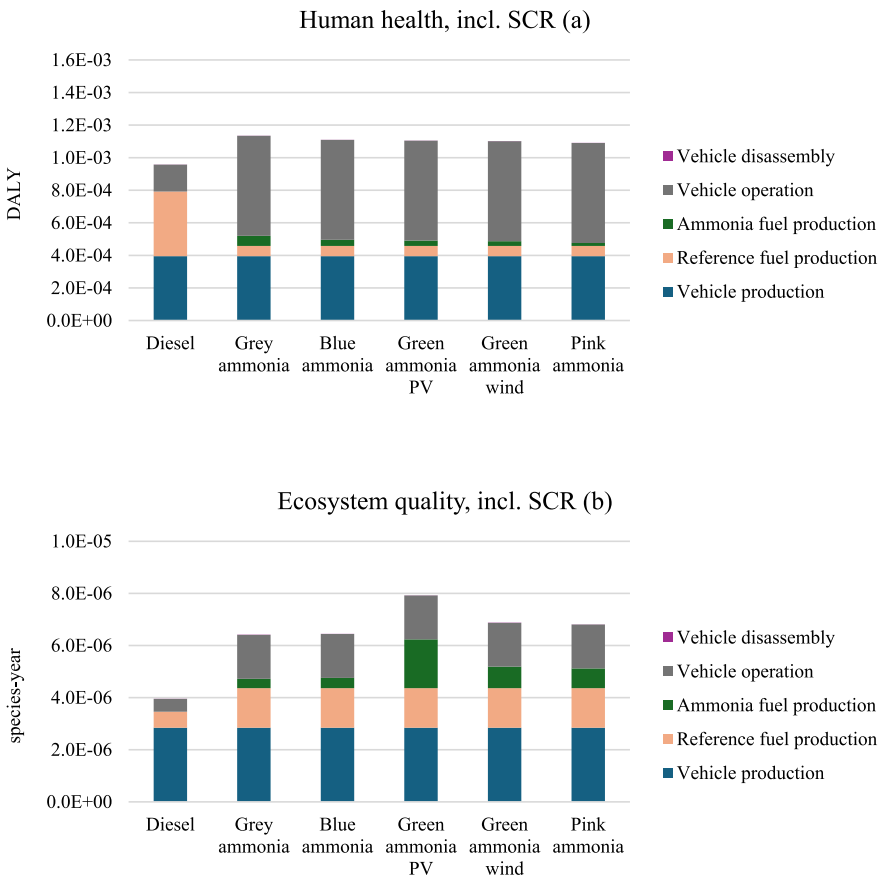

Fig. 7. Human health and ecosystem quality results incl. SCR.

via the example of diesel engines for which scaling factors have been reported by [52]. Applying power law relationship (a = 1.36, b = 0.64), a 300 kW engine (from a 13.3-tonne tractor like the John Deere 8R 370) scales down nearly 12 times to reflect the mass of 6.4 kW engine (theoretical for SCOUT 15-T). In contrast, proportional scaling suggests a 47 times reduction, indicating that linear scaling underestimates the engine's weight by nearly four times. Assuming a direct analogy between diesel engines and tractors suggests the production phase impact is significantly underestimated. However, this analogy may not be accurate due to differences in vehicle body composition and materials, making it difficult to draw definitive conclusions without validated data. This underscores the need to interpret the results with caution. Despite potential underestimation in the production phase, this issue does not affect the comparative conclusions between diesel- and ammonia-fueled tractors, as both are subject to the same scaling limitations. Therefore, the main conclusions of this work remain valid. The primary difference is that the production phase may represent a larger share of the total life cycle impact than anticipated.

Second, while operation phase data is based on steady-state engine measurements, tractors in real conditions experience varying temperatures and start from cold. High intake temperatures can elevate NO_x and N_2O emissions due to increased combustion temperatures [53]. Conversely, low temperatures may lead to incomplete combustion, raising emissions of hydrocarbons and N_2O [54]. Regarding cold starts, Ko et al. [54] found that emissions from cold engines are generally 1.5–2 times higher for most pollutants (including N_2O). In this study, the tractor starts cold 38 times annually, with each warm-up lasting 30 s – less than 1 % of its total operating time – making potential underestimation negligible. These factors influence absolute emission values but affect both diesel and ammonia-fueled tractors equally; therefore, the comparative conclusions remain valid. Differences due to cold starts or intake temperature variations can be validated via on-site experimental data.

4. Summary

From the premise presented in the introduction, ammonia fuel has the potential to decarbonize heavy-duty machinery due to its renewable nature and carbon-free emissions. While this statement remains true, the major issue revealed in this work is that dual-fuel engines still emit certain amounts of CO_2, CH_4, and N_2O – the latter being especially important due to its high GWP.

Compared to diesel, the ammonia-fueled tractor has lower operational greenhouse gas emissions (around 72 kg CO_2 eq. vs. 88 kg, an 18 % drop), but higher N_2O emissions limit this advantage. However, over its full life cycle, switching to ammonia notably lowers greenhouse gas load (about 42–44 % reduction) when produced using wind or nuclear power and considering biodiesel's footprint. Fossil fuel depletion is reduced by around 43–45 % with solar or wind-based ammonia, but it rises (about 78 % jump) with nuclear-derived ammonia. Freshwater consumption is higher for all ammonia options (about 40–50 % above diesel, and nearly doubling for the nuclear pathway).

Ammonia-fueled vehicle scenarios rise human health impact by roughly 47 % due to fine particles from NH_3/NO_x emissions and doubles ecosystem quality impact, driven by both the emissions and fuels production impacts. Adding an SCR system reduces the ammonia tractor's human health impact by about 20 % and ecosystem quality impact by around 10 %. However, human health impact remains about 19 % higher than diesel, and ecosystem quality impact is still significantly higher (around 1.6 to 2 times) even with SCR, with tractor operation being a key factor.

Consequently, it is evident that apart from engine performance, the

fuel source must be carefully considered from a life cycle perspective. While nuclear-based ammonia exhibits the lowest impact on climate change among all options, it is associated with a high fossil depletion impact, noting that nuclear energy is not renewable – a factor that should be counted in long-term analyses. Additionally, it is characterized by higher freshwater consumption compared to green pathways, and in light of limited water resources in certain areas, this should also be considered.

From the endpoint categories analysis, it is shown that high emissions of NO_x and NH_3 are responsible for the significant impact of ammonia-fueled vehicles on human health, despite the inclusion of SCR systems based on residual ammonia. Ecosystem quality is mainly influenced by tractor production and operation, so reducing emissions is crucial from this perspective as well.

Overall, electrolysis-based ammonia coupled with renewable energy sources seems to be the most viable option. However, to achieve further benefits, the following recommendations are outlined:

1. Ammonia combustion should be optimized by adjusting biodiesel/ammonia ratio under partial load conditions, or by switching from port to an advanced direct injection setup, followed by optimizing the combustion across the engine's operating map. Minimizing NO_x, N_2O, and NH_3 emissions is crucial for achieving lower impacts on climate change, human health, and ecosystem quality categories. This could also be achieved by thorough analysis of SCR systems and investigating other scenarios, such as alternative catalysts, noting their impact on N_2O.
2. Biodiesel production should be analyzed in terms of sources that do not compete with food – unlike rapeseed-based oil, which is associated with indirect land-use change (ILUC) issues. Biodiesel based on algae or waste animal fat should be considered in further research, and its environmental impact should be validated.
3. Confirmation of the obtained data could be performed by including primary data on tractor production and conducting even more detailed experimental campaigns. Considering a broader perspective and accounting for sectors like construction and agriculture, further research should focus on high-power engines.

This study proves that ammonia in a dual-fuel engine is a viable substitute that might contribute to decarbonizing difficult sectors where heavy-duty machinery is widely used. Nevertheless, more research in this area is required – especially in terms of ammonia combustion – to achieve substantial effects.

CRediT authorship contribution statement

Mateusz Proniewicz: Writing – original draft, Methodology, Investigation, Formal analysis, Conceptualization. **Karolina Petela:** Writing – review & editing, Supervision, Conceptualization. **Andrzej Szlęk:** Writing – review & editing, Supervision, Conceptualization.

Declaration of competing interest

The authors declare that they have no known competing financial interests or personal relationships that could have appeared to influence the work reported in this paper.

Acknowledgments

The authors wish to acknowledge Wojciech Adamczyk for his role in project administration and Grzegorz Przybyła for his supervision of experimental setup. The research leading to these results has received funding from the Norway Grants 2014–2021 under POLNOR2019 competition operated by the National Centre for Research and Development and from Polish State Budget (Grant No. NOR/POLNOR/ACTIVATE/ 0046/2019-00).

Appendix A. Supplementary data

Supplementary data to this article can be found online at https://doi.org/10.1016/j.fuel.2025.135809.

Data availability

Data will be made available on request.

REFERENCES

[1] Boggia, S., & Jackson, A. (2002). Some Unconventional Aero Gas Turbines Using Hydrogen Fuel. *Volume 2: Turbo Expo 2002, Parts A and B*, 683–690. Doi: 10.1115/GT2002-30412.
[2] Singla MK, Nijhawan P, Oberoi AS. Hydrogen fuel and fuel cell technology for cleaner future: A review. *Environ Sci Pollut Res* 2021;28(13):15607–26. https://doi.org/10.1007/s11356-020-12231-8.
[3] Abbasi T, Abbasi SA. 'Renewable' hydrogen: Prospects and challenges. *Renew Sustain Energy Rev* 2011;15(6):3034–40. https://doi.org/10.1016/j.rser.2011.02.026.
[4] Hwang HT, Varma A. Hydrogen storage for fuel cell vehicles. *Curr Opin Chem Eng* 2014;5:42–8. https://doi.org/10.1016/j.coche.2014.04.004.
[5] Ahluwalia RK, Hua TQ, Peng JK. On-board and Off-board performance of hydrogen storage options for light-duty vehicles. *Int J Hydrogen Energy* 2012;37(3):2891–910. https://doi.org/10.1016/j.ijhydene.2011.05.040.
[6] Zamfirescu C, Dincer I. Using ammonia as a sustainable fuel. *J Power Sources* 2008;185(1):459–65. https://doi.org/10.1016/j.jpowsour.2008.02.097.
[7] Lan R, Tao S. Ammonia as a Suitable Fuel for Fuel Cells. *Front Energy Res* 2014;2. https://doi.org/10.3389/fenrg.2014.00035.
[8] Lamb KE, Dolan MD, Kennedy DF. Ammonia for hydrogen storage; A review of catalytic ammonia decomposition and hydrogen separation and purification. *Int J Hydrogen Energy* 2019;44(7):3580–93. https://doi.org/10.1016/j.ijhydene.2018.12.024.
[9] Wan Z, Tao Y, Shao J, Zhang Y, You H. Ammonia as an effective hydrogen carrier and a clean fuel for solid oxide fuel cells. *Energ Conver Manage* 2021;228:113729. https://doi.org/10.1016/j.enconman.2020.113729.
[10] MacKenzie, J. J., & Avery, W. H. (1996). Ammonia fuel: The key to hydrogen-based transportation. *IECEC 96. Proceedings of the 31st Intersociety Energy Conversion Engineering Conference*, *3*, 1761–1766. Doi: 10.1109/IECEC.1996.553368.
[11] International Energy Agency (IEA). (2021). *Ammonia Technology Roadmap*. IEA. https://www.iea.org/reports/ammonia-technology-roadmap.
[12] Eurostat. (n.d.). *Complete energy balances* [Dataset]. Eurostat Data Browser. Retrieved October 18, 2024, from https://ec.europa.eu/eurostat/databrowser/view/NRG_BAL_C_custom_12707740/default/table?lang=en.
[13] Tornatore C, Marchitto L, Sabia P, De Joannon M. Ammonia as Green Fuel in Internal Combustion Engines: State-of-the-Art and Future Perspectives. *Frontiers in Mechanical Engineering* 2022;8:944201. https://doi.org/10.3389/fmech.2022.944201.
[14] MacFarlane DR, Cherepanov PV, Choi J, Suryanto BHR, Hodgetts RY, Bakker JM, et al. A Roadmap to the Ammonia Economy. *Joule* 2020;4(6):1186–205. https://doi.org/10.1016/j.joule.2020.04.004.
[15] Valera-Medina A, Xiao H, Owen-Jones M, David WIF, Bowen PJ. Ammonia for power. *Prog Energy Combust Sci* 2018;69:63–102. https://doi.org/10.1016/j.pecs.2018.07.001.
[16] Kumar L, Sleiti AK. Systematic review on ammonia as a sustainable fuel for combustion. *Renew Sustain Energy Rev* 2024;202:114699. https://doi.org/10.1016/j.rser.2024.114699.
[17] Chiong M-C, Chong CT, Ng J-H, Mashruk S, Chong WWF, Samiran NA, et al. Advancements of combustion technologies in the ammonia-fuelled engines. *Energ Conver Manage* 2021;244:114460. https://doi.org/10.1016/j.enconman.2021.114460.
[18] Chai WS, Bao Y, Jin P, Tang G, Zhou L. A review on ammonia, ammonia-hydrogen and ammonia-methane fuels. *Renew Sustain Energy Rev* 2021;147:111254. https://doi.org/10.1016/j.rser.2021.111254.
[19] Xu X, Liu E, Zhu N, Liu F, Qian F. Review of the Current Status of Ammonia-Blended Hydrogen Fuel Engine Development. *Energies* 2022;15(3):1023. https://doi.org/10.3390/en15031023.
[20] Qi Y, Liu W, Liu S, Wang W, Peng Y, Wang Z. A review on ammonia-hydrogen fueled internal combustion engines 2023;eTransportation, 18:100288. https://doi.org/10.1016/j.etran.2023.100288.
[21] Kurien C, Mittal M. Review on the production and utilization of green ammonia as an alternate fuel in dual-fuel compression ignition engines. *Energ Conver Manage* 2022;251:114990. https://doi.org/10.1016/j.enconman.2021.114990.
[22] Dimitriou P, Javaid R. A review of ammonia as a compression ignition engine fuel. *Int J Hydrogen Energy* 2020;45(11):7098–118. https://doi.org/10.1016/j.ijhydene.2019.12.209.
[23] Bicer Y, Dincer I, Zamfirescu C, Vezina G, Raso F. Comparative life cycle assessment of various ammonia production methods. *J Clean Prod* 2016;135:1379–95. https://doi.org/10.1016/j.jclepro.2016.07.023.
[24] Chisalita D-A, Petrescu L, Cormos C-C. Environmental evaluation of european ammonia production considering various hydrogen supply chains. *Renew Sustain Energy Rev* 2020;130:109964. https://doi.org/10.1016/j.rser.2020.109964.

[25] Singh, V., Dincer, I., & Rosen, M. A. (2018). Life Cycle Assessment of Ammonia Production Methods. In *Exergetic, Energetic and Environmental Dimensions* (pp. 935–959). Elsevier. Doi: 10.1016/B978-0-12-813734-5.00053-6.
[26] Proniewicz M, Petela K, Szlęk A, Adamczyk W. Life Cycle Assessment of Selected Ammonia Production Technologies From the Perspective of Ammonia as a Fuel for Heavy-Duty Vehicle. *J Energy Res Technol* 2024;146(3):030905. https://doi.org/10.1115/1.4064371.
[27] Cai K, Liu Y, Chen Q, Qi Y, Li L, Wang Z. Combustion Behaviors and Unregular Emission Characteristics in an Ammonia–Diesel Engine. *Energies* 2023;16(19):7004. https://doi.org/10.3390/en16197004.
[28] Nadimi E, Przybyła G, Emberson D, Løvås T, Ziółkowski Ł, Adamczyk W. Effects of using ammonia as a primary fuel on engine performance and emissions in an ammonia/biodiesel dual-fuel CI engine. *Int J Energy Res* 2022;46(11):15347–61. https://doi.org/10.1002/er.8235.
[29] Nadimi E, Przybyła G, Lewandowski MT, Adamczyk W. Effects of ammonia on combustion, emissions, and performance of the ammonia/diesel dual-fuel compression ignition engine. *J Energy Inst* 2023;107:101158. https://doi.org/10.1016/j.joei.2022.101158.
[30] Nadimi E, Przybyła G, Løvås T, Peczkis G, Adamczyk W. Experimental and numerical study on direct injection of liquid ammonia and its injection timing in an ammonia-biodiesel dual injection engine. *Energy* 2023;284:129301. https://doi.org/10.1016/j.energy.2023.129301.
[31] Sonthalia A, Geo Varuvel E, Subramanian T, Josephin Js F, Almoallim HS, Pugazhendhi A. Experimental investigation of ammonia gas as hydrogen carrier in prunus amygdalus dulcis oil fueled compression ignition engine. *Fuel* 2024;374:132337. https://doi.org/10.1016/j.fuel.2024.132337.
[32] Sonthalia A, Varuvel EG, Subramanian T, Josephin Js F, Alahmadi TA, Pugazhendhi A. Comparative analysis to reduce greenhouse gas (GHG) emission in CI engine fuelled with sweet almond oil using ammonia/after treatment system. *Fuel* 2024;371:131865. https://doi.org/10.1016/j.fuel.2024.131865.
[33] Proniewicz M, Petela K, Szlęk A, Przybyła G, Nadimi E, Ziółkowski Ł, et al. Energy and Exergy Assessments of a Diesel-, Biodiesel-, and Ammonia-Fueled Compression Ignition Engine. *Int J Energy Res* 2023;2023:1–20. https://doi.org/10.1155/2023/9920670.
[34] Dincer, I., & Bicer, Y. (n.d.). *Comprehensive Evaluation of NH3 Production and Utilization Options for Clean Energy Applications* (Mitacs Accelerate Project, pp. 92–97). University of Ontario Institute of Technology.
[35] Bicer Y, Dincer I. Life cycle assessment of ammonia utilization in city transportation and power generation. *J Clean Prod* 2018;170:1594–601. https://doi.org/10.1016/j.jclepro.2017.09.243.
[36] Chang C-C, Huang P-C, Tu J-S. Life cycle assessment of yard tractors using hydrogen fuel at the Port of Kaohsiung. Taiwan *Energy* 2019;189:116222. https://doi.org/10.1016/j.energy.2019.116222.
[37] Martelli S, Mocera F, Somà A. Carbon Footprint of an Orchard Tractor through a Life-Cycle Assessment Approach. *Agriculture* 2023;13(6):1210. https://doi.org/10.3390/agriculture13061210.
[38] Ghavam S, Vahdati M, Wilson IAG, Styring P. Sustainable Ammonia Production Processes. *Front Energy Res* 2021;9:580808. https://doi.org/10.3389/fenrg.2021.580808.
[39] Morais S, Mata TM, Martins AA, Pinto GA, Costa CAV. Simulation and life cycle assessment of process design alternatives for biodiesel production from waste vegetable oils. *J Clean Prod* 2010;18(13):1251–9. https://doi.org/10.1016/j.jclepro.2010.04.014.
[40] Sphera. (2024e). *Farm tractor production (material composition, including Maintenance, without EoL)*. Sphera LCA Database. https://lcadatabase.sphera.com/2024/xml-data/processes/77487c49-9273-4c00-9c52-52cada272812.xml.
[41] Sphera. (2024d). *Diesel mix at filling station*. Sphera LCA Database. https://lcadatabase.sphera.com/2024/xml-data/processes/99248ee9-3a59-47e4-b1f1-bb79067249ba.xml.
[42] Sphera. (2024c). *Car shredder*. Sphera LCA Database. https://lcadatabase.sphera.com/2024/xml-data/processes/9913bb52-74bc-47ae-b794-d80ee214705c.xml.
[43] Sphera. (2024a). *Ammonia (NH3) production mix, without CO2 recovery (carbon dioxide emissions to air)*. Sphera LCA Database. https://lcadatabase.sphera.com/2024/xml-data/processes/7963a3c7-823f-47a7-a761-cd04a4fecc40.xml.
[44] Sphera. (2024b). *Ammonia (NH3) synthesis with CO2 recovery, by-product carbon dioxide (without allocation)*. Sphera LCA Database. https://lcadatabase.sphera.com/2024/xml-data/processes/96cc6efb-88c1-4c06-a97c-6cb431627a26.xml.
[45] Bodner M, Hofer A, Hacker V. H $_2$ generation from alkaline electrolyzer. *WIREs Energy Environ* 2015;4(4):365–81. https://doi.org/10.1002/wene.150.
[46] Chen Z, Shen Q, Sun N, Wei W. Life cycle assessment of typical methanol production routes: The environmental impacts analysis and power optimization. *J Clean Prod* 2019;220:408–16. https://doi.org/10.1016/j.jclepro.2019.02.101.
[47] University of Maine. (n.d.). *Calendar of Apple Orchard Management Activities*. Cooperative Extension: Garden and Yard. Retrieved October 18, 2024, from https://extension.umaine.edu/gardening/manual/calendar-apple-orchard-management-activities/.
[48] Kuta K, Przybyła G, Kurzydym D, Żmudka Z. Experimental and numerical investigation of dual-fuel CI ammonia engine emissions and after-treatment with V2O5/SiO2–TiO2 SCR. *Fuel* 2023;334:126523. https://doi.org/10.1016/j.fuel.2022.126523.
[49] Park Y-K, Kim B-S. Catalytic removal of nitrogen oxides (NO, NO2, N2O) from ammonia-fueled combustion exhaust: A review of applicable technologies. *Chem Eng J* 2023;461:141958. https://doi.org/10.1016/j.cej.2023.141958.
[50] Tan P, Zhang S, Wang S, Hu Z, Lou D-M. Simulation on catalytic performance of fresh and aged SCR catalysts for diesel engines. *J Energy Inst* 2020;93(6):2280–92. https://doi.org/10.1016/j.joei.2020.06.011.
[51] Jung Y, Pyo Y, Jang J, Woo Y, Ko A, Kim G, et al. Nitrous oxide in diesel aftertreatment systems including DOC. DPF and urea-SCR *Fuel* 2022;310:122453. https://doi.org/10.1016/j.fuel.2021.122453.
[52] Caduff M, Huijbregts MAJ, Althaus H-J, Hendriks AJ. Power-Law Relationships for Estimating Mass, Fuel Consumption and Costs of Energy Conversion Equipments. *Environ Sci Tech* 2011;45(2):751–4. https://doi.org/10.1021/es103095k.
[53] Pan W, Yao C, Han G, Wei H, Wang Q. The impact of intake air temperature on performance and exhaust emissions of a diesel methanol dual fuel engine. *Fuel* 2015;162:101–10. https://doi.org/10.1016/j.fuel.2015.08.073.
[54] Ko J, Son J, Myung C-L, Park S. Comparative study on low ambient temperature regulated/unregulated emissions characteristics of idling light-duty diesel vehicles at cold start and hot restart. *Fuel* 2018;233:620–31. https://doi.org/10.1016/j.fuel.2018.05.144.

Life cycle assessment of ammonia as carbon-free fuel in internal combustion engine-driven orchard vehicle

Mateusz Proniewicz

Silesian University of Technology, Department of Thermal Technology

Konarskiego 22, 44-100, Gliwice, Poland

e–mail: mproniewicz@polsl.pl

Karolina Petela

Silesian University of Technology, Department of Thermal Technology

Konarskiego 22, 44-100, Gliwice, Poland

e–mail: karolina.petela@polsl.pl

Andrzej Szlęk

Silesian University of Technology, Department of Thermal Technology

Konarskiego 22, 44-100, Gliwice, Poland

e–mail: andrzej.szlek@polsl.pl

Corresponding author: Mateusz Proniewicz

e–mail: mproniewicz@polsl.pl

Supplementary document

Table S1. Energy content comparison of liquefied and pressurized hydrogen and ammonia (values from EES software).

	LHV, MJ/kg	LHV, MJ/l	Density, kg/m3
Liquefied NH3 (1 bar, -33.6 °C)	18.6	12.69	682
Liquefied H2 (1 bar, -252.8 °C)	120	8.50	70.9
Compressed NH3 (300 bar, 25 °C)	18.6	11.65	626
Compressed H2 (300 bar, 25 °C)	120	2.46	20.5

Table S2. Upstream processes for electrolysis definition.

Process in software database	Description
Electricity from photovoltaic (Sphera, 2024b)	Electrical energy production from photovoltaic systems, covering both manufacturing and operation phases, with a panel lifetime of 30 years. The dataset is representative for Europe.
Electricity from wind power (Sphera, 2024c)	Electrical energy production from wind turbines, including both onshore and offshore models, and covering manufacturing, transportation, installation, operation, and dismantling. The dataset is representative for Europe.
Electricity from nuclear (Sphera, 2024a)	Nuclear-based electricity production based on a mix of pressurized water and boiling water reactors, covering the entire life cycle of infrastructure, fuel (uranium), and end-of-life phases. The dataset is representative for Europe.
Water (desalinated; deionized) (Sphera, 2024j)	Desalination and deionization using ion exchange, applied to tap water sourced from groundwater. The dataset is representative for Europe.
Process steam from natural gas (90%) (Sphera, 2024f)	Steam production in heat plants powered by natural gas, considering plant efficiency, firing technology, and flue-gas treatment systems for desulfurization, NOx removal, and dedusting. The dataset is representative for Europe.
Nitrogen (gaseous) (Sphera, 2024e)	Nitrogen is produced via cryogenic air separation (Linde Process). The dataset is representative for Europe.

Table S3. Upstream processes for transesterification definition.

Process in software database	Description
Rapeseed (canola) oil, refined (Sphera, 2024i)	Rapeseed oil production considering rapeseed cultivation, harvesting, processing, milling, refining and others. The dataset is representative for Germany.
Propane at refinery (Sphera, 2024h)	Propane preparation treated as a co-product from refinery operations, with contributions allocated by mass and net calorific value. The dataset is representative for Europe.
Process steam from natural gas 95% (Sphera, 2024g)	Steam is produced in natural gas plants with 95% efficiency. The dataset is valid for Europe. It is further divided between high and medium pressure streams.
Electricity grid mix (Sphera, 2024d)	Electrical energy as an average grid mix for Europe (2020), including imports from neighboring countries.

Table S4. Experimental details: engine and fuels.

Engine	
Type	LIFAN C186F 4-stroke, 1-cylinder, forced air cooling
Displacement, cm3	418
Compression ratio, -	16.5:1
Injection pressure, bar	200
Diesel fuel	
Elementary analysis, kg/kg	C = 0.8078 H = 0.1556 O = 0.0363 N = 0.0003
LHV, MJ/kg	42.4
Biodiesel fuel	
Elementary analysis, kg/kg	C = 0.7533 H = 0.1397 O = 0.1070 N = 0.0000
LHV, MJ/kg	37.4
Ammonia fuel	
Elementary analysis, kg/kg	C = 0.0000 H = 0.1760 O = 0.0000 N = 0.8240
LHV, MJ/kg	18.6

Table S5. Specific experimental results of diesel- and ammonia-fueled engine.

Diesel scenario										
RPM, 1/min	Load, %	Pilot fuel consumption, g/s	Ammonia consumption, kg/h	Exhaust temperature, °C	CO2, %	NH3, %	N2O, %	NO, %	NO2, %	GHG, CO2 eq./s
2400	100%	0.400±0.002	0.000±0.000	525.200±0.050	9.089±0.004	0.000±0.000	0.000±0.000	0.103±0.000	0.000±0.000	1.149
2400	71%	0.276±0.000	0.000±0.000	371.700±0.025	6.336±0.008	0.000±0.000	0.000±0.000	0.092±0.000	0.006±0.000	0.813
2400	47%	0.220±0.001	0.000±0.000	295.300±0.075	4.858±0.012	0.000±0.000	0.000±0.000	0.062±0.000	0.009±0.000	0.646
2400	24%	0.163±0.000	0.000±0.000	214.900±0.124	3.327±0.014	0.000±0.000	0.000±0.000	0.031±0.000	0.014±0.000	0.472
1200	100%	0.214±0.000	0.000±0.000	418.100±0.398	8.342±0.017	0.000±0.000	0.000±0.000	0.114±0.000	0.023±0.002	0.592
1200	71%	0.152±0.000	0.000±0.000	332.600±0.085	6.471±0.017	0.000±0.000	0.000±0.000	0.129±0.000	0.028±0.003	0.442
1200	47%	0.109±0.000	0.000±0.000	251.800±0.165	4.754±0.013	0.000±0.000	0.000±0.000	0.116±0.000	0.032±0.001	0.321
1200	24%	0.078±0.000	0.000±0.000	176.600±0.257	3.207±0.025	0.000±0.000	0.000±0.000	0.065±0.000	0.032±0.002	0.229
Ammonia scenario										
2400	100%	0.184±0.000	1.770±0.000	446.200±0.108	4.652±0.027	1.540±0.002	0.012±0.000	0.161±0.000	0.001±0.000	0.864
2400	71%	0.181±0.000	1.246±0.001	360.900±0.073	4.402±0.060	1.439±0.005	0.011±0.000	0.128±0.000	0.002±0.000	0.848
2400	47%	0.180±0.000	0.631±0.000	284.900±0.023	4.466±0.022	0.879±0.001	0.016±0.000	0.084±0.000	0.005±0.000	0.989
2400	24%	0.170±0.000	0.000±0.000	214.500±0.133	3.335±0.010	0.000±0.000	0.000±0.000	0.039±0.000	0.002±0.000	0.459
1200	100%	0.093±0.000	1.022±0.000	353.000±0.071	3.606±0.033	1.528±0.004	0.009±0.000	0.213±0.000	0.230±0.036	0.418
1200	71%	0.092±0.000	0.693±0.000	279.800±0.125	3.338±0.034	1.473±0.007	0.008±0.000	0.180±0.000	0.034±0.012	0.426
1200	47%	0.090±0.000	0.378±0.000	225.400±0.161	3.584±0.015	0.984±0.003	0.014±0.000	0.110±0.001	0.009±0.001	0.511
1200	24%	0.087±0.000	0.000±0.000	165.800±0.109	3.070±0.012	0.000±0.000	0.000±0.000	0.053±0.000	0.005±0.001	0.236

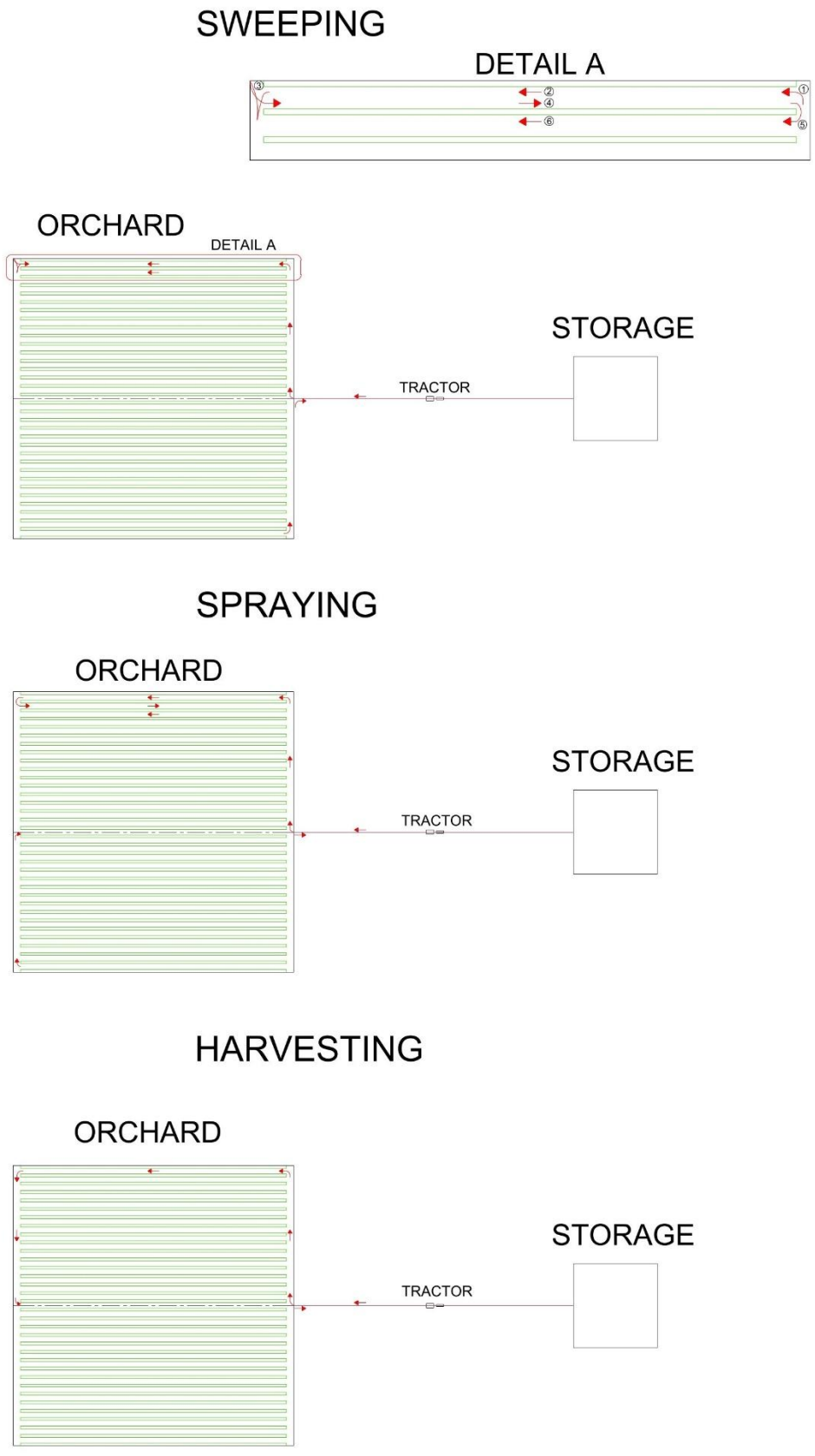

Figure S1. Orchard activities scheme.

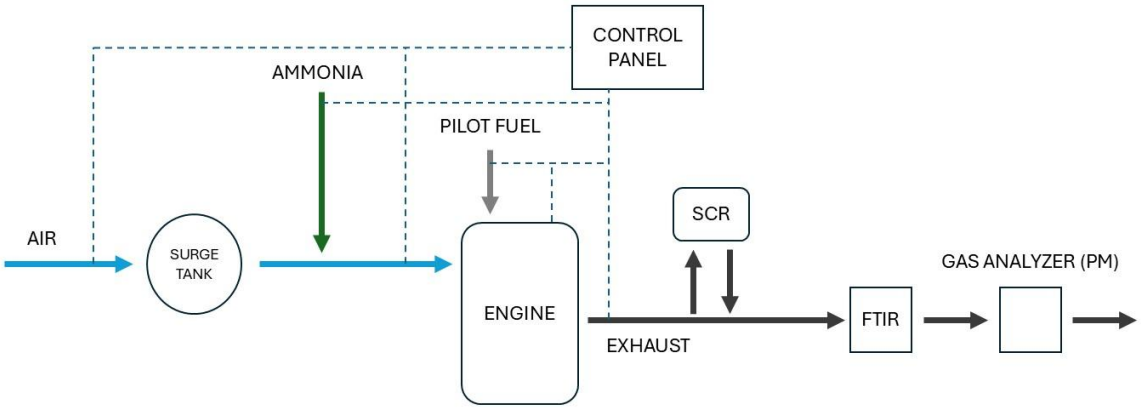

Figure S2. Schematic layout of experimental setup.

References

Sphera. (2024a). *Electricity from nuclear*. Sphera LCA Database. https://lcadatabase.sphera.com/2024/xml-data/processes/6bb9786d-dc44-4918-b328-e1b464484c3d.xml

Sphera. (2024b). *Electricity from photovoltaic*. Sphera LCA Database. https://lcadatabase.sphera.com/2024/xml-data/processes/d2842400-7718-47e1-8fea-6b35dbce7b80.xml

Sphera. (2024c). *Electricity from wind power*. Sphera LCA Database. https://lcadatabase.sphera.com/2024/xml-data/processes/fe1c3d03-072b-4da7-8fff-3505f9b01efc.xml

Sphera. (2024d). *Electricity grid mix*. Sphera LCA Database. https://lcadatabase.sphera.com/2024/xml-data/processes/001b3cb7-b868-4061-8a91-3e6d7bcc90c6.xml

Sphera. (2024e). *Nitrogen (gaseous)*. Sphera LCA Database. https://lcadatabase.sphera.com/2024/xml-data/processes/4a259aec-c66f-4375-aa9e-5b8c745addc0.xml

Sphera. (2024f). *Process steam from natural gas 90%.* Sphera LCA Database. https://lcadatabase.sphera.com/2024/xml-data/processes/d8454c30-29f7-4767-a067-978ea0447ca1.xml

Sphera. (2024g). *Process steam from natural gas 95%.* Sphera LCA Database. https://lcadatabase.sphera.com/2024/xml-data/processes/104dbecc-4f6c-456b-9e44-722bc9c41e75.xml

Sphera. (2024h). *Propane at refinery*. Sphera LCA Database. https://lcadatabase.sphera.com/2024/xml-data/processes/f8389945-6532-4128-a98b-b0fb3f461eca.xml

Sphera. (2024i). *Rapeseed (canola) oil, refined (economic allocation)*. Sphera LCA Database. https://lcadatabase.sphera.com/2024/xml-data/processes/c59ec712-064c-42b4-bbae-8bf07f46b491.xml

Sphera. (2024j). *Water (desalinated; deionised)*. Sphera LCA Database. https://lcadatabase.sphera.com/2024/xml-data/processes/ded83dc7-a169-4de2-af43-ed30a5e2bb00.xml

Paper IV

Energy 334 (2025) 137814

Contents lists available at ScienceDirect

Energy

journal homepage: www.elsevier.com/locate/energy

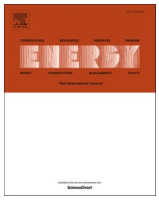

Life cycle costing of an ammonia-fueled internal combustion engine-driven orchard vehicle

Mateusz Proniewicz *, Karolina Petela, Andrzej Szlęk

Silesian University of Technology, Faculty of Energy and Environmental Engineering, Department of Thermal Technology, Konarskiego 22, 44-100, Gliwice, Poland

ARTICLE INFO

Keywords:
Ammonia
Life cycle costing
Diesel
Agriculture
Sustainability

ABSTRACT

Ammonia is gaining attention as an alternative fuel due to its carbon-free nature, the possibility of producing it from renewable sources, its existing infrastructure, and its ease of storage and transport compared to other alternatives like hydrogen. It can be particularly favorable for the decarbonization of heavy-duty machinery where electrification might pose a challenge due to high power output. In this research, the economic viability of applying ammonia, via port injection mode, as a fuel for internal combustion engine-driven mini tractor used in an orchard is tested via life cycle costing assessment. The analysis is based on a bottom-up approach i.e. the acquisition, operational and end of life costs are sourced from laboratory and literature inputs. The study considers several ammonia sources and reveals that it can economically compete with diesel: at natural gas price below 6$/MMBtu ammonia produced from natural gas-based route with CCS or electricity price below 38$/MWh for ammonia from electrolysis-based hydrogen, the ammonia is less costly on energy basis compared to diesel at 1$/l. However, an increased expenditure for constructing an ammonia-fueled vehicle results in approximately three times higher cost compared to reference diesel-fueled vehicle which is a primary challenge towards achieving economic competitiveness.

1. Introduction

The pathway to decarbonization demands the employment of alternative energy sources such as hydrogen or ammonia. Hydrogen gains attraction due to its high energy content on a mass basis [1], renewability [2] and versatility [3]. However, its storage requires either high pressure (700 bar) or liquefaction (at 20 K temperature), which are both energy-intensive and costly [4]. One way to address this is to focus on ammonia, which could be seen as a derivative of hydrogen. Interest in hydrogen and its derivatives is reflected by currently implemented projects such as The Regional Clean Hydrogen Hubs (H2Hubs) Program in the U.S. or *A hydrogen strategy for a climate-neutral Europe* published by the EU commission in 2020. *Renewable fuels of non-biological origin in the European Union* report [5] lists ammonia explicitly as one of the options.

Chemically ammonia is a carbon-free compound that can be used directly in combustion engines and fuel cells [6] or indirectly as a hydrogen carrier [7]. It can be produced from renewable sources [8] and stored more efficiently at a lower cost compared to hydrogen [9]. Since ammonia is extensively used in the agriculture and synthetic sectors, there is a well-developed infrastructure for its storage and management. According to estimates from the International Energy Agency (IEA), its production represents approximately 2 % of the world's energy use and 1.3 % of CO_2 emissions [10]. Since complete ammonia combustion produces only N_2 and H_2O, and the accompanying emissions of nitrogen oxides can be targeted via combustion optimization and after-treatment methods, it has gained interest as a promising alternative to conventional fuels.

Adopting ammonia could be particularly beneficial for sectors like agriculture, construction, and transportation, which largely rely on compression ignition (CI) internal combustion engines (ICE) used in heavy machinery. While electrification is advancing in passenger vehicles, it is less practical for heavy-duty vehicles that require both considerable power and an acceptable range. Consequently, ammonia emerges as a viable option for reducing carbon emissions in these sectors as it can directly substitute for diesel fuel, although its low flammability and high auto-ignition temperature necessitate a dual-fuel mode for practical operation [11]. Reduction of greenhouse gas emissions by over 40 % from a life cycle perspective due to the utilization of ammonia with pilot biodiesel fuel in a compression ignition engine has been confirmed by a study presented by Proniewicz et al. [12], given that ammonia production is based on hydrogen obtained from renewable- or

* Corresponding author.
E-mail addresses: mproniewicz@polsl.pl (M. Proniewicz), karolina.petela@polsl.pl (K. Petela), andrzej.szlek@polsl.pl (A. Szlęk).

https://doi.org/10.1016/j.energy.2025.137814
Received 19 February 2025; Received in revised form 8 July 2025; Accepted 29 July 2025
Available online 31 July 2025

List of abbreviations

CI –	compression ignition
EIA –	the U.S. Energy Information Administration
EoL –	end of life
ICE –	internal combustion engine
IEA –	International Energy Agency
LCA –	life cycle assessment
LCC –	life cycle costing

nuclear-based electrolysis. Therefore, low-carbon ammonia deployment is in line with SDG 7 (Affordable and Clean Energy) and SDG 13 (Climate Action).

The feasibility of ammonia-fueled internal combustion engines has been widely reported in the literature. Lasocki et al. [13] evaluated the use of ammonia in an 85 kW dual-fuel compression ignition engine on the engine's performance and emissions, using numerical simulations supported by experimental data. Gill et al. [14] presented a successful co-fueling operation achieved by substituting air intake with ammonia in an 8.6 kW CI engine. Another viable operation of such a retrofitted engine was shown by Cai et al. [15] where the authors focused specifically on irregular emissions such as hydrogen cyanide. Numerical and experimental analyses of a dual-fuel 6.4 kW CI engine utilizing liquid ammonia to assess the engine's performance and emissions were presented by Nadimi et al. [16]. For the same engine, Proniewicz et al. [17] demonstrated that the ammonia-fueled engine could achieve similar efficiency to that of diesel and biodiesel. While an ammonia-fueled engine suffers from unburned NH_3 and NO_x emissions, as noted by D, analysis of residual ammonia usage in the after-treatment selective catalytic reduction method for NO_x reduction in ammonia-fueled CI engines was presented by Kuta et al. [18], where effective emission reduction was achieved. Since these studies confirm the technical feasibility of ammonia-fueled engines, the next step toward raising their technology readiness can be achieved through an economic assessment of this solution.

The cost estimation of ammonia produced from renewable sources (green ammonia) has been explored in several studies. Zhang et al. [19] analyzed ammonia production from biomass gasification and water electrolysis based on a solid-oxide electrolyzer. The authors obtained a production cost of 450 $/t for the biomass pathway versus 400 $/t for the conventional pathway and concluded a lack of competitiveness for the electrolysis route due to high stack and electricity prices. A case study of ammonia production via renewable-powered electrolysis in Chile and its subsequent transportation to Japan was shown by Guerra et al. [20]. The investment was assessed by a positive net present value with a payback period of approximately 7.5 years. Boulamanti and Moya [21] elaborated on the complex interplay between feedstock, electricity, thermal energy, other materials, and credits due to co-products in terms of production costs for ammonia, methanol, and light olefins in several countries, highlighting the role of feedstock and the economy of credits. Fasihi et al. [22] identified the cost of ammonia from a hybrid PV-wind route to be within the range of 370–450 €/t by 2030, which could potentially decline to 285–350 €/t by 2050 in favorable locations. Cesaro et al. [23] forecasted the price of renewable-based ammonia reaching up to 400 $/t by 2040 for various locations. A least-cost optimization model of ammonia production from electrolysis with an energy storage configuration considering solar, wind, and grid sources has been presented by Campion et al. [24]. The cost of ammonia from an alkaline electrolyzer was determined to be approximately within the range of 150–200 €/MWh of NH_3 depending on the source, specific setup, and location. Adeli et al. [25] employed deep learning optimization algorithms to analyze renewable-powered ammonia supply in a case study of Dakhla, Morocco. The study showed that ammonia cost can be reduced from 575 $/t to 376 US $/t, while switching from a 20 % solar/80 % wind mix to 100 % wind. Research on green ammonia cost emphasizes its variability depending on the electrolyzer setup, electrical energy production pathway, and plant location, but the overall trend anticipates a cost drop in the upcoming years.

Vehicle capital costs are typically discussed within a wider framework of life cycle costing (LCC) in terms of diesel alternatives. Several assessments on this topic have been reported. Nylund and Koponen [26] (pp. 335–352) comprehensively compared various bus fueling technologies, showing that the price for a propulsion fuel cell bus is approximately 5.5 times higher than that of a diesel bus. Their conclusions conveyed that decreasing this gap might not be achievable merely by amplifying volumes of vehicles and power systems, and that vehicle design must become more efficient. Ally and Pryor [27] elaborated on several bus fueling options like hybrid, hydrogen fuel cell, and compressed natural gas variants for the case study of Perth. They highlighted that fuel savings for alternative buses are insufficient to compensate for increased capital and maintenance costs unless there is a noticeable diesel price increase. If the assessment includes the monetary value of emissions, an alternate conclusion might be reached, as presented by Szumska et al. [28], where hybrid buses were shown to be approximately 13 % less costly from a life cycle perspective. Thompson et al. [29] reported a price for light-duty hydrogen fuel cell vehicles within the 45–50 $/kW range and discussed a solution towards achieving the 30$/kW required for competitiveness with ICE vehicles. Halder et al. [30] comprehensively reviewed the technical and economic aspects of hydrogen fuel cell vehicles and showed that, despite lower energy consumption and greenhouse gas emissions, the increase in vehicle prices ranges from 1.2 to 12.1 times compared to typical vehicles, depending on the specific setup. A comparison of conventional, electric, hydrogen-hybrid (HEV), and hydrogen-based ICE options for buses was presented by Kuyumcu et al. [31]. Well-to-wheel costs for hydrogen ICE and hydrogen HEV were higher compared to diesel, a trend projected to change with an increase in renewable hydrogen generation by 2030. Wang et al. [32] presented a cost-based life-cycle assessment accounting for both internal and external costs in multi-scenario comparisons of hydrogen fuel-cell vehicles versus diesel and battery alternatives across China's long-distance transport sector. They found that, under the anticipated gradual drop in hydrogen price by 2035, both trucks and passenger vehicles will become the lowest-cost options, highlighting the role of supportive policy impact in achieving such results.

The aforementioned challenges associated with hydrogen storage and direct electrification solutions could lead to increased costs of decarbonizing heavy-duty machinery. From this perspective, exploring the use of ammonia in internal combustion engine setups may offer a viable and practical approach to economically achieve decarbonization goals. While the literature confirms that ammonia can be produced renewably – with an anticipated declining cost trajectory – and successfully utilized in compression ignition engines, current research focuses primarily on hydrogen-based fueling systems. Limited information on the costs of ammonia-fueled engines is the gap this work addresses. Accordingly, the study presents a life cycle costing assessment of an ammonia-fueled vehicle through a port injection mode, considering several ammonia sources, in a case study of a mini tractor used in agriculture. Results are then benchmarked against a diesel baseline to determine (i) how far ammonia-ICE capital costs must drop, and (ii) the ammonia price required for cost parity with diesel. These quantified thresholds may serve as input for policymakers in designing incentives for wider ammonia adoption.

2. Materials and methods

2.1. System boundaries

The analysis adopts the perspective of a small-orchard owner who intends to purchase a new 6.4 kW (8.6 hp) mini-tractor for field

operations. Two options are available.

1. A typical diesel-fueled mini tractor.
2. An ammonia-fueled mini tractor (same chassis as diesel-fueled vehicle, with engine's adaptation towards port injection ammonia setup).

The two options are mutually exclusive. That is, the choice between the two vehicles should be considered an independent investment decision. The life cycle cost model therefore compares the complete, standalone cost of each alternative so the orchard owner can make an informed decision, noting any potential trade-offs.

The life cycle costing assessment includes: capital expenditure for vehicle acquisition, operation (comprising fuel consumption and maintenance), and the end of life (EoL) of the vehicle body. The approach to LCC in this work is schematically presented in Fig. 1.

First, the capital expenditure is reflected by the purchase price of an ammonia-fueled tractor, and is given by eq. (1):

$$\begin{aligned} PRICE_{T,NH3} &= PRICE_{T,DIESEL} + COST_{NH3\_SETUP} \\ &= COST_{T,DIESEL} + M_{SALES} + COST_{NH3\_SETUP} \end{aligned} \quad (1)$$

where: $PRICE_{T,NH3}$ – price for ammonia-fueled mini tractor, $PRICE_{T,DIESEL}$ – price for diesel-fueled mini tractor, $COST_{NH3\_SETUP}$ – cost for an additional equipment towards ammonia utilization, $COST_{T,DIESEL}$ – cost of producing diesel-fueled tractor, M_{SALES} – dealer distribution and margin.

In this perspective, the sum of $COST_{T,DIESEL}$ and M_{SALES} constitute the price for diesel-fueled vehicle. Therefore, the price of the ammonia-fueled mini tractor is derived on the premise that it requires the incorporation of additional equipment. However, the distribution cost and dealer margin remain the same in both scenarios, i.e. there is a single dealer margin applied in both cases.

Secondly, fuel costs – covering both ammonia and a biodiesel pilot fuel – along with maintenance costs, constitute the operational costs. Since ammonia can be produced from both conventional, fossil-based methods and renewable pathways, several options are investigated. Finally, the end of life cost of the vehicle body is accounted for. While capital expenditures and fuel costs are investigated in detail, a simplified approach to the maintenance and EoL costs of the ammonia-fueled tractor is applied, as they are calculated as parts of the capital expenditure. A detailed discussion is provided in the following subsections. The data have been primarily drawn from the U.S. marketplace, and the monetary values are expressed in 2024 U S. dollars. The LCC is calculated before purchase incentives, tax credits, or financing charges – i.e. the resulting diesel-to-ammonia cost gap can then be interpreted directly as the required incentive level.

2.2. Capital expenditure and associated costs

The simplest method of utilizing ammonia in a compression ignition engine is to introduce it via port injection mode, where gaseous ammonia is sent to the intake manifold to mix with air before entering the engine's cylinder. Such an engine has been constructed at the Silesian University of Technology in Poland; its technical performance has been elaborated by Proniewicz et al. [17]. The experimental work concluded with assembling a fully operational vehicle; laboratory work inputs served as a baseline for cost aggregation.

An ammonia-fueled engine with a port injection setup is technically similar to diesel-gas hybrid solutions (LPG or CNG). Capital expenditure aggregation, presented numerically in Table 1, is based on the following assumptions.

i. The mini tractor analyzed is the SCOUT T-15. Its baseline price is reflected by its net market price available in Poland, where it was purchased for the purpose of experimental work, and this price is considered to be an internationally valid value. Major metrics regarding the vehicle and its engine are provided in Table 2.
ii. The cost of the ammonia tank includes three components: a 10-liter tank (300 $), compliant with ISO 9809/GB 5099

Table 1
Capital expenditure aggregation for ammonia-fueled tractor (port injection).

Item	Cost, $
SCOUT T-15 (baseline; diesel)	**2500**
Ammonia tank	580
Ammonia implementation equipment	900
Selective catalytic reduction	330
Factory service	3960
Total	**8270**

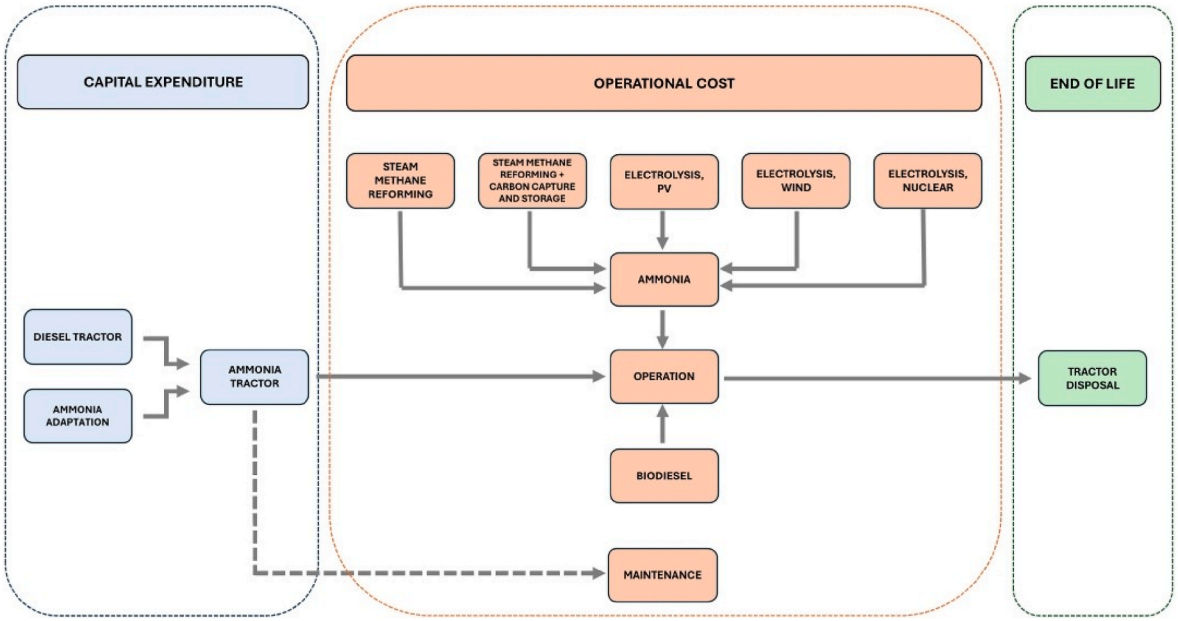

Fig. 1. Life cycle costing of an ammonia-fueled tractor – system boundaries.

Table 2
Analyzed mini tractor specification.

Vehicle	
Model	SCOUT T-15
Main dimensions, length x width x height, mm	2415 x 1350 x 1190
Gearbox	Manual
Nominal pulling force, kN	4.32
Engine	
Model	LIFAN CI, 4-stroke, 1-cylinder, forced air
Bore x stroke, mm x mm	86 x 70
Displacement, cm^3	418
Compression ratio, -	16.5 : 1
Injection pressure, bar	200

standards, shipping with insurance from China (200 $), and a customs duty using 15 % duty rate (75 $). The values have been sourced from online market research. The total cost obtained – 580 $ – is very close to the 560 $ price that was incurred for the experimental work. The transportation scenario, including shipping and customs duty, has been selected as a conservative approach; it is understood that a locally produced tank would likely result in lower costs, as shipping and customs duties would not be considered.

iii. The cost for ammonia implementation equipment is based on an analogy to a diesel LPG/CNG adaptation unit – a commercially available equipment set which includes the fuel line, reducer, injectors, ECU (electronic control unit), switch, and sensors, in compliance with ISO 15500 standards. Additionally, a separate oxygen lambda sensor (110 $) is considered. Such setup can be linked to the ammonia tank, allowing for straightforward operation of the engine.

iv. A Selective Catalytic Reduction (SCR) unit is needed to control the NO_x emissions of an ammonia-based engine, as discussed in the literature [18,33]. Therefore, a vanadium-based SCR cost is included, sourced from Posada et al. [34], who analyzed SCR unit cost in detail and presented the total manufacturing cost regarding 9.0 L, 12.0 L, and 15.0 L engines for the Euro V standard. The cost of the SCR for the mini tractor considered in this study is interpolated from a 9.0 L case to a 1.0 L engine. Since the paper was published in 2016, the inflation rate was utilized to express the value in 2024 U S. dollars [35].

v. Factory service costs account for: i) front-end assembly (controller, reducer, sensors, injectors): 32 man-hours; ii) rear-end assembly (ammonia tank, mounting, connection): 8 man-hours; iii) ammonia refueling valve: 4 man-hours. Assigning a factory rate of 90 $/hour as an average rate of factory services, a total cost is obtained. Assembly steps and price estimations have been determined based on consultation with an industrial company.

The capital expenditure of a vehicle not only represents its upfront cost but also influences its maintenance and EoL costs, as these expenses are often defined as a proportion of the capital expenditure. Based on values reported by Ally & Pryor [27], the annual maintenance costs for diesel and CNG buses are calculated at 1.62 % and 1.74 % of their acquisition values, respectively. Additionally, EoL costs constitute 20 % of the acquisition value.

For tractors, which are designed to perform various activities, the annual maintenance cost in this study is set at 2 % of the acquisition cost for both diesel- and ammonia-fueled options, reflecting their potentially higher wear compared to the bus-related literature study. In the case of EoL cost for tractors, the bus analogy is considered to be adequate, and therefore EoL is set at 20 % of the acquisition value.

2.3. Operational costs

Operational cost aggregates the costs for fuel and maintenance. The estimation of maintenance cost is referenced in section 2.2. The cost of fuel requires defining both its consumption and price.

2.3.1. Fuel consumption

The mini tractor equipped with a low-power engine analyzed in this study is suitable for work in applications like a fruit orchard. An apple orchard scenario is assumed in this study, which serves as a baseline for defining the activities performed by the vehicle and the corresponding fuel consumptions while performing these tasks. Inputs for fuel consumption calculation are provided in Table 3. The following assumptions apply.

i. A set of activities performed by the tractor on the orchard and their annual frequency are based on recommendations given by the University of Maine [36].

ii. A CAD model of a 1 ha apple orchard to scale has been drawn to define the movement of the vehicle while performing these activities and to calculate distances.

iii. Specific average fuel consumption while performing each activity has been estimated from measurements performed on the engine, measured separately for diesel and ammonia. Dataset with experimental data published has been presented in a paper [17].

Since ammonia requires pilot fuel for combustion, as explained in 1, it is combusted with pilot biodiesel. Experiments on the engine were conducted on a test rig; to reflect particular orchard activities, a theoretical gearbox model was developed. This model breaks down orchard activities into sub-activities (like moving forward along the road, turning, moving through the alley, etc.) and matches them with appropriate gear and speed settings to define engine operating points (shaft speed and torque). This considers factors like rolling resistance and additional weight from attachments required to perform the activities (such as a mower). High load while activating dedicated devices has also been accounted for. The engine's operation procedure focused on achieving maximum fuel substitution, i.e., ammonia's maximum share with biodiesel at its minimum dose, however this may be a subject to further optimization in terms of engine's thermal efficiency and emissions under partial load conditions.

For activities like pruning and harvesting, the ammonia consumption in the ammonia-fueled scenario might seem unexpectedly low; this is because these activities are performed at low speed (the tractor pulls a trailer while moving through the orchard alley and operates at low ground speed, while workers toss prunings or fruit into the trailer as it proceeds). The experimental procedure revealed that a minimum flow rate of the biodiesel pilot dose resulted in 4 Nm torque on the shaft at all shaft speeds. Considering ammonia's high auto-ignition temperature and low flammability, it can be efficiently combusted only above this threshold, which equals a 24 % torque load (17 Nm maximum). Therefore, under low-speed and low-torque engine conditions – such as in the case of pruning and harvesting – the pilot dose is sufficient for the tractor's operation. However, once that torque threshold is passed (e.g., during sweeping, mowing, or hoeing, where the attached device increases the engine load at a given speed), ammonia consumption rises, consistent with the values reported in Table 3. Integrating fuel consumption over distances and accounting for activities' frequencies leads to the final value of fuel consumption per 1 ha of orchard.

Additionally, a fuel efficiency comparison is presented in Table 4. It is defined as the ratio of annual mechanical work performed by the engine throughout the orchard activities – 100.6 kWh ha^{-1} – to the energy delivered as fuel input (diesel or ammonia with biodiesel) on lower heating value basis. Diesel shows slightly higher efficiency (28.06 % vs. 26.83 %), which is expected because the engine was originally optimized for single-fuel diesel combustion; dual-fuel would require

Table 3
Fuel consumption estimation – assumptions per 1 ha of orchard operations.

Activity	Frequency during a year	Covered distance, km	Diesel scenario – fuel consumption g/km	Ammonia scenario – fuel consumption, g/km	Ammonia scenario – pilot fuel consumption, g/km
Sweeping (branch and leaves)	2	6.97	258	362	123
Hoeing	1	6.97	258	362	123
Mowing	8	6.97	166	226	81
Pruning	2	15.14	110	19	120
Harvesting	1	15.14	127	39	131
Fertilizing	4	3.67	120	52	119
Spraying (insecticide and fungicide)	20	3.67	120	52	119

Table 4
Fuel efficiency comparison.

Mini tractor fuel	Fuel efficiency, %
Diesel	28.06
Ammonia	26.83

further optimization of pilot-injection timing and ammonia/biodiesel ratios, especially under partial load conditions. Still, the difference is modest, indicating that ammonia can still be utilized effectively in this engine configuration.

2.3.2. Fuel unit cost

Having established the quantity of fuels, their unit costs must be defined to determine the fuel cost throughout the vehicle's life cycle. The U.S. Department of Energy publishes information on average retail fuel prices; the cost of diesel and biodiesel in this study is sourced from statistical data [37]. However, the cost of producing ammonia requires thorough investigation, as the primary reason for introducing ammonia as a fuel in internal combustion engines is its renewable nature and decarbonization potential, which has been elaborated in detail by Proniewicz et al. [38]. Therefore, several ammonia production pathways are investigated. All cases are based on the Haber-Bosch process due to its maturity and high-volume capacity [39].

i. Grey ammonia – ammonia produced from hydrogen obtained in a steam methane reforming process (SMR).
ii. Blue ammonia – ammonia produced from hydrogen obtained in a steam methane reforming process coupled with carbon capture and storage (SMR + CCS).
iii. Green ammonia – ammonia produced from hydrogen obtained in a water electrolysis process with electrical energy supplied by photovoltaic or wind sources.
iv. Pink ammonia – ammonia produced from hydrogen obtained in a water electrolysis process with electrical energy supplied by a nuclear source.

2.3.2.1. Fossil-based ammonia. The cost of producing ammonia using hydrogen from steam methane reforming of natural gas, as the most common method, follows the guidelines published by the IEA [40]. It is defined as a variable dependent on a fixed cost term, which accounts for all capital investments needed to build and commission the plant, along with the ongoing expenses that do not change significantly with production level (such as labour, administration, and maintenance). Additionally, there is a variable cost term that depends on the natural gas price. No specific reformer technologies are modeled; the cost values reported by the IEA [40] reflect averaged data. For hydrogen plants coupled with carbon capture and storage (CCS), an additional fixed cost term is added. The ammonia production cost estimation can be expressed in the form of the following equation:

$$TC_{ng} = FC_{ng} + VC_{ng} + CCS = FC_{ng} + X_{ng} \cdot NG + Y_{ng} + CCS \quad (1)$$

where: TC_{ng} – total cost of ammonia production ($/tNH$_3$) for the natural gas-based route; FC_{ng} – fixed cost for the natural gas-based route ($/tNH$_3$), VC_{ng} – variable cost for the natural gas-based route ($/tNH$_3$), CCS – fixed term for carbon capture and storage ($/tNH$_3$), X_{ng} and Y_{ng} – empirical coefficients of a linear function linking the natural gas price ($/MMBtu) and ammonia variable cost, NG – natural gas price ($/MMBtu).

In the report shown by IEA [40] a comparison of ammonia production costs is outlined, which has been further discussed in an article published by the Ammonia Energy Association [41]. In the latter source, a typical range for the fixed cost was indicated; an average of 110 $/tNH$_3$ (2019 U S. dollars) is used in this study. Based on the total ammonia production costs at two gas prices and the defined fixed cost term, a variable cost function was defined using empirical coefficients. Since the IEA report was published in 2019, all values have been adjusted to 2024 U S. dollars.

The estimated value is a pre-shipment cost; if the ammonia were produced in Asia, additional freight transport costs would need to be considered. Seo et al. [42] estimated the transport distance between South Korea and the U.S. to be within a range of 70–130 $/tNH$_3$, depending on the fueling system. Alternative, if the ammonia were produced in the U.S., it could be subject to a carbon-pricing system (e.g., California's Cap-and-Trade). Considering the carbon allowance price to be at 35$/tCO$_2$ (average for 2024), the added emission-compliance cost would result in an extra 80.5 $/tNH$_3$ for grey ammonia with a CO_2 intensity of 2.3 tCO$_2$/tNH$_3$ and 45.5 $/tNH$_3$ for blue ammonia with a CO_2 intensity of 1.3 tCO$_2$/tNH$_3$ [40], assuming that only process emissions are captured (CO_2 from high-pressure synthesis gas obtained via the methane reforming reaction). No specific chemical absorption method for CCS is analyzed; the values reported in IEA [40] pertain to averaged data for the capture, transport, and geological storage of CO_2. Fossil-based ammonia cost aggregation is shown in Table 5.

2.3.2.2. Electrolysis-based ammonia. The production of ammonia using hydrogen from water electrolysis was also addressed in report from IEA [40], which investigated electrolyzer CAPEX within a range of 455–$894 $/kWe and efficiency (on an LHV basis) within 64–74 %, defining

Table 5
Fossil-based ammonia cost aggregation.

Cost, $/tNH$_3$	Natural gas price at 3.5 $/MMBtu	Natural gas price at 12 $/MMBtu
FC_{ng}	131	131
VC_{ng}	131	405.5
CCS[a]	95.5	95.5
TC_{ng} grey ammonia	262	536.5
TC_{ng} blue ammonia	357.5	632

[a] CCS – refers to the blue ammonia production pathway.

"low" and "high" electrolysis cost scenarios. In the "low" scenario, corresponding to the lower CAPEX (455 $/kWe) and higher efficiency (74 %), data from the report were used to extract total ammonia costs at different electricity prices, allowing for the determination of fixed and variable cost components. The equation was solved considering that a variable cost portion is directly dependent on the electricity price, while the fixed cost remains constant regardless of operating conditions. Similarly, the "high" cost scenario was processed, and the results of the cost breakdown for both variants are presented in Table 6.

However, a more recent paper by Vartiainen et al. [43] reported a lower electrolyzer CAPEX of 400 $/kWe, with projections to drop further to 240 $/kWe by 2030, and an average efficiency for an alkaline electrolyzer to be 67 %. Accordingly, in this study, the following assumptions are utilized: firstly, the fixed cost of ammonia production using a 400 $/kWe alkaline electrolyzer (as the most mature and commercially widespread technology) is calculated proportionally to the 455 $/kWe case. Secondly, from variable cost functions for "low" and "high" scenarios corresponding to 74 % and 64 % electrolyzer efficiencies, respectively, a cost function for 67 % efficiency was derived, as shown in Table 6. Finally, the total cost of ammonia production based on electrolysis is defined analogously as fossil-based ammonia, via equation:

$$TC_{el} = FC_{el} + VC_{el} = FC_{el} + X_{el} \cdot EL + Y_{el} \quad (2)$$

where variables are defined analogically as in the case of equation (1), with the difference being in X_{el} and Y_{el} which represent empirical coefficients of a linear function linking the electrical energy price ($/MWh) and ammonia variable cost, and EL being the price of electricity.

2.3.2.3. Retail price. Subsections elaborate on the ammonia production costs; however, to define ammonia's market price prior to its use in an ICE, additional factors must be considered.

i. Distribution: expenses associated with transporting ammonia from the production site to storage facilities and later to distributors.
ii. Storage: expenses associated with the maintenance of storage facilities.
iii. Regulatory costs: expenses associated with duties/taxes for using ammonia in ICE.
iv. Profit margin: ammonia used as fuel in ICE would be sold at retail gas stations; the profit margin of the seller constitutes the final cost.

In a large-volume scale, ammonia transport from the plant to storage facilities could be realized by pipelines, as discussed by Bartels [44], who also reported on pipeline transport and storage costs, which are utilized in this study and are provided in Table 7 (in 2024 U S. dollars). In the US, ammonia is also subject to the Superfund Chemical Excise Tax under 26 USC 466. However, several cost factors remain unaddressed, including local distribution from storage facilities to refueling stations (likely involving vehicle transport), profit margins, and other potential taxes. An additional cost of 10 $/tNH$_3$ has been added as a mark-up to account for these factors. The sum of total production costs and discussed expenses constitute the ammonia retail price which can be compared to conventional fuel.

Fig. 2 aggregates all cost contributions discussed. The variable term dominates in three of the four scenarios. In the low natural gas price case, it matches the fixed term. The CCS charge (applicable solely to blue ammonia) and the retail markup each add a noticeable increment, showcasing that no cost component can be ignored when defining the final ammonia price.

Table 6
Electrolysis-based ammonia cost aggregation.

Electrolyser: CAPEX = 455 $/kWe, η = 0.74, "low" cost scenario		
Electricity price, $/MWh	21.5	62
TC_{el}, $/tNH$_3$	262	632
FC_{el}, $/tNH$_3$	65.5	65.5
VC_{el}, $/tNH$_3$	196.5	566.5
Electrolyser: CAPEX = 894 $/kWe, η = 0.64, "high" cost scenario		
Electricity price, $/MWh	21.5	46.5
TC_{el}, $/tNH$_3$	357.5	632
FC_{el}, $/tNH$_3$	141	141
VC_{el}, $/tNH$_3$	216.5	491
Electrolyser: CAPEX = 400 $/kWe, η = 0.67, applied scenario		
Electricity price, $/MWh	21.5	62
TC_{el}, $/tNH$_3$	273.5	681
FC_{el}, $/tNH$_3$	57.5	57.5
VC_{el}, $/tNH$_3$	216	623.5

2.4. Life cycle costing assumptions

Life cycle costing assessment of a mini tractor is based on the following assumptions.

i. Timeframe: the analysis spans a 10-year period.
ii. Fuel consumption follows the approach discussed in Section 2.3.1. The starting prices of diesel and biodiesel (in the first year of analysis) are taken from the U.S. Department of Energy (*Alternative Fuels Data Center*, 2024) as the average retail price for 2024. Changes in diesel price over time follow the U.S. Energy Information Administration (EIA) predictions [46]. All values have been expressed in 2024 U S. dollars. Biodiesel price is assumed to follow the same trend as diesel but starts from a different baseline value. After determining the annual pilot fuel cost, a 5 % discount rate is applied. Exact values of initial fuel prices are provided in Table 8.
iii. Ammonia cost: ammonia consumption is calculated based on the approach discussed in Section 2.3.1. The unit price of ammonia from respective sources follows Section 2.3.2. For natural-gas-based ammonia, the natural gas price in the initial year is based on the EIA forecasts, and subsequent years follow the EIA's projected price trajectory [47]. For green (solar PV and wind) and pink (nuclear) ammonia, the electricity price is derived from the *Levelised Cost of Electricity Calculator* [48], applied to: i) green PV – utility-scale solar PV (median case, 100 MW), ii) green wind – onshore wind (≥1 MW, median case, 100 MW), iii) pink – LTO (10 years, 1000 MW). No additional year-to-year variation is considered for the green or pink ammonia pathways. However, the resulting annual ammonia costs (for both natural gas and renewable/nuclear pathways) are discounted over time, similarly to diesel and biodiesel. The ammonia price is based on the pre-shipment cost and excludes the carbon-emission compliance cost in the default scenario; these factors are included in the sensitivity analysis in Section 3.3.2.
iv. Maintenance and EoL costs follow the approach outlined in Section 2.2, and both have been discounted over time, consistent with the method used to define fuel costs.

Table 7
Retail price cost aggregation.

Cost	Value, $/tNH$_3$
Production	Depending on the source
Pipeline transport [44]	49
Short-term storage [44]	15.5
Tax rate [45]	5.28
Local delivery and retail markup	10

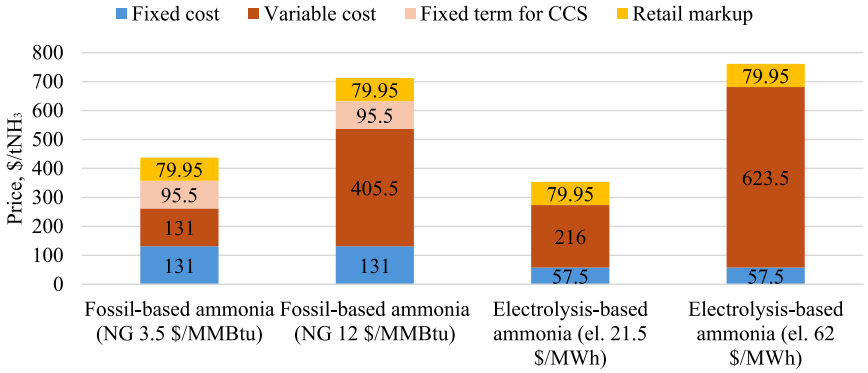

Fig. 2. Price structure of ammonia for fossil- and electrolysis-based pathways.

Table 8
Initial prices used for the LCC calculation (first year).

Fuel/electrical energy	Value	Unit
Diesel	1.06	$/l
Biodiesel	1.20	$/l
Natural gas	4.58	$/MMBtu
Electrical energy, PV	52.7	$/MWh
Electrical energy, wind	46.5	$/MWh
Electrical energy, nuclear	43.0	$/MWh

Exact values of prices used for the first year of analysis are summarized in Table 8. Fig. 3 shows the 10-year price fluctuation indexes for diesel/biodiesel and natural gas, expressed as a percentage of their initial values (year 1 = 100 %).

A real discount rate of 5 % has been applied to all operating cash flows, treating it as a midpoint between the 3 % stable-market and 7 % high-risk benchmarks presented in Ref. [49]. Because the cost of green ammonia is dominated by electricity price, using the same factor for ammonia as for the LCOE is treated as a consistent approach. This value also aligns with the historical 3–5 % range used in transportation sector life cycle studies [50], making it an appropriate sector-specific choice.

Since the study addresses a first-generation ammonia tractor and relies on multiple assumptions, its results should be interpreted given these methodological boundaries.

i. Capital expenditure is derived from a bottom-up estimate based on laboratory inputs and as such it should be viewed as an estimate rather than a precise quotation.
ii. Green ammonia cost is based on linear cost function models that assume an alkaline electrolyser. A detailed investigation of other electrolyser types with varying efficiencies could alter the cost functions.
iii. Blue ammonia cost assumes a single CCS surcharge. Advances in carbon capture and storage technologies, transport distances, or storage fees could lower this cost and improve ammonia's profitability.
iv. Diesel, biodiesel, and natural-gas price projections over the 10-year period, the carbon emissions compliance cost that affect grey and blue ammonia within the sensitivity analysis, the maintenance and EoL cost factors, as well as the retail-price build-up for ammonia (pipeline transport, short-term storage, local delivery, retail markup) are literature-based estimates that could shift in a region-specific case study.
v. Fuel consumption values are derived from the vehicle's movement in a 1 ha apple orchard example. Different crops, row spacings, terrain, or agronomic practices may change operating patterns and, therefore, fuel use.
vi. Ammonia consumption is based on a port-injection (indirect) setup at minimum pilot fuel dose; retuning the ammonia/biodiesel ratio or redesigning the engine for direct injection towards better performance would alter the NH_3 share and therefore its consumption.

The objective of this study is to establish the technology-driven cost gap between a first-generation ammonia tractor and its diesel counterpart. Accordingly, the LCC is calculated before any purchase incentives, tax credits, or financing charges, and the resulting gap is taken as the numerical basis for policy design. In this way, the analysis indicates the one-time subsidy that would be required for an ammonia-fueled tractor or the ammonia price needed to reach operational cost parity with diesel (or how diesel price should be raised e.g. due to carbon emissions

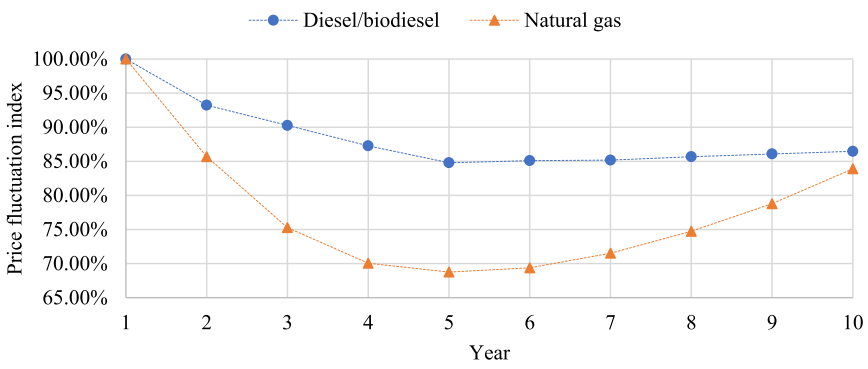

Fig. 3. Price fluctuation indexes regarding diesel/biodiesel and natural gas prices.

involved). Detailed modelling of specific support instruments can be undertaken at a higher stage of technology development and lies outside the scope of this paper. Such work would need to be tailored to a specific case study considering interest, depreciation schedules, investment tax credits, local carbon market, and overall public-finance mechanisms. There is a variety of options how incentives can be designed to promote clean energy investments; the present study limits itself to calculating the incentive level rather than assuming fixed scenarios.

3. Results

3.1. Fuel cost break-even analysis

Since in ICE applications ammonia directly competes with diesel, a price comparison of fuels on an LHV energy basis (per 1 GJ) is presented in Fig. 4. The following cases are assumed.

i. Green – ammonia based on electrolysis, directly depending on the price of electrical energy.
ii. Grey low – ammonia based on natural gas, with natural gas priced at 3.5 $/MMBtu.
iii. Grey high – ammonia based on natural gas, with natural gas priced at 12 $/MMBtu.
iv. Blue low – ammonia based on natural gas with carbon capture and storage, with natural gas at 3.5 $/MMBtu.
v. Blue high – ammonia based on natural gas with carbon capture and storage, with natural gas at 12 $/MMBtu.
vi. Diesel low – diesel price determined from the average retail diesel price analysis between 2013 and 2023 in the U.S., reported by the U.S. Department of Energy (*Alternative Fuels Data Center*, 2024). The low price corresponds to the lowest noted value equal to 0.74 $/l in 2024 U S. dollars.
vii. Diesel high – determined analogously as the diesel low case, with a fuel price at 1.70 $/l in 2024 U S. dollars.
viii. Biodiesel low – determined analogously as the diesel cases, with a fuel price at 0.98 $/l in 2024 U S. dollars.
ix. Biodiesel high – determined analogously as the biodiesel low case, with a fuel price at 1.71 $/l in 2024 U S. dollars.

Fuel comparison shows that at low gas prices, the break-point for green ammonia is at 20.5 $/MWh compared to the grey ammonia low case, and increases to 30 $/MWh for the blue low ammonia variant. The Levelised Cost of Electricity Calculator prepared by the IEA (2020) indicates the lowest Levelized Cost of Electricity (LCOE), recalculated to 2024 U S. dollars, as low as 40 $/MWh for nuclear (LTO; 1000 MW), onshore wind (≥1 MW), and solar PV (utility scale) at the most advantageous locations. As such, at low gas prices, green (or pink) ammonia cannot compete with natural gas-based ammonia, especially without CCS installation.

At high gas prices, the break-point for electrolysis as a cheaper option is at 47 $ and 57 $/MWh, respectively, for the grey and blue high scenarios. In addition to the mentioned wind, solar PV, and nuclear sources, the IEA (2020) gives an example of a hydro reservoir (≥5 MW) allowing for a cost around 46 $/MWh. This illustrates that electrolysis-based ammonia can offer a lower price compared to the natural-gas-based route, but a specific case study must be considered in terms of gas and electricity prices.

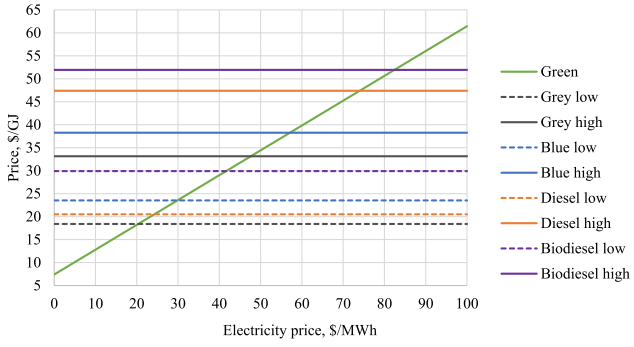

Fig. 4. Price comparison of ammonia and conventional fuels per 1 GJ.

The low diesel price is set between the grey and blue low ammonia production scenarios, resulting in a break-point versus green ammonia at 24 $/MWh. However, for high diesel prices, this break-point is set at around 74 $/MWh. At a low diesel price, green ammonia might not compete with diesel, as reaching an electricity price below 24 $/MWh may not be feasible. The break-point for low biodiesel price with green ammonia is at 42 $/MWh, while for high biodiesel, it is at 82.5 $/MWh. Biodiesel is generally shown as the most expensive source, highlighting the need to consider alternatives, like ammonia, however, this might also result in a high cost for exploiting dual-fuel engines where biodiesel is used as a pilot fuel.

Ammonia prices discussed in Fig. 4 exclude shipping and carbon-emission compliance costs (which might apply to grey and blue ammonia). This omission may underestimate the true ammonia price; depending on the location of ammonia production and legislative framework, its production may incur shipping costs, carbon-compliance costs, or both. Because this study does not assume a specific plant location, break-point prices versus electrolysis-based ammonia under four scenarios (A–D) are shown in Table 9.

i. Scenario A: Baseline scenario, no ammonia shipping and carbon emissions compliance (same as in Fig. 4).
ii. Scenario B: Ammonia shipping is excluded. Carbon emission compliance cost for grey and blue ammonia at 35 $/t$CO_2$ is added.
iii. Scenario C: Ammonia shipping at 70 $/t$NH_3$ is considered for all ammonia sources. Carbon emission compliance cost is excluded.
iv. Scenario D: Ammonia shipping at 70 $/t$NH_3$ is considered for all ammonia sources. Carbon emission compliance cost for grey and blue ammonia at 35 $/t$CO_2$ is added.

Including carbon emission costs for grey and blue ammonia makes electrolysis-based ammonia more attractive, as the higher break-even prices are more likely to be achieved. Nonetheless, green ammonia still requires electricity to be priced below 28 $/MWh to undercut low grey ammonia, whereas blue ammonia (both low and high scenarios) and high grey ammonia can potentially reach competitive levels with renewable electricity sources. In scenario B, there is no change for either green ammonia or conventional fuels, so break-even prices remain the same as in the baseline scenario.

In scenario C, shipping costs are added to all ammonia sources equally, leaving the break-even prices between green and grey/blue ammonia unchanged. However, this increases the cost gap between green ammonia and conventional fuels, favoring the latter. This effect is especially evident for low diesel prices, since achieving an electricity price below 17.5 $/MWh may not be feasible with current renewable

Table 9
Break-point prices for green ammonia versus fossil-based ammonia and conventional fuels used in diesel engines. Values in $/MWh.

Fuel price/scenario	Scenario A	Scenario B	Scenario C	Scenario D
Grey low	20.5	28	20.5	28
Grey high	47	56	47	56
Blue low	30	34	30	34
Blue high	57	62	57	62
Diesel low	24	24	17.5	17.5
Diesel high	74	74	67	67
Biodiesel low	42	42	35	35
Biodiesel high	82.5	82.5	76	76

and nuclear technologies. Finally, scenario D combines the two effects from scenarios B and C: while it makes green ammonia more competitive against natural gas-based ammonia, it also shows that, at low diesel prices, diesel remains more economical choice.

3.2. Life cycle costing results

Aggregating all cost components of the ammonia-fueled tractor – considering several ammonia sources – and comparing them to diesel results in the comparison outlined in Fig. 5. Baseline refers to the capital expenditure discussed in Section 2.2. Adaptation denotes the difference between the total price of an ammonia-fueled tractor and the reference diesel tractor. Pilot fuel refers to diesel in the diesel-fueled scenario, and to biodiesel in the ammonia-fueled scenario.

An LCC comparison of the ammonia-fueled mini tractor shows that it is around three times more expensive than the reference diesel vehicle, regardless of the ammonia source. The main reason is that the cost of converting the vehicle to an ammonia-fueling mode is roughly 2.3 times higher than purchasing the diesel tractor alone. This is due to the relatively high cost of equipment and factory services, based on the bottom-up approach adopted to define these costs.

The pilot fuel cost for the diesel scenario is higher than in the ammonia-fueled vehicle. This stems from greater diesel consumption in the diesel-only case, compared to the lower quantity of biodiesel utilized in the ammonia-fueled engine.

Ammonia costs contribute the smallest share to total life cycle cost (2–3 %). For grey and blue ammonia, this can be explained by a natural gas price ranging from 3.15 to 4.58 $/MMBtu in this assessment, which is on the lower end of typical natural gas prices, as discussed in Section 3.1. In contrast, electrolysis-based ammonia – produced with electricity priced at 43–53 $/MWh – is more expensive than natural gas-based pathways at low gas prices, which aligns with the values illustrated in Fig. 4. Ammonia costs exclude shipping and emission compliance costs.

Diesel prices in this analysis oscillate around 1 $/l, translating to approximately 28 $/GJ. Under these conditions, grey and blue ammonia at low gas prices are less expensive than diesel on an energy basis; particularly, if the natural gas price remains below 6 $/MMBtu, blue ammonia remains less costly. For green ammonia to be cheaper at the same diesel price, electricity cost would need to drop below about 38 $/MWh, which is less than the electricity prices considered in this work. Finally, because biodiesel is about 1.1 $/l in this analysis – and the ammonia-fueled setup still consumes a notable amount of biodiesel as pilot fuel – the combined cost for fuels in the ammonia-fueled vehicle is 10–30 % higher than in the diesel-fueled scenario.

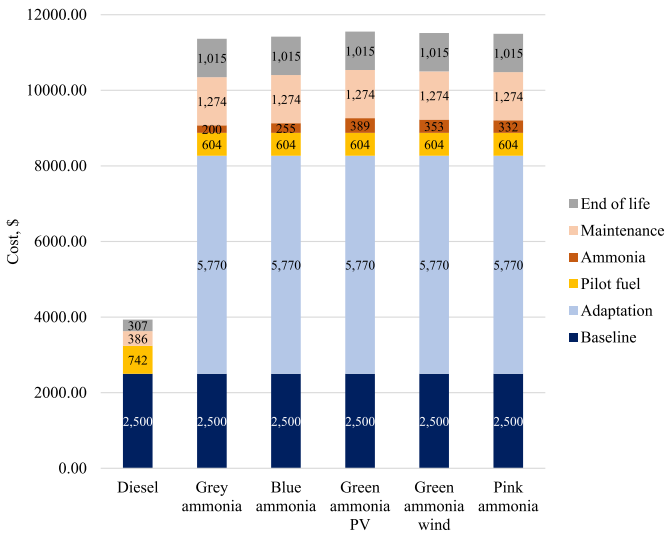

Fig. 5. Life cycle costing of an ammonia-fueled mini tractor results.

Both maintenance and EoL costs are defined in a simplified manner as a portion of the initial acquisition cost; consequently, the maintenance and EoL costs for the ammonia-fueled vehicle are approximately 3.3 times higher than those for the diesel case.

3.3. Sensitivity analysis

3.3.1. Capital expenditure variation

The results presented in Fig. 5 indicate that the ammonia-fueled vehicle is considerably more expensive, primarily due to its high acquisition cost. Conversely, the bottom-up approach adopted in this study may not precisely reflect actual costs; capital expenditure may differ as broad adoption of ammonia systems for compression ignition engines, especially among large manufacturers, could achieve lower vehicle modernization costs through high-volume production translating into lower equipment cost or factory service rate. However, these cost projections might also be underestimated; while the design allows the ammonia-fueled engine to operate and avoid excessive nitrogen oxide emission, additional safety concerns or equipment to enhance the engine's efficiency might increase this value. Similarly, the SCR cost depends on its sizing and catalyst used; the value used for the LCC calculation might be imprecise if further engine optimization reveals that a different catalyst than vanadium might perform better. Finally, the baseline price which refers to the typical mini tractor might vary from the adopted value if manufactured by another company.

Ammonia and diesel/biodiesel costs in this study are based on informed trends; however, in reality, electricity and natural gas prices may change differently, either underestimated or overestimated, depending on the market situation. Therefore, there is a need to define an impact from changing input variables on the cost estimation results. Since ammonia-fueled vehicle should be treated as an early-stage technology development, a conservative range of ±30 % is considered for the sensitivity analysis, reflecting the typical accuracy range for early-stage cost estimates in process-equipment studies [51].

Capital expenditure, presented in detail in Table 1, and is broken down into four items.

i) Baseline cost
ii) Ammonia's hardware (tank with adaptation unit)
iii) SCR
iv) Factory service

Given that the cost of each item is varied under ± 30 %, the results are plotted in Fig. 6 (a). Because capital expenditure is an arithmetic sum, varying any one item shifts the total proportionally. Factory service contributes to the capital expenditure the most (48 % at default scenario), and so its reduction would deliver the largest saving; baseline, hardware, and SCR follow in that order. Reducing factory service cost by 30 % results in a ≈1200 $ saving. Interpreting these results from the policy perspective, the value of incentive matches the sum of hardware, SCR and factory service. Assuming that only a single item cost varies from the default scenario, as in the case of this calculation, this would fall within the range of 4500–7000 U S. dollars.

Since annual maintenance and EoL costs are defined as shares of capital expenditure, under these scenarios they take values between 142 and 189 $ for annual maintenance and 1416–1892 $ for EoL. The distribution of these costs across scenarios is provided in Fig. 6 (b).

3.3.2. Fuel variation

Since the LCC model is an arithmetic sum of all cost components (acquisition, adaptation, and others), and the cost of ammonia is based on cost-function linear models elaborated in Section 2.3.2, changes in natural gas or electricity prices linearly impact the ammonia value, and therefore linearly affect the total ammonia cost from the LCC perspective. The impact of electricity price on total discounted ammonia cost is illustrated in Fig. 5, considering green ammonia from PV, green

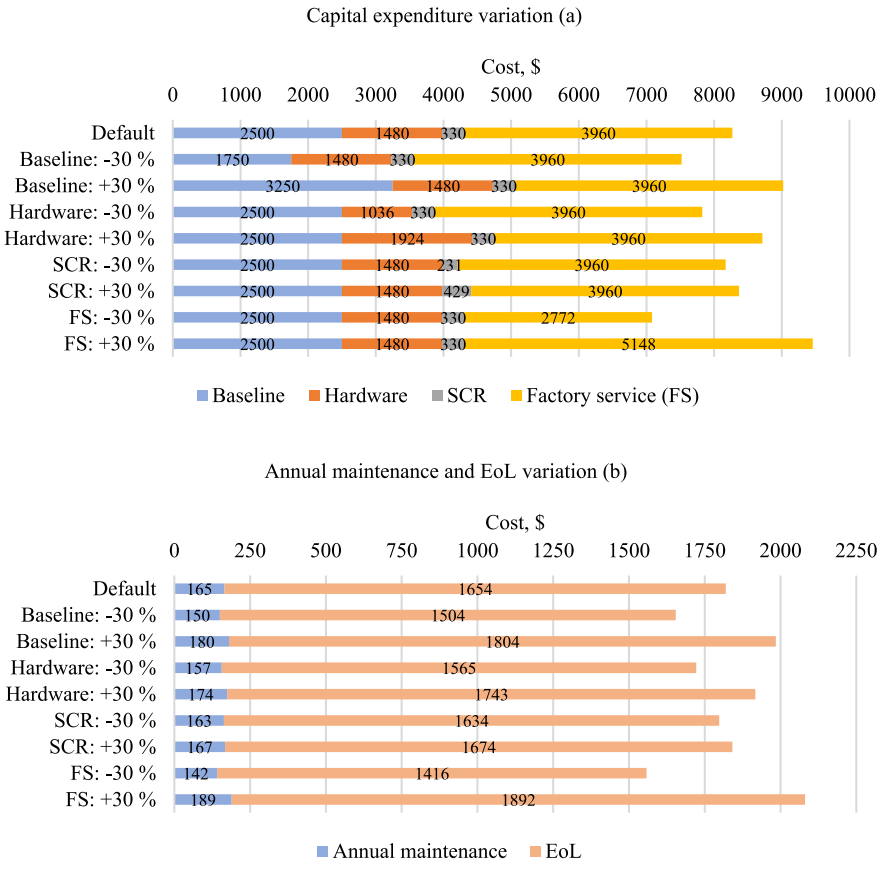

Fig. 6. Capital expenditure (a), maintenance and EoL (b) – sensitivity analysis.

ammonia from wind, and pink ammonia. In these cases, the ammonia cost amounts to 389, 353, and 332 $, respectively, for electricity prices of 52.7, 46.5, and 43 $/MWh.

However, as mentioned in Section 3.2, the results presented in Fig. 5 exclude shipping and carbon emission compliance costs associated with ammonia production. If these factors were added – using the same levels as described previously in Section 3.1, namely an ammonia shipping cost of 70 $/t$NH_3$ for all ammonia sources and a carbon emission compliance cost of 35 $/t$CO_2$ for grey and blue ammonia – the contribution of ammonia cost to the total life cycle cost of the ammonia-fueled vehicle would increase by approximately one percentage point (from 2–3 % to 3–4 %, depending on the scenario). This situation is shown in Fig. 7, where LCC results are presented including these additional ammonia-related cost factors. Due to the low share of ammonia in the overall LCC results, accounting for these effects does not alter the conclusions of this assessment. Parity between diesel and ammonia can be reached at the break-point prices discussed in Section 3.1.

Additional consideration is required for the pilot fuel impact on the results. For the 10-year analysis horizon, annual prices of diesel, biodiesel and natural gas follow the trajectories described in Section 2.4. Each trajectory of fuel can be reduced into a discounted-average price: the single unit price that, when applied uniformly over the time horizon and discounted, produces the same total fuel cost as the total fuel cost from year-by-year projection. This is presented in Table 10. The electrical energy price from PV is used as a conservative estimate representing the upper range of electricity prices (referred to as electrolysis-based ammonia).

As mentioned in Section 3.2, the combined cost for fuels in the ammonia-fueled vehicle is 10–30 % higher than in the diesel-fueled scenario, depending on the ammonia production pathway. To illustrate this, the following scenarios are defined.

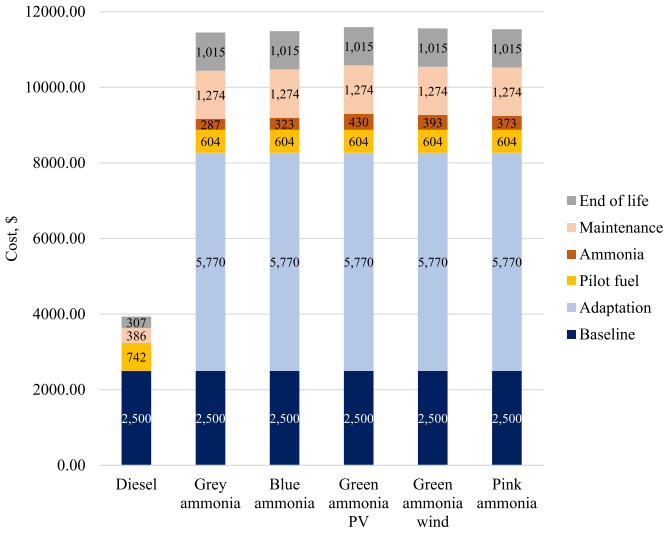

Fig. 7. Life cycle costing of an ammonia-fueled mini tractor results including shipping and carbon-emission compliance for ammonia.

i. Scenario A: Default scenario (no changes). The results are consistent with values plotted in Fig. 5.
ii. Scenario B: Biodiesel levelized value is set at 0.98 $/l (lower bound from Section 3.1).
iii. Scenario C: Biodiesel is set to 0.96 $/l for grey ammonia, 0.86 $/l for blue ammonia, and 0.62 $/l for electrolysis-based ammonia.

Table 10
Discounted-average prices of fuels and electrical energy.

Fuel	Value
Diesel, $/l	0.94
Biodiesel, $/l	1.07
Natural gas price, $/MMBtu	3.59
Electrical energy price, $/MWh	52.7

Pilot fuel impact on the LCC results is plotted in Fig. 8. Even though in an ammonia-fueled mini tractor more ammonia is consumed than pilot fuel, high price of biodiesel makes its contribution a dominant factor for all cases. To determine if reducing biodiesel price to its lower bound would equalize the total fuels costs, a calculation shown through scenario B was performed. While a reduction in pilot fuel cost of ≈50 $ almost allowed for equalizing diesel case with grey ammonia variant, further reduction would be required to achieve parity with blue or electrolysis-based ammonia. Diesel-parity solutions varying biodiesel prices are outlined in scenario C. Due to their low values, they might not be achievable.

3.3.3. *Life cycle costing results variation*

Based on the variations in capital expenditure and fuel prices elaborated in previous sections, a range of LCC results can be defined by considering best-case and worst-case scenarios. The best-case scenario (BS) represents favorable market conditions based on the assumptions discussed in this work. These include.

i. Capital expenditure −30 % for all cost items.
ii. Biodiesel set at 0.98 $/l.
iii. Natural gas set at 3.5 $/MMBtu.
iv. Electrical energy set at 43.0 $/MWh.

Conversely, the worst-case scenario (WS) represents opposite market conditions, including.

i. Capital expenditure +30 % for all cost items.
ii. Biodiesel set at 1.71 $/l.
iii. Natural gas set at 12 $/MMBtu.
iv. Electrical energy set at 52.7 $/MWh.
v. Carbon-compliance and transportation costs added to the ammonia price.

The best-versus worst-case comparison is presented in Fig. 9. Since ammonia's contribution to the total LCC is small (2–3 % at default scenario), the three options for the best-case scenario achieve similar value; same applies to worst-case scenario. This comparison serves to estimate the range of expected LCC results, given the uncertainty in the assumptions related to the default case (Fig. 5). Depending on the market conditions, the following results are obtained.

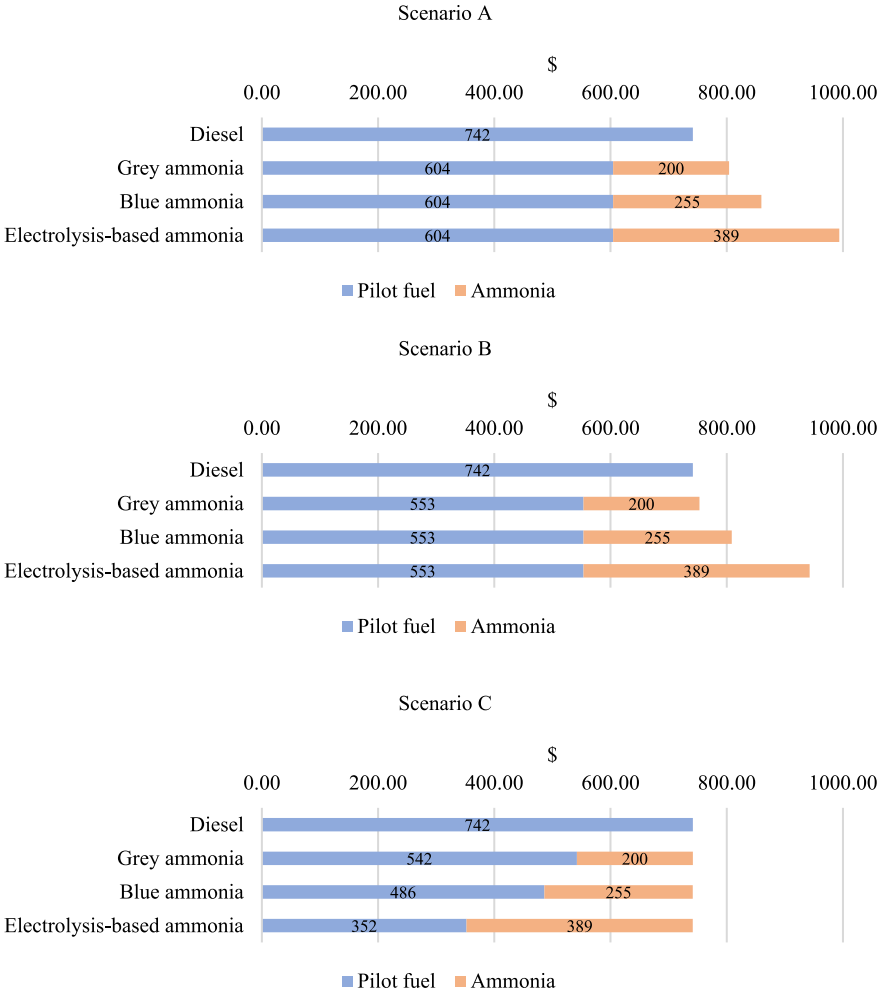

Fig. 8. Pilot fuel impact on the LCC results.

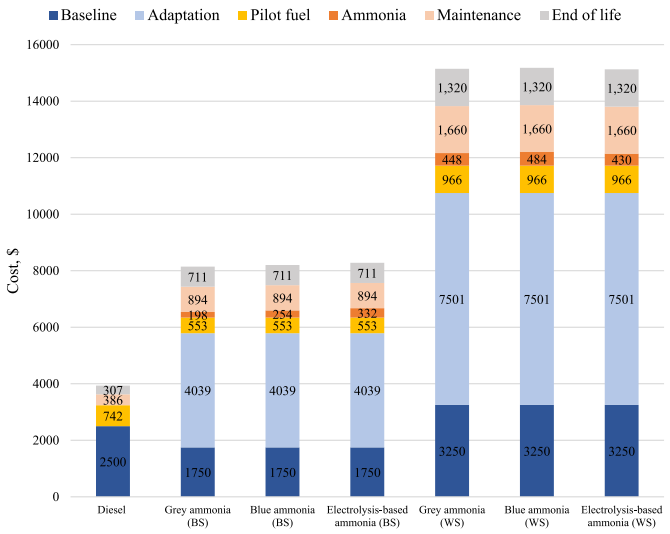

Fig. 9. Range of estimated LCC results.

i. Capital expenditure for the ammonia-fueled tractor is between 2.3 and 4.3 times higher than the diesel tractor.
ii. Fueling cost (ammonia with pilot fuel) is between 1.1 and 2 times higher compared to the diesel cost for diesel tractor. The exception is grey ammonia, which under low biodiesel and natural gas prices achieves a cost similar to diesel.
iii. Maintenance and EoL are 2.3–4.3 times higher for the ammonia tractor compared to the diesel tractor.

4. Summary

Ammonia's potential for decarbonization and its advantages over hydrogen make it an attractive alternative within a hydrogen-based economy. It can be stored and refueled similarly to LPG or CNG and its existing infrastructure in agriculture makes its management and deployment towards vehicle fueling easier. In this research, a life cycle costing assessment of an ammonia-fueled mini tractor – focusing on several ammonia sources – leads to the following conclusions.

First, whether the ammonia produced from natural gas or electrolysis-based pathways is less costly depends on the prices of gas and electricity. Generally, at a low natural gas price (3.5 $/MMBtu), the electrical energy price would need to be below 20–30 $/MWh, which is unlikely to be achieved. However, at high gas prices (around 12 $/MMBtu), electrolysis-based ammonia can become cheaper if electricity costs are sufficiently low (about 47–57 $/MWh), which is possible under renewable or nuclear energy generation sources in optimal scenarios (40–46 $/MWh). While these conclusions, derived from the determined cost-function relationships, can be applied to other ammonia use cases, the ammonia consumption will differ in each specific case study.

Second, at low diesel prices (0.74 $/l), only ammonia from natural gas at low gas prices can compete with diesel; the electrical energy price would have to be below 24 $/MWh, which is unlikely. However, at a diesel price of 1.70 $/l, the electricity price would need to be under 74 $/MWh, which is feasible in many cases.

Life cycle costing results for the case study show that a CI mini tractor using ammonia via indirect injection mode is approximately 3.3 times more expensive than a standard diesel vehicle under the presented assumptions. Maintenance, end of life and fuel contributions follow. The combined cost for fuels in the ammonia-fueled vehicle is 10–30 % higher than in the diesel-fueled scenario. This can be reduced either by decreasing ammonia or biodiesel costs; however, since biodiesel contributes a larger share of the combined fuel cost, reducing its price would be particularly beneficial. It would need to fall within the range of 0.62–0.96 $/l depending on the ammonia source. Shipping and carbon-compliance costs for ammonia production raise the total LCC only marginally.

The estimated results may not precisely reflect real-world conditions due to the bottom-up cost aggregation approach. Considering uncertainties related to capital expenditure and a range of potential market conditions affecting fuel prices, the LCC of the ammonia-fueled vehicle is estimated to be 2–4 times higher than that of a diesel mini tractor. Other limiting factors include public perception of ammonia safety and the resulting increase in maintenance costs for ammonia-fueled vehicles, required to ensure safety through periodic inspections.

To achieve cost-effectiveness for an ammonia-fueled vehicle, several strategies could be employed. One solution is for decision-makers to introduce a direct incentive for purchasing a carbon-free vehicle, which could offset the orchard owner's acquisition costs. The level of these would be in a range of 3000–8000 $, with around 6000 $ in the default scenario. Another option is to offer direct incentives for ammonia and biodiesel so that they reach parity with diesel. Alternatively, parity could be reached if the price of diesel reflected the carbon-emission compliance cost associated with greenhouse gas emissions from its combustion. Accounting for these factors might shift the profitability in favor of the ammonia-fueled mini tractor, which may serve as a viable option for reducing the carbon footprint from agriculture while also enhancing energy security through diversified fueling options.

CRediT authorship contribution statement

Mateusz Proniewicz: Writing – original draft, Methodology, Investigation, Formal analysis, Conceptualization. **Karolina Petela:** Writing – review & editing, Supervision, Conceptualization. **Andrzej Szlęk:** Writing – review & editing, Supervision, Conceptualization.

Declaration of competing interest

The authors declare that they have no known competing financial interests or personal relationships that could have appeared to influence the work reported in this paper.

Acknowledgments

The authors wish to acknowledge Wojciech Adamczyk for his role in project administration and Grzegorz Przybyła for his supervision of experimental setup. The research leading to these results has received funding from the Norway Grants 2014–2021 under POLNOR2019 competition operated by the National Centre for Research and Development and from Polish State Budget (Grant No. NOR/POLNOR/ACTIVATE/0046/2019-00).

Data availability

Data will be made available on request.

References

[1] Boggia S, Jackson A. Some unconventional aero gas turbines using hydrogen fuel. Turbo Expo 2002, Parts A and B 2002;2:683–90. https://doi.org/10.1115/GT2002-30412.
[2] Turner J, Sverdrup G, Mann MK, Maness P-C, Kroposki B, Ghirardi M, Evans RJ, Blake D. Renewable hydrogen production. Int J Energy Res 2008;32(5):379–407. https://doi.org/10.1002/er.1372.
[3] Singla MK, Nijhawan P, Oberoi AS. Hydrogen fuel and fuel cell technology for cleaner future: a review. Environ Sci Pollut Control Ser 2021;28(13):15607–26. https://doi.org/10.1007/s11356-020-12231-8.
[4] Taylor JB, Alderson JEA, Kalyanam KM, Lyle AB, Phillips LA. Technical and economic assessment of methods for the storage of large quantities of hydrogen, international journal of hydrogen energy. Int J Hydrogen Energy 1986;11(1):5–22. https://doi.org/10.1016/0360-3199(86)90104-7.
[5] Buffi M, Scarlat N, Hurtig O, Motola V, Georgakaki A, Letout S, Mountraki A, Joanny G. *Clean energy technology observatory: renewable fuels of non-biological origin*

in the European Union – 2022 status report on technology development, trends, value chains and markets (No. JRC130729). Publications Office of the European Union; 2022. https://doi.org/10.2760/76717.
[6] Zamfirescu C, Dincer I. Using ammonia as a sustainable fuel. J Power Sources 2008; 185(1):459–65. https://doi.org/10.1016/j.jpowsour.2008.02.097.
[7] Lamb KE, Dolan MD, Kennedy DF. Ammonia for hydrogen storage; A review of catalytic ammonia decomposition and hydrogen separation and purification. Int J Hydrogen Energy 2019;44(7):3580–93. https://doi.org/10.1016/j.ijhydene.2018.12.024.
[8] Giddey S, Badwal SPS, Munnings C, Dolan M. Ammonia as a renewable energy transportation media. ACS Sustainable Chem Eng 2017;5(11):10231–9. https://doi.org/10.1021/acssuschemeng.7b02219.
[9] Wijayanta AT, Oda T, Purnomo CW, Kashiwagi T, Aziz M. Liquid hydrogen, methylcyclohexane, and ammonia as potential hydrogen storage: comparison review. Int J Hydrogen Energy 2019;44(29):15026–44. https://doi.org/10.1016/j.ijhydene.2019.04.112.
[10] International Energy Agency (IEA). Ammonia technology roadmap. IEA; 2021. https://www.iea.org/reports/ammonia-technology-roadmap.
[11] Tornatore C, Marchitto L, Sabia P, De Joannon M. Ammonia as green fuel in internal combustion engines: state-of-the-art and future perspectives. Front Mech Eng 2022;8:944201. https://doi.org/10.3389/fmech.2022.944201.
[12] Proniewicz M, Petela K, Szlęk A. Life cycle assessment of ammonia as carbon-free fuel in internal combustion engine-driven orchard vehicle. Fuel 2025;400:135809. https://doi.org/10.1016/j.fuel.2025.135809.
[13] Lasocki J, Bednarski M, Sikora M. Simulation of ammonia combustion in dual-fuel compression-ignition engine. IOP Conf Ser Earth Environ Sci 2019;214:012081. https://doi.org/10.1088/1755-1315/214/1/012081.
[14] Gill SS, Chatha GS, Tsolakis A, Golunski SE, York APE. Assessing the effects of partially decarbonising a diesel engine by co-fuelling with dissociated ammonia. Int J Hydrogen Energy 2012;37(7):6074–83. https://doi.org/10.1016/j.ijhydene.2011.12.137.
[15] Cai K, Liu Y, Chen Q, Qi Y, Li L, Wang Z. Combustion behaviors and unregular emission characteristics in an ammonia–diesel engine. Energies 2023;16(19):7004. https://doi.org/10.3390/en16197004.
[16] Nadimi E, Przybyła G, Løvås T, Peczkis G, Adamczyk W. Experimental and numerical study on direct injection of liquid ammonia and its injection timing in an ammonia-biodiesel dual injection engine. Energy 2023;284:129301. https://doi.org/10.1016/j.energy.2023.129301.
[17] Proniewicz M, Petela K, Szlęk A, Przybyła G, Nadimi E, Ziółkowski Ł, Løvås T, Adamczyk W. Energy and exergy assessments of a Diesel-, Biodiesel-, and ammonia-fueled compression ignition engine. Int J Energy Res 2023;2023:1–20. https://doi.org/10.1155/2023/9920670.
[18] Kuta K, Przybyła G, Kurzydym D, Żmudka Z. Experimental and numerical investigation of dual-fuel CI ammonia engine emissions and after-treatment with V2O5/SiO2–TiO2 SCR. Fuel 2023;334:126523. https://doi.org/10.1016/j.fuel.2022.126523.
[19] Zhang H, Wang L, Van Herle J, Maréchal F, Desideri U. Techno-economic comparison of green ammonia production processes. Appl Energy 2020;259:114135. https://doi.org/10.1016/j.apenergy.2019.114135.
[20] Fúnez Guerra C, Reyes-Bozo L, Vyhmeister E, Jaén Caparrós M, Salazar JL, Clemente-Jul C. Technical-economic analysis for a green ammonia production plant in Chile and its subsequent transport to Japan. Renew Energy 2020;157:404–14. https://doi.org/10.1016/j.renene.2020.05.041.
[21] Boulamanti A, Moya JA. Production costs of the chemical industry in the EU and other countries: ammonia, methanol and light olefins. Renew Sustain Energy Rev 2017;68:1205–12. https://doi.org/10.1016/j.rser.2016.02.021.
[22] Fasihi M, Weiss R, Savolainen J, Breyer C. Global potential of green ammonia based on hybrid PV-wind power plants. Appl Energy 2021;294:116170. https://doi.org/10.1016/j.apenergy.2020.116170.
[23] Cesaro Z, Ives M, Nayak-Luke R, Mason M, Bañares-Alcántara R. Ammonia to power: forecasting the levelized cost of electricity from green ammonia in large-scale power plants. Appl Energy 2021;282. https://doi.org/10.1016/j.apenergy.2020.116009.
[24] Campion N, Nami H, Swisher PR, Vang Hendriksen P, Münster M. Techno-economic assessment of green ammonia production with different wind and solar potentials. Renew Sustain Energy Rev 2023;173:113057. https://doi.org/10.1016/j.rser.2022.113057.
[25] Adeli K, Nachtane M, Tarfaoui M, Faik A, Pollet BG, Saifaoui D. Deep learning analysis of green ammonia synthesis: evaluating techno-economic feasibility for sustainable production. Int J Hydrogen Energy 2024;87:1224–32. https://doi.org/10.1016/j.ijhydene.2024.09.127.
[26] Nylund N-O, Koponen K. Fuel and technology alternatives for buses: overall energy efficiency and emission performance. VTT; 2012.
[27] Ally J, Pryor T. Life cycle costing of diesel, natural gas, hybrid and hydrogen fuel cell bus systems: an Australian case study. Energy Policy 2016;94:285–94. https://doi.org/10.1016/j.enpol.2016.03.039.
[28] Szumska E, Pawełczyk M, Pistek V. Evaluation of the life cycle costs for urban buses equipped with conventional and hybrid drive trains. The Archives of Automotive Engineering – Archiwum Motoryzacji 2019;83(1):73–86. https://doi.org/10.14669/AM.VOL83.ART5.
[29] Thompson ST, James BD, Huya-Kouadio JM, Houchins C, DeSantis DA, Ahluwalia R, Wilson AR, Kleen G, Papageorgopoulos D. Direct hydrogen fuel cell electric vehicle cost analysis: system and high-volume manufacturing description, validation, and outlook. J Power Sources 2018;399:304–13. https://doi.org/10.1016/j.jpowsour.2018.07.100.
[30] Halder P, Babaie M, Salek F, Shah K, Stevanovic S, Bodisco TA, Zare A. Performance, emissions and economic analyses of hydrogen fuel cell vehicles. Renew Sustain Energy Rev 2024;199:114543. https://doi.org/10.1016/j.rser.2024.114543.
[31] Kuyumcu AM, Bingül B, Akar F, Yıldız A. Well-to-wheel carbon footprint and cost analysis of gasoline, diesel, hydrogen ICE, hybrid and fully electric city buses. Energy 2024;301:131685. https://doi.org/10.1016/j.energy.2024.131685.
[32] Wang B, Li Z, Zhou J, Cong Y, Li Z. Technological-economic assessment and optimization of hydrogen-based transportation systems in China: a life cycle perspective. Int J Hydrogen Energy 2023;48(33):12155–67. https://doi.org/10.1016/j.ijhydene.2022.12.189.
[33] Dimitriou P, Javaid R. A review of ammonia as a compression ignition engine fuel. Int J Hydrogen Energy 2020;45(11):7098–118. https://doi.org/10.1016/j.ijhydene.2019.12.209.
[34] Posada F, Chambliss S, Blumberg K. Costs of emission reduction technologies for heavy-duty diesel vehicles. The International Council on Clean Transportation; 2016.
[35] U.S. Inflation Rate 1960-2025. (n.d.). macrotrends. Retrieved January 23, 2025, from, https://www.macrotrends.net/global-metrics/countries/USA/united-states/inflation-rate-cpi.
[36] University of Maine. (n.d.). calendar of apple orchard management activities. Cooperative extension: garden and yard. Retrieved October 18, 2024, from, https://extension.umaine.edu/gardening/manual/calendar-apple-orchard-management-activities/.
[37] Alternative Fuels Data Center. U.S. department of energy, energy efficiency & renewable energy. https://afdc.energy.gov/fuels/prices.html; 2024, December.
[38] Proniewicz M, Petela K, Szlęk A, Adamczyk W. Life cycle assessment of selected ammonia production technologies from the perspective of ammonia as a fuel for heavy-duty vehicle. J Energy Resour Technol 2024;146(3):030905. https://doi.org/10.1115/1.4064371.
[39] Ghavam S, Vahdati M, Wilson IAG, Styring P. Sustainable ammonia production processes. Front Energy Res 2021;9:580808. https://doi.org/10.3389/fenrg.2021.580808.
[40] IEA. The future of hydrogen. 2019. p. 105–8. https://www.iea.org/reports/the-future-of-hydrogen.
[41] Shiozawa B. The cost of CO2-free ammonia. Ammonia Energy Association; 2020. https://ammoniaenergy.org/articles/the-cost-of-co2-free-ammonia/.
[42] Seo Y, An J, Park E, Kim J, Cho M, Han S, Lee J. Technical–economic analysis for ammonia ocean transportation using an ammonia-fueled carrier. Sustainability 2024;16(2):827. https://doi.org/10.3390/su16020827.
[43] Vartiainen E, Breyer C, Moser D, Román Medina E, Busto C, Masson G, Bosch E, Jäger-Waldau A. True cost of solar hydrogen. Sol RRL 2022;6(5):2100487. https://doi.org/10.1002/solr.202100487.
[44] Bartels JR. A feasibility study of implementing an ammonia economy. Master of Science, Iowa State University, Digital Repository]; 2008, 2807317. https://doi.org/10.31274/etd-180810-1374.
[45] Charter Brokerage. *Superfund taxable chemicals*. List of taxable chemicals and rates (26 USC 4661) as specified under the infrastructure investment and jobs act (P.L. 177-58) of 2021. https://charterbrokerage.net/superfund-taxable-chemicals/; 2022.
[46] Annual Energy Outlook 2023 Table: Table 12. Petroleum and Other Liquids Prices. U.S. energy information administration. 2023. https://www.eia.gov/outlooks/aeo/data/browser/#/?id=12-AEO2023&region=0-0&cases=ref2023&start=2021&end=2050&f=A&linechart=ref2023-d020623a.3-12-AEO2023~&map=&ctype=linechart&sourcekey=0.
[47] Annual Energy Outlook 2023 Table: Table 13. Natural Gas Supply, Disposition, and Prices. U.S. energy information administration. https://www.eia.gov/outlooks/aeo/data/browser/#/?id=13-AEO2023&cases=ref2023&sourcekey=0; 2023.
[48] IEA. Levelised cost of electricity calculator. https://www.iea.org/data-and-statistics/data-tools/levelised-cost-of-electricity-calculator; 2020.
[49] IEA. Projected costs of generating electricity 2020. https://www.iea.org/reports/projected-costs-of-generating-electricity-2020; 2020.
[50] Jawad D, Ozbay K. The discount rate in life-cycle cost analysis of transportation projects. In: Transportation Research Board 85th Annual Meeting, Washington, DC; 2006. https://trid.trb.org/View/777599. Paper No. 06-2662.
[51] AACE International. Cost estimate classification system – as applied in engineering, procurement, and construction for the process industries (recommended practice nos. 18R-97; TCM framework: 7.3 – cost estimating and budgeting). International: AACE; 2016.